NOVEL SUBSTRATE INTEGRATED WAVEGUIDES AND COMPONENTS

A thesis submitted to the University of KENT
for the degree of Doctor of Philosophy
in Electronic Engineering

by
Nikolaos Grigoropoulos
September 2005

Abstract

This thesis examines the properties of novel waveguides at mm-wave frequencies as advanced alternatives to the conventional components used today in research as well as in commercial applications. The analysis begins with the folded waveguide, a space saving substitute for the well known Rectangular Waveguide (RWG). Folded waveguides are dielectric-filled metallic structures that preserve the original modes of a rectangular waveguide in a more compact geometry. There are two types of folded waveguides, type 1 and type 2 both of which are narrower than RWGs. Furthermore it is proved that the bandwidth characteristics of type 1 are by far superior to those of an RWG.

Due to the closed nature of folded structures the dispersion characteristics are identical to those of RWG. This thesis presents design equations for type 1 and type 2 guides and discusses their fabrication process as well as their ability to form multilayer stacks with even greater benefits in bandwidth and reduced dimensions.

By introducing discontinuities in the transmission line of a folded guide we create resonating cavities with controllable response i.e. a filter. Hence it is shown that folded guides form the basis for a new class of folded-based components with the benefit of small widths.

Another novel type of waveguide analysed in this thesis is the Non Radiative Perforated Dielectric Waveguide (NRPD). The structure is based on the operating principle of the conventional Nonradiative Dielectric Waveguide (NRD) but, instead of air, the slab is surrounded by perforated dielectric. Our structure uses the same theory as the NRD with the only difference being the value of the surrounding permittivity which is equal to the *equivalent* permittivity of the perforated lattice. NRPD shows manufacturing superiority over conventional NRDs and allows the fabrication of NRPD components such as filters, based on the resonating cavity principle.

CONTENTS

Acknowledgement

I would like to thank Dr P.R.Young, my supervisor, for his inspiration and his innovative ideas that raised my research to high scientific standards and produced numerous publications for journals and conferences. Dr P.R.Young has not only been an excellent supervisor but a good friend as well.

I would also like to thank Dr. Batchelor, Simon Tse and B. Sanz Izquierdo for their collaboration with my area of research and all the staff in the mechanical workshop of the University of KENT.

List of publications arising from this thesis:

- *Low Cost Non-Radiative Perforated Dielectric Waveguides*, N. Grigoropoulos, P.R. Young, 33rd European Microwave Conference, Munich 2003 October

- *Compact folded waveguides*, N. Grigoropoulos, P. R. Young, 34th European Microwave Conference, Amsterdam 2004 October

- *Non-Radiative Perforated Dielectric Waveguide (NRPD) with Integrated Transition to Slotline for Millimetre-Wave Components*, N. Grigoropoulos, S. Tse, P. R. Young, IEEE 2004 High Frequency Postgraduate Student Colloquium, Manchester, pp. 127-131 2004

- *Substrate-Integrated Folded Waveguide Slot Antenna*, B. Sanz-Izquierdo, P. R. Young, N. Grigoropoulos, J. C. Batchelor, R. J. Langley, IEEE International Workshop on Antenna Technology, Singapore, March 2005

- *Slot Array Antenna using Folded Waveguides*, B. Sanz-Izquierdo, P. R. Young, N. Grigoropoulos, J. C. Batchelor, R. J. Langley, Loughborough Antennas & Propagation Conference, Loughborough, April 2005

- Slot Antenna on C Type Compact Substrate Integrated Waveguide, B. Sanz Izquierdo, P. R. Young, N. Grigoropoulos, J. C. Batchelor, R. J. Langley, To be presented at the 35th European Microwave Conference, Paris, October 2005.

- Substrate Integrated waveguides and filters, P.R.Young, N. Grigoropoulos, B. Sanz Izquierdo, Submitted to the IEEE letter

A brief history of Microwaves

"Those who fail to remember the past are condemned to repeat it"

- George Santayana

The historical journey of Microwave technology and its evolution has to begin with Michael Faraday (1791-1867). The discovery of magneto-electric induction, the law of electro-chemical decomposition, the magnetization of light, and diamagnetism, were some of his most important contributions to science. Faraday's concepts, which came directly from experiment, are today's common ideas in modern research. In 1873, James Clerk Maxwell laid the foundations of electromagnetic theory in his work, "A Treatise on Electricity and Magnetism" in Scotland. In this treatise, Maxwell theorized that, if combined, electrical and magnetic energy would be able to travel through space in a wave. Maxwell's equations are routinely solved many thousands of times per second by today's three-dimensional structural simulators using finite element analysis. Several years later, German Heinrich Hertz conducted experiments that proved Maxwell's theories were correct. Hertz began testing these theories by using a high-voltage spark discharge to excite a half-wave dipole antenna. A receive antenna consisted of an adjustable loop of wire with another spark gap. When both transmit and receive antennas were adjusted for the same resonant frequency, Hertz was able to demonstrate propagation of electromagnetic waves.

In the following years, much progress was done in transmission line theory and the propagation of waves over long distances, mostly through air. It was not before the 1930s, when Dr. George C. Southworth of Bell Telephone Labs discovered that radio waves could be transmitted efficiently through a hollow, water-filled copper pipe. He and his team at Bell found that electromagnetic energy travelling through an enclosed structure moved in distinct patterns that we call today "modes", and that the optimum diameter for a waveguide pipe was slightly greater than one-half wave length. They also experimented successfully with square, rectangular and oval waveguides.

In the 1950s and 1960s scientists began to study the properties of electromagnetic waves of higher frequencies, thus entering the Microwave Communications Era. High frequencies implied the need for Microwave Integrated Circuits (MICs), i.e. compact, planar circuit configurations. Planar waveguides such as the microstrip

line, slotline, co-planar waveguide (Cheng P. Wen 1969) and stripline, were invented to form the elementary blocks of MIC circuits.

1. Introduction

The ever-increasing demand for bandwidth has pushed the applications of microwaves into the millimetre-wave region. Upcoming mass consumer market applications at millimetre-wave frequencies include wireless local area networks (WLAN), vehicle radar systems and intelligent transportation systems (ITS). It is clear that for large scale fabrication, future millimetre-wave systems need to have small dimensions, good performance and a cheap, simple manufacturing procedure. Conventional microwave circuits fabricated on microwave ceramic/PTFE substrates have the benefit of low cost fabrication based on standard PCB techniques. Unfortunately the large conduction and radiation loss from microstrip lines and coplanar waveguides commonly found on PCB boards limits their use at microwave frequencies. Various dielectric waveguides such as image guides [1] and insular guides [2] have been proposed as possible substitutes for microstrip lines but are of limited use at curved sections due to additional radiation losses.

Rectangular waveguides (RWG), on the other hand, are electromagnetic transmission lines without radiation problems. They are popular among microwave circuits for their excellent power handling capabilities and their immunity to radiation and crosstalk. The rectangular waveguide is today present in a plethora of applications from wireless local area networks to airborne radar and intelligent transportation systems. It can be found in large array formations and also in High Q filters and broadband couplers. Unfortunately, rectangular waveguides, are by nature three dimensional, and can be difficult to integrate with microstrip lines and planar circuitry in general. Furthermore, at the lower part of mm-wave region, RWGs have large dimensions and a considerable weight which makes them unsuitable for microwave systems.

To overcome these problems several novel techniques relying on existing circuit fabrication have been proposed for the fabrication of waveguides. They include micromachining of silicon and photoimageable spin-on materials [3]. Nevertheless, both of these methods require many steps and integration with planar circuits remains a problem. Unfortunately, even with this reduction in size, substrate integrated

waveguides can be much wider than their microstrip counterparts particularly at low microwave frequencies. An alternative method is to use dielectric filled waveguides. Such a technique is the fabrication of RWGs photolithografically by employing multilayer processing and using photoimageable thick film materials [4]. A low loss glass filled technique at millimetre wave has been demonstrated by Kinayaman [5] where guides are formed by etching pedestals from a silicon wafer. His method has been proved to integrate RGWs with planar circuits at frequencies up to 77GHz.

Dielectric filled waveguides have also been made using laminate technology [6]. More recently, multilayer co-fired ceramic has been used [7]. The sidewalls of the waveguides have been realised using series of vias, while on the top and bottom metallisation has been employed. These techniques allow easy integration with planar transmission lines and are relatively simple and low-cost. Single layer alternatives have also been produced. In [8] a 2D lattice of plated via holes are used to form the sidewalls of a RWG using microwave laminates. All of these techniques have the advantage of easy integration with planar circuitry. In addition, because they are dielectric filled the cross-sectional area of the guide is reduced by a factor of $\varepsilon_r^{-1/2}$, where ε_r is the permittivity of the dielectric material. Unfortunately the width of these structures still remains much wider compared to their microstrip counterparts at microwave frequencies.

In order to cope with today's fast growing Microwave industry, dielectric waveguides are required that offer good performance at low cost. In this thesis we propose two novel types of substrate integrated microwave guides. The first is the Substrate Integrated Folded Waveguide and the second is the Non Radiative Perforated Dielectric Waveguide (NRPD).

The folded waveguide, figure 1.1, is an advanced alternative to the rectangular waveguide. The structure is easy to fabricate and retains the advantages of a rectangular waveguide in a much smaller and lighter package. It is shown that the folded waveguide results in a size reduction of $\varepsilon_r^{-1/2}/2$ over standard waveguide. This results in structures with 1/6 the width of conventional air filled waveguide when using a substrate with relative permittivity $\varepsilon_r = 9$. Furthermore, since the structures are, by their nature, easily integrated with planar devices they present a viable small size waveguide that can be used even at low microwave frequencies.

The second type of waveguide that we propose, the NRPD guide, is based on the technology of the Nonradiative dielectric waveguide (NRD). The NRD guide has seen renewed interest as a low cost, high performance alternative to conventional planar structures. Although NRDs are not as small as RWGs, they have demonstrated their simplicity in mechanical assembling, ease of fabrication and low loss nature. The NRD was first proposed by Yoneyama and Nishida [9] and is formed by a block of dielectric placed between two conducting planes, figure 1.2. The structure is very

similar to the H guide [10] but it is based on a different principle of operation. Whereas in the H guide the distance between the metal plates is rather arbitrary, in the NRD this distance has been reduced to suppress radiation from the structure.

By periodically introducing air columns in the dielectric material between the metal plates of the NRD we create the NRPD structure, figure 1.3.

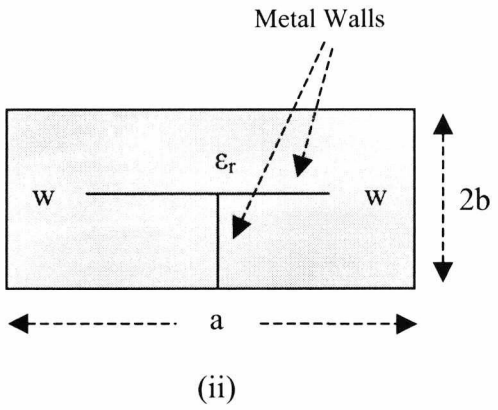

Figure 1.1. The cross-sectional view of the substrate integrated folded guide

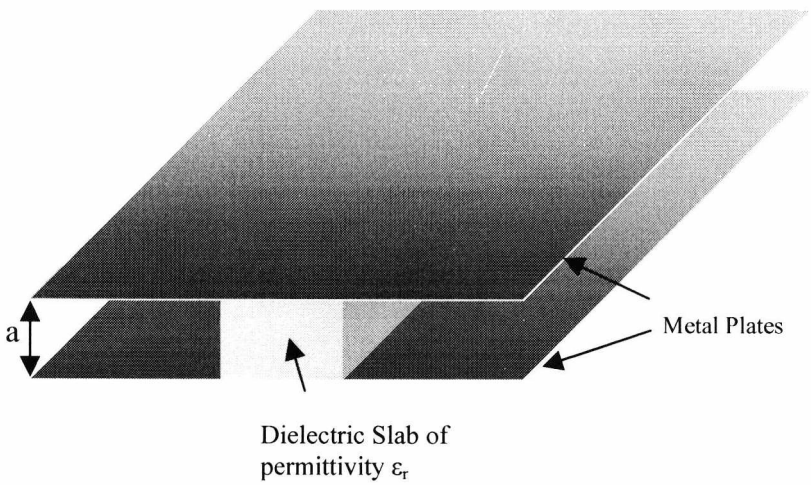

Figure 1.2. The nonradiative dielectric waveguide

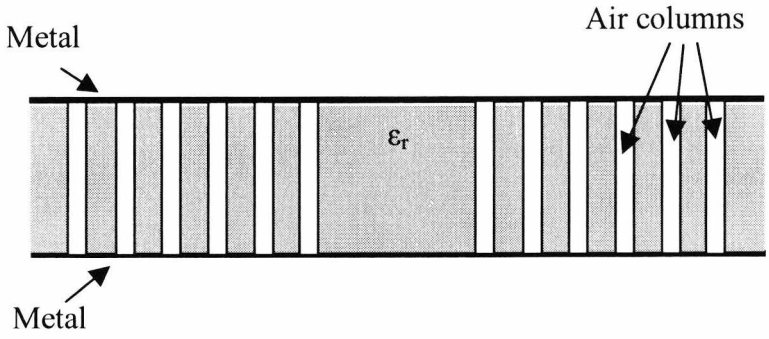

Figure 1.3. Cross section of the NRPD structure

1.1 Outline of thesis

This thesis is an extensive analysis of two novel types of waveguide; the substrate integrated folded waveguide and the NRPD.

The folded waveguide is a closed structure with dispersion characteristics identical to those of rectangular waveguides. Therefore chapter 2 begins with the analysis of the rectangular waveguide starting from Maxwell's equations and derives expressions for the propagation constants of the modes. The theory is then modified to fit the folded guide.

In the same chapter, design equations are produced for the folded guide and simulated results are given for the bandwidth and cutoff frequencies. Towards the end of chapter 2 the capability of a folded guide to form multilayer stacks is analysed and presented with simulated results. Furthermore, we discuss the losses of folded guides and compare them to those of RWGs.

Chapter 3 analyses the fabrication methods of folded guides. It is shown shown how planar types of transmission lines can form hybrid structures with folded guides and furthermore we introduce the via-hole technology for the fabrication of folded structures in the X-band. Two waveguides were manufactured in the workshop and the measurements are presented along with simulated results.

In addition, we describe the fabrication of folded structures using thick films in collaboration with the University of Surrey. Thick films allow the fabrication of very small waveguides with operating frequencies up to 110 GHz.

Chapter 4 explains how folded guides form the basis for a new class of microwave components. More specifically, we design filters based on folded guide technology which deliver good performance with reduced dimensions. The operation of the filters is based on the theory of *direct coupled cavities*, formed by introducing discontinuities in the transmission line of the folded guide. We fabricated a filter in the workshop using conventional PCB technology and the results are presented with simulated results.

Chapter 5 is an analysis of the NRPD waveguide which is based on the conventional NRD. The theory of an NRD guide is an extension of the slab waveguide theory, the simplest form of dielectric waveguide and therefore chapter 5 begins with an analysis of the dielectric slab. Modifying the theory of the slab produces formulae for the dispersion curves of the NRD. Then, by substituting the air regions of the NRD with perforated regions of dielectric material we get the NRPD waveguide. The principle of operation is based on the total internal reflection of the waves in the boundaries between the perforated regions and the central NRPD core. We fabricate an NRPD guide in the workshop and the measurements are presented together with simulated results. This chapter also deals with excitation methods, comparisons of perforated regions and several manufacturing issues.

Chapter 6 uses the theory of *direct coupled cavities* from chapter 4 to form filters using NRPD guides. Two types of discontinuities are analysed, the cylindrical air columns and the rectangular cavities. The filters have been simulated and the results are encouraging.

Chapter 7 gives some suggestions for further work on the NRPD guide and chapter 8 summarises the results of the thesis.

References

[1] R. M. Knox, "Integrated circuits for the millimeter through optical frequency range," in *Proc. Symp. Submillimeter Waves, pp. 497-516, 1970*

[2] J.E. Kietzer, A.R.Kaurs, and B.J.Levin, "A V-band communication transmitter and receiver system using dielectric waveguide integrated circuits," *IEEE Trans. Microwave Theory Tech.,* vol MTT-24, pp. 297-803, Nov. 1976

[3] Digby, J. McIntosh, C.E. "Fabrication and characterization of micromachined rectangular waveguide components for use at mm-wave and THz frerquencies" *IEEE Transactions on Microwave Theory and Techniques*, 48 pp1293-1302

[4] M. S. Aftanasar, P. R. Young, I. D. Robertson, J. Minalgiene and S. Lucyszyn, "Photoimageable thick-film millimetre-wave metal-pipe rectangular waveguides," *Electron. Lett.*, vol. 37, No. 18, August 2001, pp. 1122-1123.

[5] N. Kinayman, C. Eswarappa, N. Jatin and A. Buckle, "A novel surface-mountable millimetre-wave bandpass filter," *IEEE Microwave Wireless Compon. Lett.*, vol. 12, no. 3, pp. 76-78, March 2002.

[6] U. Hiroshi, T. Takeshi and M. Fujii, "Development of a 'laminated waveguide," *IEEE Trans. Microwave Theory Tech.*, vol. 46, no. 12, pp. 2438-2443, December 1998.

[7] W. Menzal and J. Kassner, "Millimeter-wave 3D integration techniques using LTCC and related multilayer circuits," *30th European Microwave conference proceedings*, pp. 33-53, Paris 2000.

[8] C. Y. Chang and W. C. Hsu, "Photonic bandgap dielectric waveguide filter," *IEEE Microwave wireless Compon. Lett.*, Vol. 12, no. 4, pp. 137-139, April 2002.

[9] T. Yoneyama and S. Nishida, "Non Radiative Dielectric waveguide for Millimeter- wave Integrated Circuits," *IEEE Transactions on Microwave Theory and Techniques,* Vol.MTT-29, No.11, November 1981

[10] F. J. Tisher, "A waveguide structure with low losses," *Arch. Elec Ubertragung*, vol 7, pp.592-596, Dec 1953

2. Folded Waveguides

Although rectangular waveguides are one of the earliest types of transmission lines, they are used today in many applications. A lot of components such as polarizers [1], filters and resonators [2-5], junctions [6,7] diplexers [8] and slot antennas [9-10] are designed for various standard waveguide bands from 1 GHz to above 220 GHz. RWGs are simple structures with easily predictable cutoff frequency and sufficient bandwidth. However, the microwave industry is constantly shifting to more efficient structures with easy integration to planar transmission lines and compact dimensions. RWGs are heavy structures and are difficult to form hybrid designs with microstrip lines.

In this chapter we introduce the folded waveguide, a substrate integrated waveguide structure made from microwave laminates. The folded guide can have two different geometrical variations, type 1 and type 2, both of which are double-layered. We show that these designs offer 50% more bandwidth and up to $\varepsilon_r^{-1/2}/3$ width reduction compared to standard air-filled rectangular waveguide. Furthermore, we explore the ability of folded guides to form multilayer stacks with even greater benefits in bandwidth and reduced dimensions.

The theory of a folded guide is similar to that of a rectangular waveguide. Therefore, in this section, we analyze the rectangular waveguide first and derive formulae for the propagation constants and cut-off frequencies of its modes. These formulas are then modified to fit the folded waveguide. Both types of folded guide have been analyzed and they are presented in this chapter together with design equations.

Losses of folded guides are also discussed and they are compared to those of rectangular waveguides.

2.1 The hollow rectangular waveguide

The rectangular waveguide in figure 2.1 is of finite width and height and extends infinitely in the x direction. There can be no TEM waves inside the rectangular waveguide due to the metal boundary conditions. Instead we are dealing with TE (transverse electric) and TM (transverse magnetic) waves. Certain properties of this waveguide can be obtained by considering that the TE or TM modes are the result of superimposing two TEM component waves and applying the metal boundary conditions. The more accurate method however starts with Maxwell's equations and proceeds to the solution of the wave equation in rectangular coordinates. This solution gives us complete expressions for the electric and magnetic fields inside the waveguide.

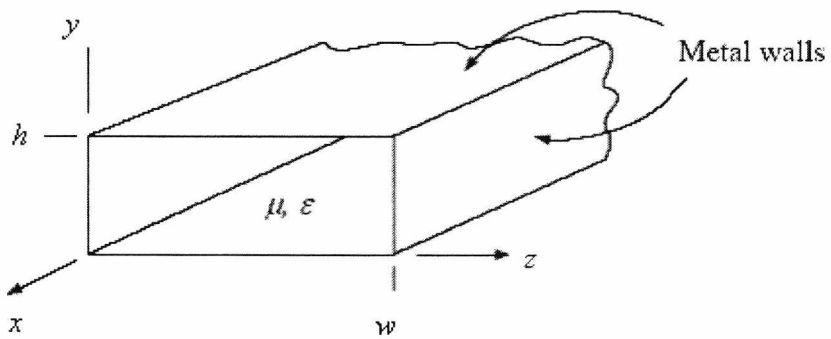

Figure 2.1. The hollow rectangular waveguide

The electromagnetic analysis of any waveguide begins with a statement of Maxwell's four equations in differential form:

$$\textit{First Curl equation: } \nabla \times \widetilde{H} = \widetilde{J} + \frac{\partial D}{\partial t} \tag{2.1}$$

Maxwell's First Curl equation represents an extension of Ampere's law which states that the magnetic field $\widetilde{H}$ around a finite closed path is related to the total current passing through the area enclosed by that path. $\widetilde{J}$ represents current density.

$$\textit{Second curl equation: } \nabla \times \widetilde{E} = -\frac{\partial \widetilde{B}}{\partial t} \tag{2.2}$$

Maxwell's second curl equation comes from Faraday's law of Electromotive force (EMF). This law states that the EMF force induced on a fixed, closed electrical circuit is equal to the normal component of the rate of change of magnetic flux density $\widetilde{B}$ passing through the circuit. $\widetilde{E}$ is the electric field intensity.

$$\textit{Third equation: } \nabla \cdot \widetilde{D} = \widetilde{\rho} \tag{2.3}$$

Maxwell's third equation comes from Gauss's first law which explains that the electric flux density $\widetilde{D}$ though any closed surface equals the total charge enclosed by that surface. $\widetilde{\rho}$ is the electric charge density.

$$\textit{Fourth equation: } \nabla \cdot \widetilde{B} = 0 \tag{2.4}$$

Maxwell's fourth equation comes from Gauss's second law which states that magnetic flux tubes are continuous i.e. they have no sources or sinks. Thus as many magnetic flux tubes must enter a volume leave it.

In the above equations the tildes (~) represent functions of space and time. Also the (.) sign is the *dot* product of two vectors which yields a scalar function. The (x) sign represents vector product and yields another vector function. Also, Maxwell's equations are supplemented with: $\widetilde{J} = \sigma\widetilde{E}$, $\widetilde{D} = \varepsilon\widetilde{E}$ and $\widetilde{B} = \mu\widetilde{H}$, where ε is the permittivity and μ is the permeability of the medium.

From Maxwell's curl equations, i.e. (2.1) and (2.2) we get the following set of six scalar equations:

$$\frac{\partial \widetilde{H}_z}{\partial y} - \frac{\partial \widetilde{H}_y}{\partial z} - \sigma \widetilde{E}_x - \varepsilon \frac{\partial \widetilde{E}_x}{\partial t} = 0 \quad (2.5)$$

$$\frac{\partial \widetilde{H}_x}{\partial z} - \frac{\partial \widetilde{H}_z}{\partial x} - \sigma \widetilde{E}_y - \varepsilon \frac{\partial \widetilde{E}_y}{\partial t} = 0 \quad (2.6)$$

$$\frac{\partial \widetilde{H}_y}{\partial x} - \frac{\partial \widetilde{H}_x}{\partial y} - \sigma \widetilde{E}_z - \varepsilon \frac{\partial \widetilde{E}_z}{\partial t} = 0 \quad (2.7)$$

$$\frac{\partial \widetilde{E}_z}{\partial y} - \frac{\partial \widetilde{E}_y}{\partial z} + \mu \frac{\partial \widetilde{H}_x}{\partial t} = 0 \quad (2.8)$$

$$\frac{\partial \widetilde{E}_z}{\partial z} - \frac{\partial \widetilde{E}_z}{\partial x} + \mu \frac{\partial \widetilde{H}_y}{\partial t} = 0 \quad (2.9)$$

$$\frac{\partial \widetilde{E}_y}{\partial x} - \frac{\partial \widetilde{E}_x}{\partial y} + \mu \frac{\partial \widetilde{H}_z}{\partial t} = 0 \quad (2.10)$$

where σ is the conductivity of the medium. From the divergence conditions, i.e. (2.3) and (2.4) in rectangular coordinates, in space free of charge (ρ=0), we get:

$$\nabla \cdot D = 0 \Rightarrow \frac{\partial \widetilde{E}_x}{\partial x} + \frac{\partial \widetilde{E}_y}{\partial y} + \frac{\partial \widetilde{E}_z}{\partial z} = 0 \quad (2.11)$$

$$\nabla \cdot B = 0 \Rightarrow \frac{\partial \widetilde{H}_x}{\partial x} + \frac{\partial \widetilde{H}_y}{\partial y} + \frac{\partial \widetilde{H}_z}{\partial z} = 0 \quad (2.12)$$

For the purposes of this analysis we assume harmonic time dependence and distance attenuation for the field components inside the rectangular waveguide. Hence for the y component of the electric field in the positive x direction we have:

$$\widetilde{E}_y = E_A e^{j\omega t - \gamma x} \quad (2.13)$$

where the $j\omega$t term denotes the harmonic time dependence and γ is the propagation constant, typically expressed as $\gamma = \alpha + j\beta$, with α = attenuation constant and β = phase constant. Applying the condition of (2.13) on equations (2.5) to (2.12) we get:

$$\frac{\partial H_z}{\partial y} + \frac{\gamma H_y}{\partial z} - (\sigma + j\omega\varepsilon)E_x = 0 \quad (2.14)$$

$$\frac{\partial H_x}{\partial z} + \gamma H_z - (\sigma + j\omega\varepsilon)E_y = 0 \quad (2.15)$$

$$-\gamma H_y - \frac{\partial H_x}{\partial y} - (\sigma + j\omega\varepsilon)E_z = 0 \quad (2.16) \qquad \frac{\partial E_z}{\partial y} - \frac{\partial E_y}{\partial z} + j\omega\mu H_x = 0 \quad (2.17)$$

$$\frac{\partial E_x}{\partial z} - \gamma E_z + j\omega\mu H_y = 0 \quad (2.18) \qquad -\gamma E_y - \frac{\partial E_x}{\partial y} + j\omega\mu H_z = 0 \quad (2.19)$$

$$-\gamma E_x - \frac{\partial E_y}{\partial y} + \frac{\partial E_z}{\partial z} = 0 \quad (2.20) \qquad -\gamma H_x - \frac{\partial H_y}{\partial y} + \frac{\partial H_z}{\partial z} = 0 \quad (2.21)$$

where the $e^{j\omega t}$ factor has been omitted for simplicity.

Since the rectangular waveguide is a typical transmission line we can apply the expressions for series impedance and shunt admittance, commonly used in transmission line theory [11]. Thus we introduce the series impedance Z and shunt admittance Y with:

$$Z = -j\omega\mu \quad (2.22) \qquad \text{and} \qquad Y = \sigma + j\omega\varepsilon \quad (2.23)$$

Substituting for (2.22) and (2.23) to equations (2.14) through (2.21) we get the following set of equations

$$\frac{\partial H_z}{\partial y} - \frac{\partial H_y}{\partial z} - YE_x = 0 \quad (2.24) \qquad \frac{\partial H_x}{\partial z} + \gamma H_z - YE_y = 0 \quad (2.25)$$

$$-\gamma H_y - \frac{\partial H_z}{\partial y} - YE_z = 0 \quad (2.26) \qquad \frac{\partial E_z}{\partial y} - \frac{\partial E_y}{\partial z} - ZH_x = 0 \quad (2.27)$$

$$\frac{\partial E_x}{\partial z} - \gamma E_z - ZH_y = 0 \quad (2.28) \qquad -\gamma E_y + \frac{\partial E_x}{\partial y} - ZH_z = 0 \quad (2.29)$$

$$-\gamma E_x + \frac{\partial E_y}{\partial y} + \frac{\partial E_z}{\partial z} = 0 \quad (2.30) \qquad -\gamma H_x + \frac{\partial H_y}{\partial y} + \frac{\partial H_z}{\partial z} = 0 \quad (2.31)$$

We now apply the restriction for the transverse electric modes of the rectangular waveguide.

Transverse electric or TE modes are the field configurations whose electric field components lie in a plane that is transverse to a given direction. That direction is often chosen to be the direction of propagation. In the rectangular waveguide of figure 2.1, if the wave is traveling in the positive x direction, the TE condition specifies that $E_x = 0$. The remaining components, the two electric field components (E_z and E_y) and the three magnetic field components (H_x, H_y and H_z), may or may not exist at all. The objective of our analysis is hence to determine analytical expressions for all the modes that can propagate inside the rectangular waveguide.

Equations (2.24) to (2.31), for TE mode solution, reduce to

$$\frac{\partial H_z}{\partial y} - \frac{\partial H_y}{\partial z} = 0 \qquad (2.24')$$

$$\frac{\partial H_x}{\partial z} + \gamma H_z - YE_y = 0 \qquad (2.25')$$

$$-\gamma H_y - \frac{\partial H_x}{\partial y} - YE_z = 0 \qquad (2.26')$$

$$\frac{\partial E_z}{\partial y} - \frac{\partial E_y}{\partial z} - ZH_x = 0 \qquad (2.27')$$

$$\gamma E_z - ZH_y = 0 \qquad (2.28')$$

$$-\gamma E_y - ZH_z = 0 \qquad (2.29')$$

$$\frac{\partial E_y}{\partial y} + \frac{\partial E_z}{\partial z} = 0 \qquad (2.30')$$

$$-\gamma H_x + \frac{\partial H_y}{\partial y} + \frac{\partial H_z}{\partial z} = 0 \qquad (2.31')$$

Equations (2.28') and (2.29') can be rewritten as

$$\frac{E_z}{H_y} = \frac{Z}{\gamma} \qquad (2.32) \qquad \text{and} \qquad -\frac{E_y}{H_z} = \frac{Z}{\gamma} \qquad (2.33)$$

The ratios E_z / H_y and E_y / H_z represent, in the case of a waveguide, the characteristic impedance of the transmission line. Since (2.32) and (2.33) contain only transverse field components they are called *transverse-wave impedance* Z_{yz} of the waveguide. We can then write

$$Z_{yz} = \frac{E_y}{H_z} = -\frac{E_z}{H_y} = -\frac{Z}{\gamma} = \frac{j\omega\mu}{\gamma} \tag{2.34}$$

Using equation (2.34) we substitute for E_z in equation (2.26) and then solve for H_y. Thus

$$H_y = \frac{-1}{\gamma - YZ_{yz}} \frac{\partial H_x}{\partial y} \tag{2.35}$$

In the same way, from (2.25)

$$H_z = \frac{-1}{\gamma - YZ_{yz}} \frac{\partial H_x}{\partial z} \tag{2.36}$$

Substituting (2.36) into (2.34) gives

$$E_y = \frac{-Z_{yz}}{\gamma - YZ_{yz}} \frac{\partial H_x}{\partial z} \tag{2.37}$$

and substituting (2.35) into (2.34) gives

$$E_z = \frac{-Z_{yz}}{\gamma - YZ_{yz}} \frac{\partial H_x}{\partial y} \tag{2.38}$$

The last four equations give the four transverse field components as a function of H_x. We can obtain an analytical expression for H_x by taking the y derivative of (2.35), the z derivative of (3.36) and substituting both into (2.31). This gives

$$\frac{\partial^2 H_x}{\partial y^2} + \frac{\partial^2 H_x}{\partial z^2} + \gamma(\gamma - YZ_{yz})H_x = 0 \tag{2.39}$$

Let $k^2 = \gamma(\gamma - YZ_{yz})$. Equation (2.39) then becomes

$$\frac{\partial^2 H_x}{\partial y^2} + \frac{\partial^2 H_x}{\partial z^2} + k^2 H_x = 0 \tag{2.40}$$

Equation (2.40) is a second order partial differential equation of first degree. We seek a solution to equation (2.40) that fits the boundary conditions of the rectangular waveguide. More specifically, assuming that the walls are perfectly conducting, the tangential components of the electric field must vanish on the wall surface. In (2.40), H_x is a function of y and z. The solution we are looking for should be of the form

$$H_x = f(y)f(z) \tag{2.41}$$

Where $f(y)$ and $f(z)$ are functions of y and z respectively.

Substituting into (2.40) gives

$$f(z)\frac{d^2 f(y)}{dy^2} + f(y)\frac{d^2 f(z)}{dz^2} + k^2 f(y)f(z) = 0 \tag{2.42}$$

or

$$\frac{1}{f(y)}\frac{d^2 f(y)}{dy^2} + \frac{1}{f(z)}\frac{d^2 f(z)}{dz^2} = -k^2 \tag{2.43}$$

The term k in equation (2.43) does not depend on either y or z and is treated as a constant. Consequently, both of the y and z terms are also constants. We hence write

$$\frac{1}{f(y)}\frac{d^2 f(y)}{dy^2} = -A_1 \quad (2.44) \qquad \text{and,} \qquad \frac{1}{f(z)}\frac{d^2 f(z)}{dz^2} = -A_2 \quad (2.45)$$

where A_1 and A_2 are constants. A solution of (2.44) is

$$f(y) = c_1 \sin b_1 y \tag{2.46}$$

where c_1 and b_1 are constants. Substituting into equation (2.44) gives

$$b_1 = \sqrt{A_1} \tag{2.47}$$

Hence (2.46) is a solution if (2.47) is fulfilled. In the same fashion, another solution is

$$f(y) = c_2 \cos b_1 y \tag{2.48}$$

If (2.46) and (2.48) are both solutions for $f(y)$, their sum would also be a solution. Thus

$$f(y) = c_1 \sin \sqrt{A_1}\, y + c_2 \cos \sqrt{A_1}\, y \tag{2.49}$$

The same procedure can be followed to reveal solutions for $f(z)$, such as

$$f(z) = c_3 \sin \sqrt{A_2}\, z + c_4 \cos \sqrt{A_2}\, z \tag{2.50}$$

Equations (2.49) and (2.50) are substituted into (2.41) to the solution for H_x as

$$\begin{aligned} H_x = {} & c_1 c_2 \sin \sqrt{A_1}\, y \sin \sqrt{A_2}\, z + c_2 c_3 \cos \sqrt{A_1}\, y \sin \sqrt{A_2}\, z \\ & + c_1 c_4 \sin \sqrt{A_1}\, y \cos \sqrt{A_2}\, z + c_2 c_4 \cos \sqrt{A_1}\, y \cos \sqrt{A_2}\, z \end{aligned} \tag{2.51}$$

Substituting (2.51) into (2.37) and (2.38) and applying the boundary conditions for the rectangular waveguide, we find that only the last term of (2.51) satisfies the boundary conditions provided that

$$\sqrt{A_1} = \frac{n\pi}{h} \qquad (2.52) \qquad \text{and,} \qquad \sqrt{A_2} = \frac{m\pi}{w} \qquad (2.53)$$

where m and n are integers (0, 1, 2, ...m or n) and w and h are the width and height of the rectangular waveguide of figure 2.1. The solution for H_x becomes

$$H_x(y,z) = H_0 \cos\frac{n\pi y}{h}\cos\frac{m\pi z}{w} \qquad (2.54) \qquad \text{where,} \qquad H_0 = c_2\, c_4 \qquad (2.55)$$

Equation (2.54) is substituted into (2.35) to (2.38) to give expressions for the transverse field components

$$H_y = \frac{\gamma H_0}{k^2}\frac{n\pi}{h}\sin\frac{n\pi y}{h}\cos\frac{m\pi z}{w}e^{-\gamma x} \qquad (2.56)$$

$$H_z = \frac{\gamma H_0}{k^2}\frac{m\pi}{w}\cos\frac{n\pi y}{h}\sin\frac{m\pi z}{w}e^{-\gamma x} \qquad (2.57)$$

$$E_y = \frac{\gamma Z_{yz} H_0}{k^2}\frac{m\pi}{w}\cos\frac{n\pi y}{h}\sin\frac{m\pi z}{w}e^{-\gamma z} \qquad (2.58)$$

$$E_y = -\frac{\gamma Z_{yz} H_0}{k^2}\frac{n\pi}{h}\sin\frac{n\pi y}{h}\cos\frac{m\pi z}{w}e^{-\gamma z} \qquad (2.59)$$

Also, from (2.52), (2.53) and (2.43) we have

$$\left(\frac{n\pi}{h}\right)^2+\left(\frac{m\pi}{w}\right)^2=k^2 \tag{2.60}$$

and since $k^2=\gamma^2-j\omega\mu(\sigma+j\omega\varepsilon)$ we get

$$\gamma=\sqrt{\left(\frac{n\pi}{h}\right)^2+\left(\frac{m\pi}{w}\right)^2-\omega^2\mu\varepsilon} \tag{2.61}$$

This is the well-known formula for the propagation constant of the rectangular waveguide (σ =0)

For cutoff frequency condition $\gamma=0$. Hence from (2.61)

$$(f_c)_{mn}=\frac{1}{2\pi\sqrt{\mu\varepsilon}}\sqrt{\left(\frac{n\pi}{h}\right)^2+\left(\frac{m\pi}{w}\right)^2} \tag{2.62}$$

For completeness we need to discuss the topology of the rectangular waveguide modes as well as the significance of integers *m* and *n*. If in the above field equations we substitute m=1 and n=0 we only have three field components H_x, H_z and E_y. In addition, the component E_y will have no variation with respect to *z* and the variation of amplitude is half a cycle with respect to x. This mode is referred to as TE_{10}. If m=2 then the variation along *x* is two half cycle variations and the mode is the TE_{20}. Figure 2.2 shows the field variations inside the rectangular waveguide for the TE_{10} and TE_{20}.

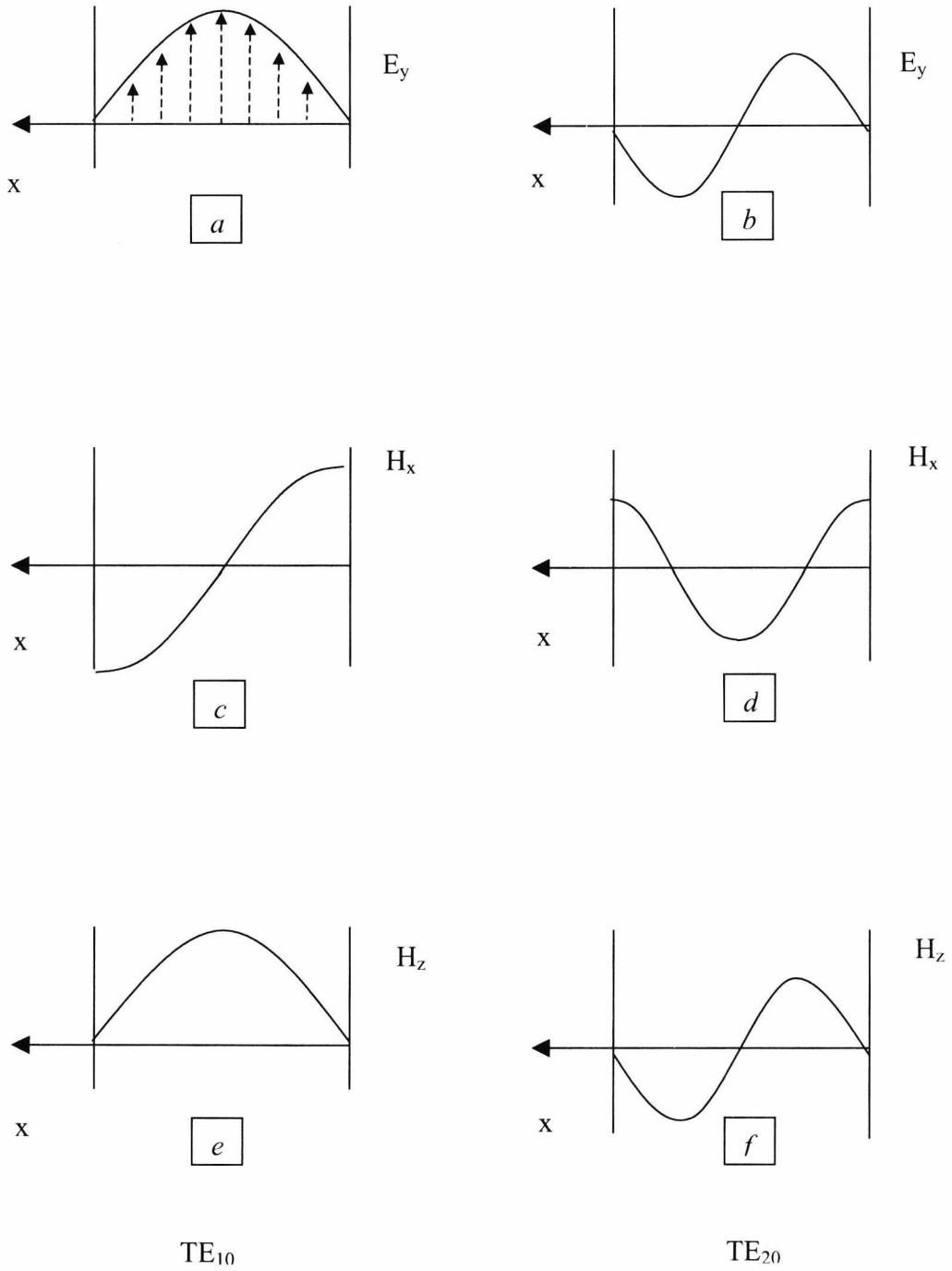

Figure 2.2. Field profiles for the modes TE_{10} and TE_{20} of the rectangular waveguide

2.2 Principle of operation of the folded guide

The folded waveguide, as the name suggests, is a dielectric-filled rectangular waveguide whose sides have been folded to achieve width reduction while preserving the original modes. There are two types of folded waveguides, depending on the orientation of the geometrical disfigurement, figure 2.3. The first type is folded in the vertical direction while the second folds the waveguide in the horizontal. Both types are two-layer structures, with each layer having a height *b*.

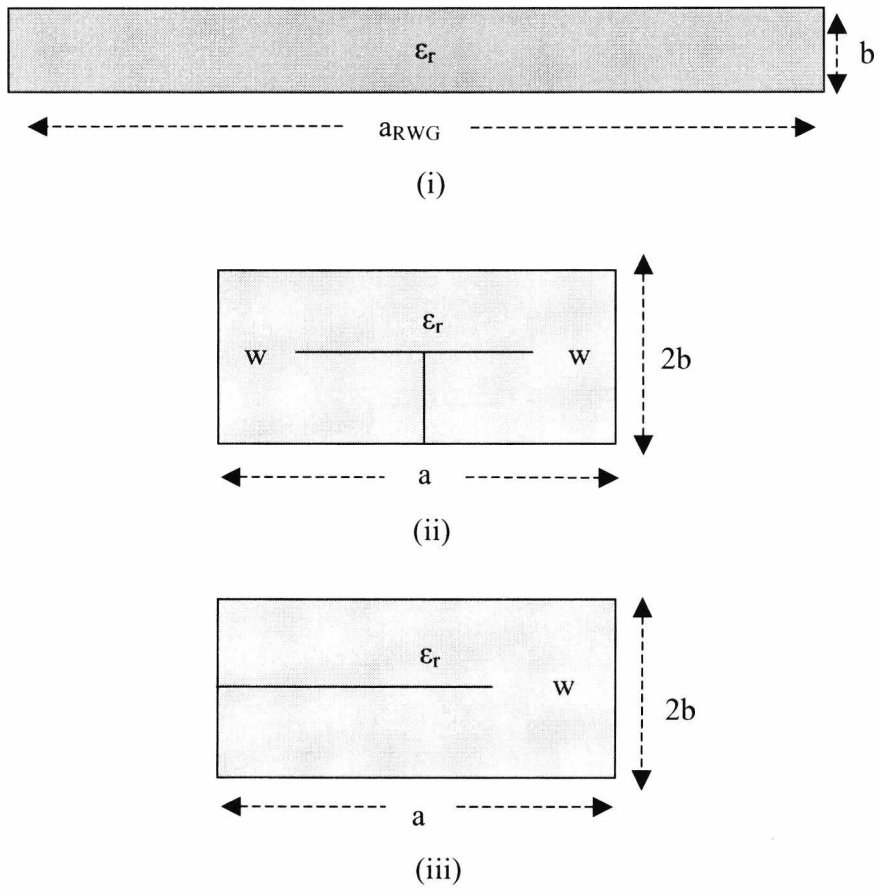

Figure 2.3. Cross-sectional view of (i) Rectangular waveguide, (ii) Folded type 1, (iii) Folded type 2

Figures 2.4 and 2.5 show electric vector plots for the fundamental and second order modes for both types of folded guide and figure 2.6 shows vector plots for rectangular waveguide.

The dominant mode of a rectangular waveguide (TE_{10}) varies sinusoidally in the transverse direction and has a maximum at the centre and nulls at the two side walls. The fundamental mode in the folded waveguide type 1 maintains the maximum in the middle but allows the electric field to shift 180 degrees at both sides before it finally goes to zero on the lower central part of the guide. For the second type of folded waveguide, the Electric field is at maximum over the right edge of the guide, rather than in the centre, and reduces to zero at the top and bottom left walls. So, for both types of folded guides, the fundamental modes can be thought of as folded versions of the TE_{10} mode inside the RWG. The second order mode TE_{20} varies sinusoidally with two maxima. The corresponding mode in the type1 peaks at the two edges and gets to zero at the top half of the waveguide. The second order mode of the folded guide type 2 is the TE_{10} mode of a half width RWG. This mode is cutoff from the folded guide type 1 because the vertical wall in the centre shorts the electric filed which is at maximum.

Overall, although the two folded waveguides have different geometries compared to the rectangular waveguide, they still preserve the same modes. For that reason folded guides are valid alternatives to the rectangular waveguide. This statement is fully justified in the following paragraphs, where we examine bandwidth properties and dispersion curves for the folded guides.

Equivalent to the TE_{10} mode of a rectangular waveguide

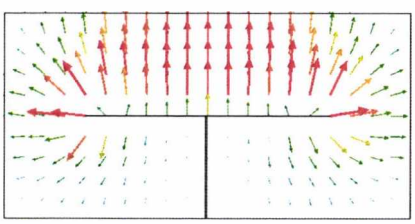

Fundamental Mode of folded guide type1

Equivalent to the TE_{20} mode of a rectangular waveguide

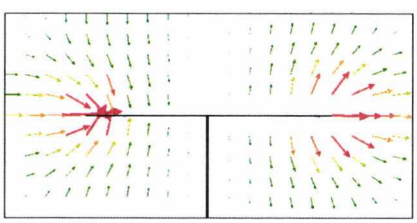

Second order Mode of folded guide type1

Figure 2.4. Simulated vector plots for the 1st and 2nd order modes for the folded guide type 1. Red vectors denote high field intensity

Equivalent to the TE_{10} mode of a rectangular waveguide

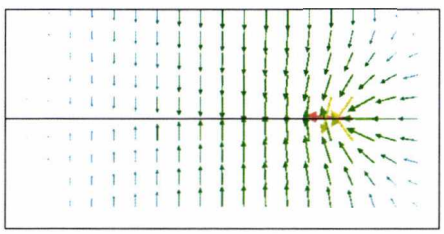

Fundamental Mode of folded guide type2

Equivalent to the TE_{10} mode of a half width rectangular waveguide

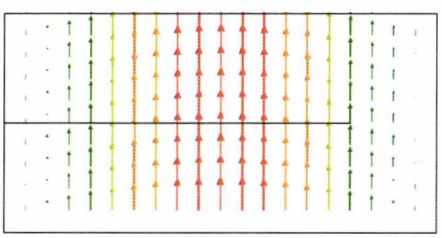

Second order Mode of folded guide type2

Figure 2.5. Simulated vector plots for the 1st and 2nd order modes for the folded guide type 2. Red vectors denote high filed intensity

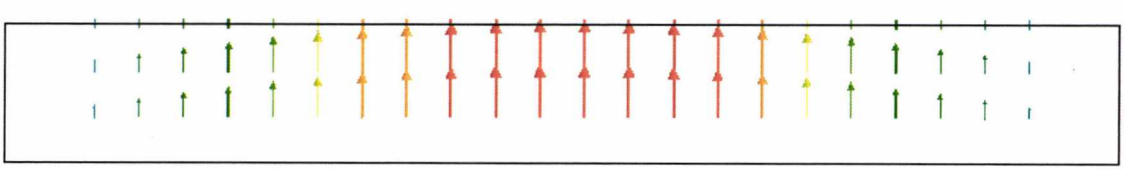

(a)

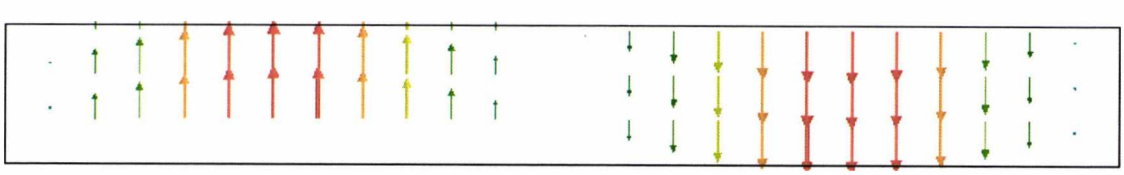

(b)

Figure 2.6. Simulated E vector plots for rectangular waveguide a) TE_{10} mode b) TE_{20} mode. Red vectors denote high filed intensity.

2.2.1 Design methodology

Our proposed folded waveguides are double-layered structures comprised of two narrow sheets of dielectric material attached together. Although, the height of these layers does not significantly affect the phase constant of the guide, the attenuation constant tends to increase with reducing the layer thickness. Hence, if very small height is required, only the highest quality dielectric sheets should be used, with minimum loss tangent.

Due to the small overall height, modes whose electric field varies along the vertical axis do not propagate in the frequency range of interest. Overall, the folded waveguide analysis is based around the theory of propagation of rectangular waveguides. From section 2.1, the longitudinal propagation constant of the TE_{m0} mode of a rectangular waveguide is given by the formula (assume perfect conducting walls, $\gamma=j\beta$, $\sigma=0$):

$$\beta = \sqrt{\varepsilon_r k_0^2 - \left(\frac{m\pi}{a_{RWG}}\right)^2} \qquad (2.63)$$

where ε_r is the relative electric permittivity of the guide, a_{RWG} and b are the width and height of the guide respectively, k_0 is the free space wavenumber ($k_0=\omega/c$), and m is the mode order, or the number of field variations across the width of the RGW. When dealing with the fundamental mode of the guide, $m=1$. This formula shows that the propagation constant β is dependent only on the operating frequency (i.e. the k_0 term) and the values of ε_r and a.

At first, the cutoff frequency of a folded guide can be thought of as being equal to that of a rectangular waveguide having twice the width. However, apart from the width a and the electric permittivity, the propagation characteristics of folded guides depend on the value of gap w. Fortunately, due to the closed nature of the folded guides, we find that their dispersion characteristics are identical to those of RWG as long as we select the appropriate values of a, b, w for our folded waveguide. Figure 2.7 demonstrates such a case. The parameters of the folded guide have been carefully chosen such that the dispersion curves of the two waveguides are coincidental.

Nevertheless, the influence of the gap width w is more than just a tuning variable. In order to form a theory that describes the association of w to the other parameters of a folded guide, and its propagation characteristics, we introduce an effective width a_{eff}. The parameter a_{eff} is the width of a rectangular waveguide that has exactly the same

dispersion curve as a folded waveguide of width a. Equation (2.63), for the folded waveguide, becomes:

$$\beta = \sqrt{\varepsilon_r k_0^2 - \left(\frac{m\pi}{a_{\text{eff}}}\right)^2} \tag{2.64}$$

The expression for cutoff frequency is also similar to that of rectangular waveguides. Hence:

$$f_c = \frac{c}{2a_{\text{eff}}\sqrt{\varepsilon_r}} \tag{2.65}$$

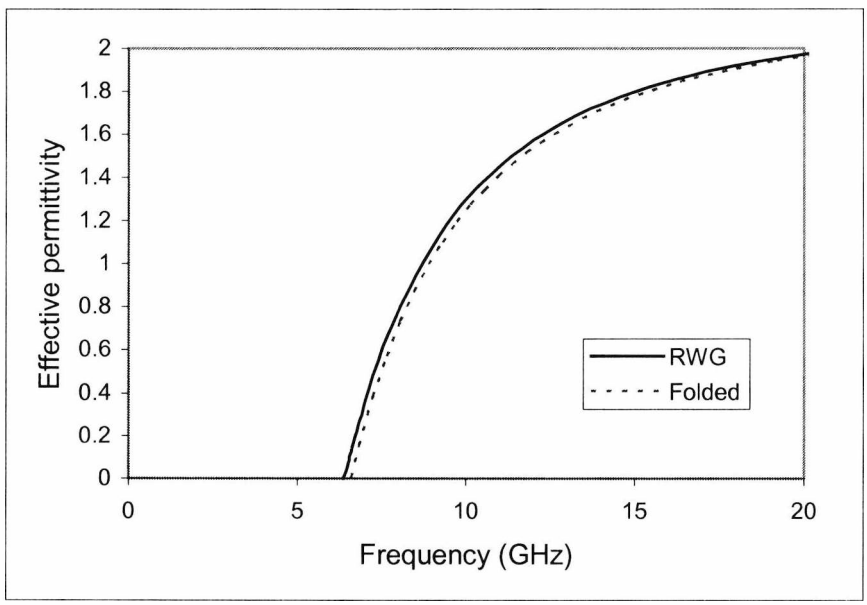

Figure 2.7. The parameters w, a, b of the folded guide have been selected such that its dispersion curve is identical to that of the RWG. In this particular case the width of the RWG is referred to as a_{eff}.

For the analysis of folded guides we have developed an efficient method which comprehends the useful results of a high frequency simulation package and applies error correction to extract accurate values for the propagation constants. More specifically, the method examines the dependence of a, b, w on the cutoff frequency of the waveguide.

By squaring equation (2.64) we get:

$$\beta^2 = \varepsilon_r k_0^2 - \left(\frac{m\pi}{a_{\text{eff}}}\right)^2 \tag{2.66}$$

which in turn can be written as:

$$\beta^2 = Af^2 - C \tag{2.67}$$

where

$$A = \varepsilon_r \left(\frac{2\pi}{c}\right)^2 \tag{2.68}$$

and

$$C = \left(\frac{m\pi}{a_{eff}}\right)^2 \tag{2.69}$$

where c is the speed of light. Equation (2.67) is quadratic of the form $y = ax^2 + b$, where, instead of y we have the squared propagation constant β^2 and instead of the constants a and b we have A and C respectively. The value of β^2 for the folded guide can be calculated using a high frequency electromagnetic simulator and the value of constant

A is also known. Ultimately, the unknown parameter is the effective width of the guide a_{eff} and therefore the constant C. It is essential to note that for every folded waveguide there is a value of a_{eff} that fully characterises its dispersion curve. In addition, obtaining the value of a_{eff} reveals the cutoff frequency of the guide since the two parameters are directly related through equation (2.65).

Nevertheless in order to generate plots for the folded guide we cannot depend entirely on simulation, as, near the cutoff frequency, the wavelength of the structure becomes infinite and cannot be calculated with efficient precision. Consequently, in every frequency sweep, there will be a *true* value of propagation constant and a *simulated* value and by subtracting those two we obtain the error. As such:

$$y - \beta^2 = e \tag{2.70}$$

where y is the parameter containing the true value of propagation constant, β^2 is the squared simulated propagation constant and e is the error. The *least squares* technique aims to find the minimum error by adding the square of error over the entire frequency range. If N is the number of points in a frequency sweep, equation (2.70) becomes:

$$\sum_{i=1}^{N}\left[y_i - \beta_i^2\right]^2 = e^2 \tag{2.71}$$

and remembering that $y = Af^2 - C$ gives

$$\sum_{i=1}^{N}\left[Af_i^2 - C - \beta_i^2\right]^2 = e^2 \tag{2.72}$$

To obtain the value of C that gives the minimum error, we differentiate with respect to C and then set the result equal to zero. Hence

$$\frac{\partial}{\partial C}\sum_{i=1}^{N}\left[Af_i^2 - C - \beta_i^2\right]^2 = 0 \tag{2.73}$$

which solving for C gives

$$C = \frac{1}{N}\left[\sum_{i=1}^{N} Af_i - \sum_{i=1}^{N} \beta_i^2\right] \tag{2.74}$$

where A is known and β is calculated from simulation. Equation (2.74) is of great importance to the analysis of folded guides since it allows the calculation of C and surpasses the error caused by simulation around the cutoff frequency. This principle is illustrated in figure 2.8 where we plot the simulated value of propagation constant, together with the corrected value trough the *least squares* technique. For most of the 41-point frequency sweep, both lines are coincidental with almost no visible error. However, around the cutoff region the corrected line is much closer to the true value of frequency cutoff, figure 2.9. The folded guide under test was designed with f_c=138 GHz.

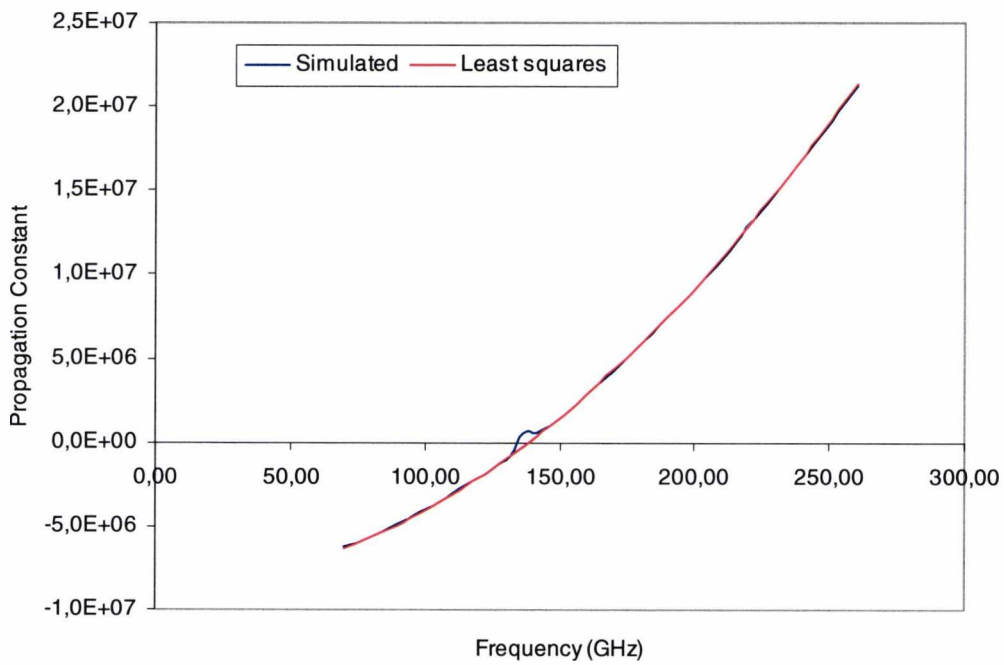

Figure 2.8. Typical example: comparison of simulated values and corrected values through least squares technique for folded guide with f_c= 138 GHz. Prop. Cost. in rad/m.

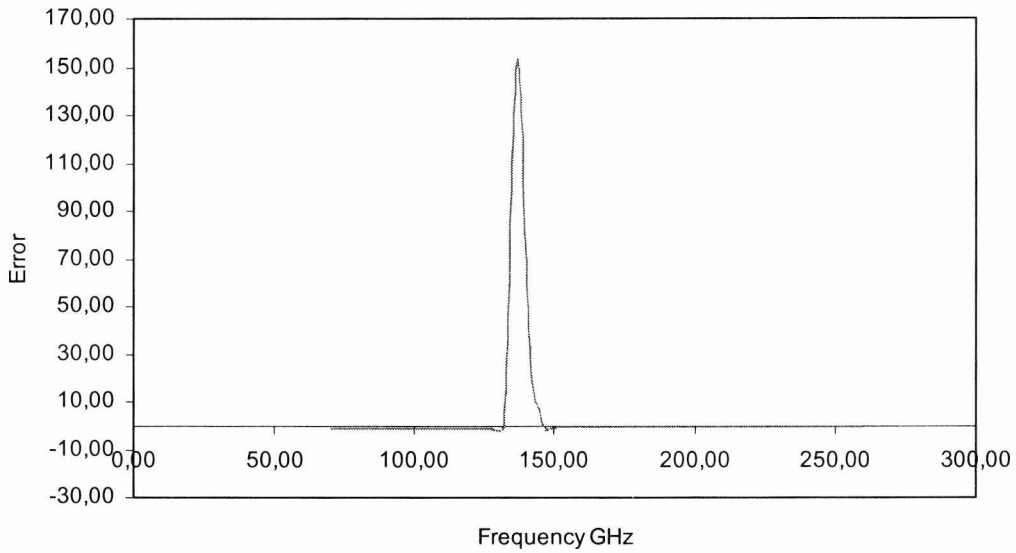

Figure 2.9. Plot of error caused by simulation. The error is max on the cutoff frequency of the folded guide since the operating wavelength becomes infinite.

By repeatedly simulating the folded waveguide, and applying the least squares technique, we can generate graphs of normalised effective width a_{eff}/a against normalised gap width w/a for a range of different b/a values. Then, using Mathcad, we implement a linear multivariate least squares fit to these graphs and generate general expression for the value of a_{eff}. Figures 2.10 and 2.11 show plots of normalised effective width a_{eff}/a for guides type1 and type2 respectively. We notice that both types have very similar characteristics. In both cases a_{eff}/a decreases with w/a. This phenomenon occurs because increasing w/a will result in an increase in cutoff frequency. Hence the rectangular waveguide that matches this new cutoff needs to be thinner.

By observing the graphs we also see that a_{eff} varies almost linearly with w/a as long as $w/a<2b/a$. We have fitted a linear function to both graphs to provide design equations. For type 1 it is:

$$a_{\text{eff}} = a\left(1.976+1.030\frac{b}{a}-2.008\frac{w}{a}\right) \tag{2.75}$$

and for type2

$$a_{eff} = a\left(1.977 + 1.103\frac{b}{a} - 2.028\frac{w}{a}\right) \tag{2.76}$$

The accuracy of both expressions is to within 3% over the range

$$0.05 \le \frac{b}{a} \le 0.45 \quad \text{and} \quad \frac{w}{a} \ge 2\frac{b}{a}$$

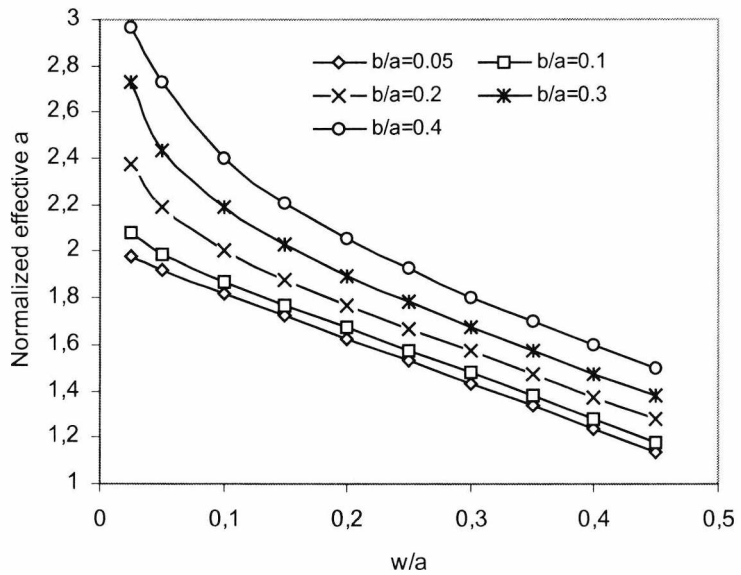

Figure 2.10. Normalized effective width (a_{eff}/a) for type 1 folded waveguide.

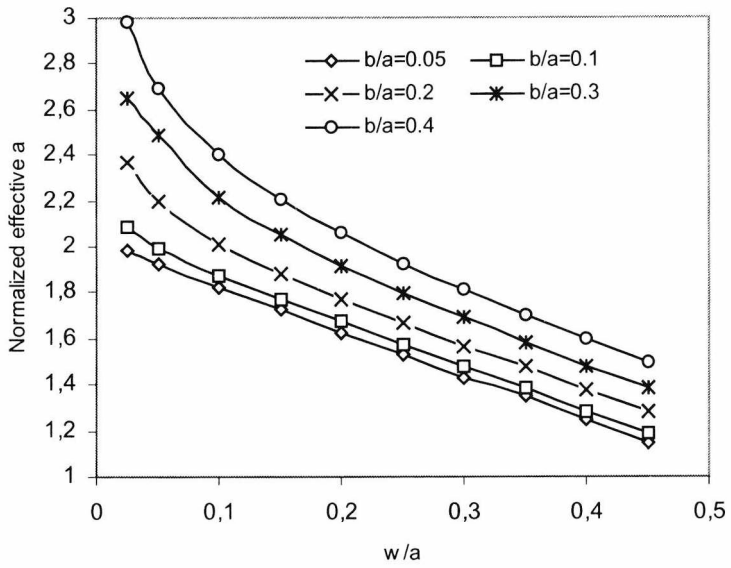

Figure 2.11. Normalized effective width (a_{eff}/a) for type 2 folded waveguide

2.3 Bandwidth and size of folded waveguides

We have seen how folded waveguides have reduced width compared to rectangular waveguides while preserving the same modes and propagation characteristics. However the most important advantage of a folded guide over rectangular guides is the bandwidth. The bandwidth of folded guides type 1 and type 2 are shown in figures 2.12 and 2.13 respectively. We notice, from figure 1, that the relative bandwidth of folded guides reaches a maximum of 3. This value is 50% higher than the bandwidth of a rectangular waveguide. This result is not new since type 1 folded guide is similar to the T-septum waveguide [12-14]. However in the T-septum case the emphasis is to increase the bandwidth whereas in our case the emphasis is on size reduction. The graph of bandwidth is also different for the two types of folded guide. For type 1, the bandwidth initially increases, reaches a maximum and then declines again. For the second type the bandwidth decreases monotonically with w/a.

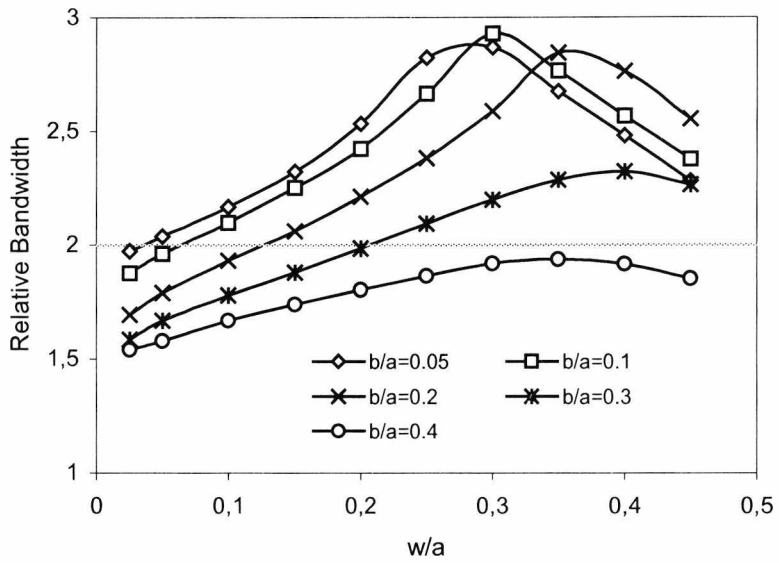

Figure 2.12. Relative bandwidth (f_{c2}/f_{c1}) of type 1 folded guide. f_{c1} is the cutoff frequency of the fundamental mode and f_{c2} the cutoff frequency of the next higher order mode.

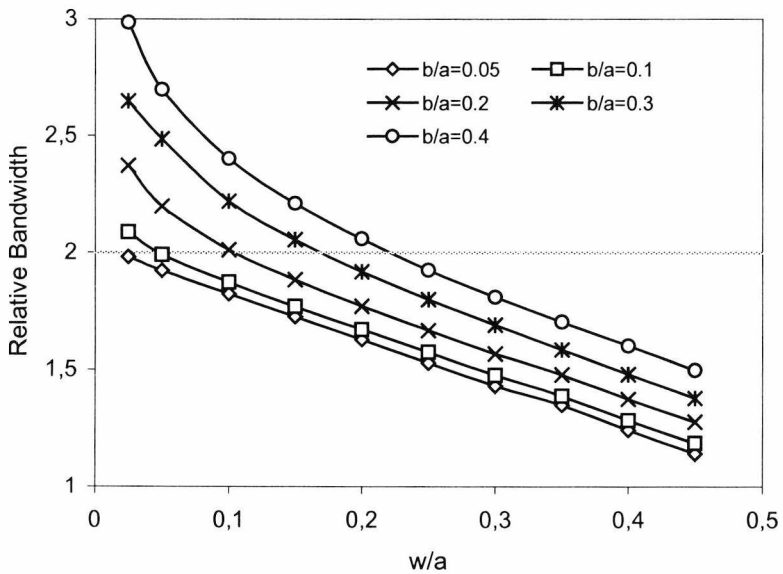

Fig. 2.13. Relative bandwidth (f_{c2}/f_c) of type 2 folded guide. f_{c1} is the cutoff frequency of the fundamental mode and f_{c2} the cutoff frequency of the next higher order mode.

The difference in bandwidths has to do with the geometry of the guides. Type 1 guide cuts off the TE_{10} RWG mode due to the extra wall in the centre whereas the type 2 guide does not. As a result the cut-off of the second order mode in type 1 is dependent on *w/a* and *b/a*. In contrast, the second mode in the type 2 folded guide is similar to the TE_{10} of the RWG and has a cut-off that is independent of *b/a* and *w/a*.

Increased Bandwidth and reduced width are the two major advantages of using a folded waveguide over its conventional rectangular counterpart. As a first approximation, a folded guide has half the width of its equivalent rectangular waveguide. However, when the maximum relative bandwidth of 3 is required, the folded guide gets a bit wider, although it never gets as wide as the rectangular waveguide. The graph that follows describes the relationship between maximum achievable bandwidth and width for a folded guide type1. The results for type 2 are almost identical.

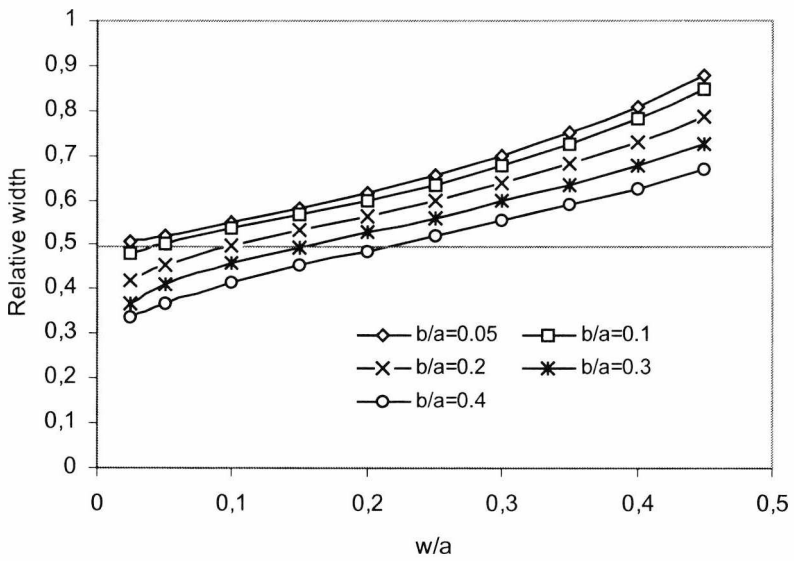

Fig. 2.14. Relative width (a/a_{eff}) of type 1 folded waveguide. Type 2 results are almost identical.

There have been attempts of folded guide type 2 in previous papers [15] but those waveguides are big and bulky whereas our design is very light and compact.

Summarizing the results of the above figures, for type one, the maximum bandwidth is achieved at b/a=0.1 and w/a=0.3 and is equal to three. At these dimensions, the size reduction is only 0.7. If greater size reduction is required, then we choose b/a=2w/a. Is this case, the width of the folded guide is half that of the rectangular waveguide but at the expense of bandwidth. The new bandwidth is 2.

For type 2 folded waveguide, for size reduction of 0.5 and bandwidths of approximately f_{c2}/f_c=2, we find that b/a=2w/a. However, type 2 folded waveguides with relative bandwidth of 3 are difficult to manufacture due to the small b/a dimensions and the extremely narrow gap w required. On the other hand, b/a ratios in the 0.05-0.2 range are easily fabricated using the various fabrication techniques. At those specifications, the bandwidth of the folded guide is 2 and its width is approximately half that of a rectangular waveguide.

2.4 Multilayer folded waveguides

So far, we have seen how a folded waveguide is a two-layer representation of a rectangular waveguide. We examined the bandwidth properties of folded guides and found them to be greater compared to RWGs of twice the width. This paragraph takes the design of folded guides to the next logical step and introduces the multilayer stack. In the pages that follow we study the properties of folded guides with more than two layers and show that increasing the number of layers results in narrower designs with even wider bandwidth compared to the known two layer case.

As before we examine type 1 and type 2 folded stacks of three and four layers separately.

2.4.1 The multilayer stack

Figure 2.15 shows three and four layer examples for the two types of folded waveguide. For an n layer structure, the total width reduction compared to the width of a rectangular guide, of the same cutoff frequency, is 1/n. Inevitably, there will be a proportional

increase in waveguide height, due to the additional dielectric sheets required to form the multilayer design, but because the thickness of these sheets is less than 1mm the ratio *b/a* is small and hence that height increase is not significant.

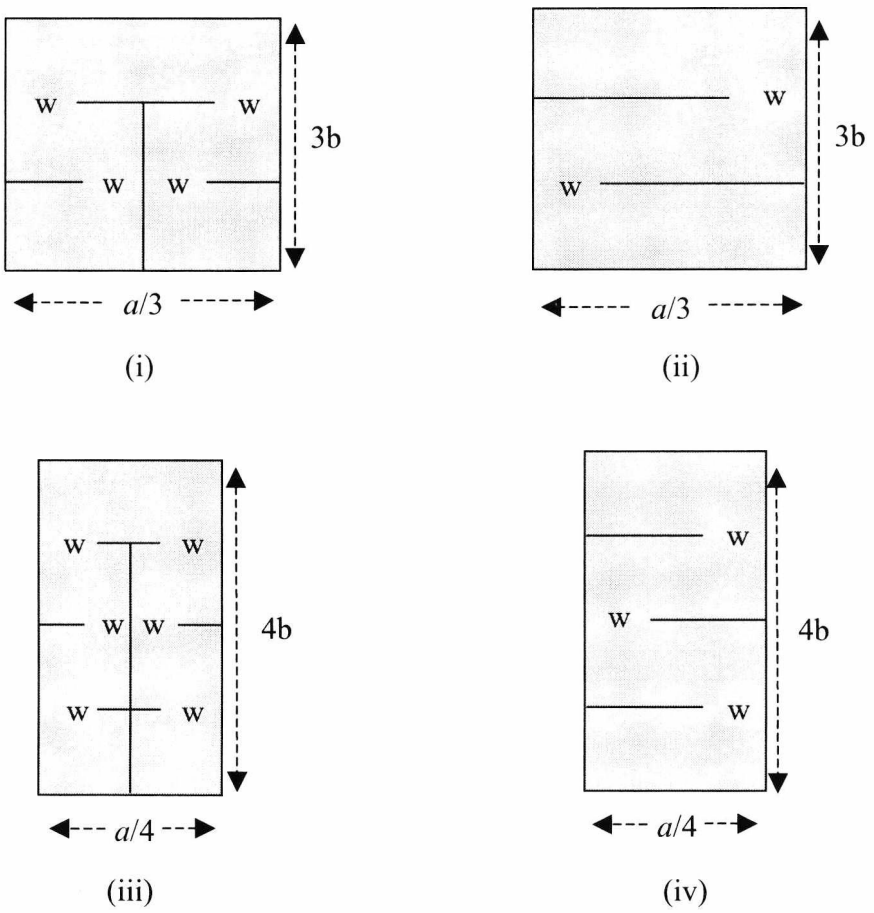

Figure 2.15. i) three layer type1 ii) three layer type2 iii) four layer type 1 iv) four layer type2

In the pages that follow we present characteristic graphs for the three and four layer folded guides. Same as before, we use the least squares technique to generate plots of relative bandwith, normalised a_{eff} and relative width for all types of guide.

Three layers folded guide type 1

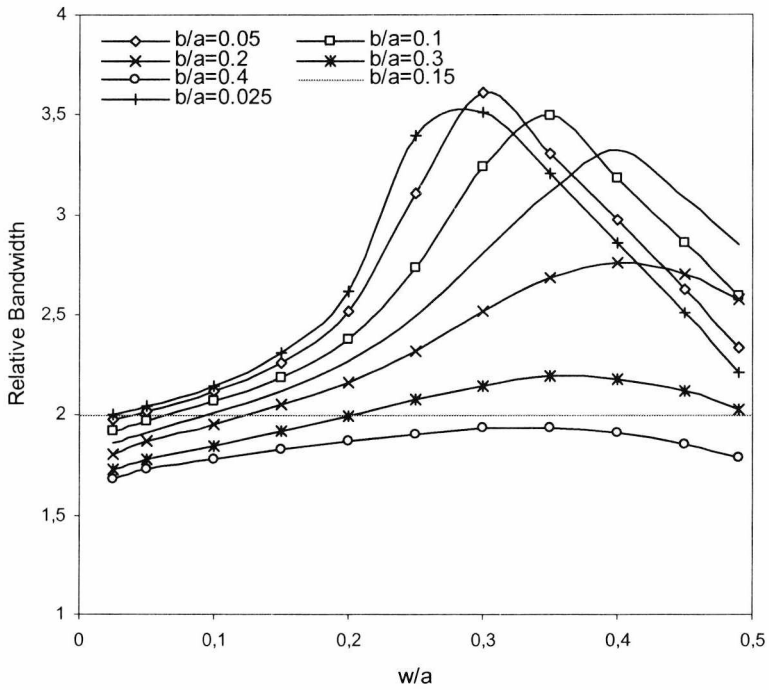

Figure 2.16. Relative bandwidth (f_{c2}/f_{c1}) vs w/a

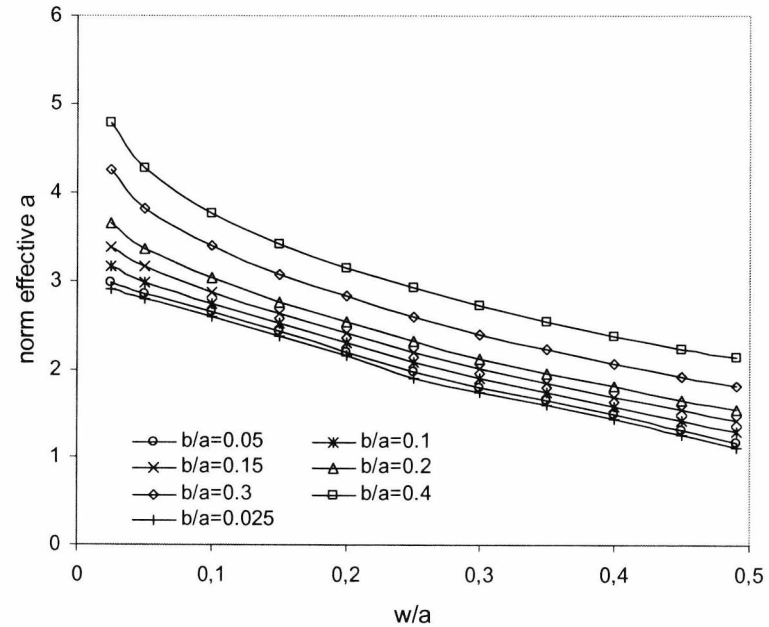

Figure 2.17. Normalized effective a (a_{eff}/a) vs w/a

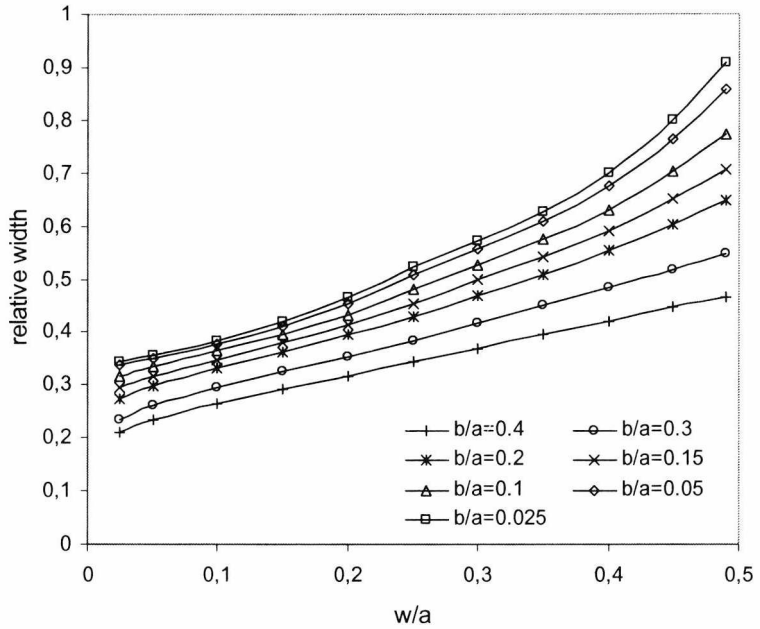

Figure 2.18. Relative width (a/a_{eff}) vs w/a

Three Layers folded guide type 2

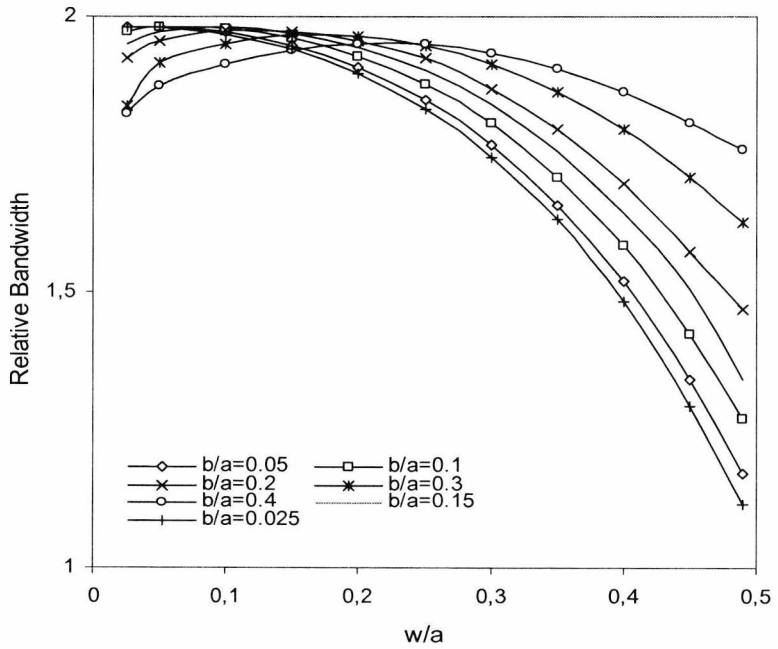

Figure 2.19 Relative bandwidth (f_{c2}/f_{c1}) versus w/a

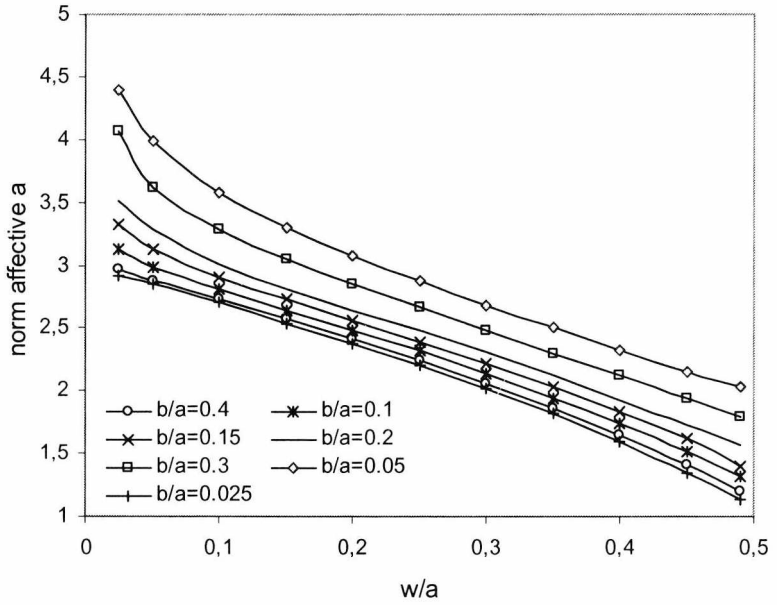

Figure 2.20 Normalized effective a (a_{eff}/a) vs w/a

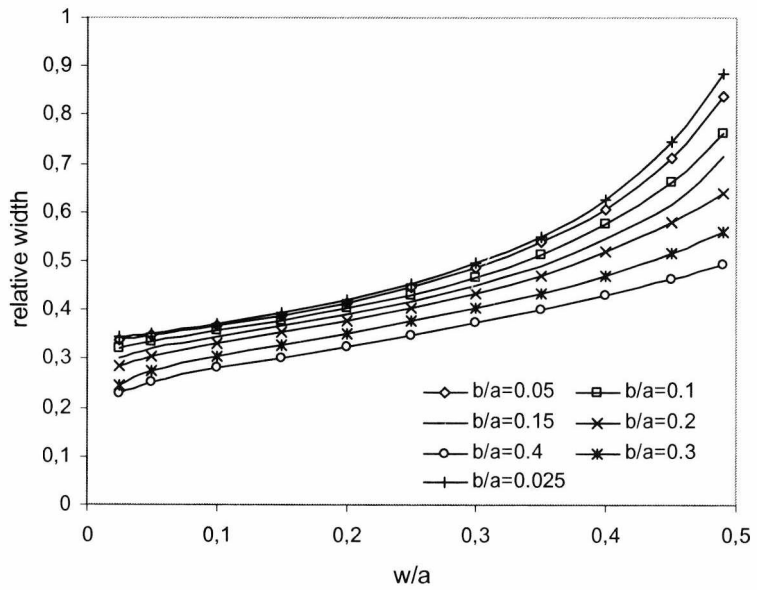

Figure 2.21. Relative width (a/a_{eff}) versus w/a

Four layers Folded guide type 1

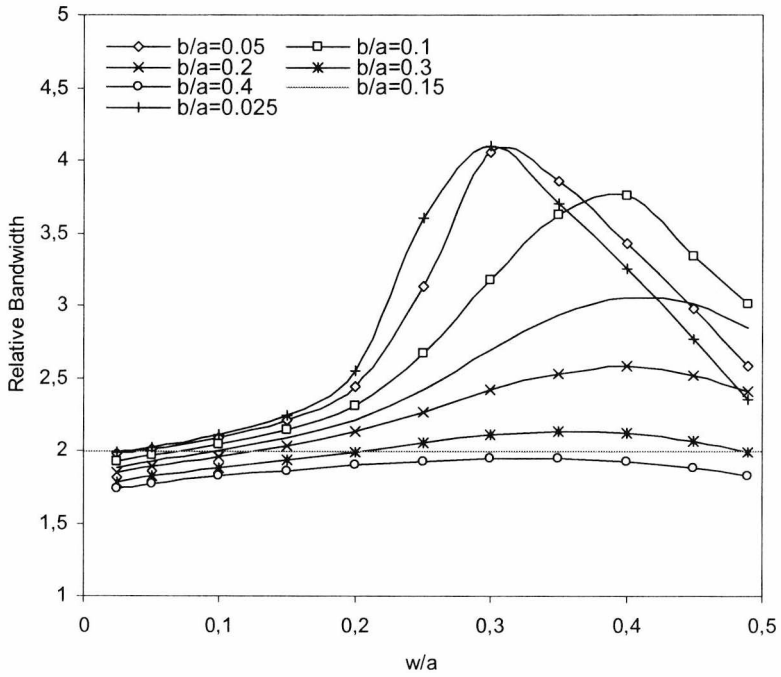

Figure 2.22. Relative bandwidth (f_{c2}/f_{c1}) versus *w/a*

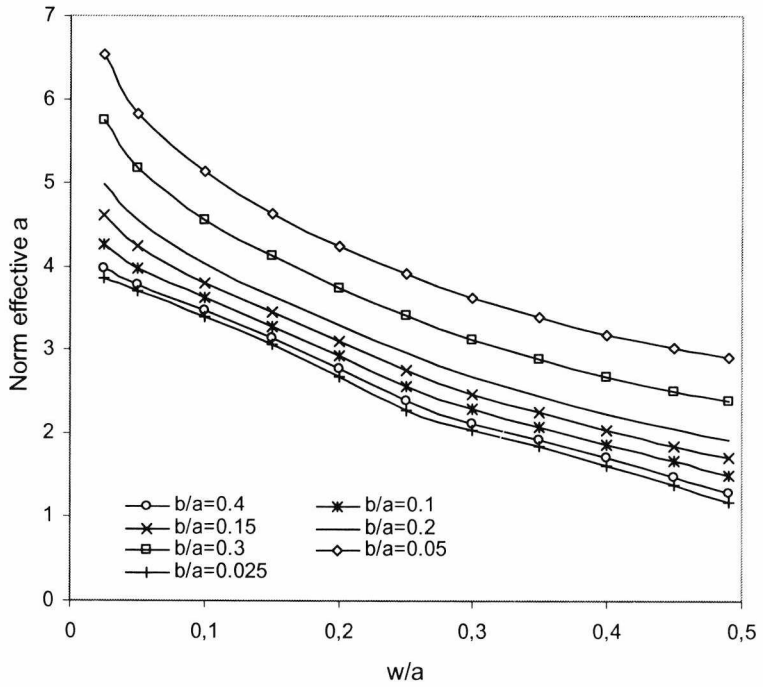

Figure 2.23 Normalised effective *a* (a_{eff}/a) vs *w/a*

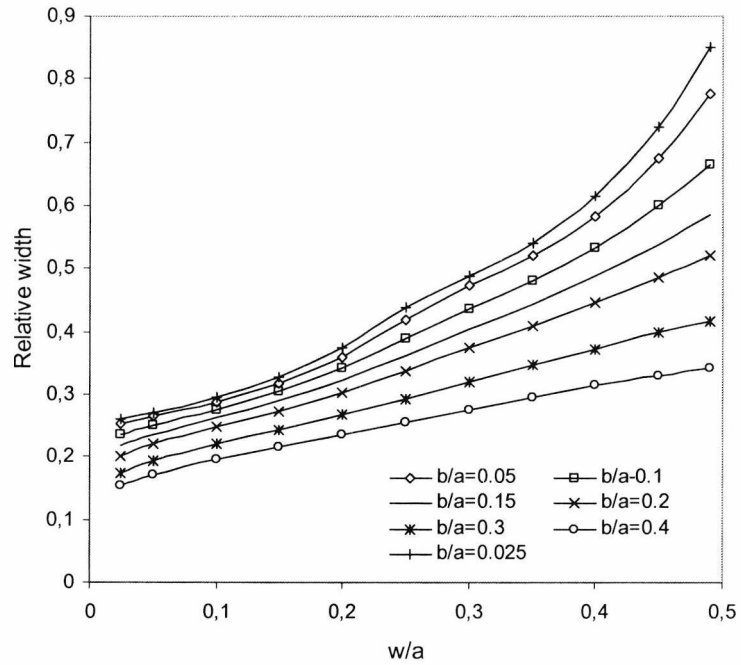

Figure 2.24. Relative width (a/a_{eff}) versus w/a

Four layers Folded guide type 2

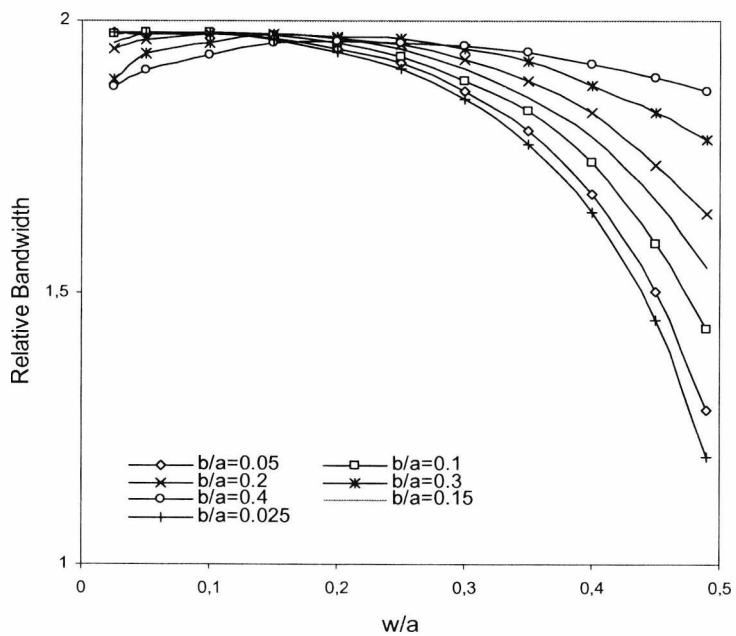

Figure 2.25. Relative bandwidth (f_{c2}/f_{c1}) vs w/a

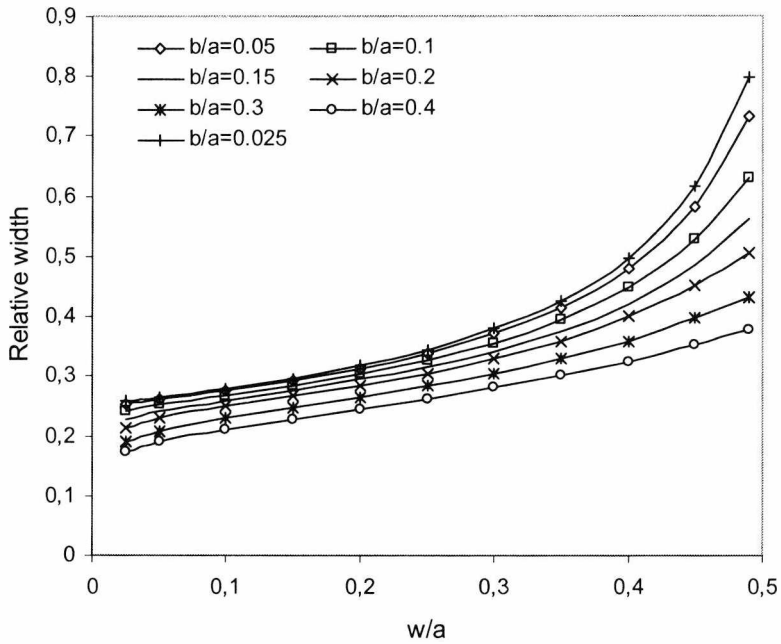

Figure 2.26. Relative width (a/a_{eff}) vs w/a

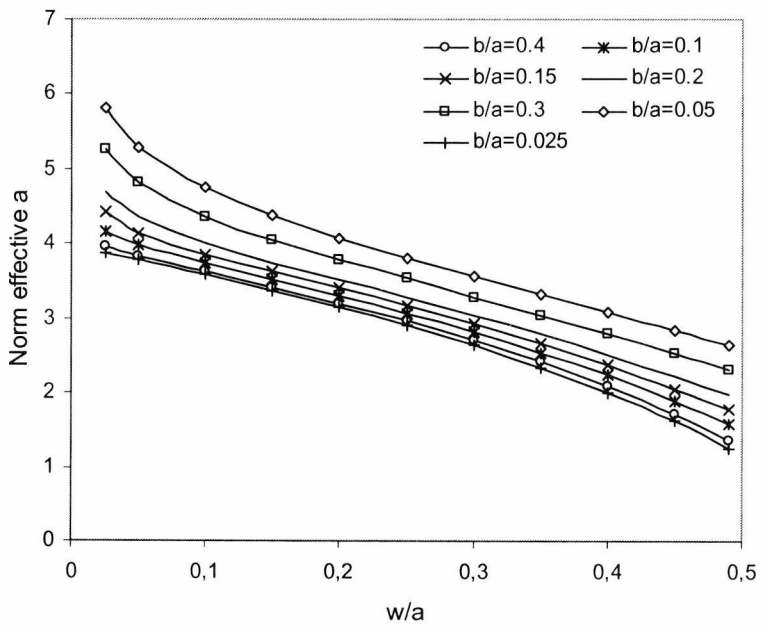

Figure 2.27. Normalised effective a (a_{eff}/a) vs w/a

Figures 2.16 and 2.22 show the relative bandwidth for the three and four layer type 1 guides respectively. We notice that both of these graphs have the same pattern as the two layer case i.e. initially the bandwidth increases until it reaches a maximum and then starts to decrease. The maximum value of bandwidth for two, three and four layer guides takes place at w/a=0.1 but it is different for each case. As the number of layers in the folded guide is increased, so does the bandwidth. From figure 2.22, the maximum relative bandwidth of the four layer guide is 4. This value is double compared to the bandwidth of a standard rectangular waveguide.

The situation is very different for type 2 folded guide. Increasing the number of layers has no apparent effect on the maximum bandwidth of the structure. Also the pattern of bandwidth for type 2 is different for the three and four layers, than what it is for the two layer case. The explanation for this phenomenon is that in the three and four layer guides, the upper limit of bandwidth, mode TE_{10} appears only for $w/a > 0.6$. Whereas for the two layer guide the TE_{10} mode is always present. Figures 2.25 and 2.21 show the relative bandwidth of the three and four layer type 2 guide.

Independent of bandwidth, both types of guide, type 1 and type 2, offer reduced width. Compared to the width of a rectangular waveguide, the three and four layer guides are 3 and 4 times narrower respectively. In the special case where max bandwidth is required, type 1 folded guides get a bit wider than RWG, similar to the analysis for the two layers.

2.4.2 Losses

Losses in microwave integrated guides are undoubtedly an important issue. As a first approximation, both the folded waveguide and the RWG are closed metallic waveguides and have no radiation problems. Therefore the main cause of energy loss is associated to the finite conductivity of the waveguide walls and furthermore, if the guides are not hollow, to the loss tangent of the dielectric material. Since the geometry of the RWG is different to that of a folded guide, a comparison of losses in the two waveguides cannot be valid unless both guides have the same cross sectional area and hence the same, or almost the same, metal wall area.

Figure 2.28 shows the field profile of multilayer folded guides and the first comparison of losses is illustrated in figure 2.29 where we plot attenuation constant versus frequency for four waveguides: one, two and three layer folded guides type 1 and the rectangular guide. All four designs have the same cross sectional area and the same cutoff frequency. We notice from the graph that the rectangular waveguide has the lowest attenuation compared to the folded structures. The explanation for this phenomenon is that as we increase the number of layers, each electric field component has to shift its direction more times. The difference in attenuation is not significant as long as the there are less than three layers.

Overall, graph 2.29 explains that a two layer folded guide has 10% higher attenuation constant compared to the rectangular case and the three and four layer guides have 20% and 30% more attenuation respectively. These percentages are preserved for type 2 folded guides as well.

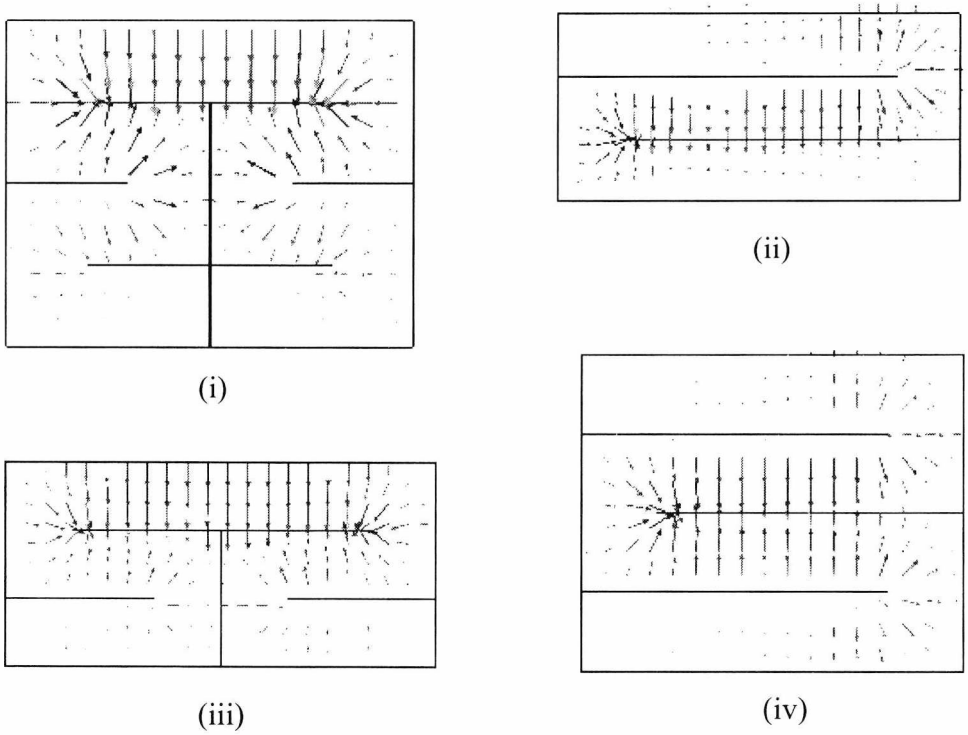

Figure 2.28. Electric vector plots for i) Four layer Type1, ii) Three layer type 2, iii) Three layer type 2, iv) Four layer type 2. Increasing the number of layers in a folded guide causes the E field to shift its direction more times

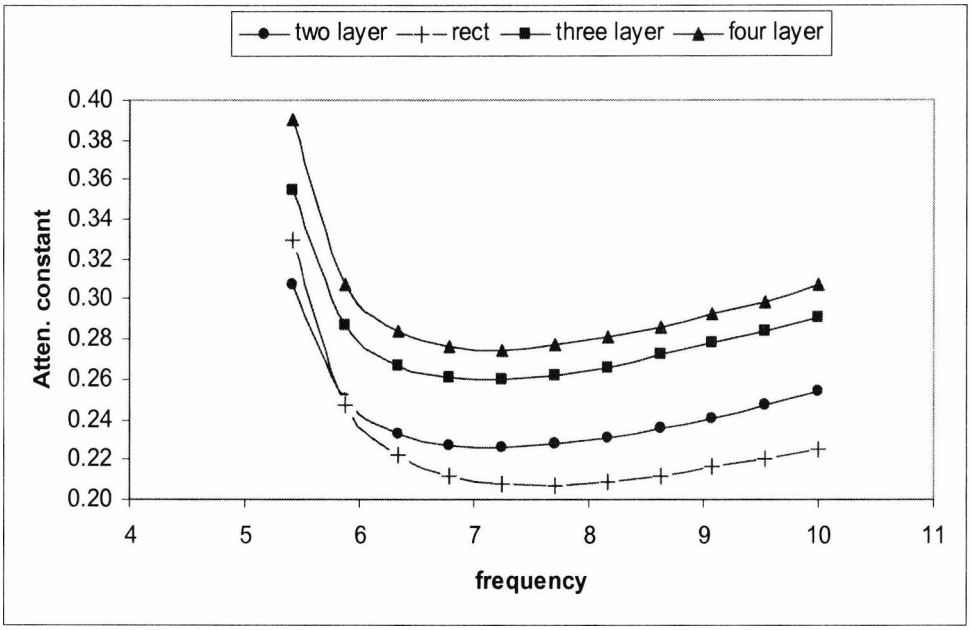

Figure 2.29. Plot of attenuation constant (Np/meter) versus frequency (GHz). Dielectric material used: Rogers^{TM} Duroid (ε_r=2.2, tanδ=0.0009).

In the following pages we analyze the effect of *b/a* and *w/a* on the attenuation constant of folded guides. We start the analysis with the two layer case first. Figures 2.30 and 2.31 describe the variation of b/a for both types of guide. As expected, a small value of *b/a* corresponds to higher attenuation constant since the waveguide becomes narrower. On the other hand, increasing *b/a* reduces the attenuation constant until *b/a*=3. Increasing b/a further does not have any noticeable effect.

Furthermore, comparing figures 2.30 and 2.31 shows that the two types of folded guide have very similar attenuation constants.

The variation of attenuation constant with *w/a* is very small. Hence for every *w/a* value we normalize the frequency axis, so that all curves phenomenally have the same cutoff frequency. Figures 2.32 and 2.33 show the variation of attenuation constant with *w/a*. We notice that *w/a* has little effect on the losses of folded guide. Also type 1 and type 2 plots look very similar.

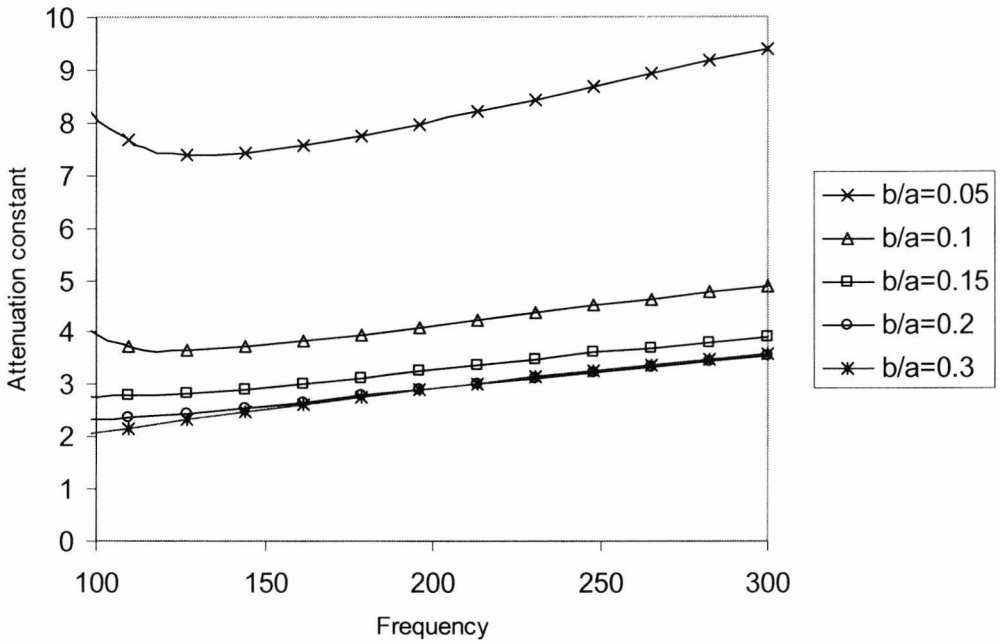

Figure 2.30. Attenuation constant (Np/meter) versus frequency for two layer type 1

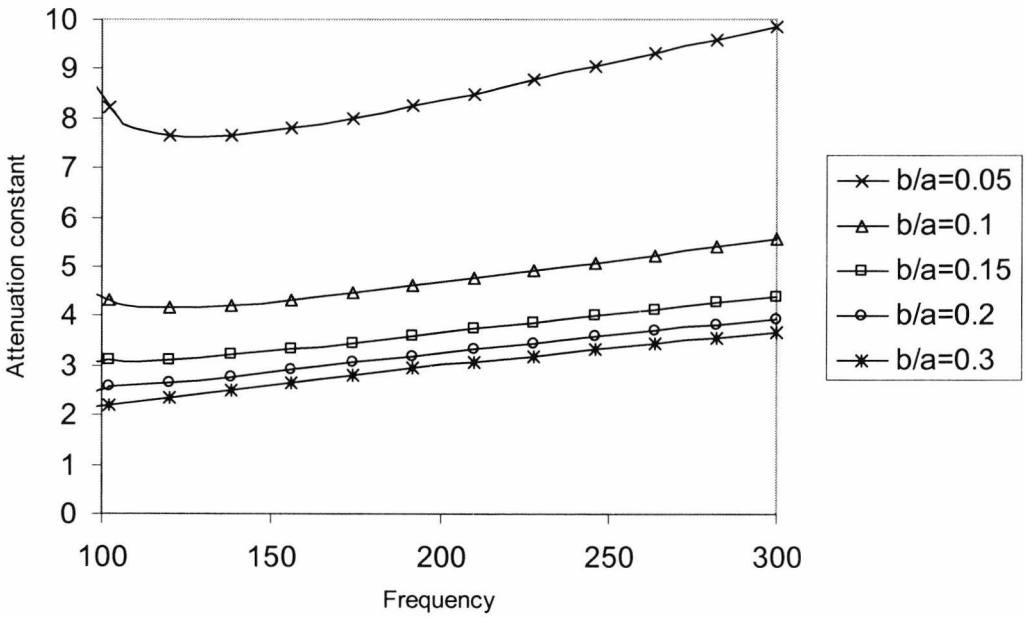

Figure 2.31. Attenuation constant (Np/meter) versus frequency for two layer type 2

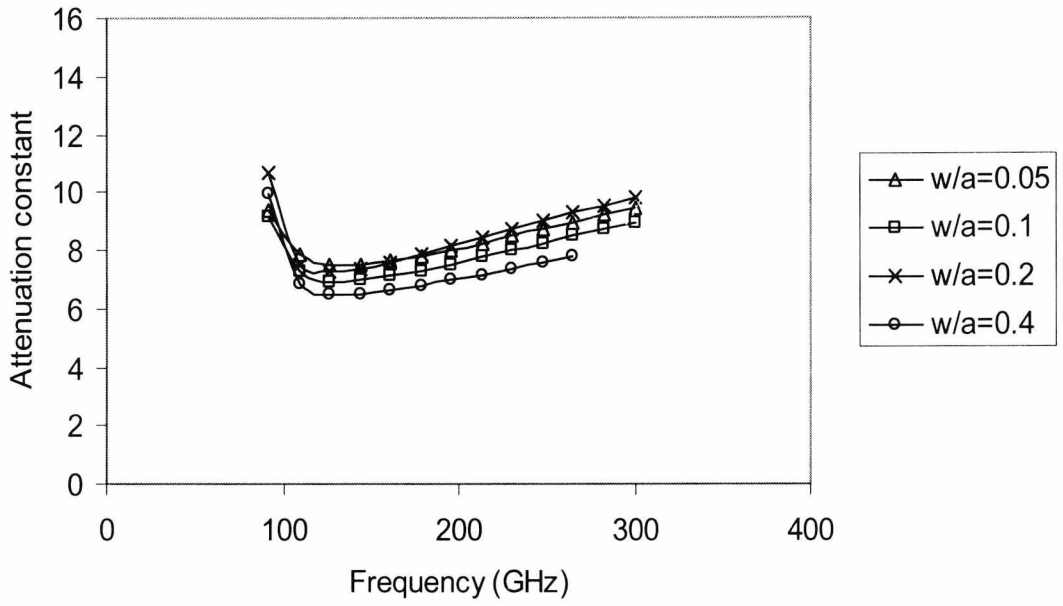

Figure 2.32. T-Type folded guide two layers. Att. constant (Np/meter) versus frequency

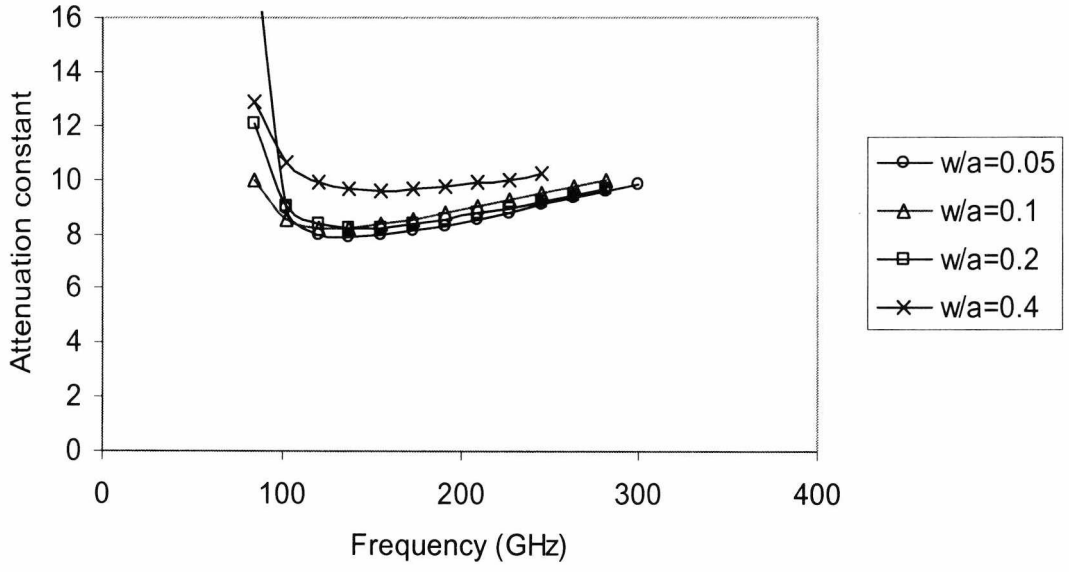

Figure 2.33. Type 2 folded guide two layers. Att. constant (Np/meter) versus frequency

2.4.3. Power handling capabilities of folded waveguide

The power handling capabilities of folded waveguides, similar to the RWG, are limited by voltage breakdown which occurs at a field strength of about E_d=3x10^6 V/m for room temperature at sea level. In general, the maximum power capacity of an air-filled transmission line is given by

$$P_{\max} = \frac{V_{\max}^2}{2Z_0} \tag{2.77}$$

where V_{max} is the peak to peak voltage along the transmission line and Z_0 its characteristic impedance. In the case of an air-filled rectangular waveguide of width a the voltage varies as E_y=E_0sin(πx/a), which has a maximum at x=$a/2$. Thus the maximum power capacity before breakdown can be shown to be

$$P_{\max} = \frac{abE_0^2}{2Z_w} \tag{2.78}$$

where Z_w is the impedance of the RWG and a and b is the width and height respectively. From (2.78) it can be seen that P_{max} reduces with small size. Since the folded waveguides are manufactured on small dimensions it can be presumed that P_{max} will be much smaller compared to the P_{max} of a WR10 rectangular waveguide. Also, it is good engineering to limit the maximum power handling of a waveguide by ½ for safety reasons.

However, since the folded waveguides are substrate integrated the power capacity will be increased compared to the air-filled counterparts. The dielectric strength of most dielectrics is greater than that of air but it maybe limited due to heating of the dielectric. The folded waveguides of this thesis were mostly fabricated using Rogers ™ duroid materials. Power handling capacity is usually associated with temperature rise and maintaining the operating temperature below the rated value for the given material. When the operating temperature is too high over prolonged periods of time, the concern is that the traces will loose adhesion to base dielectric and eventually delaminate. In general, maintaining the continuous operating temperature below 125°C is

recommended which means that the temperature rise should be less than 100°C (assuming 25°C ambient temperature)

A comparison of RO4350B™ high frequency material, PTFE/woven glass (GX), and FR4 illustrates the advantage of selecting a material with higher thermal conductivity when it comes to power handling [16]. Table 2.1 provides material properties

	RO4350B	FR4
Dielectric Constant	3.48	4.2
Loss Tangent	0.004	0.012
Thermal Conductivity	0.62	0.27
UL Rating (94V-0)	Yes	Yes

Table 2.1. Material Properties Needed in Temperature Rise Calculations. Table from Rogers website.

Figure 2.34 illustrates the RF power required to raise the temperature of the microstrip 50W trace by 100°C on the various materials. It can be seen that selecting materials with low loss tangent is important in maximizing the power to be fed through the circuit. This is evident when comparing RO4350B material and PTFE/woven glass to FR4. Also For high frequency materials, the most important factor in increasing power handling capacity is thermal conductivity. Although RO4350B material has a higher loss tangent than PTFE/woven glass, it can still carry more power because of the higher value of this property. And finally for a given power level, selecting a thinner dielectric layer of RO4350B material instead of PTFE/woven glass would reduce material costs.

Although microwave laminates are available at a wide range of specifications the basic idea is the same: higher thermal conductivity is the key factor when trying to minimize high power related failures. In the case of RO4350B material, better heat conduction is achieved because of the lack of PTFE in the material and the use of thermoset resins and ceramic powder [17].

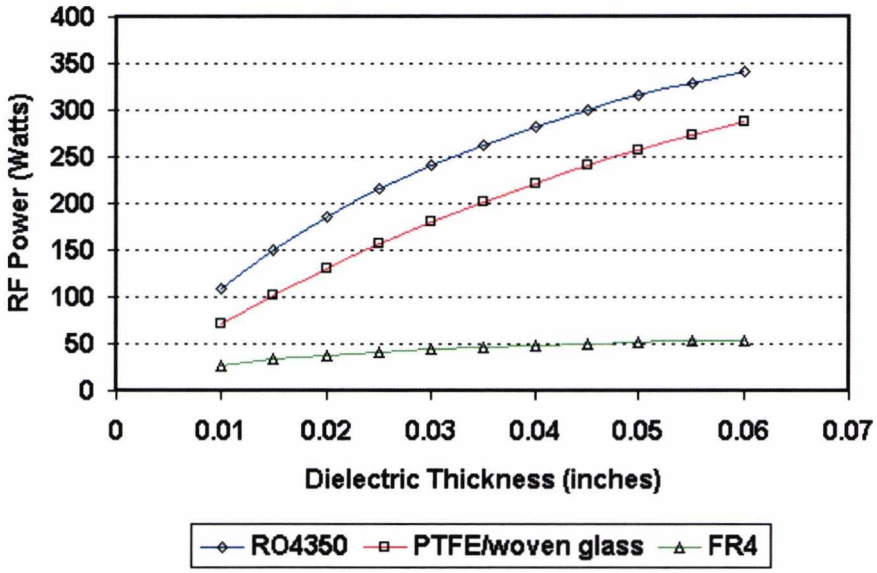

Figure 2.34. RF Power Input for 100°C Temperature Rise on 50W Microstrip Transmission Line @2GHz. Figure from Rogers Website.

2.5 Summary

The hollow rectangular waveguide, although popular in many microwave applications, suffers from usage limitations due to its large size and weight. In this chapter we proposed two alternative structures which preserve the modes of a RWG in a folded geometry. Both guides are substrate integrated and offer reduced dimensions and increased bandwidth compared to conventional rectangular waveguide. The folded waveguides of both types are flexible novel designs suitable for microwave applications where space saving is an important issue.

We presented design equations and graphs for the two types of folded guide and analyzed their bandwidth properties. In the case of folded guide type 2, although the bandwidth is similar to that of a rectangular waveguide the width is narrower by a factor of two. In other words type 2 is a space saving alternative to the rectangular waveguide.

In the case of type 1 the benefits of folded technology are more than just width reduction. We find that the bandwidth of type 1 increases by 50% over rectangular waveguide for the two-layer folded guide and up to 100% for the four layer folded guide. Essentially, type 1 folded guide is a superior alternative to the RWG since is offers much higher bandwidth and reduced width.

Attenuation properties of folded guides, as expected, follow those of rectangular waveguides. i.e. thin guides tend to have the highest attenuation constant. Power handling properties were also discussed.

References

[1] "Analysis of rectangular waveguide filters and polarizers with reduced width E plane stubsTun," S.M.;Computation in Electromagnetics, 1996. *Third International Conference on* (Conf. Publ. No. 420) 10-12 April 1996 Page(s):421 - 424

[2] "Dual mode coupling by square corner cut in resonators and filters," Xiao-Peng Liang; Zaki, K.A.; Atia, A.E.;Microwave Symposium Digest, 1992., *IEEE MTT-S International1*-5 June 1992 Page(s):1327 - 1330 vol.3

[3] "Rectangular waveguide resonators in planar form for filter applications" Helkovnikov, A.; Budimir, D.;*Antennas and Propagation Society Symposium*, 2004. IEEE Volume2, 20-25 June 2004 Page(s):2167 - 2170 Vol.2

[4] "Novel TE10δ rectangular-waveguide-type resonators and their bandpass filter applications." Hee Yong Hwang; Sang-Won Yun; *Microwave Theory and Techniques, IEEE Transactions on* Volume 50, Issue 7, July 2002 Page(s):1821 - 1831

[5] Low-cost dual-mode asymmetric filters in rectangular waveguideGuglielmi, M.; Roquebrun, O.; Jarry, P.; Kerherve, E.; Capurso, M.; Piloni, M.;*Microwave Symposium Digest*, 2001 IEEE MTT-S InternationalVolume 3, 20-25 May 2001 Page(s):1787 - 1790 vol.3

[6] "Rigorous analysis of the rectangular waveguide six-port cross junction Sieverding," T.; Arndt, F.;*Microwave and Guided Wave Letters*, IEEE [see also IEEE Microwave and Wireless Components Letters, Volume 3, Issue 7, July 1993 Page(s):224 – 226

[7] "A simple and rigorous analysis of the transmission properties of a sector horn junction in a rectangular waveguideTsushima," T.; Kuwano, S.; Kokubun, K.; *Microwave Theory and Techniques, IEEE Transactions on* Volume 39, Issue 2, Feb. 1991 Page(s):287 - 293

[8] "Rectangular waveguide diplexers with a circular waveguide common port" Tao Shen; Zaki, K.A.; Dolan, T.G.;*Microwave Theory and Techniques, IEEE Transactions on* Volume 51, Issue 2, Feb. 2003 Page(s):578 – 582

[9] "A ferrite-filled rectangular waveguide slot antenna arrayShan", X.; Shen, Z.;Antennas and Propagation, 2003. (ICAP 2003). *Twelfth International Conference on* (Conf. Publ. No. 491)Volume 2, 31 March-3 April 2003 Page(s):678 - 681 vol.2

[10] "60 GHz band radial line slot array antenna fed by rectangular waveguide," Kim, Y.; Lee, J.; Chae, H.; Park, J.; Kim, S.-C.; Nam, S.;*Electronics Letters* Volume 38, Issue 2, 17 Jan. 2002 Page(s):59 - 60

[11] John D. Krauss "Electromagnetics" fourth edition, McGraw-Hill International Editions, Electrical engineering series, ISBNM 0-07-035621-1

[12] G.G. Mazumder and P.K.Saha, "A novel rectangular waveguide with double T-septums," *IEEE Trans. Microwave Theory and Techs*, vol 33, no 11, pp. 1235-1238, November 1985

[13] "G.G. Mazumder and P.K.Saha,"Rectangular waveguide with P-shaped septa,"*IEEE Trans. Microwave Theory Tech.*, vol 35, no 2, pp.201-204, February 1987

[14] Y. Zhang and W. T. Joines, "Some properties of the T-septum waveguides,"*IEEE Trans. Microwave theory and Techs.*, vol 35, no 8 pp.769-775, August 1987

[15] "Theoretical study of the folded waveguide", G.L.Chen. T.L.Owens, and J.H.Whealton, *IEEE Transactions on plasma Science*, vol. 16, No. 2, Aprill 1988

[16] http://www.rogerscorporation.com/mwu/tip12.htm

[17] Rogers Technical Note RT3.3.2, "Temperature Rise Estimations in RT/duroid® Circuit Boards Carrying Direct or RF Current", Revised 1993, 4 Pages.

3. Fabrication and measurement of folded waveguides

3.1 Excitation of folded waveguides

Folded waveguides are attractive alternatives to the various types of substrate integrated waveguides discussed in chapter 1 not only for their wide bandwidth but also for the hybrid schemes they can form with planar circuits. This chapter explains how folded waveguides can be integrated with planar transmission lines and also discusses the fabrication process for both types of folded guide.

3.1.1 Explanation of basic planar transmission lines

When speaking about planar transmission lines in high frequency engineering, microstrip line comes to mind first. The microstrip line is the most fundamental type of planar waveguide in microwave electronics and is present in most applications. It consists of a single conducting strip of width W placed on a dielectric of thickness H and located on a ground plane, figure 3.1. The electric field of a microstrip line is mainly concentrated in the dielectric region between the two metal strips but there is also field in the air region. For that reason, the mode of a microstrip line is not pure TEM but rather quasi-TEM figure 3.2. Other basic types of planar transmission lines are the co-planar line, the slot line and the stripline shown in figure 3.3.

It is possible to integrate folded waveguides to more than one type of planar line. For example, depending on the requirements of each application, we can integrate folded waveguide to microstrip line as well as co-planar waveguide. However, for smoother integration, we choose the transmission line whose electric field profile is closer to that of a folded waveguide. Under these circumstances, the field profile of

a stripline, figure 3.4, is closest to the field profile of both type 1 and type 2 of folded waveguides.

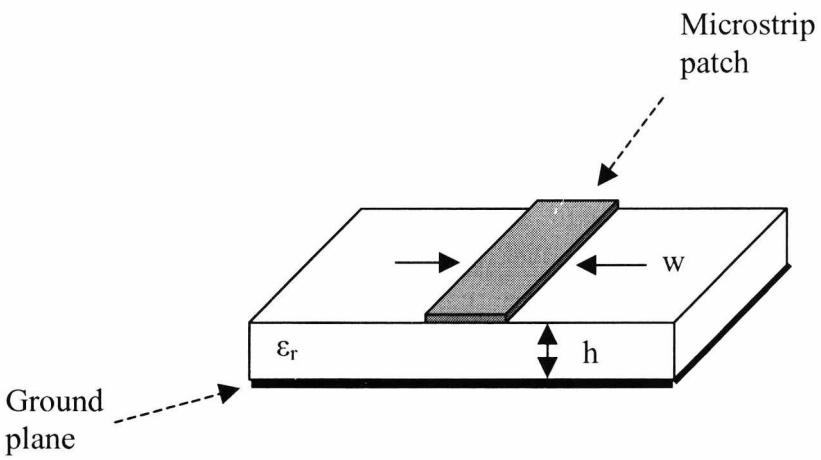

Figure 3.1. The Microstrip line

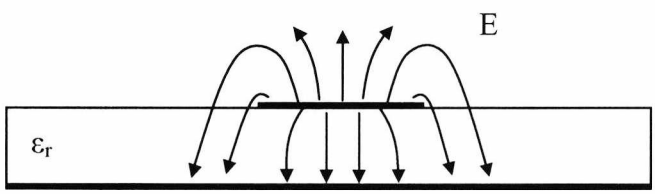

Figure 3.2. Electric field profile for the microstrip line; cross sectional view. The field is partially extended to the air regions above the dielectric strip of permittivity ε_r. Dark lines represent metal patches.

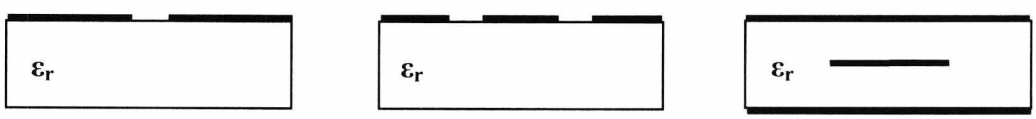

(a) (b) (c)

Figure 3.3. Cross-sectional view of characteristic types of planar transmission lines. Dark lines represent metal patches. a) Slotline b) Coplanar line c) Stripline

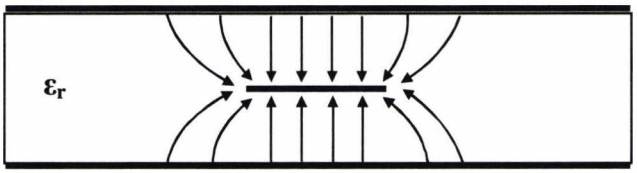

(a)

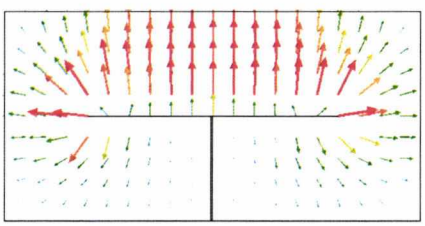

(b)

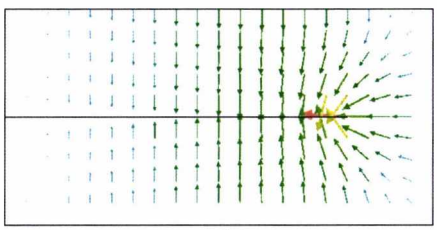

(c)

Figure 3.4. The electric field profile of a stripline (a) is very similar to that of a folded guide type 1 (b) and type 2 (c). Dark lines are metal patches

3.1.2 Optimization of the excitation

We have seen how the stripline is the most suitable type of planar transmission line, for integration to our folded waveguide. We start the analysis with folded guide type 1 excited through a tapered stripline. As a first approximation, the transition is shown in figure 3.5.

We include a lamda/4 section of stripline to account for smoother energy excitation in the structure. Depending on the thickness of the dielectric substrate used and its electric permittivity, the width of the stripline section is carefully adjusted to deliver an input impedance of 50 Ohms.

The parameter that needs to be optimized is the taper length L. Tapers are generally used as impedance transformers and are known for their broadband characteristics. In this case, the taper is used to transform the 50 ohm input impedance to the impedance of our folded waveguide. However, apart from the taper length, the length of the outer walls of the structure is another parameter that requires attention. As the wave travels through the taper and reaches the folded guide, the outer walls

of the guide are an obstacle to the field lines. The middle wall disrupts the mode too, but not to the same extent because it is only half the height of the outside walls. Simulating the structure of figure 3.5 showed mediocre performance over the operating frequencies, with return loss less than -20dBs at some points. Nevertheless, the design appeared to have problems in back-to-back configuration, with unwanted spikes in the S-Parameters. The electric field profile, figure 3.6, reveals that the structure has radiation problems.

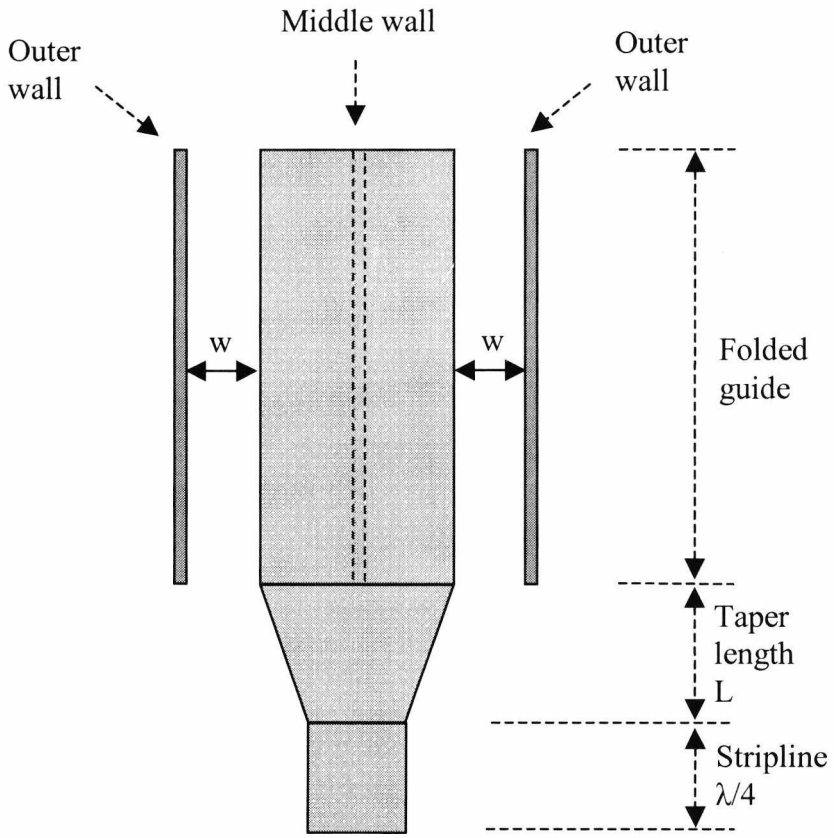

Figure 3.5. Transition for folded guide type 1, top view.

The solution to the radiating modes of our structure is to extend the outer walls up to the input of our design. The mode can no longer radiate, but the design of the folded waveguide gets a bit more complicated. At the input, we have a stripline shielded inside a rectangular waveguide whose TE_{10} is not affected by the middle patch of the stripline. Care needs to be taken, to avoid exciting the TE_{10} mode of the rectangular waveguide, or at least to operate the folded waveguide at frequencies

below the cutoff frequency of the rectangular waveguide through which it is being excited.

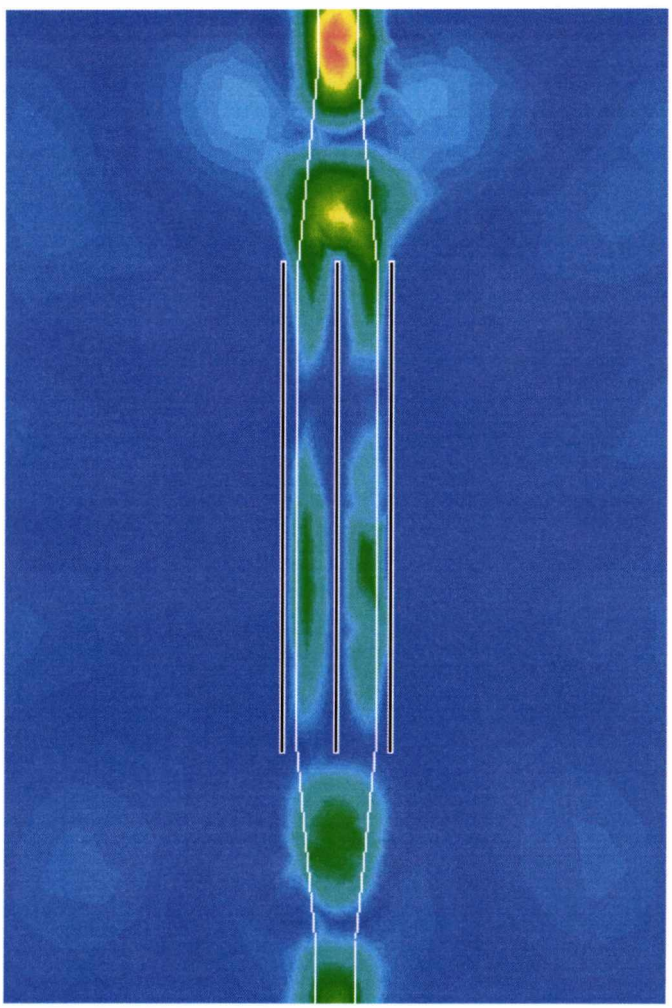

Figure 3.6. Electric field profile of folded waveguide type 1 in back-to back configuration, excited through tapered stripline.

Optimization of the taper is carried out automatically, after repeated trial-and-error simulations on the structure. High frequency electromagnetic software packages were used to adjust the taper length for the lowest possible return loss over the centre frequency (HFSS). The new optimized transition is shown in figure 3.7 and the simulated return loss is shown in figure 3.8. It is clear that the optimized return loss over the centre frequency f_c=10 GHz is much less compared to the non-optimised case.

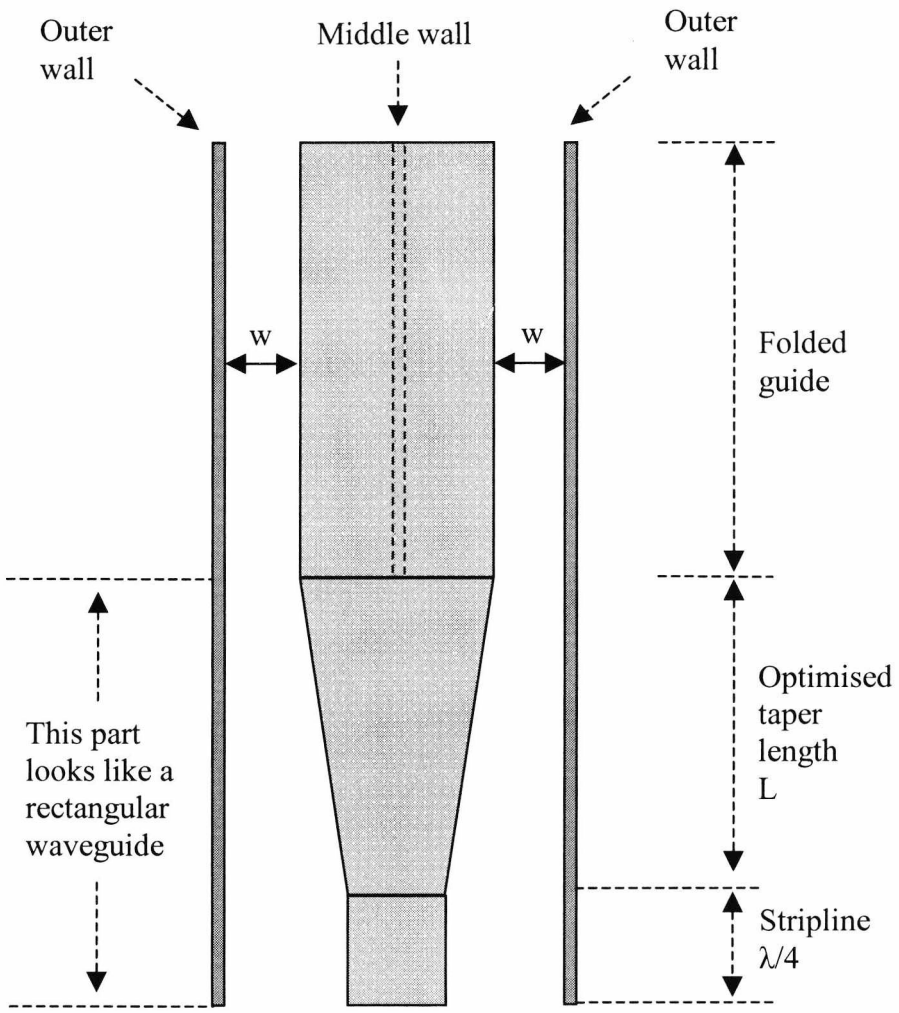

Figure 3.7. Transition for folded guide type1, top view.

For type 2 folded guide the optimization procedure is identical. The outer walls of the guide are again extended to the input of the structure. The taper length is optimized using electromagnetic simulation package (HFSS). The difference, compared to the taper used for type 1, is that this time the taper is asymmetric as there is only one gap *w*. On one side the taper extends until it reaches the outer metal wall of the folded guide and a proper electrical contact is established.

Although type 2 folded guides are not as broadband as type 1, they have the benefit of easier design-fabrication. There are fewer design parameters, i.e. one gap *w*, and therefore less possibility of fabrication error. Furthermore, there is no middle wall as in the case of folded guide type 1.

Nevertheless, the ease of fabrication of either guide depends on the method used and the amount of human supervision required. These factors are discussed further in the next sections.

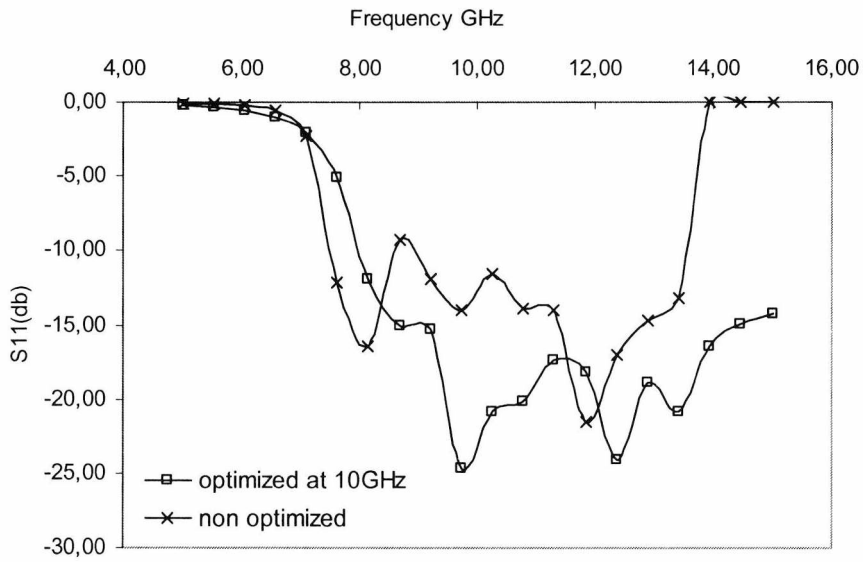

Figure 3.8. Simulated return loss for optimized and non-optimized transition for folded guide type 1. b=8 mm (7.875 mm), f_c=6.5 GHz, f_u=12.9 GHz, w=1 mm, a=3.15 mm, ε_r=2.2. Losses were accounted for.

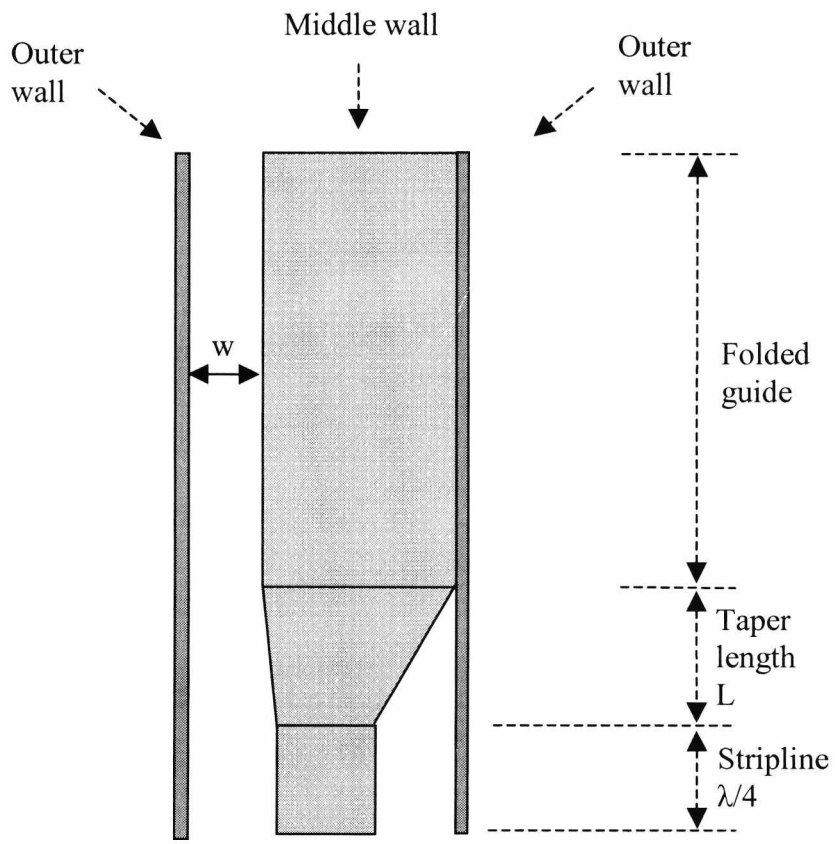

Figure 3.9 Tapered transition for folded guide type 2

3.1.3 Using the series of vias

The folded waveguides and their transitions were realized using conventional PCB fabrication techniques in the workshop. Hence most of the work required is relatively low cost and straight forward. We should note however that it is not very simple to manufacture the conducting walls of the guides, i.e. the three walls for type 1 and the two walls for type 2. For that reason we emulate the conducting walls using series of vias. It is known [1] that series of conducting vias with spacing much shorter than the operating wavelength are equivalent to a conducting wall. This technique has recently become very common in microwave circuit design, as it is practical and requires only standard drilling methods. Consequently we have seen couplers [2] using vias rather than some form of continuous conducting wall. Figure 3.10 illustrates the principle of the vias. The top and bottom plates are metal conductors. In this case two series of vias are effectively working as a rectangular waveguide.

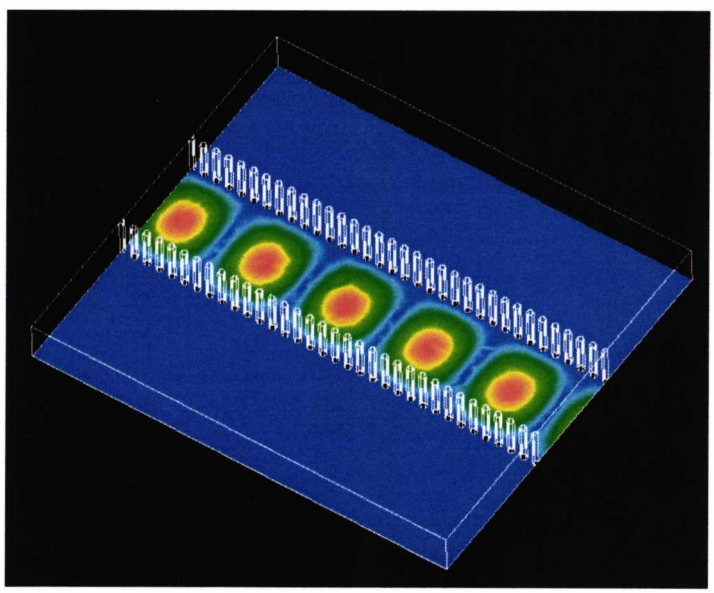

Figure 3.10. Simulated field plot where series of vias substitute conducting walls.

Using the via-hole technology, the final form of folded waveguide-to-stripline transition, for type 1 waveguide, is shown in Figure 3.11. Series of vias were used to synthesize the conducting walls. There are three walls, two on the outside and one in the centre. The middle wall is half the height of the other two, such that its

vias are in electrical contact with the central patch. The dashed line around the structure shows the separation of the two layers.

The transition of figure 3.11 has been simulated, and the electric field profile is shown in figure 3.12. The blue areas denote negligible electric field while the red areas indicate that the field is at maximum. We notice that the energy is kept entirely in the area between the vias and hence this is the proof that the series of vias work as proper conducting walls. Furthermore, due to the symmetry of type 1 folded waveguide, we can see that the maximum electric field is always in the centre of the guide.

The transition to stripline for guide type 2 is shown in figure 3.13. The overall layout of the design is similar to that for type 1. There are two series of vias, but no middle wall this time. Also, notice that the central patch is asymmetric. To the right, the distance between the patch and the series of vias forms the gap w. To the left, the patch extends outside the series to ensure electrical connection with each of the vias. Figure 3.14 shows the electric field plot for this transition. In contrast with the field profile of type 1, this waveguide concentrates its electric field on the right side, over the gap w. In the next section, it is shown that type 2 waveguide has a better measured response because of its simplicity over type 1.

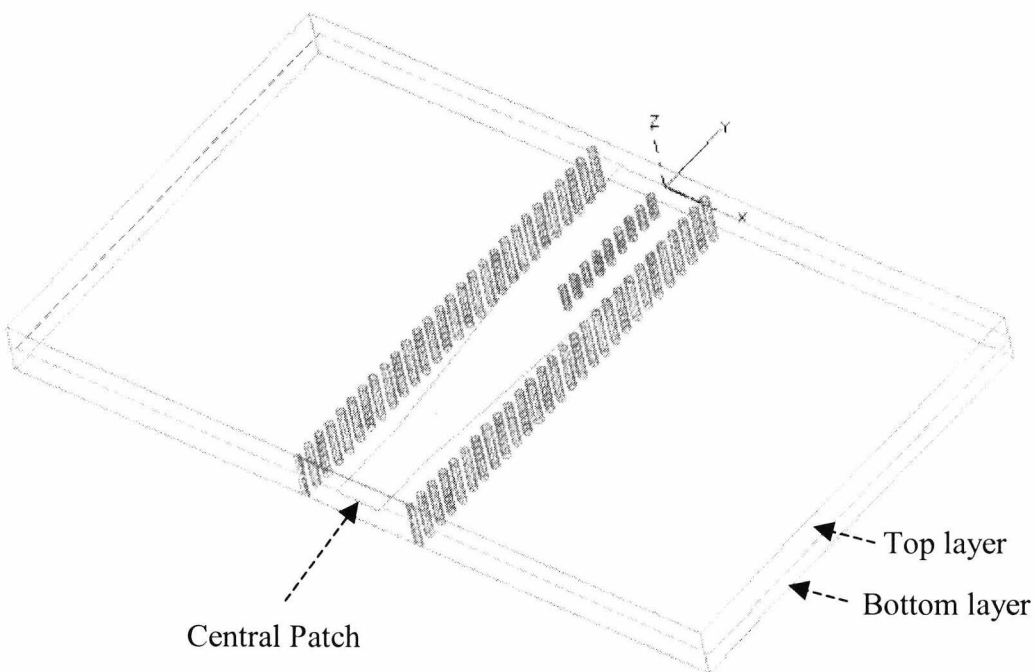

Figure 3.11. Stripline-to-folded waveguide transition for Type1

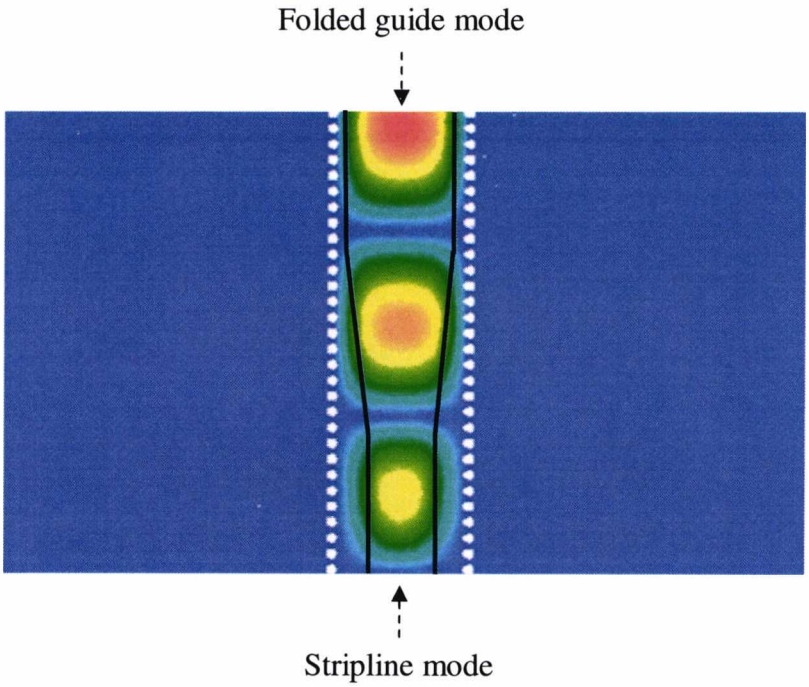

Figure 3.12. Field profile of folded waveguide type 1. The black line shows the position of the central patch

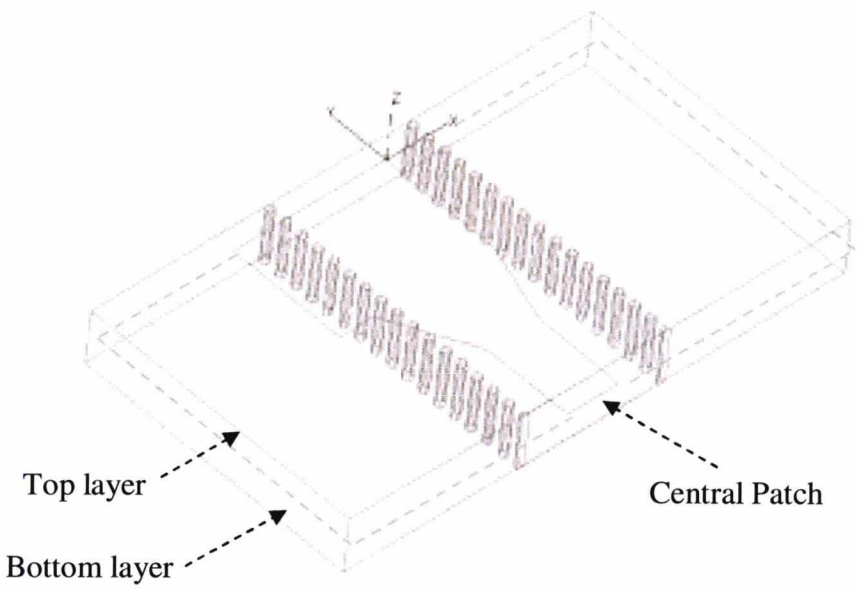

Figure 3.13. Stripline-to-folded guide transition for type2

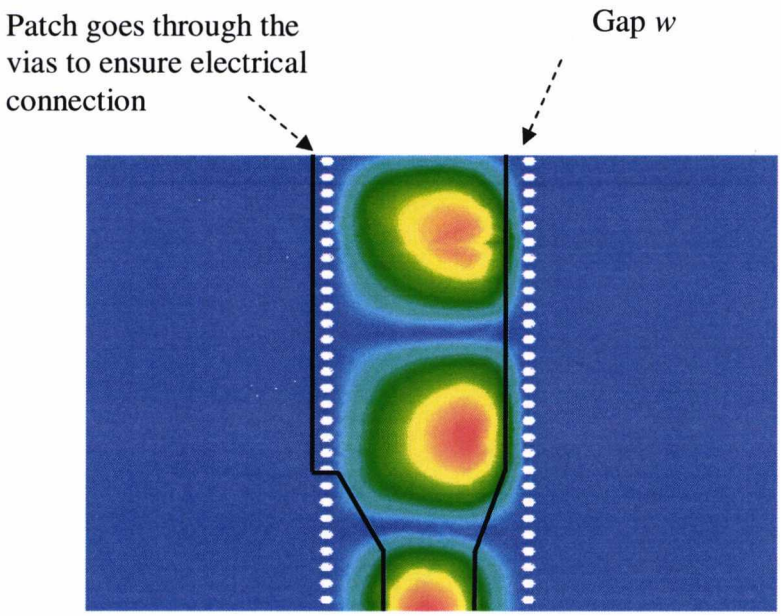

Figure 3.14. Electric field profile for type 2 folded waveguide. The black line shows the position of the central patch. We notice, as the mode propagates, how the maximum field shifts from the centre to the right of the folded guide.

3.2 Fabrication process

Fabrication of folded waveguides is a relatively simple process which, if the right method is followed, does not require a great deal of time. The top, bottom and central conductors of the guide are formed by patterned metallisations on the surfaces of the respective layer laminates. In order to form these metallisations some of the metal has to be removed. There are two methods of removing the copper from a microwave laminate. The first method requires etching the metal off the dielectric by spraying with photo resist, exposing to UV light and washing off the exposed areas with acid solution. Although etching is a very effective method of removing the copper without damaging the dielectric, it is rather time consuming as it may require many attempts until a good result is obtained. This method also requires extra alignments with the series of vias that are drilled independently. Hence the possibility of human error in the design is high.

The second method of removing the copper is milling the metal off the dielectric sheet using a computer controlled milling machine. This method is automatic and does not require any extra alignments for the vias and hence is more accurate. A

single data file, containing both the information for the drilling and the position of the vias, is interpreted by the machine, and the waveguides are manufactured with minimum human supervision. It is essential to notice that automated milling requires a great amount of experience in using the milling equipment. If the job is not done carefully, the milling machine might take off not just the copper but a bit of the dielectric underneath too. Nevertheless, if the technician has had enough experience on the milling machine and in working with the specific microwave laminates, it is possible to manufacture the waveguides at a high level of accuracy.

The waveguide shown in figure 3.15 has been manufactured in this fashion in the workshop. The orange coloured area is copper. We notice how the metal on the top side of the bottom layer has been selectively removed to form the central conductor of the folded waveguide. Two sections of stripline, $\lambda/4$ long, are included in the design for smoother excitation. Energy is launched in the waveguides using SMA connectors attached to the ends of the striplines. The series of holes that can be seen on both layers are going to be filled with copper wire i.e. metal vias.

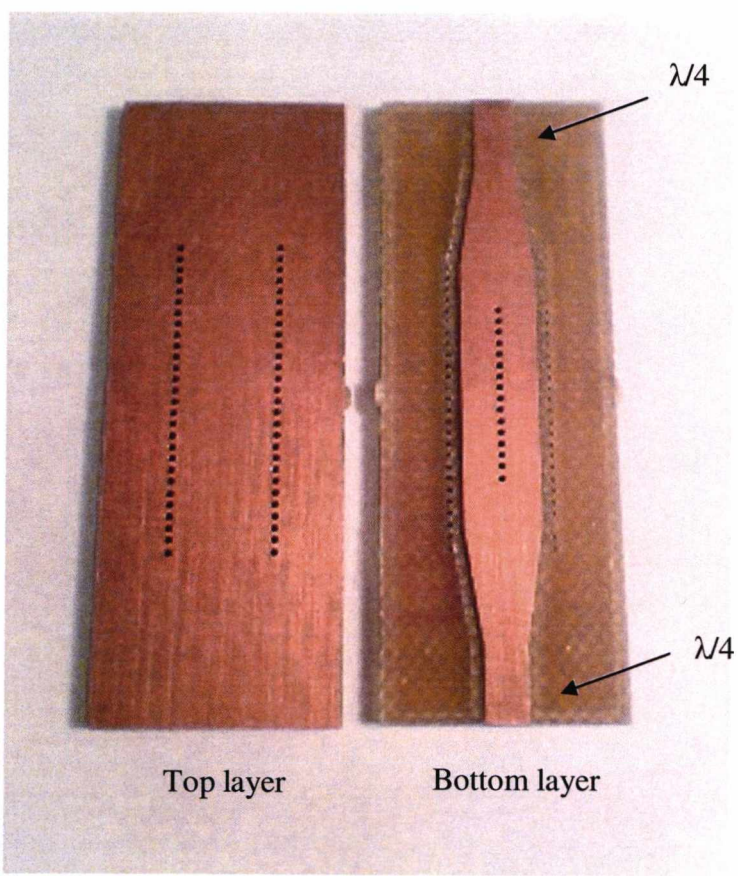

Figure 3.15. The two layers of folded waveguide type 1.

Should you choose to perfect the manufacturing process, making it entirely automated, the holes can be metallised using special equipment in the workshop. For this reason two extra sections of microstrip line should be used on layer two around the outside series of holes.

The fabrication process for waveguide type 2 is very similar to that used for type 1 with just a couple of differences due to the geometry of the guide. The first difference is the absence of the middle wall. The second difference is related to the issue of electrical contact between the middle patch and one of the side walls. In order to achieve proper electrical contact on that side of the guide the vias need to be metalised separately, before the two layers of the folded guide have been attached. Then electrical contact is achieved through the simple contact of the two layers.

3.2.1 Measurements

Type 1 and type 2 folded waveguides have been fabricated, one of each, using Rogers^{TM} Duroid (ε_r=2.2, tanδ=0.0009). The total length of the structures, including the feeding lines is 51 mm for type 1 and 33mm for type 2. The stripline width of 3mm was selected to give 50 Ohms impedance at the centre frequency of operation. The taper lengths are 13.76 mm for type 1 and 4.56 mm for type 2. These values have been optimized to achieve a return loss of less than 20 dB.

Also, for both waveguides b=1.575 mm and w=0.9 mm, with a=7.5 mm for type 1 and a=7.75 mm for type 2 respectively. Using these parameters the cutoff frequencies of the two designs are 6.8 GHz for type 1 and 6.6 GHz for type 2. The waveguides are designed to operate in the X band. In both cases the relative bandwidth is two.

The measured results are shown in figure 3.16, for type 1 and figure 3.17 for type 2. The comparison of measurements to simulated results shows good agreement for both types of folded waveguide. Also, for both types of guide the cutoff frequencies occur below 7 GHz, i.e. as expected, and the higher order mode starts to propagate at about 13 GHz. The measured return loss is worse than expected but this is probably due to the SMA connectors that were not de-embedded. Also a more professional fabrication process would improve the results further since the fabrication method used in our case was not the most rigorous.

We notice that the type 1 results are not in such a good agreement as type 2. This is, as expected, due to the presence of the extra wall in the middle of the waveguide. For that reason, as mentioned above, folded waveguides of type 1 are also more

difficult to manufacture. In addition, the width of the middle wall *d* alters the propagation characteristics of the guide. To avoid something like this happening we choose *d*<<a.

For measurement purposes, an Anritsu 3739C analyzer was used, with coaxial calibration.

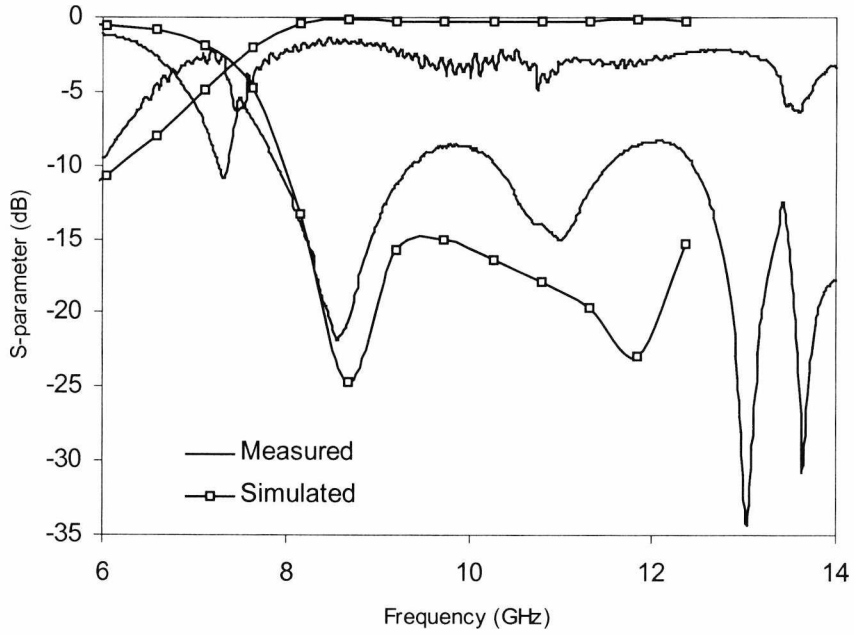

Figure 3.16. Simulated results and measurement for folded guide type 1

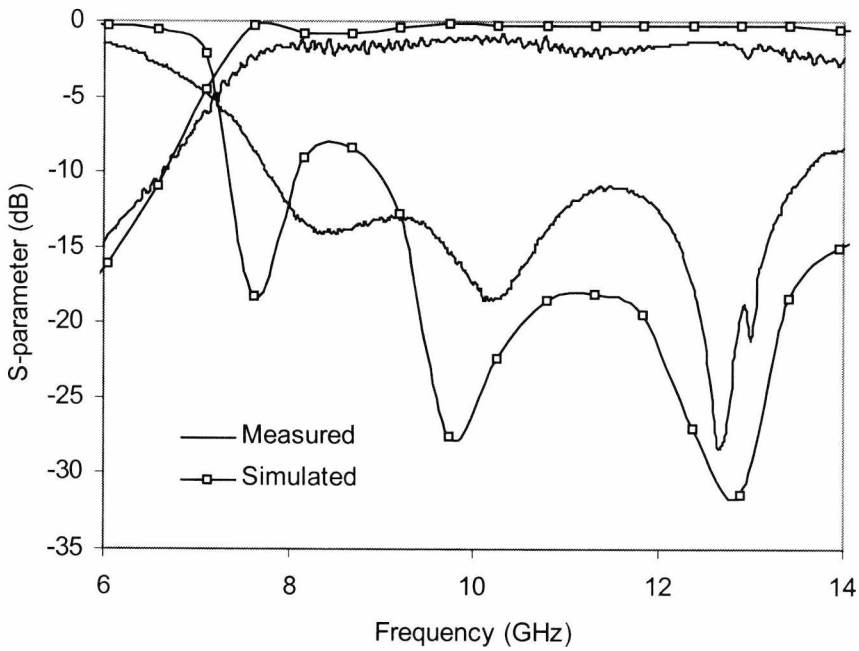

Figure 3.17. Simulated results and measurement for folded guide type 2

3.2.2 Fabrication of folded waveguide in large scale

The mass consumer market applications of millimeter wave technology require the production of simple, low-cost products in the minimum amount of time. Millimeter-wave components are hence required to have small dimensions and good performance at low cost.

So far, we have seen the important advantages of folded waveguides over various other types of guides. This paragraph proves how folded guides can be produced in large scale using conventional PCB fabrication techniques. Figure 3.18 shows such an example. From a single sheet of dielectric material you can cut, at once, many folded waveguides at different lengths. To the left of the picture, we have the top layers of folded waveguides of different lengths and to the right we have the respective bottom layers. The two layers are held together through four alignment points, one at each corner. The process is entirely automatic, timesaving and low cost.

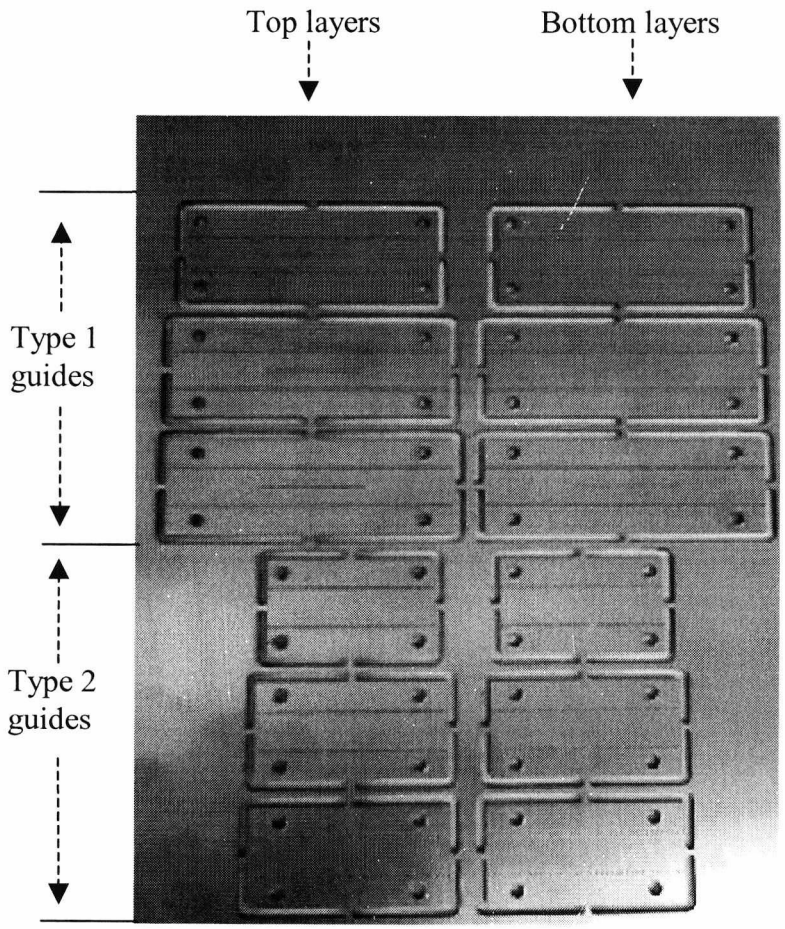

Figure 3.18. Fabrication of many folded waveguides out of a single dielectric sheet.

3.3 Alternative excitation methods for the folded guides

Folded waveguides can form hybrid integrated schemes with planar transmission lines such as the stripline and the microstrip line. Nevertheless, there are numerous other integration techniques that can be used. In this paragraph we present two more alternative excitation methods for the two types of folded guides and show some simulated results.

3.3.1 Excitation of folded guide type1 through coaxial waveguide

Figure 3.19 shows a coaxial waveguide for mm wave applications. It is comprised of an outer conductor which is earthed and an inner conductor which carries the signal. The outer conductor is filled with dielectric and both conductors have the same centre. The impedance of a coaxial waveguide is given by equation 3.1 and is not dependent on the length of the conductors but on their diameter ratio. Usually the dielectric used for coaxial waveguides is PTFE with $\varepsilon_r = 2.1$. Typical conductor diameters for an input impedance of 50 Ohms are $d_o = 3.34$ and $d_{in} = 1$mm.

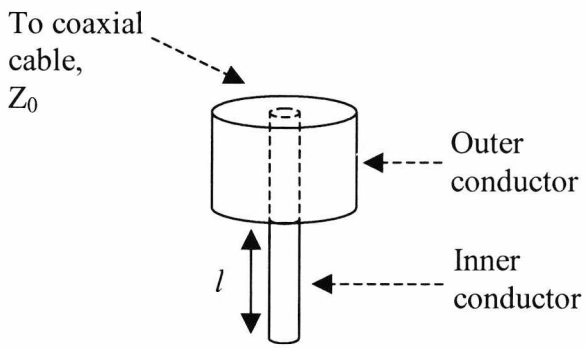

Figure 3.19. The coaxial waveguide. Both conductors are usually made of gold

$$Z_0 = \frac{60}{\sqrt{\varepsilon_r}} \ln\left(\frac{d_o}{d_{in}}\right) \tag{3.1}$$

where: d_0 is the diameter of the outer conductor and d_1 is the diameter of the inner conductor, l is the length by which the inner conductor extends under the outer conductor

A coaxial waveguide can be used to excite the folded waveguide type 1 as shown in figure 3.20. The inner conductor should be $\lambda/4$ away from a short circuit such that the reflected waves are in phase with the transmitted ones. Normally, if we were exciting a rectangular waveguide, the length of the inner conductor extends approximately to the middle of the rectangular waveguide. In the case of the folded waveguide, the structure is made of two layers and the middle carries the central conductor. Repeated simulations have shown that the performance of the excitation is better when the inner conductor is very close to the central conductor but without touching it. The optimum distance between the two was calculated to around 100 microns. Figure 3.21 shows the field profile of the structure and figure 3.22 shows the frequency response for a folded waveguide with a=7.875 mm, b=3.15 mm, ε_r=2.2 and w=1 mm for different values of d i.e the distance between the inner conductor and the central patch of the folded guide. The thickness of each layer is 1.575 mm.

The disadvantage of this excitation method is that distances of the order of 100 microns are not easy to achieve. Very precise machinery needs to be used, and the overall manufacturing procedure is slow. For the purposes of our design this type of excitation was not very practical and was not chosen. Nevertheless, if a very accurate drilling machine is available, and if the planar type of transmission line is not an option then this excitation method is an alternative solution.

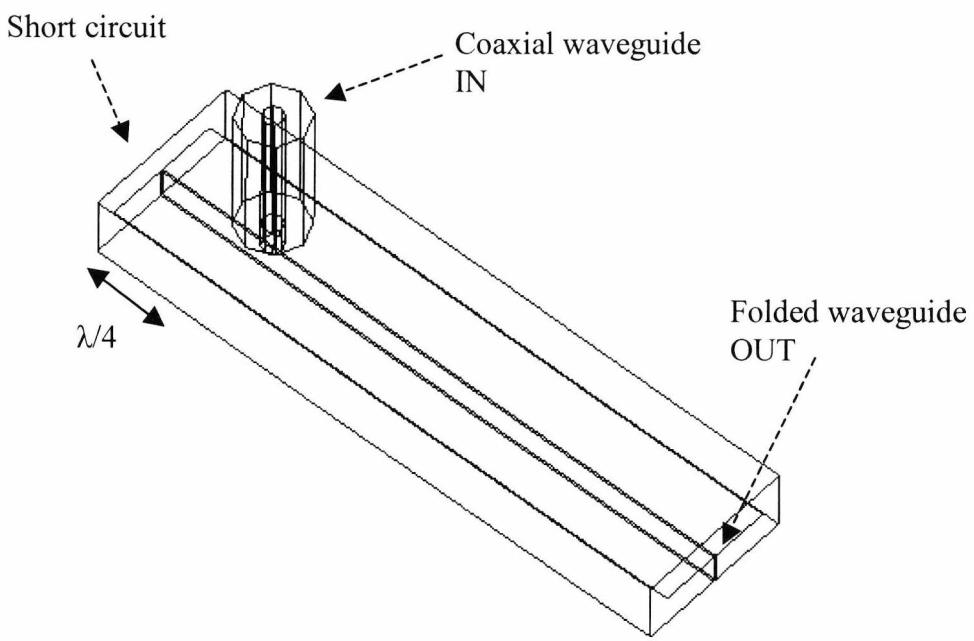

Figure 3.20. Folded guide type 1 excited with coaxial waveguide. Model used for simulation. The coaxial waveguide and the inner conductor are octagons rather than perfect circles, to reduce the simulation time.

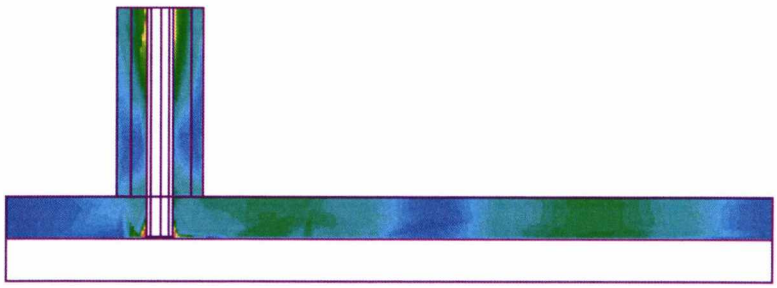

Figure 3.21. Field profile of the coaxial transition. Green-yellow areas denote high electric field

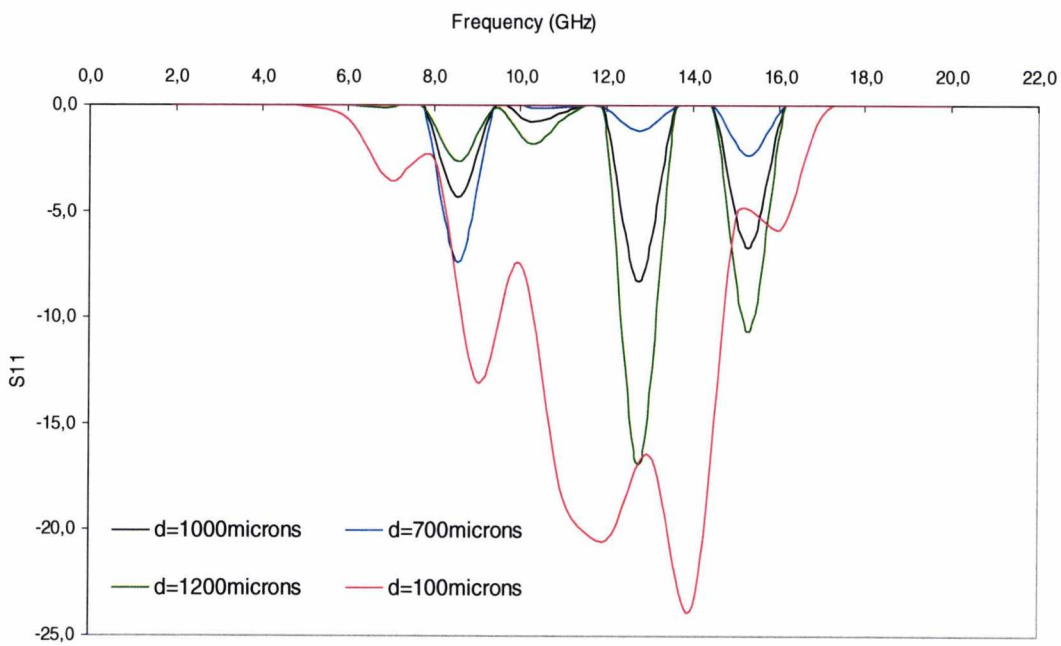

Figure 3.22. Frequency response of the coaxially fed folded waveguide; *d* is the distance of the inner coaxial conductor from the middle patch.

3.3.2 Type 2 folded guide excited with a via

We have seen the folded guide type 2 being excited using the stripline method. In this paragraph the folded guide is being excited using a vertical via and a microstrip line at right angles to each other. This method requires very high manufacturing

accuracy and hence thick film fabrication is required. The properties of this method are discussed in detail in the next section. The structure that follows is designed according to multilayer thick film standards. Figure 3.23 shows the simulation model and figure 3.24 shows a close view of the transition.

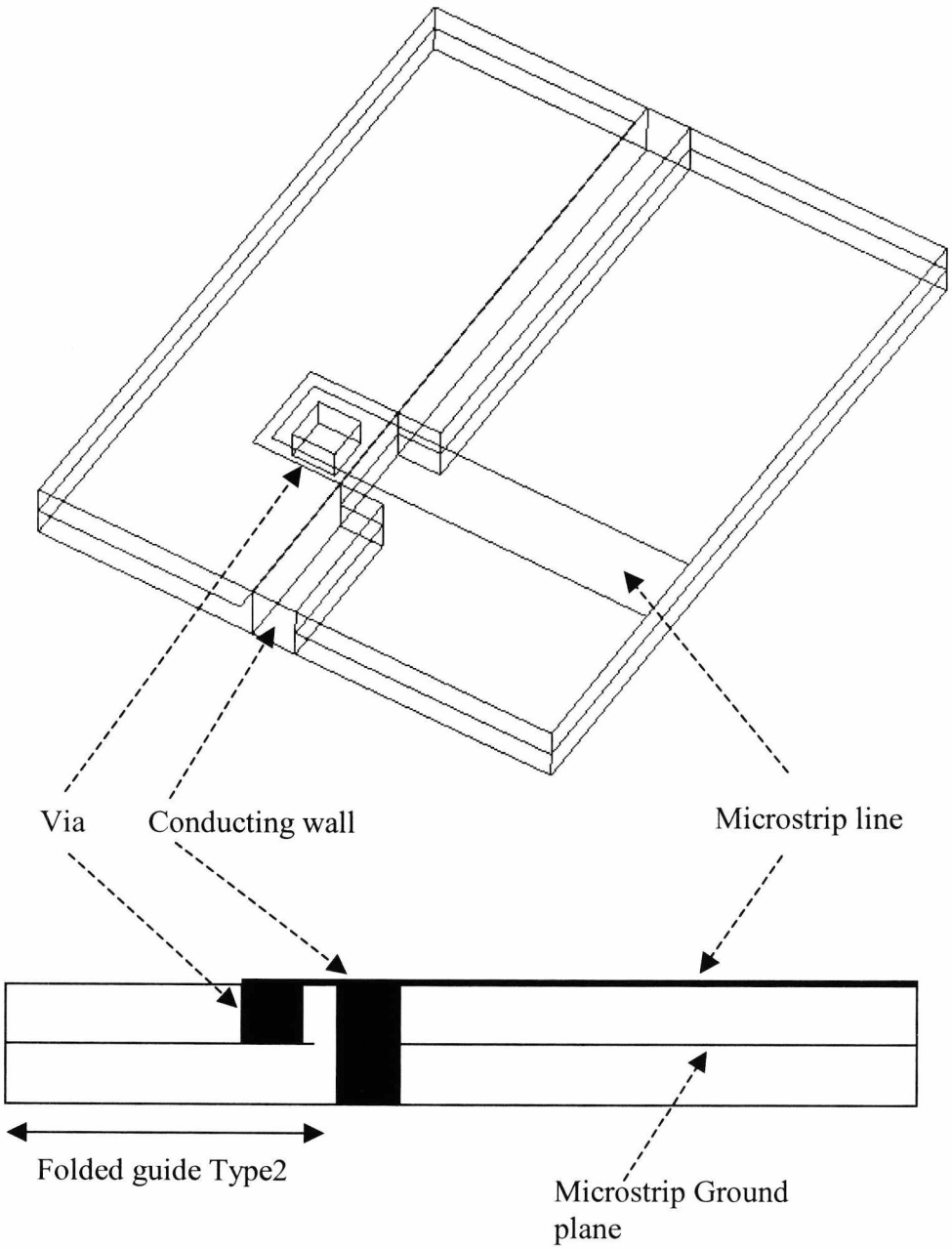

Figure 3.23. Folded guide type 2 excited using via and microstrip line

The dimensions for the transition of figure 3.24 were selected on a trial-and-error-basis to obtain the best return loss. The parametric values are: I) the sideways distance between the top plate of the folded guide and the microstrip patch w_1, II) the respective front distance d_1, III) the distance of the vertical via from the end of the central patch d_2, IV) the separation of the walls and the central patch w_2. For the return loss the values of these parameters where adjusted to w_1=26 μm, w_2=26 μm, d_1= 20 μm, d_2= 20 μm.

As mentioned before these dimensions are only possible to achieve through thick film fabrication, a method which is explained in the next section.

Figure 3.25 demonstrates the field profile of the transition and the simulated S-parameters for the structure, including losses, are shown in figure 3.26. The waveguide operates from 60 to 100 GHz and its dimensions are width a=500 μm, height b=120 μm, gapwidth w=30 μm. We notice that the S-parameters are not very good since the S_{11} does not go below -13 dB in the best case, figure 3.26. We should also add that optimizing the structure was very time consuming and the results could not be dramatically improved compared to the non-optimized case. Nevertheless we believe that this design has more prospects given a more persistent analysis.

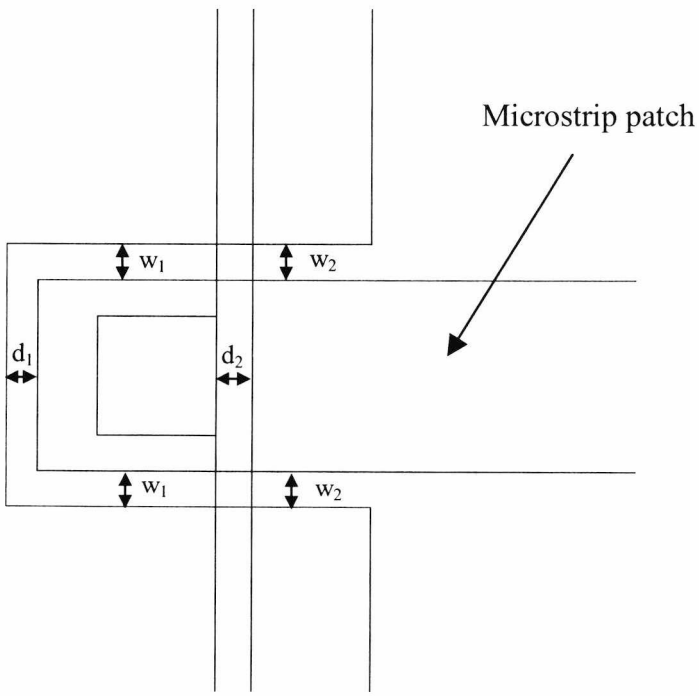

Figure 3.24. Detailed figure of the parametric variables in the via-excited folded waveguide

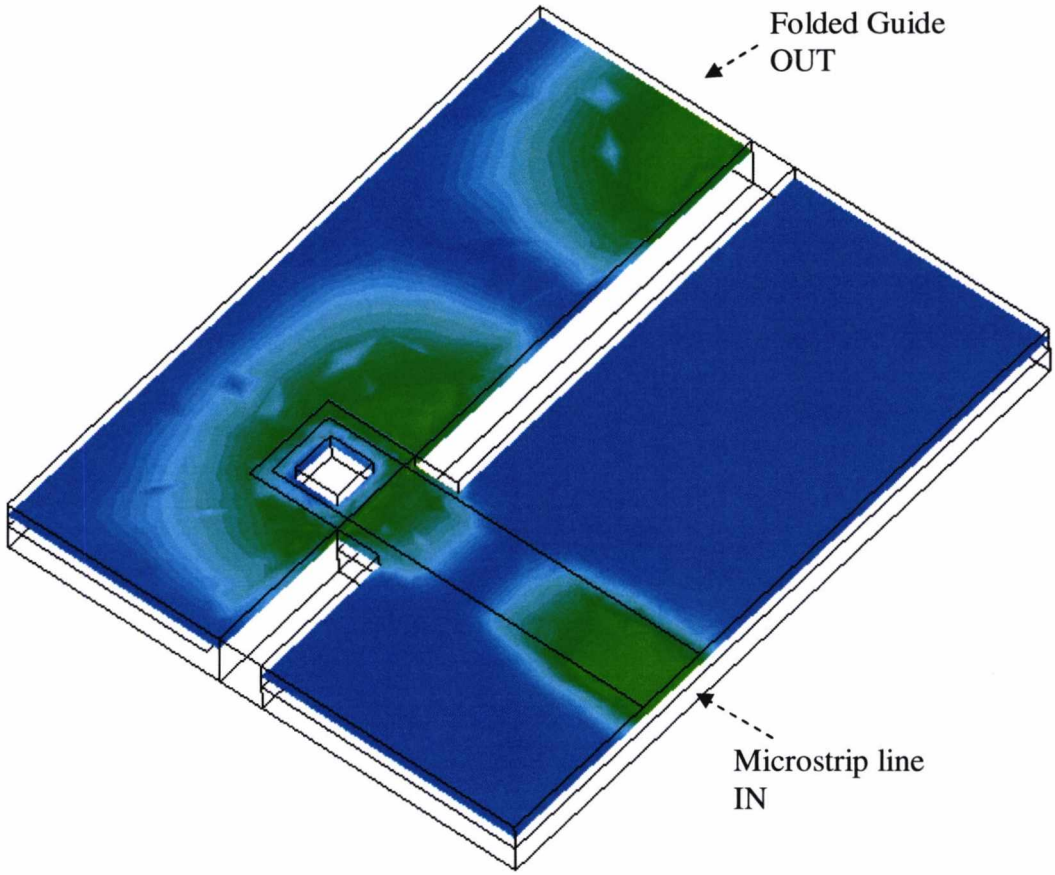

Figure 3.25 Field profile of the transition

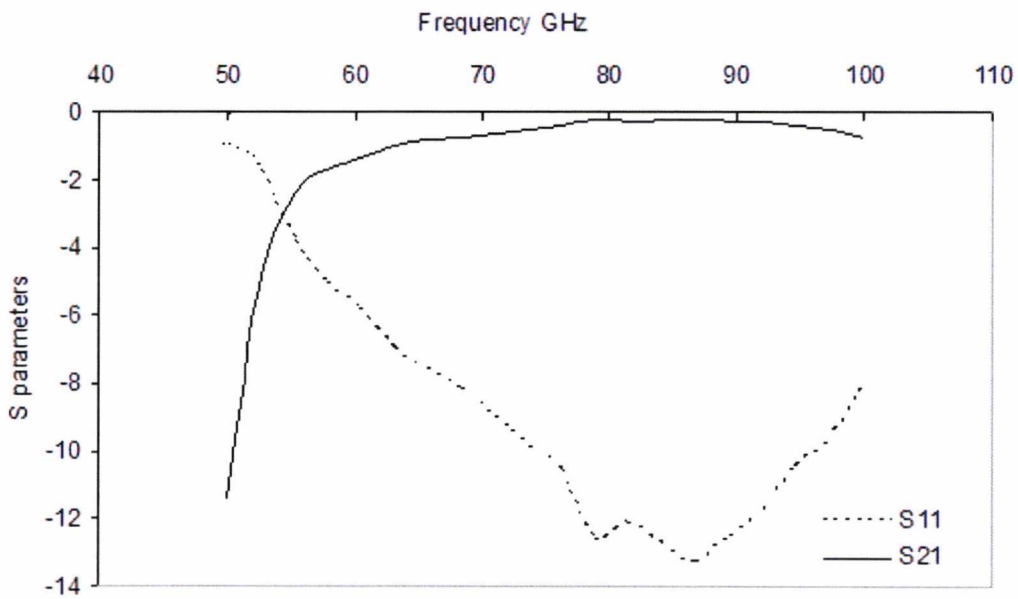

Figure 3.26. Frequency response of via-excited folded guide

3.4 Folded waveguides using the thick-film method

So far, we have seen the fabrication method of folded guides using conventional low-cost PCB drilling techniques in the workshop. In this section we discuss a more advanced fabrication method which involves the use of thick films and allows the manufacturing of extremely small folded waveguides.

Until now, thin film technology yielded poor line resolution and high losses. But rapid development in novel thick-film materials and advanced thick-film circuit-patterning techniques has brought improvements that allow current thick-film technology to reach beyond its previous limitations. Advanced thick-film techniques such as photolithography over fired layer, and photoimaging over photosensitive dried layer, yield conductor strips with resolution and edge definition comparable to thin-film technology. Thick-film technology allows designers to combine microwave and digital functions on common high-thermal-conductivity alumina substrates and to incorporate capacitors and laser-trimmable thick-film resistors into the main microwave structures. The self-smoothing tendency of thick films at the substrate interface permits the use of less-expensive, 96-percent alumina substrates. Additionally, thick film technology provides significant advantages such as low-cost and feasibility for mass production. The microwave components designed today in this fashion have very small dimensions and operate in the 60GHz + range [3-8].

The waveguides presented in this section have been designed for fabrication in collaboration with the University of Surrey. Researchers in the Microwave laboratory of Surrey University are currently using multilayer thick film technology with dielectric pastes of permittivity ε_r=8, figure 3.27.

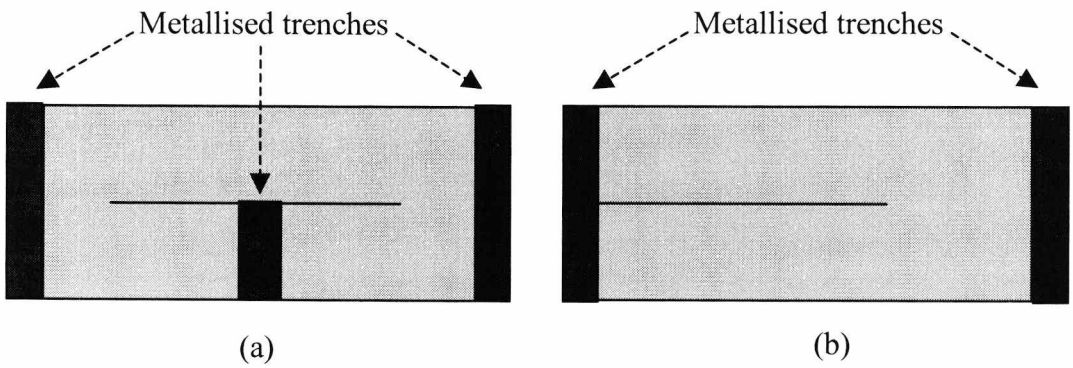

Figure 3.27. Cross-sectional views of: a) type 1 folded guide, b) type2 folded guide

In this case rather than vias we have metallised trenches and instead of dielectric sheets we have layers of dielectric paste. The thickness of the paste is 60 microns and the minimum width of the metallised trenches is 100 microns.

3.4.1 Excitation for the thick film folded waveguides

The excitation method is realized, inevitably, through microstrip line which lies on the top of the structure. That is because the energy is induced into the system via the probes of the network analyzer, which touch-on the surface of the structure. It is therefore impossible to launch the wave through the middle layer, or through some other method which does not use the top of the structure. Two waveguides have been designed. The first is a broadband example of type 1 and the second is a type 2 folded waveguide for the U band (40-60 GHz). The microstrip line on both structures is 70 microns wide so that impedance at the input is 50 ohms, the same as the impedance of analyzer probes. Figure 3.28 shows the type 1 folded waveguide, modified for fabrication in thick film multilayer method.

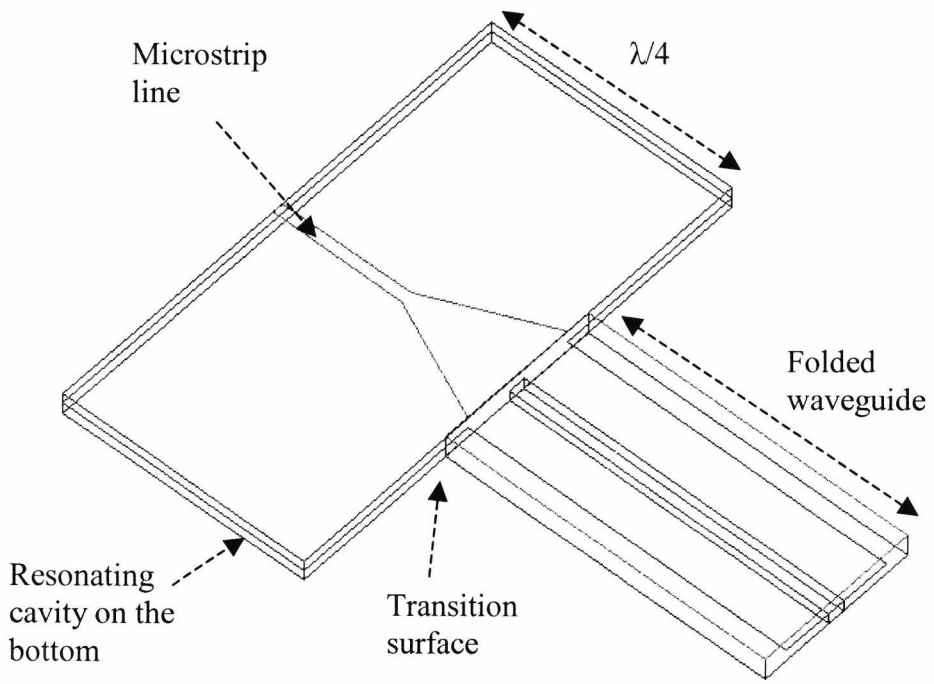

Figure 3.28. Folded guide type 1 modified for thick film fabrication.

We use a tapered transition to launch the energy from the microstrip line to the folded waveguide. The length and width of the taper is optimized for the lowest return loss, S_{11}, using electromagnetic simulation packages (HFSS). Repeated simulations have shown that the overall frequency response of the structure is improved if the substrate, which holds the microstrip line, is shielded with conducting walls for both layers. However, care needs to be taken to avoid the mode TE_{10} which propagates on the bottom layer, under the ground plane of the microstrip line. By making the length of the microstrip substrate equal to $\lambda/4$ we create a resonating cavity underneath the ground plane of the microstrip line. At the transition surface with the folded guide, the RWG mode under the microstrip mode sees an open circuit and cannot propagate further.

Figure 3.29 shows the field profile. The frequency response is shown in figure 3.30. This waveguide is a broadband example of type 1 folded waveguide. As the graph clearly shows, the operating bandwidth is from 40 to 100GHz.

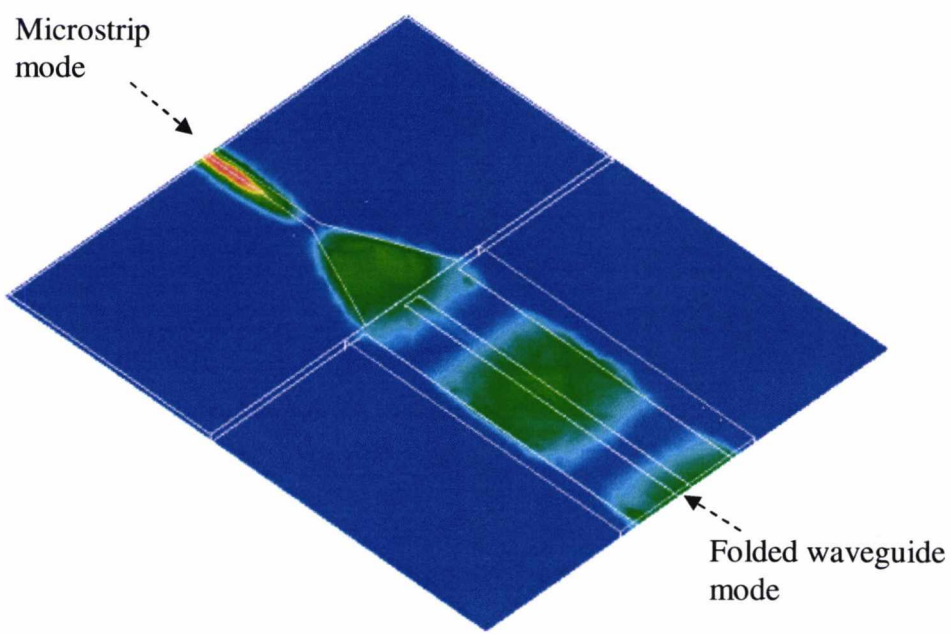

Figure 3.29. Field profile of folded guide type2

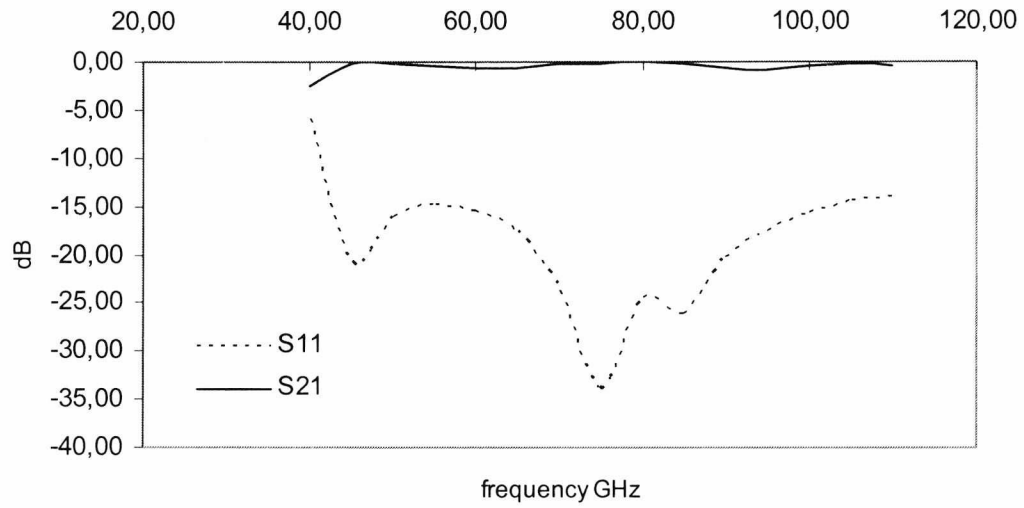

Figure 3.30. Frequency response of folded guide type 2, frequency Hz

The procedure for exciting folded guide type 2 is the same. Figure 3.31 shows the outline of the excitation and figure 3.32 the electric field profile. The taper used in this case is asymmetric. This waveguide is not as broad band as type 1 but the structure works well from 55 to 90 GHz, figure 3.33.

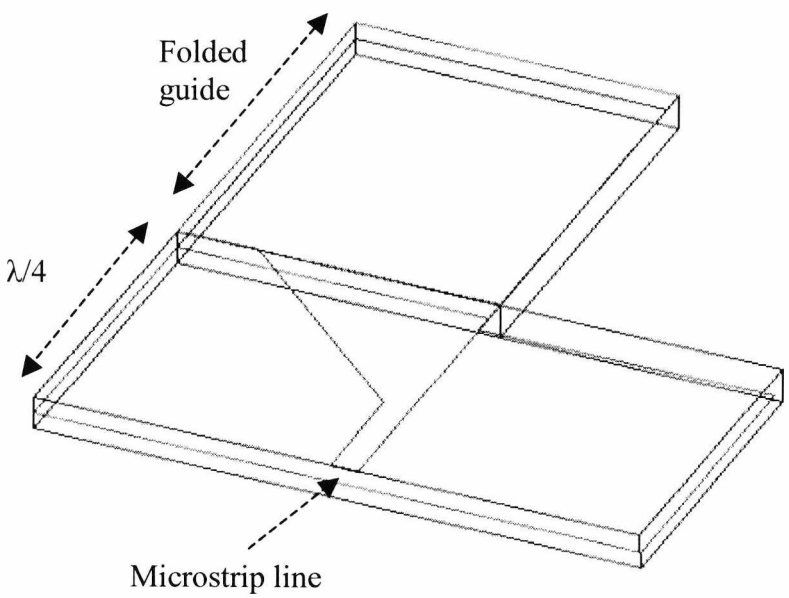

Figure 3.31. Folded guide type2 for thick film.

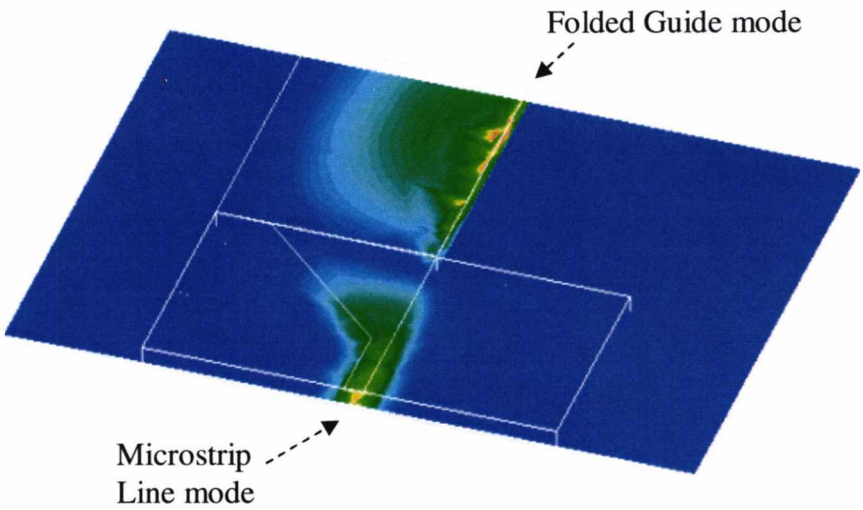

Figure 3.32 electric field profiled for transition to folded guide type2

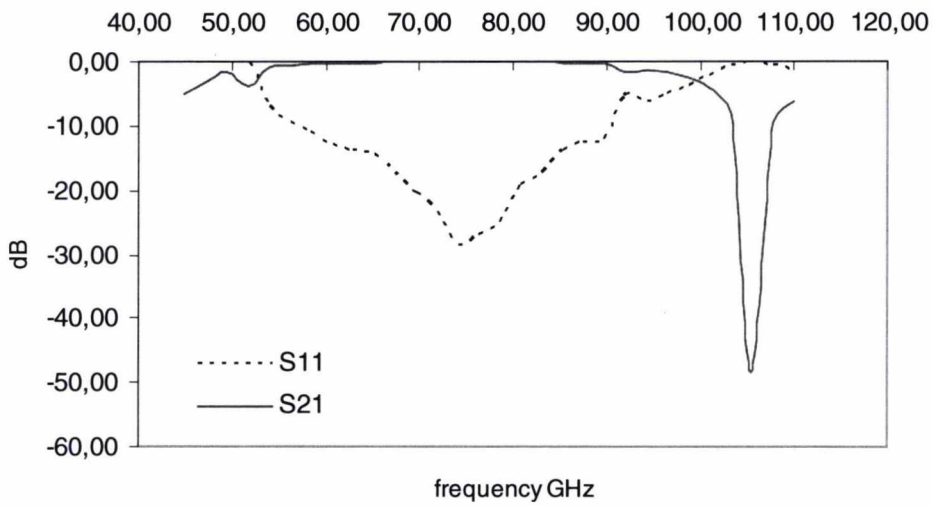

Figure 3.33. Frequency response for transition to type 2

The wave guides shown in this section where sent to the University of Surrey in the form of multilayer Autocad files, for fabrication. For each waveguide we prepared four different lengths as required by the TRL de-embedding method, refer to Appendix A. Unfortunately, at the time that this thesis was written the waveguides had not been fabricated and therefore we were unable to present any measurements. Nevertheless we already know from section 3.2.1 that folded guides work well in

the X frequency range. Hence the successful of folded waveguides in thick films is only a matter of careful fabrication.

3.5 Summary

New microwave components are being developed in intelligent transportation systems and wireless communication systems. Increased use of substrate integrated devices has led to the search for new technologies offering advanced circuit functions at low cost. In this chapter we presented low-cost and efficient fabrication methods for the folded waveguides of type 1 and type 2 using conventional PCB fabrication techniques. We demonstrated how both types of guide can form hybrid circuits and combine with planar transmission lines, such as the stripline, and therefore showed the high potential of folded guides. Integration with other types of waveguides is today an essential feature of every microwave device and this is why the novel guides that we present in this thesis are sure to attract attention in the microwave field.

The measurement of folded guides showed good agreement with simulated results. Both types had efficient responses over the X band frequency range with only type1 having some minor problems in the transmission parameters. In any case, if instead of using copper wire the vias are metallised the S-parameters are bound to improve for both types of guide.

Furthermore in this chapter we explained how to automate the fabrication process of the folded guides for large scale production. The process is low cost and required minimal human supervision. It is therefore suitable for the production standards of intelligent transportation systems.

Towards the end of the chapter we talked about thick films a new technology with advanced circuit functions at low cost. Moving much further than standard PCB methods thick films offer high electrical conductivity, fine-line and space resolution, well defined conductor edges, nearly vertical walls, and smooth upper surfaces. All these features are essential for achieving low losses in both types of folded guides at very high frequencies.

References

[1] D. Deslandes and K.Wu, "Integrated microstrip and rectangular waveguide in planar form," *IEEE Microwave and Wireless Comp.* Lett., vol. 11, No. 2 February 2001.

[2] "Substrate Integrated Rectangular Waveguides", A. J. Farrall, P. R. Young, IEEE 2004 *High Frequency Postgraduate Student Colloquium*, Manchester, pp. 133-138 2004

[3] C. Y. Ng, M. Chongcheawchamnan, M. S. Aftanasar, I. D. Robertson, P. R. Young and J. Minalgiene, "Characterization of TFMS lines fabricated using photoimageable thick-film technology", *IEE Proc. - Microwave, Antennas and Propagation*, Volume 150, Issue 03. June 2003, pp. 125-130.

[4] R. Sobrany and I. D. Robertson, "Ruthroff Transmission Line Transformers using Multilayer Technology" , *European Microwave Conference*, October 2003.

[5] C. E. Free, D. Stephens, P. Camina and I. D. Robertson, "Microwave Planar Circuits using Modern Thick-Film Technologies", *Broadband Wireless Forum*, Cambridge, Nov. 2003.

[6] "Hibridas' photoimageable thick film process and materials for microwave and sensor component applications" Muckett, S.; Minalgene, J.;*IEMT/IMC Symposium*, 2nd 1998 15-17 April 1998 Page(s):154 - 160

[7] "Analysis of thick film thermistor geometries" Aleksic, O.S.; Nikolic, P.M.; Jokic, V.D.; Pejovic, V.Z.; Pavlovic, J.M.; Duric, S.;Microelectronics, 1997. Proceedings., 1997 *21st International Conference on* Volume 1, 14-17 Sept. 1997 Page(s):431 - 434 vol.1

[8] Influence of the Substrate on the Electrical Properties of Thick-Film ResistorsCattaneo, A.; Pirozzi, L.; Morten, B.; Prudenziati, M.;Components, Hybrids, and Manufacturing Technology, *IEEE Transactions on* [see also IEEE Trans. on Components, Packaging, and Manufacturing Technology, Part A, B, C] Volume 3, Issue 1, Mar 1980 Page(s):181 - 186

4. Folded Waveguide filters

The folded waveguides that we presented in chapter 2 form the basis for the design of a new class of folded-based substrate integrated components. In this chapter we analyze the design of folded waveguide filters and analyze their fabrication methods and measurements. The filters are formed by introducing discontinuities in the transmission line of the folded waveguide and offer compact dimensions and good performance at low cost.

4.1 Filter Design

Microwave filter design is a sophisticated procedure which goes through many steps until the desired filter has been realized. The first step is the selection of an electrical circuit, comprised of capacitors and inductors, which has the desired frequency response. Then it is possible to replace those components by suitable microwave circuit elements that have similar frequency characteristics over the same frequency range. To start with, we consider the two basic methods of filter design. The first is the *image parameter* method and the second is called the *insertion loss* method.

4.1.1 Filter Design using the Image parameter method

Filters using the image parameter method consist of a cascade of simple two-port networks to provide the required cutoff frequencies and attenuation characteristics [1]. This method is mostly used to describe simple filter structures and provides practical responses. Nevertheless the disadvantage is that it does not allow the specification of frequency response over the complete frequency range and for this reason we are not going to examine this method any further. On the contrary, the

insertion loss method allows a degree of control in the frequency response of the passband.

4.1.2 Filter Design using the Insertion loss method

The insertion loss method allows the control of a filter response by means of its amplitude in the passband and stopband as well as the phase characteristics. The power loss ratio of a network is defined as the incident power divided by the power delivered to the load:

$$P_{LR} = \frac{\text{Power from source}}{\text{Power delivered to load}} = \frac{1}{1-\left(\left|\Gamma(\omega)\right|\right)^2} \tag{4.1}$$

where Γ is the input reflection coefficient of a lossless network terminated in a resistive load impedance.

There are different types of filter responses which correspond to different expressions for the power loss ratio. Some of the most important types of responses are the *maximally flat*, the *equal ripple* (or *Chebyshev*), the *elliptic function* and the *linear phase*. We discuss the first two types, since they are the most commonly used.

Maximally flat is the response of a low-pass filter, when the power loss ratio is described by the equation:

$$P_{LR} = 1 + k^2\left(\frac{\omega}{\omega_c}\right)^{2N} \tag{4.2}$$

where N is the order of the filter and ω_c is the cutoff frequency. The passband of the filter extends from ω=0 to ω_c. The maximum value of P_{LR} in the passband is $1+k^2$, and therefore k is called the passband tolerance. We usually choose $1+k^2$ to be the half power point (-3db) and in that case we have k=1. In addition, the minimum value of P_{LR} is 1. The *maximally flat* filter provides the flattest possible response in the passband and hence the name given. Figure 4.1 shows the shape of a maximally flat response.

Chebyshev filters have power loss ratio given by the expression:

$$P_{LR} = 1 + k^2 T_N^2 \left(\frac{\omega}{\omega_c} \right)^{2N} \tag{4.3}$$

where $T_N(\omega/\omega_c)$ is the Chebyshev polynomial of degree N which oscillates between plus and minus 1 for $|\omega/\omega_c| \leq 1$ and increases monotonically for $\omega/\omega_c > 1$. Hence the power loss ration will oscillate in the pass band and will increase for $\omega/\omega_c > 1$. The response curve is shown in figure 4.1.

The difference compared to the *maximally flat* response is that the Chebyshev filter will have ripples in the passband. The number of these ripples is equal to the filter order N, although during the oscillations the power loss ratio does not exceed the value of $1+k^2$.However, the most important feature of the Chebyshev response is that its power loss ratio has a much greater rate of rise compared to *maximally flat*. Effectively, Chebyshev filters have a much sharper cutoff region separating the passband and the stopband and for this reason they are usually preferred in microwave filter design.

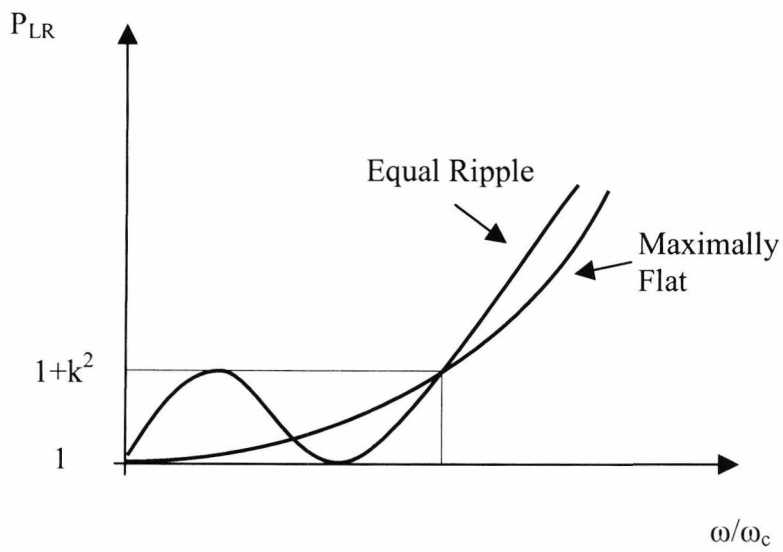

Figure 4.1. The two types of filter response, Chebyshev and Maximally flat

4.1.3 The ladder Network

Throughout this thesis, the type of filter response that we use is the Chebyshev, mainly due to its sharp cutoff frequencies separating the passband and stopband. To realize this type of filter we use a ladder network comprised of capacitors and inductors [2]. The elements in that network are numbered from 1 to N for a filter having N reactive elements. For Chebyshev response in the pass band the circuit must be symmetrical with respect to the middle. Figure 4.2 describes the ladder networks for a Chebyshev low-pass filter. The two networks shown are the dual of each other and the elements alternate between series and shunt connections. The element values are denoted as g_k.

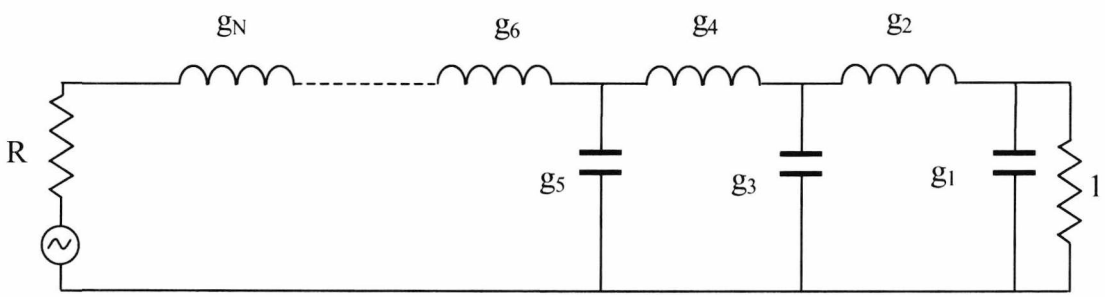

(i)

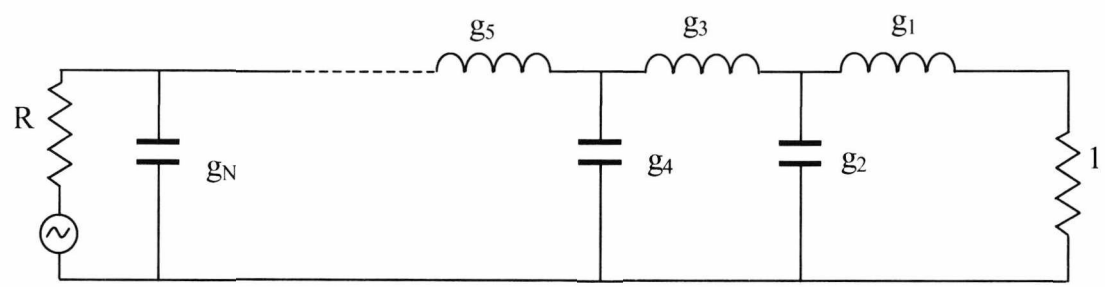

(ii)

Figure 4.2. i) Ladder network with capacitors and inductors for Chebyshev passband filter ii) Dual version of the network above it.

For N small the values of inductors and capacitors are given by simple analytical solutions. For larger values of N general solutions have been worked out [3]. Hence, for a Chebyshev low-pass filter with ω_c=1 we get:

$$g_{N+1} = \begin{cases} 1 & \text{N odd} \\ 2k^2 + 1 - 2k\sqrt{1+k^2} & \text{N even} \end{cases} \tag{4.4}$$

When g_N is a capacitor, $g_{N+1} = R$ but when g_N is an inductor, $g_{N+1} = 1/R$

The rest of the elements in the ladder network are given by

$$g_k = \frac{4a_{k-1}a_k}{b_{k-1}g_{k-1}} \tag{4.5}$$

where

$$a_k = \sin\frac{2k-1}{2N}\pi \tag{4.6}$$

$$b_k = \sinh^2\frac{\beta}{2N} + \sin^2\frac{k\pi}{N} \tag{4.7}$$

$$\beta = \ln\frac{\sqrt{1+k^2}+1}{\sqrt{1+k^2}-1} \tag{4.8}$$

$$g_1 = \frac{2a_1}{\sinh\beta/2N} \tag{4.9}$$

Using the above equations it is possible to derive tables for the values of filter elements for any number N which also stands for the filter order. Choosing the correct filter order is a procedure which requires careful consideration. A low value of N represents a short filter which, in microwave terms, is very practical since it has low losses. On the other hand, high filter order means a longer filter and hence higher losses, but with more accurate cutoffs. Usually a compromise between the two is necessary. The table that follows shows typical values for the g_k elements of the ladder network [4].

	N (filter order)			
K	**2**	**3**	**4**	**5**
1	0.843	1.0315	1.1088	1.1468
2	0.6220	1.474	1.3061	1.3712
3		1.0315	1.7703	1.9750
4			0.8180	1.3712
5				1.1468

Table 4.1. Values of elements for a Chebyshev filter with k^2=0.0233

The formulae derived in this section and the element tables, similar to the one above (table 4.1), are sufficient for the design of Chebyshev filters. Nevertheless, filters designed in this fashion are based on alternative occurrence of series and parallel elements as shown in figure 4.2. At microwave frequencies such networks are not very practical because they are difficult to manufacture from microwave elements. An impedance transformation is necessary to convert the filter into an equivalent circuit with only parallel cascaded tuned circuits or to convert the filter into one containing only series elements. This impedance transformation is achieved through the use of impedance and admittance inverters [5], [6], [7] which are useful for filters with narrow bandwidths (<10%).

An impedance inverter is an ideal quarter-wave transformer. Without going into too much detail, figure 4.3 shows the operation of the inverter for parallel and series transformation. Figure 4.3.a and figure 4.3.b show the general case scenario, while Fig.4.3.c shows the simplest form of inverter constructed by using a $\lambda/4$ line with the appropriate characteristic impedance. Figure 4.3.d shows another type of impedance inverter in which an inductive element is transformed into capacitive circuit by the correct selection of line lengths. The $\theta/2$ sections are generally required to be negative for this type of inverter but this is not a problem since they can be incorporated into the design by connecting transmission lines on either side of the circuit.

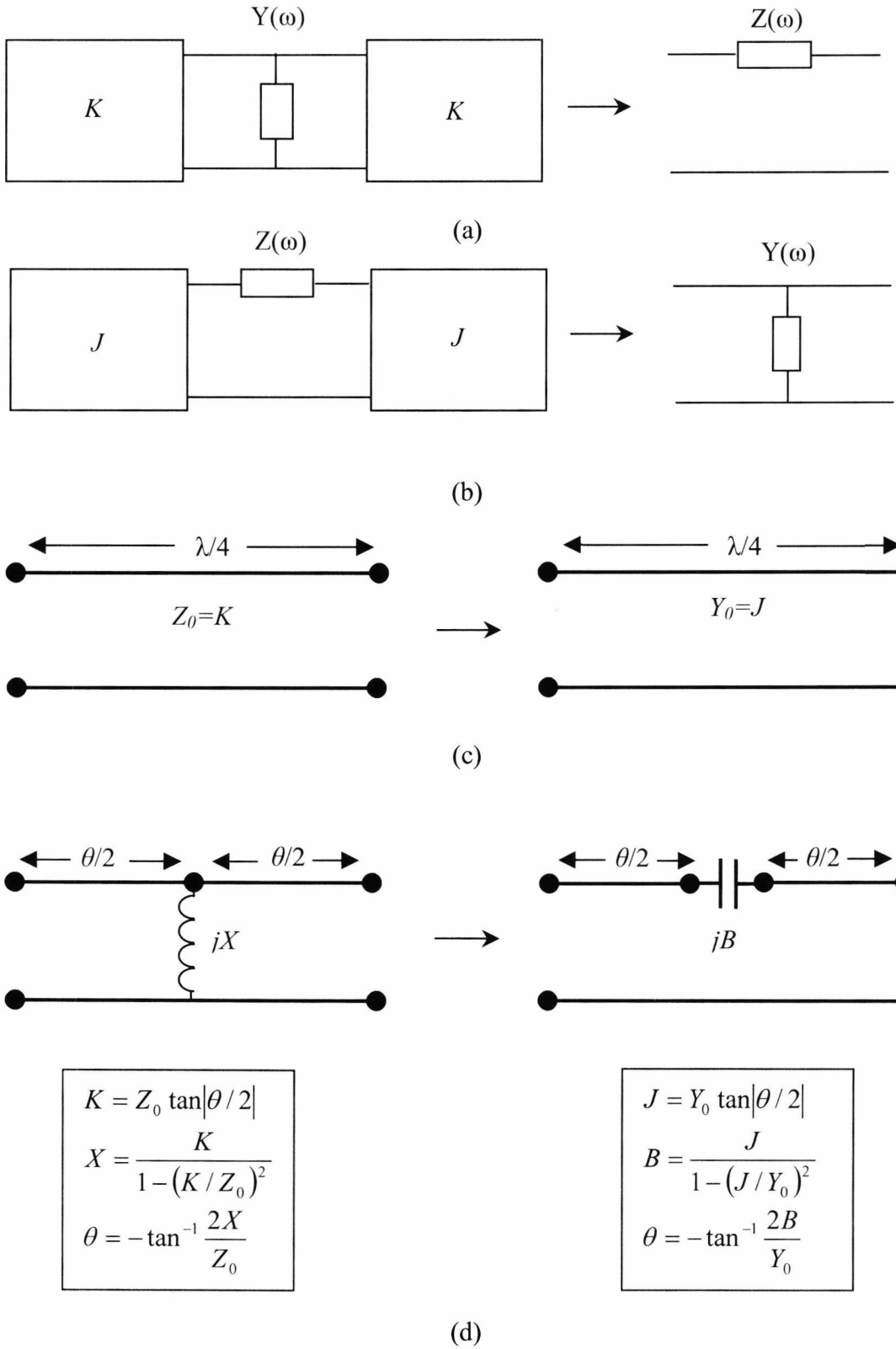

Figure 4.3. Impedance and admittance inverters. a) Operation of impedance and admittance inverter, b) Inverters using quarter-wave transformers, c) Implementation using transmission lines and reactive elements.

4.2 Resonators for Microwave filters

We mentioned in the beginning of the chapter that introducing diaphragms or other form of discontinuities, inside a waveguide produces attenuation characteristics at certain frequencies. The filtering property of the loaded waveguide is based on the resonating cavity between each of the two diaphragms. For that reason we refer to the structures as *Series Resonators.* A first approach to the theory behind these circuits is based on the equivalent circuit of figure 4.4. The rectangular waveguide of figure 4.4.a has been loaded with two inductive diaphragms with normalized susceptance $-jB_k$. The exact equivalent circuit is shown in figure 4.4.b. To design a filter we need to replace the exact equivalent circuit by an approximate shunt circuit. Mumford has proved that an equivalent circuit such as the one shown in figure 4.4.c has the same frequency characteristics as the exact circuit over a narrow band [8]. The type of filter designed by Mumford is referred to as *Quarter-Wave Cavity Filter* as there is a single *quarter-wave coupling line* every two adjacent cavities. Formulae for the calculation of shunt susceptances and the physical length of the coupling lines are given by Mumford.

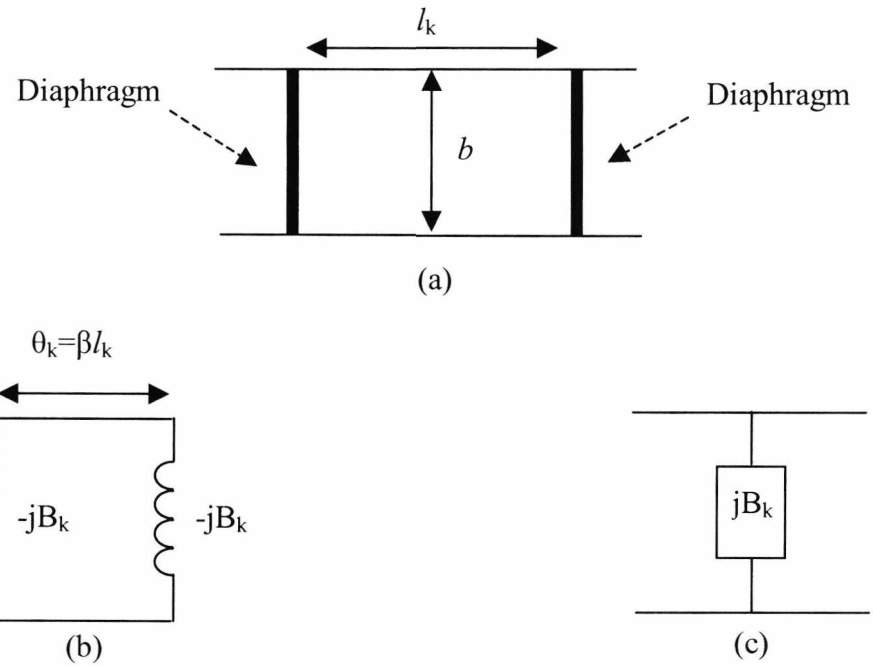

Figure 4.4. a) rectangular waveguide loaded with two diaphragms to form a cavity, b) exact equivalent circuit, c) approximate equivalent circuit

A second, more efficient approach to the design of microwave filters is given by Cohn [9] in his paper on *Direct Coupled Cavity filters.* This type of filter is more compact than the corresponding quarter-wave-coupled cavity filter and hence is the type that we prefer throughout this thesis. The filters are accurate for bandwidths up to 20 percent.

The design of *Direct coupled cavity filter* is based on the use of the ladder network and the equivalent circuit of figure 4.5. The circuit shown in figure 4.4.a can be represented using a Π network using inductive susceptances at each end. The two susceptances B= -cot(θ_k/2) can be neglected because the value of B_k is large and θ_k is close to π.

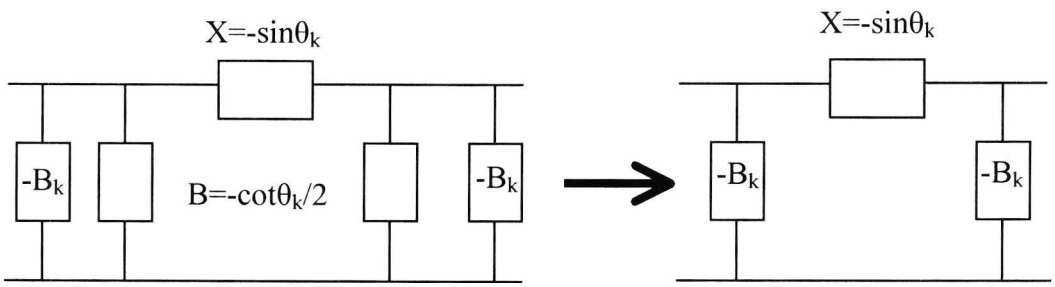

Figure 4.5. Equivalent circuit for waveguide cavity

For impedance inverters Cohn uses the shunt inductive reactances plus the two short sections of waveguide shown in figure 4.6. The use of impedance inverters is quite common in filters, especially those with narrow bandwidths. For practical purposes we always prefer to use circuits of only shunt or series elements. In cases where both series and shunt elements are present impedance inverters are used to simplify the circuit.

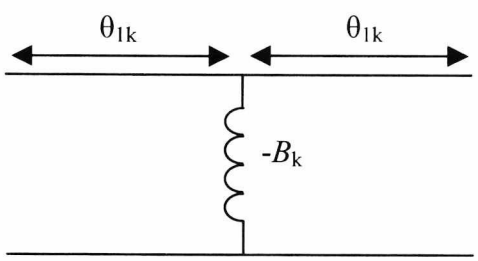

Figure 4.6. Impedance-inverted equivalent circuit for waveguide cavity

Where

$$\theta_{1k} = -\frac{1}{2}\tan^{-1}\frac{2}{B_k} \tag{4.10}$$

and

$$B_k = \frac{1-K^2}{K} \tag{4.11}$$

K is the characteristic impedance of the quarter wave impedance inverter.

The expressions that follow are applicable for a bandwidth of 20%. Also, in the vicinity of $\omega = \omega_0$ where $\theta_k = \pi$, the series reactance X is given by:

$$X = \sin\theta_k = \sin(\theta_k - \pi + \pi) = -(\theta_k - \pi) = -(\beta - \beta_0)l = \frac{\beta_0 - \beta}{\beta_0}\pi = -\frac{\pi}{2}\left(\frac{\beta}{\beta_0} - \frac{\beta_0}{\beta}\right) \tag{4.12}$$

The negative lengths of the impedance inverters are incorporated into the design as part of the cavity length. The physical length of the k_{th} cavity becomes.

$$l_k = \frac{\lambda_{g0}}{2} + \frac{\lambda_{g0}}{2\pi}(\theta_{1k} + \theta_{1k+1}) \tag{4.13}$$

The total equivalent circuit becomes:

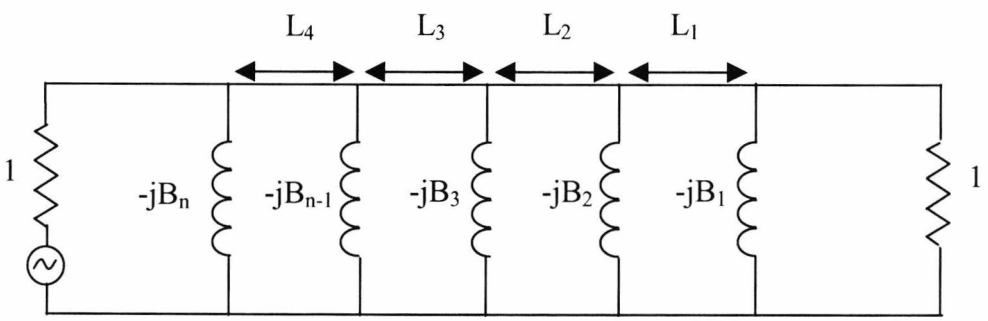

Figure 4.7. Direct coupled cavity filter

Design equations for the filter are given by Cohn over 20 percent band

$$B_1 = \frac{1-\omega/g_1}{\sqrt{\omega/g_1}} \tag{4.14}$$

$$B_2 = \frac{1}{\omega}\left(1-\frac{\omega^2}{g_1 g_2}\right)\sqrt{g_1 g_2} \tag{4.15}$$

$$B_k = \frac{1}{\omega}\left(1-\frac{\omega^2}{g_k g_{k-1}}\right)\sqrt{g_k g_{k-1}} \tag{4.16}$$

$$B_N = \frac{1-\omega R/g_{N-1}}{\sqrt{\omega R/g_{N-1}}} \tag{4.17}$$

Where

$$\omega = \frac{\pi}{2}\frac{\beta_2-\beta_1}{\beta_0} \tag{4.18}$$

and g_k are the element values from the prototype filter.

The length of the k_{th} cavity at $b=b_o$ is given by:

$$l_k = \frac{\lambda_{g0}}{2} - \frac{\lambda_{g0}}{4\pi}\left(\tan^{-1}\frac{2}{B_{K+1}} + \tan\frac{2}{B_k}\right) \tag{4.19}$$

Although the value of l_k can be easily found from λ_{go} and the B values, it cannot be used in filter realization as it is. To obtain the correct values of lengths we need to consider the negative lengths given by 4.13. The final corrected values are given by the subtraction of 4.13 from 4.19.

4.2.1 Direct coupled cavity filters on folded waveguides

We have seen how rectangular waveguides, set up with diaphragms or some other form of discontinuity, can have filtering properties. In this section we describe how, following the same principle, we can introduce discontinuities inside a folded waveguide and create a filter with controllable response.

The type of discontinuity used in this case is short circuits in the transmission line of the folded waveguide type 2, figure 4.8.

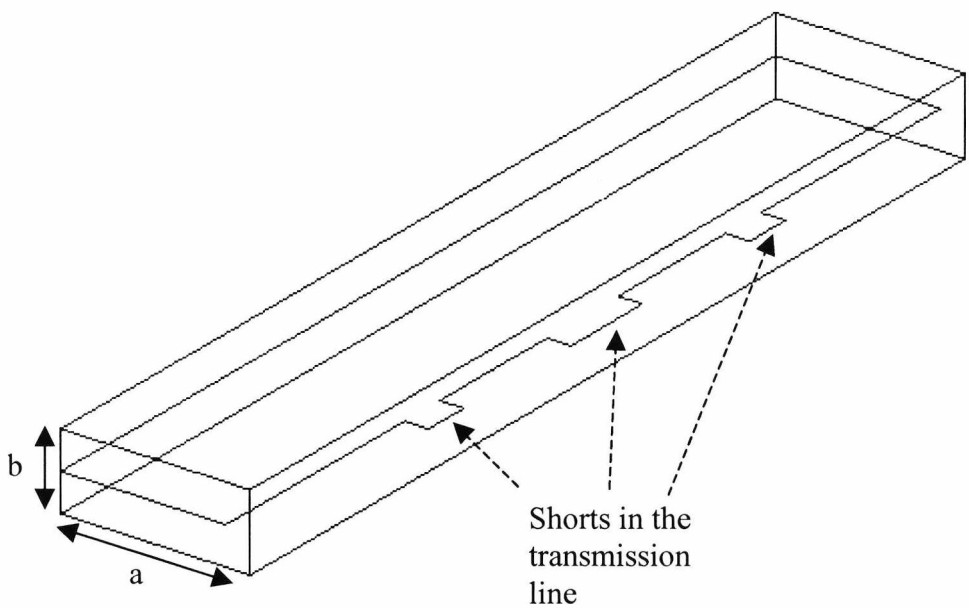

(i)

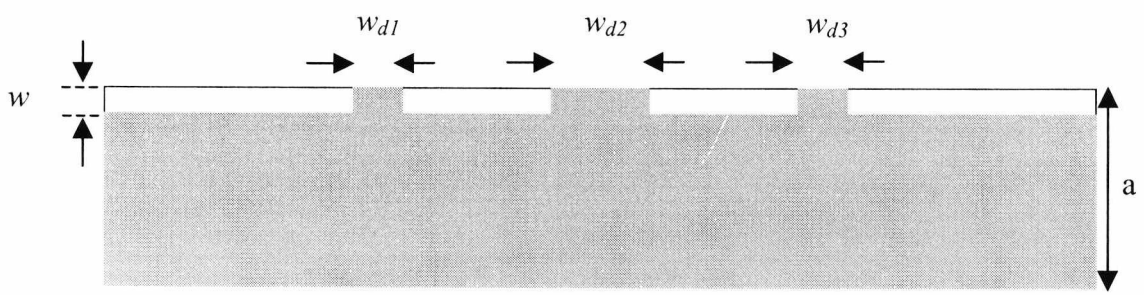

(ii)

Figure 4.8. Filter using the folded waveguide discontinuities. (i) 3D view (ii) Top view

The study of filter design relies on finding the exact position and length of each of the discontinuities such that the desired response can be obtained. The analysis begins with calculating the parameters of a single discontinuity first. We design a short section of folded waveguide that contains a single discontinuity of variable length w_d, figure 4.9. From an electromagnetic point of view, the discontinuity in the folded guide is similar to a short circuit in the centre of a rectangular waveguide. We therefore treat these discontinuities in the equivalent circuit as shunt inductors. Figure 4.10 justifies this statement as it plots the S-parameters of a short circuit inside the folded guide. At low frequencies the signal transmission is minimal while, at high frequencies, the waveguide becomes transparent similar to a shunt inductor.

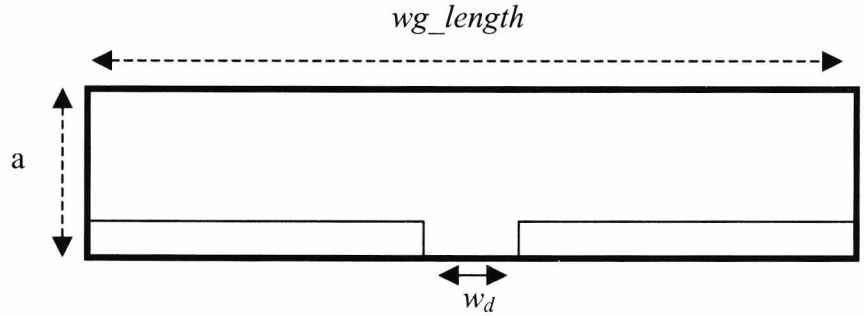

Figure 4.9. Folded guide with a single discontinuity.

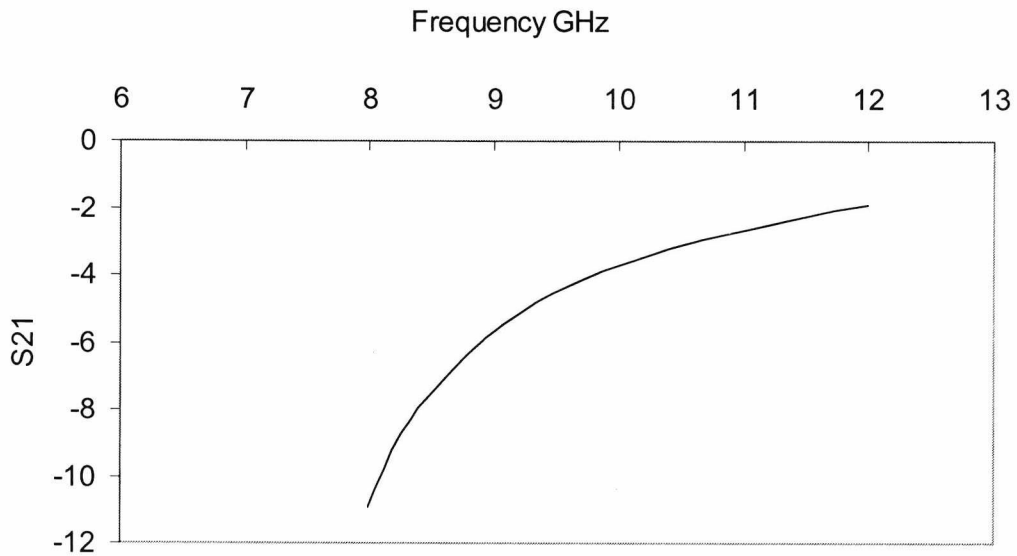

Figure 4.10. The transmission properties of a single discontinuity inside a folded guide are similar to those of a shunt inductor. Waveguide f_c=7.6 GHz used a= 7.875 mm, b=3.15 mm, discontinuity length w_d = 1.6 mm, gap with w= 2 mm,

The most important step in the design of folded filters is the combination of Cohn's expressions with simulated results. More specifically, given the proper specifications and using equations 4.14 through 4.18 we calculate the B values and the required lengths L for the cavities of the filter. Then the module of figure 4.9 is repeatedly simulated using high a frequency electromagnetic package for different values of w_d until we can obtain a graphical representation that associates w_d to θ. The parameter θ is the phase shift caused by the sections of lines surrounding the discontinuity in the folded guide. We cannot calculate θ directly from HFSS but we can derive an expression for its value using standard methods of scattering coefficients and circuit analysis. Consider the equivalent circuit of figure 4.11.

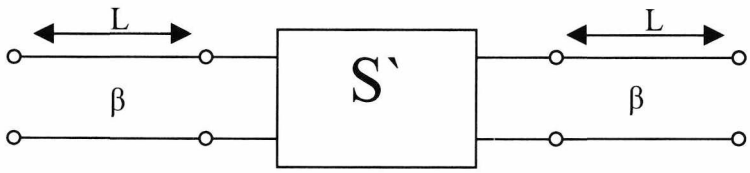

Figure 4.11 Two-port device represented by S-parameter matrix

where β is the propagation constant of the folded guide. The sections of line L just give phase delay. We can write for S`:

$$S' = Se^{2j\beta L} = \begin{bmatrix} S_{11} & S_{12} \\ S_{21} & S_{22} \end{bmatrix} e^{2j\beta L} \tag{4.20}$$

We have already discussed in the previous pages that S` is assumed to be of the form:

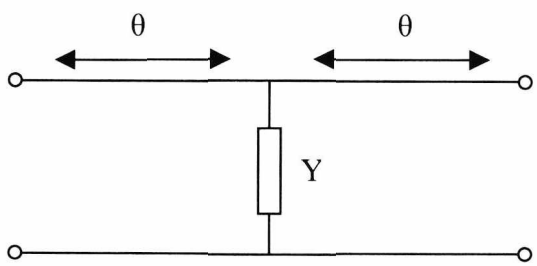

Figure 4.12. Shunt admittance Y

We have

$$S' = \begin{bmatrix} \frac{-Y}{2+Y} & \frac{2}{Y+2} \\ \frac{2}{Y+2} & \frac{-Y}{2+Y} \end{bmatrix} e^{-j2\theta} \tag{4.21}$$

where Y has been normalized to the characteristic admittance of the waveguide. Therefore in terms of the simulated S parameters

$$\begin{bmatrix} S_{11} & S_{12} \\ S_{21} & S_{22} \end{bmatrix} = \begin{bmatrix} \frac{-Y}{2+Y} & \frac{2}{Y+2} \\ \frac{2}{Y+2} & \frac{-Y}{2+Y} \end{bmatrix} e^{-j2\theta - j2\beta L} \tag{4.22}$$

We assume that the admittance Y is a shunt inductor

$$Y = -jB \tag{4.23}$$

Then for the S-parameters it is

$$S_{11} = \frac{jB}{2-jB} e^{-2j(\theta+BL)} \tag{4.24}$$

and

$$S_{21} = \frac{2}{2-jB} e^{-2j(\theta+BL)} \tag{4.25}$$

therefore, for the amplitudes, it is

$$|S_{11}| = \frac{B}{\sqrt{4+B^2}} \tag{4.26}$$

and

$$|S_{21}| = \frac{2}{\sqrt{4+B^2}} \tag{4.27}$$

dividing the last two equations gives

$$B = 2\frac{|S_{11}|}{|S_{12}|} \tag{4.28}$$

Hence the value of B can be easily calculated from simulation using HFSS or other electromagnetic package. Now

$$\frac{jB}{2-jB} = \frac{Be^{j\pi/2}}{\sqrt{4+B^2} * e^{-j\phi}} \tag{4.29}$$

where

$$\phi = \tan^{-1}\left(\frac{B}{2}\right) \tag{4.30}$$

Which gives

$$S_{11} = \frac{B}{\sqrt{4+B^2}} e^{j(\pi/2+\phi-2\theta-2\beta L)} \tag{4.31}$$

For the phase of S_{11} we have

$$\angle S_{11} = \pi/2 + \phi - 2\theta - 2\beta L \tag{4.32}$$

and finally for the phase

$$2\theta = \pi/2 + \tan^{-1}\left(\frac{B}{2}\right) - \angle S_{11} - 2\beta L \tag{4.33}$$

or

$$2\theta = 0 + \tan^{-1}\left(\frac{B}{2}\right) - \angle S_{21} - 2\beta L \tag{4.34}$$

Thus

$$\theta = \frac{\pi}{4} + \frac{1}{2}\tan^{-1}\left(\frac{B}{2}\right) - \frac{1}{2}\angle S_{11} - \beta L \tag{4.35}$$

or

$$\theta = \frac{1}{2}\tan\left(\frac{B}{2}\right) - \frac{1}{2}\angle S_{21} - \beta L \tag{4.36}$$

The values of S-parameters and B can be calculated through simulation. In HFSS the angle θ is calculated in degrees. So the above equations need to be converted from radians to degrees. Then

$$\theta = (90 + a\tan(B/2) - s11\_ph - 2*g\_im*wg\_l/2*1e-3*180/\pi)/2 \tag{4.37}$$

where *s11_ph* is the phase of S_{11}, *g_im* is the magnitude of the imaginary part of the propagation constant of the dominant mode in the folded guide, *wg_l* is the total length of the module circuit of figure 2.

4.2.2 Filter design in the X band

In this section we design a 5% percent Chebyshev passband filter based on the folded waveguide analysis that we have already explained.

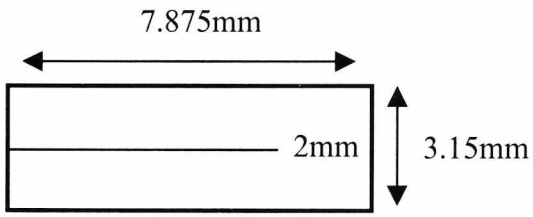

Figure 4.13. Folded guide type 2

The bandwidth of the waveguide in figure 4.13 is from 7.6 GHz to 12.9 GHz and the centre frequency is estimated to be at 10.25 GHz. In that frequency of operation the wavelength inside the folded waveguide is 29 mm. Since the filter has 5% bandwidth we calculate the propagation constants at plus and minus 2.5% of the centre frequency i.e. at β_1 (9.993 GHz) = 199.046 rad/m and β_2 (10.50 GHz) = 223.112 rad/m. We prepare an elementary circuit in the dimensions of the folded waveguide and an arbitrary length of discontinuity. The circuit is simulated repeatedly at the centre frequency for different lengths of w_d and the following plots are obtained:

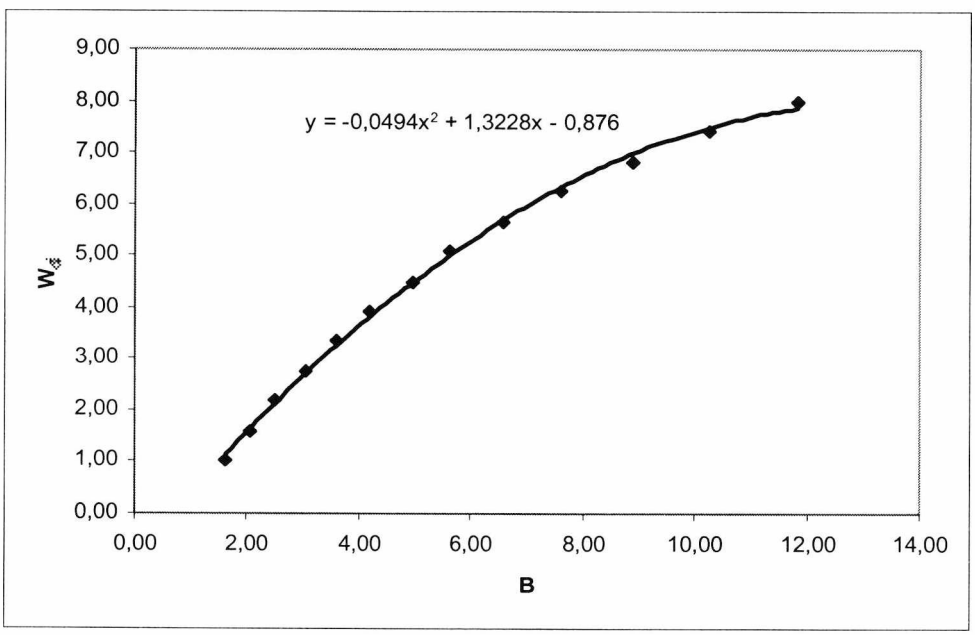

Figure 4.14. Simulated results, w_d versus B (from equation 4.28)

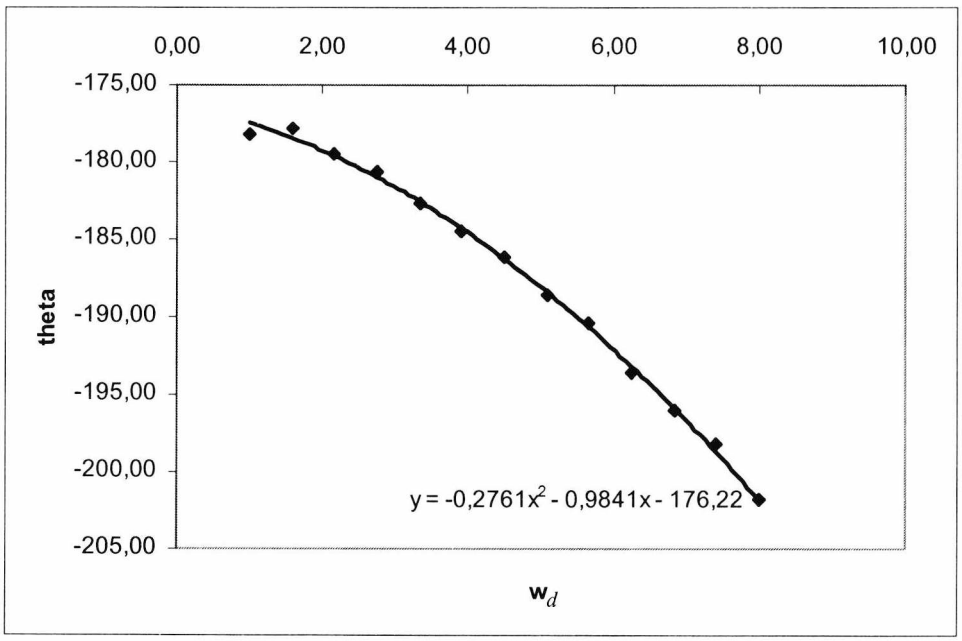

Figure 4.15. Simulated results, *theta* (θ) versus w_d

We now calculate the inductor values of a ladder network representing a filter with N=5 and ripple=0.1.

B	Required Resonator Length (mm)
2.1364	12.5
6.8645	13.7
9.0869	13.9
9.0869	13.7
6.8645	12.5
2.1364	

Table 4.2. B values and required lengths for the X-band filter

Using the simulated results and the formulas derived from excel we get the values required for the filters.

w_d(mm)	Θ
1.7178	-1.262
5.861	-11.538
7.050	-16.955
7.050	-16.955
5.861	-11.538
1.7178	-1.262

Table 4.3. Length of discontinuities and theta values

The only step left is the correct resonator lengths. We know that the lengths that we have calculated are not accurate because they do not include the negative lengths of the impedance inverters. The negative lengths are absorbed as part of the cavity length and are calculated through equation 4.13. Subtracting these values from table 4.3 gives the corrected values of lengths. Hence table 4.4 summarizes the results of the analysis.

B	Resonator Length(mm)	Correct Resonator lengths
2.1364	12.5	13.35
6.8645	13.7	16.05
9.0869	13.9	16.7
9.0869	13.7	16.05
6.8645	12.5	13.35
2.1364		

Table 4.4. B values and corrected resonator lengths

Using the above table as a guideline, we design the microwave filter of figure 4.17 and its response is shown in figure 4.16. The resonator lengths are measured between the centres of the discontinuities. Two extra parts of folded waveguide have been included at each side to allow for the smoother excitation of energy into the

filter. The length of these parts is left to the designer's discretion. In any case however they should not be much shorter than λ/4. The filter has been simulated and the results are shown in figure 4.16.

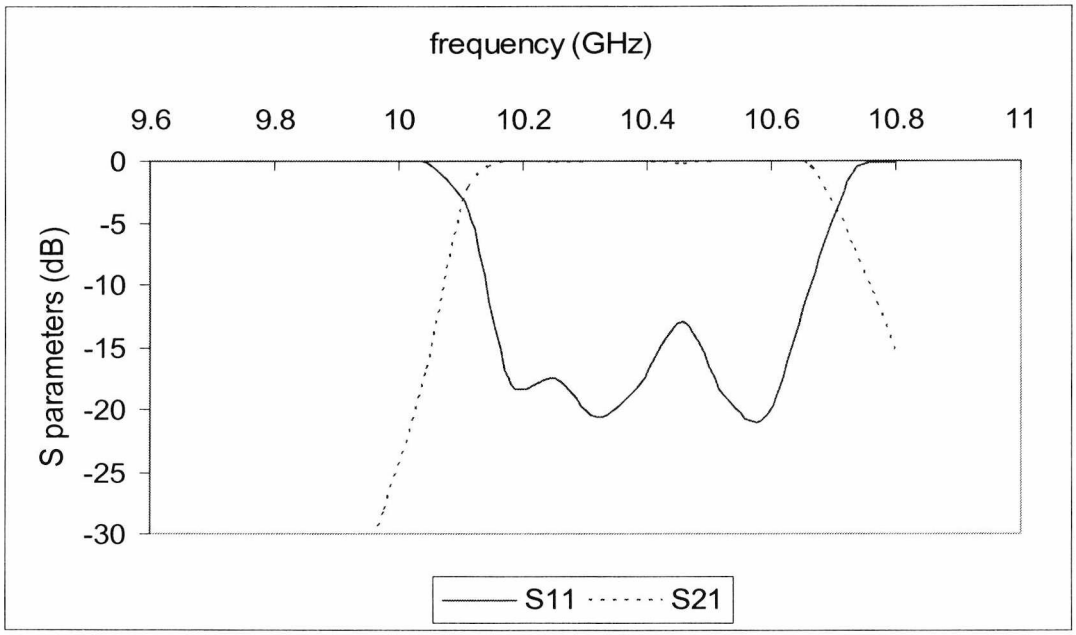

Figure 4.16. Frequency response of the microwave filter of figure 3.

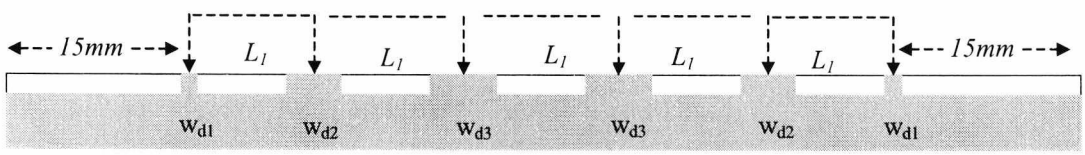

Figure 4.17. The final form of filter. Length=115 mm; the values of 15 mm are arbitrary. Although, it is preferable to keep these sections as short as possible to avoid extra losses.

Filter design for type 1 folded guide is the same as for type 2. The only difference is the structure for simulation. We have two short circuits one for each side, but we treat them as one, figure 4.18. The entire procedure is then identical to the one described until now.

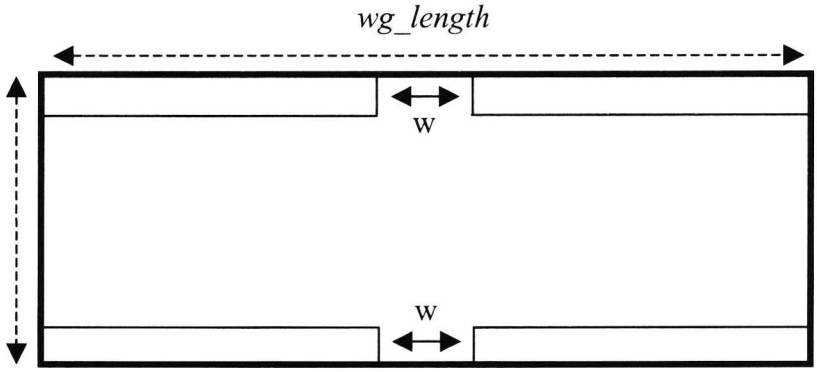

Figure 4.18. The module for T-Type filter

4.3 Filter Realization-Fabrication

So far we have achieved the design of microwave filters using short circuits in the transmission line of a folded waveguide. The principle of operation is based on the theory of *direct coupled cavity resonators* and is very flexible, allowing the user to manufacture a filter at virtually any centre frequency. Since the analysis up to this point has been theoretical, this section deals with the practical realization of filters and discusses the fabrication aspects. Furthermore we discuss the materials used and any limitations that might arise during fabrication. The fabrication method is similar for both types of folded guide, so anything that is mentioned in the next pages for type 2 applies for type 1 as well.

4.3.1 Fabrication method

The filters analyzed in the previous section are built inside folded waveguides made of conducting walls. Instead of using conducting walls at the two sides of the guide we use series of vias which, as we have seen in the previous chapter, completely isolate the field in the space between them.

Using the vias method might look simple at first. The most obvious solution that comes to mind is the direct substitution of the side walls with two series of vias. However simulated results have shown that this method is not feasible for practical reasons. Because the exact length of each discontinuity in the folded waveguide is of critical importance for the correct response of the filter, the series of vias perturb

those lengths and effect the position of the passband. Figure 4.19 demonstrates this manufacturing limitation, focusing on a single discontinuity of a microwave filter. The patch itself is defined by chemical etching and is therefore made at high precision. However the length of discontinuity in Figure 4.19.i is dependent on the number of vias that the patch is touching and therefore is different compared to that of Figure 4.19.ii; L1≠L2. Since a microwave filter requires 4 or 5 discontinuities, immediately this method becomes impractical.

The solution to the discontinuity problem is to introduce a metal patch surrounding the series of vias. The patch extends 250 microns at either side of the via wall and forms accurate lengths of discontinuities. Figure 4.19.iii demonstrates this new addition on a single discontinuity.

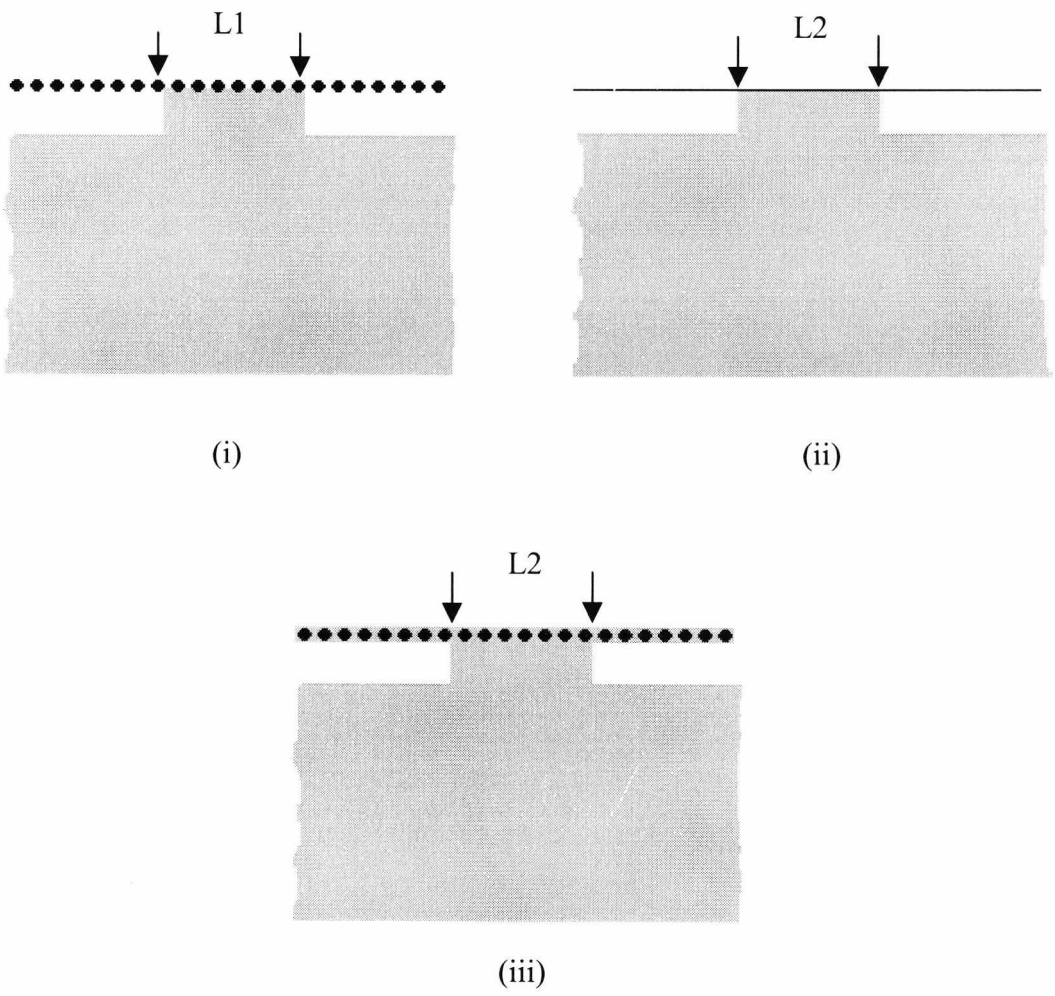

Figure 4.19. Top view of i) Waveguide using vias, ii) Conductive wall iii) The solution to the via problem. A patch surrounds the series of vias and delivers precise lengths of discontinuity

Using this patch method we fabricated a filter, type 2, from microwave laminates of $\varepsilon_r = 2.33$. The filter was excited using asymmetrically tapered microstrip line like the one used in chapter 2. The microstrip with was adjusted to 2.5 mm for 50 Ohms input impedance. The taper length has been optimised to 5.2 mm for minimum return loss. The folded guide specifications are width=7.75 mm, height=3.15 mm and gap=0.9 mm. The frequency of operation is the X band.

The filter was measured using an Anritsu 37392C network analyzer with coaxial calibration. Figure 4.20 shows the measured and simulated result of the filter. The return loss is a bit worse than expected because adapters, SMA connectors, stripline feeds and tapered transition were not de-embedded from the measurement. We also note that the response is shifted to a slightly higher frequency than the design value but this is probable due to variations in the dielectric constant of the substrate and the crude fabrication technique. Overall the theoretical and measured results are in good agreement.

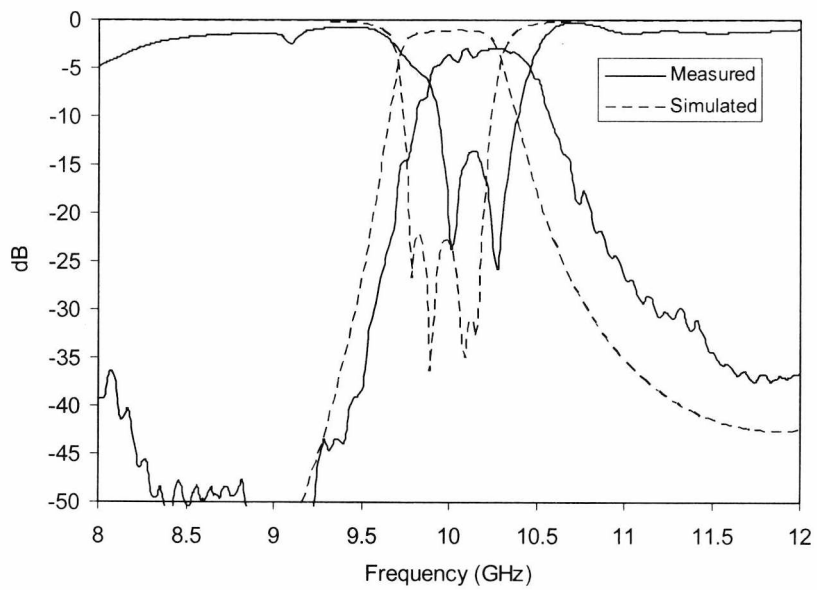

Figure 4.20. Measure and simulated response of Folded microwave filter

4.3.2 Fabrication of filters using thick films

We have seen the fabrication of folded filters using conventional PCB drilling techniques. This method, although it is low cost and efficient it has a few drawbacks, such as low frequency of operation and large size of filters. For example the folded

filter of type 2 proved to be 115 mm and that is quite long for today's microwave standards.

To overcome these manufacturing limitations we can use the thick film fabrication method to design microwave filters of minimal dimensions. Thick films, already discussed in chapter 3, deliver well defined conductor edges, nearly vertical walls, and smooth upper surfaces. Hence they are ideal for folded filters at high frequencies.

We have designed folded filters of both types and sent them for thick film fabrication at the University of Surrey. Unfortunately. At the time that this thesis was written the filters were not ready and hence we could not present any measured results. We do however present a simulated graph of return loss for such a filter. The filter is type 2 and the centre frequency of operation is 77 GHz. The bandwidth is 5% i.e. 2.5% either side of the centre frequency. Bearing in mind that the graph includes losses the results look promising since, for most of the bandwidth S_{11} is lower than -15dBs

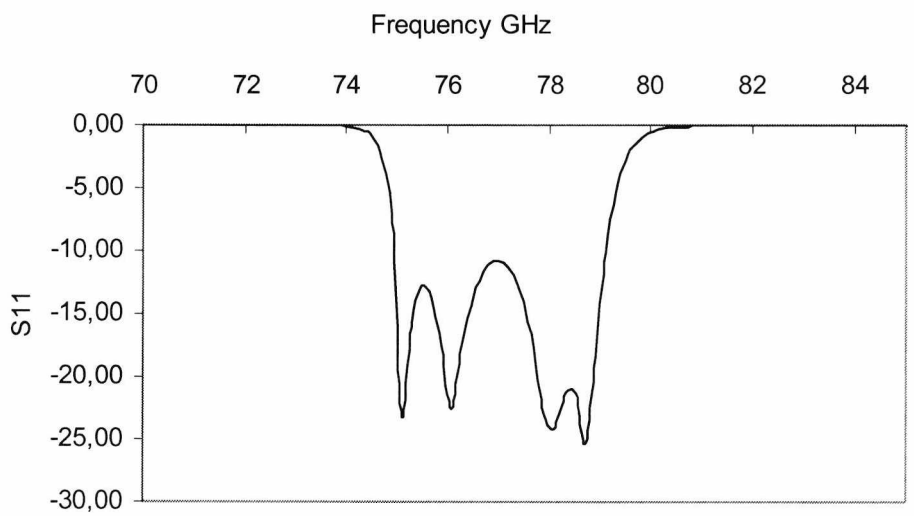

Figure 4.21. Filter response at 77GHz, 5th order, length=4.78mm, width=0.5mm, Simulation includes losses

4.4 Summary

The folded waveguides of chapter 2 form the basis for a new class of folded-based components. In this chapter we presented substrate integrated folded filters. The

filters are formed by introducing discontinuities in the transmission line of the folded guide, thus creating succession of resonating cavities with controllable response.

Although both types of folded guide are suitable for filter design, we prefer type 2 mainly due to its manufacturing simplicity using conventional PCB technology. Furthermore, as we already discussed in chapter 3 for the folded waveguides, folded filters can be manufactured using thick films and LTCC methods.

Unlike other substrate integrated filters the characteristics are determined purely in terms of the metallization on a planar layer which can be accurately defined using photolithography. Furthermore, the filter is at least half the width of other substrate integrated waveguide filters. Since multilayer fabrication is becoming more and more common place, folded waveguides may provide a valid miniaturized alternative to other types of filters.

References

[1] David M. Pozar, "Microwave engineering" 3rd edition, John Wiley and sons Inc. Copyright 2005.

[2] Robert E. Collin "Foundations for microwave engineering" The IEEE press series on electromagnetic wave theory, John Wiley and sons, Classic Reissue 2001

[3] V. Belevitch, "Chebyshev Filters and Amplifier networks", Wireless Eng., vol. 29, pp.106-107, April 1952

[4] L. Weinberg, "Network Design by use of modern Synthesis Techniques and Tables", *Proc. Natl. Electron*, Conf., vol 12, 1956

[5] G. L. Matthaei, L Young and E. M. Jones, "Microwave filters, Impedance-Matching Networks and coupling Structures", Artech House, Dedham, Mass., 1980

[6] W.A Davis, "Microwave Semiconductor Circuit design, Van Nostrad Reinhold, N. Y., 1984

[7] S. B. Cohn, "Parallel- Coupled Transmission –Line –Resonator Filters" *IRE Trans Microwave Theory and techs*, vlo. MTT-6, pp. 223-231, April 1958.

[8] W.W. Mumford, "Maximally flat Filters in Waveguides", *Bell System Tech. J.* vol. 27 pp.684-714, October1948

[9] S. B. Cohn, "Direct Coupled Resonator Filters", *Proc. IRE*, vlo 45, pp. 187-196, February, 1957

[10] M. S. Aftanasar, P. R. Young, I. D. Robertson, J. Minalgiene and S. Lucyszyn, "Photoimageable thick-film millimetre-wave metal-pipe rectangular waveguides," *Electron. Lett.*, vol. 37, No. 18, August 2001, pp. 1122-1123.

5. The Non-Radiative Dielectric waveguide (NRD) and the perforated NRD (NRPD)

In chapter 1, we talked about the about the Non-Radiative dielectric waveguide (NRD) and the increased role that it plays in Microwave applications. This chapter presents an analysis of the NRD guide and then proceeds to a new type of waveguide which we name NRPD. The new structure is based on NRD principles but employs the volume averaged permittivity method and poses significant manufacturing superiority over its conventional counterpart. In order to analyze the NRD we consider the simplest form of dielectric waveguide, the dielectric slab.

5.1 The slab waveguide theory

The slab waveguide is essentially a dielectric slab, infinite in the y and z directions, that guides the energy in the positive z direction, Figure 5.1. The slab has a permittivity ε_1 and it is surrounded by a material of lower permittivity ε_2. The structure operates on the principle of total internal reflection at the boundary between the two different dielectrics.

We begin the analysis by writing expressions for the electric and magnetic field inside the slab. We consider the time harmonic case $e^{j\omega t}$ where ω is the frequency in radians and t is the time is seconds. Then we have

$$\widetilde{E} = E_s e^{j\omega t} \tag{5.1}$$

and

$$\widetilde{H} = H_s e^{j\omega t} \tag{5.2}$$

where the subscript s denotes function of space

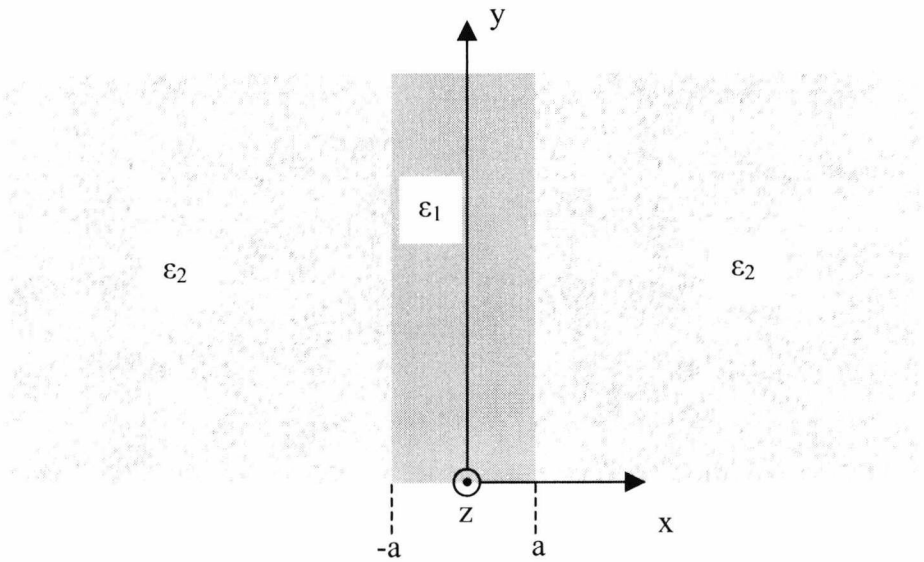

Figure 5.1. The Dielectric slab waveguide, ε_1, inside a dielectric medium ε_2

Maxwell's four equations, from chapter 2, become

$$\nabla \times \mathrm{E} = -j\omega\mu\mathrm{H} \tag{5.3}$$

$$\nabla \times \mathrm{H} = -j\omega\varepsilon\left(1 - j\frac{\sigma}{\omega\varepsilon}\right)\mathrm{E} \tag{5.4}$$

$$\nabla \cdot (\mu\mathrm{H}) = 0 \tag{5.5}$$

$$\nabla \cdot (\varepsilon\mathrm{E}) = 0 \tag{5.6}$$

where the $e^{j\omega t}$ term and the s subscript have been neglected for simplicity. We also assumed that $\rho=0$ since all the media is source free.

We are going to consider the lossless case, $\sigma = 0$. Also the field dependence along the direction of propagation z is of the form $\mathrm{e}^{-\gamma_z z}$, where $\gamma_z = j\beta_z$ is the longitudinal propagation constant. Hence,

$$\mathbf{E}_s = \mathbf{E}(x, y)\mathrm{e}^{-\beta_z z} \tag{5.7}$$

and

$$\mathbf{H}_s = \mathbf{H}(x, y)\mathrm{e}^{-\beta_z z} \tag{5.8}$$

Apart from the direction of propagation z, the transverse field variation of a dielectric slab is assumed to be in the x direction only. Since the guide is uniform and infinite in height the field variation along the y is zero. Hence the above expressions can be simplified as:

$$\mathbf{E}_s = \mathbf{E}(x)\mathrm{e}^{-\beta_z z} \tag{5.9}$$

and

$$\mathbf{H}_s = \mathbf{H}(x)\mathrm{e}^{-\beta_z z} \tag{5.10}$$

Substituting into 5.3 and 5.4 we get

$$j\beta_z E_y = -j\omega\mu H_x \tag{5.11}$$

$$\frac{dE_y}{dx} = -j\omega\mu H_z \tag{5.12}$$

$$-j\beta_z H_x - \frac{dH_z}{dx} = j\omega\varepsilon E_y \tag{5.13}$$

and

$$j\beta_z H_y = j\omega\varepsilon E_x \tag{5.14}$$

$$\frac{dH_y}{dx} = j\omega\varepsilon E_z \tag{5.15}$$

$$-j\beta_z E_x - \frac{dE_z}{dx} = -j\omega\mu H_y . \tag{5.16}$$

The first three equations, 5.11 to 5.13 do not contain electric field component in the z direction or, in other words, the electric field is transverse in the direction of propagation z. These equations define the transverse electric (TE) mode solutions of the dielectric slab. Eliminating H_x and H_z from equations 5.11 to 5.13 gives the characteristic equation for TE mode solutions

$$\frac{d^2E_y}{dx^2} + k_x^2 E_y = 0 \tag{5.17}$$

Following a similar procedure, i.e. eliminating E_x and E_y from 5.14 to 5.16 we get the characteristic equation for the TM modes of the dielectric slab

$$\frac{d^2H_y}{dx^2} + k_x^2 H_y = 0 \tag{5.18}$$

where k_x is the eigenvalue for the transverse propagation constant and it is given by the dispersion relation

$$\varepsilon_r k_0^2 = \beta_z^2 + k_x^2 \tag{5.19}$$

or

$$k_x^2 = \beta_z^2 - \varepsilon_r k_0^2 \tag{5.20}$$

5.1.1 TE mode solutions

Based on the common explanation of guidance, we anticipate that for guided mode solutions the electric and magnetic fields should be evanescent, that is, exponentially decaying as x approaches plus or minus infinity. In the slab region however, the field distribution is of standing-wave nature.

In any case the modes have two types of symmetries: even and odd. For the field profile inside the slab we have

$$E_y(x) = \begin{cases} A_1 \cos(k_{x1}x), & even \quad \text{modes}, \quad for|x| \le -a \\ A_1 \sin(k_{x1}x), & odd \quad \text{modes}, \quad for|x| \le -a \end{cases} \tag{5.21}$$

A_1 is a complex amplitude constant.

and for the field profiles outside the dielectric slab it is

$$E_y(x) = \begin{cases} \pm A_2 \exp[a_d(x+a)], & for \quad x < -a \\ A_2 \exp[-a_d(x-a)] & for \quad x > a \end{cases} \tag{5.22}$$

where A_2 is a complex constant and a_d is a decay constant in the x direction, in the region outside the dielectric slab. From equation (5.12) we get

$$H_z = \frac{j}{\omega\mu}\frac{dE_y}{dx} \tag{5.23}$$

Substituting for E_y from the previous equations we get expressions for the magnetic field of the TE solutions inside the slab:

$$H_z(x) = \begin{cases} -\frac{j}{\omega\mu} k_{x1} A_1 \sin(k_{x1}x) & TE \quad even \quad for \quad |x| \le a \\ -\frac{j}{\omega\mu} k_{x1} A_1 \cos(k_{x1}x) & TE \quad odd \quad for \quad |x| \le a \end{cases} \tag{5.24}$$

The exponentially decaying magnetic field in the region surrounding the dielectric slab is given by

$$H_z(x) = \begin{cases} \pm\frac{j}{\omega\mu} a_d A_2 \exp[a_d(x+a)] & TE \quad for \quad x < -a \\ \pm\frac{j}{\omega\mu} a_d A_2 \exp[-a_d(x-a)] & TE \quad for \quad x > a \end{cases} \tag{5.25}$$

The continuity principle requires the tangential components of the fields to be continuous across the boundaries. Hence

$$E_y(|a^-|) = E_y(|a^+|) \tag{5.26}$$

and

$$H_z(|a^-|) = H_z(|a^+|), \tag{5.27}$$

where the + and – superscripts denote the left and right sides of the $x= \pm a$ boundaries.

Applying the boundary conditions at the $x=a$ boundary yields

$$even \quad \text{modes} \begin{cases} A_1 \cos(k_{x1}a) = A_2 \\ k_{x1} A_1 \sin(k_{x1}a) = a_d A_2 \end{cases} \tag{5.28}$$

$$odd \quad \text{modes} \begin{cases} A_1 \sin(k_{x1}a) = A_2 \\ k_{x1} A_1 \cos(k_{x1}a) = -a_d A_2 \end{cases} \tag{5.29}$$

Dividing the two expressions of (5.28) gives the guidance condition for the TE modes with even symmetry:

$$k_{x1} \tan(k_{x1}a) = \alpha_d \tag{5.30}$$

Similarly, (5.29) gives the guidance condition for TE odd modes:

$$k_{x1} \cot(k_{x1}a) = -\alpha_d \tag{5.31}$$

Squaring equation (5.30) and remembering that $k_{x1}^2 = \varepsilon_1 k_0^2 - \beta_z^2$ and $a_d^2 = \beta_z^2 - \varepsilon_2 k_0^2$ gives the guidance condition for TE even modes:

$$k_{x1}^2\left[1+\tan^2(k_{x1}a)\right]=k_0^2(\varepsilon_1-\varepsilon_2) \tag{5.32}$$

Following the same procedure we get the guidance condition for the TE odd modes

$$k_{x1}^2\left[1+\cot^2(k_{x1}a)\right]=k_0^2(\varepsilon_1-\varepsilon_2) \tag{5.33}$$

where ε_1 and ε_2 are the relative permittivities of media 1 and 2.

Since we have not considered any losses in the waveguide, equations 5.32 and 5.33 are sufficient to provide solutions for each of the propagating modes. However, it is the nature of these equations that does not allow for analytical solution. Instead, a graphical solution is preffered. Equation 5.32 can be rewritten as a second degree polynomial with respect to x:

$$x^2\left(1+\tan^2(x)\right)=k_0^2a^2(\varepsilon_1-\varepsilon_2) \tag{5.34}$$

or

$$x^2\left(1+\tan^2(x)\right)-k_0^2a^2(\varepsilon_1-\varepsilon_2)=0 \tag{5.35}$$

where $x=k_{x1}a$ and ε_1 and ε_2 are the relative values of permittivities.

The general idea in the graphical solution is based on implementing equation (5.35). We develop a programming code which calculates the value of $x^2\left(1+\tan^2(x)\right)$ and plots it against $k_{x1}a$. The programming code uses the *bisection* technique, which does not calculate the exact solution but it gets closer than 99% of the true value. For a given frequency f, the parameter $k_0^2a^2(\varepsilon_1-\varepsilon_2)$ will have a constant value. Since we already know the graph of $x^2\left(1+\tan^2(x)\right)$ versus $x=k_{x1}a$, the graph of $x^2\left(1+\tan^2(x)\right)-k_0^2a^2(\varepsilon_1-\varepsilon_2)$ versus $x=k_{x1}a$ will be the same but shifted downwards by $k_0^2a^2(\varepsilon_1-\varepsilon_2)$. In that case the solutions are the values of x for which $x^2\left(1+\tan^2(x)\right)-k_0^2a^2(\varepsilon_1-\varepsilon_2)=0$. Figure 5.2 shows plots [1] of the right hand side of equations (5.32) and (5.33) where both side have been multiplied by a^2.

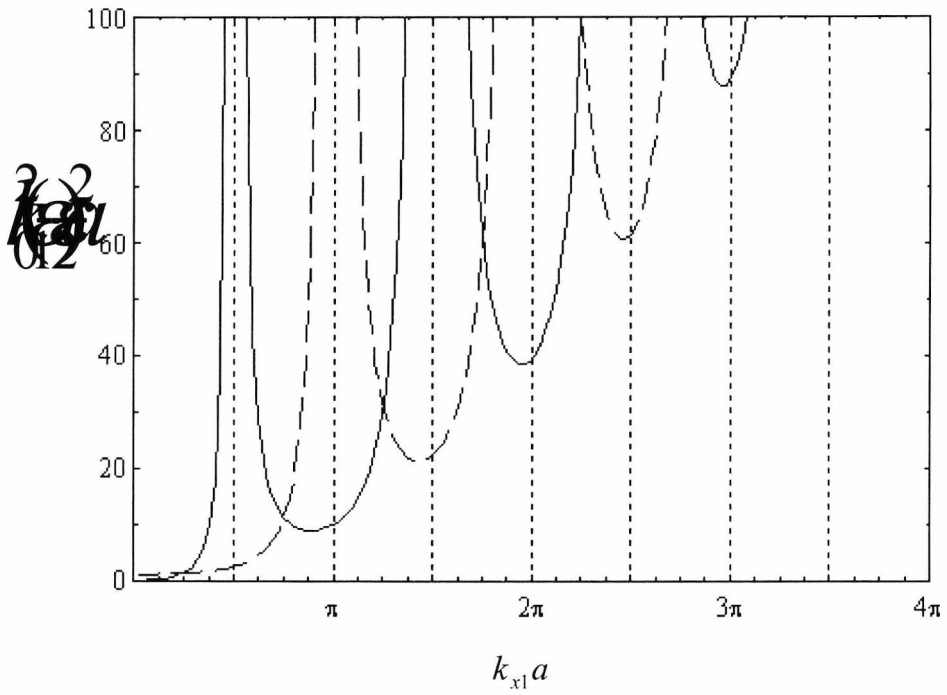

Figure 5.2. Graph of guidance condition for TE slab guide. Solid lines show even mode solutions, dashed lines show odd mode solutions, ε_1=2.07 and ε_2=1

Negative values result in field solutions that diverge away from the guiding region. These so-called improper or leaky modes carry infinite power and are of limited practical significance. The range for which TE even solutions are defined is

$$n\pi < k_{x1}a < \frac{\pi}{2}(2n+1) \qquad n=0, 1, 2, \ldots, m_e\text{-}1$$

where m_e is the number of modes with even symmetry supported by the guide. The range for which TE odd solutions are defined is as follows

$$\frac{\pi}{2}(2n-1) < k_{x1}a < n\pi \qquad n=1, 2, \ldots, m_o$$

where m_o is the number of antisymmetrical modes supported by the guide. The total number of modes the guide supports is given by $m_e + m_o$. In general, TE_n refers to the

(n+1)th mode of the waveguide. For example, TE_0 is the lowest order even mode, TE_1 is the lowest order odd mode, TE_2 is the next highest order even mode, etc.

5.1.2 TM Mode Solutions

The analysis of TM modes is the same. Again, we start by assuming the following field solutions over the three regions

$$H_y(z) = \begin{cases} B_1 \cos(k_{x1}x) & even \quad \text{mod}es, \quad |x| \le a \\ B_1 \sin(k_{x1}x) & odd \quad \text{mod}es, \quad |x| \le a \end{cases} \tag{5.36}$$

The field outside the slab will decay exponentially. Hence,

$$H_y(z) = \begin{cases} \pm B_2 \exp[a_d(x+a)] & even \quad \text{mod}es, \quad x > a \\ B_2 \exp[-a_d(x-a)] & odd \quad \text{mod}es, \quad x < -a \end{cases} \tag{5.37}$$

From equation (4.15) we have

$$E_z = -\frac{j}{\omega\varepsilon}\frac{dH_y}{dx}. \tag{5.38}$$

Therefore, the longitudinal electric field for the TM mode solutions within the guiding region is given by

$$E_z(x) = \begin{cases} \frac{j}{\omega\varepsilon_1} k_{x1} B_1 \sin(k_{x1}x) & even \quad \text{mod}es, \quad |x| \le a \\ -\frac{j}{\omega\varepsilon_1} k_{x1} B_1 \cos(k_{x1}x) & odd \quad \text{mod}es, \quad |x| \le a \end{cases} \tag{5.39}$$

In the surrounding region, the exponentially decaying electric fields are given by

$$E_z(x) = \begin{cases} \pm \dfrac{j}{\omega\varepsilon_2} a_d B_2 \exp[a_{x2}(x+a)] & for \quad x < -a \\ \dfrac{j}{\omega\varepsilon_2} a_d B_2 \exp[-a_{x2}(x-a)] & for \quad x > a \end{cases} \tag{5.40}$$

Applying the continuity principle and following the same steps as for the TE case, we finally obtain the TM guidance condition for even modes:

we obtain, after some work, the guidance condition:

$$k_{x1}^2 \left[1 + \frac{\varepsilon_2^2}{\varepsilon_1^2} \tan^2(k_{x1}a) \right] = k_0^2(\varepsilon_1 - \varepsilon_2) \tag{5.41}$$

Similarly, for the odd modes we obtain

$$k_{x1}^2 \left[1 + \frac{\varepsilon_2^2}{\varepsilon_1^2} \cot^2(k_{x1}a) \right] = k_0^2(\varepsilon_1 - \varepsilon_2) \tag{5.42}$$

Figure 5.3 shows plots of equations 5.41 and 5.42. Again the two sides of the equations have been multiplied by a^2. Even mode solutions are shown as solid lines, odd modes as dashed lines. The range for which TM even and odd mode solutions are identical to that of the TE modes.

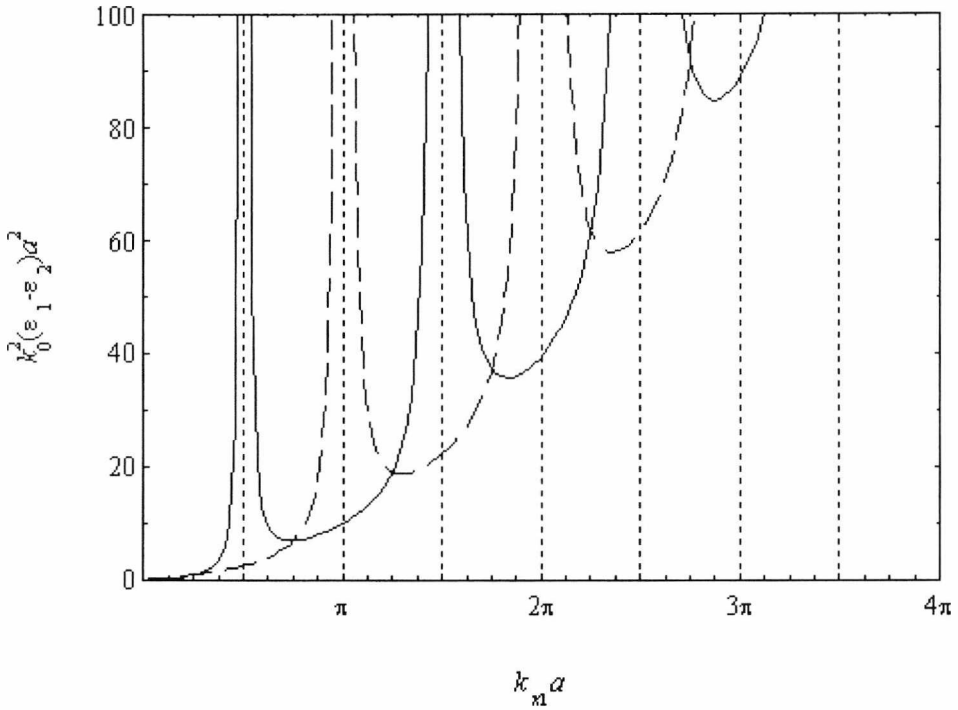

Figure 5.3. Graph of guidance condition for TM slab guide with ε_1=2.07 and ε_2=1. Solid lines show even mode solutions; dashed lines show odd mode solutions.

5.1.3 Dispersion characteristics

We have already seen that, for the lossless case the longitudinal propagation constant of the dielectric slab is given by:

$$\beta_z = \sqrt{\varepsilon_1' k_0^2 - k_{x1}'^2} \tag{5.43}$$

Usually, when analysing dispersion plots of dielectric waveguides we prefer to look at the *effective permittivity* of the structure against frequency. The effective permittivity of the slab is derived as follows:

Squaring (5.43) we get:

$$\beta_Z^2 = \varepsilon_1 k_0^2 - k_{x1}^2 \tag{5.44}$$

then dividing by k_0^2 gives:

$$\frac{\beta_z^2}{k_0^2} = \varepsilon_1 - \frac{k_{x1}^2}{k_0^2} \tag{5.45}$$

the term β_z^2 / k_0^2 is the squared normalized propagation constant of the slab which we also call effective permittivity. By calculating the value of k_{x1} we plot the dispersion characteristics for TE and TM modes of the slab, figure 5.4. We note that the TE modes start to propagate earlier than the respective TM modes. Also, at high frequency, all of the modes are asymptotic to the relative permittivity of the slab. Figure 5.4 gives such an example with ε_r= 9.8.

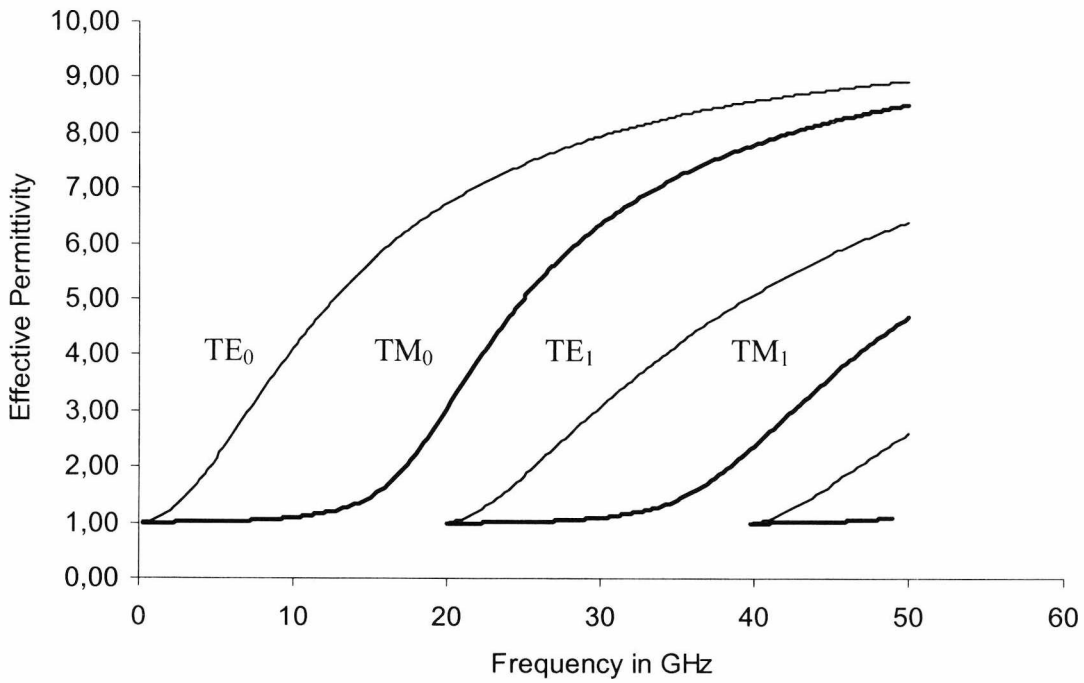

Figure 5.4. Effective permittivity for TE (thin lines) and TM (thick lines) of a slab waveguide with width=2.54 mm, permittivity of slab = 9.8, loss tangent of slab=0.0009

5.2 Introduction to the NRD

The modes that propagate inside the NRD are of the form LSE_{mn} and LSM_{mn}, where the initials LS stand for "longitudinal section" and the third letter denotes either electric or magnetic field; "m" and "n" are indices for the x (horizontal) and y (vertical) variation of the field respectively. The LSEmn mode propagating inside the dielectric slab of the NRD would have its electric field predominantly transverse to the direction of propagation. The same principle applies for the LSM_{mn} mode. For every NRD guide, the LSE_{mn} and LSM_{mn} modes ($n > 0$) are non-radiative as long as the plate separation is less than $\lambda/2$, where λ is the wavelength in the dielectric surrounding the guiding structure (conventionally air). Under these conditions the wave in the surrounding region must be evanescent due to the parallel plate cut-off and no radiation can exist outside the dielectric region. NRD guides exhibit low losses, particularly when operated using the LSM_{11} mode of propagation, which displays a decrease in conduction loss with increasing frequency [2] figure 5.5. It is therefore the benefit of this structure that it is capable of guiding electromagnetic waves around curved sections or discontinuities with potentially no radiation loss.

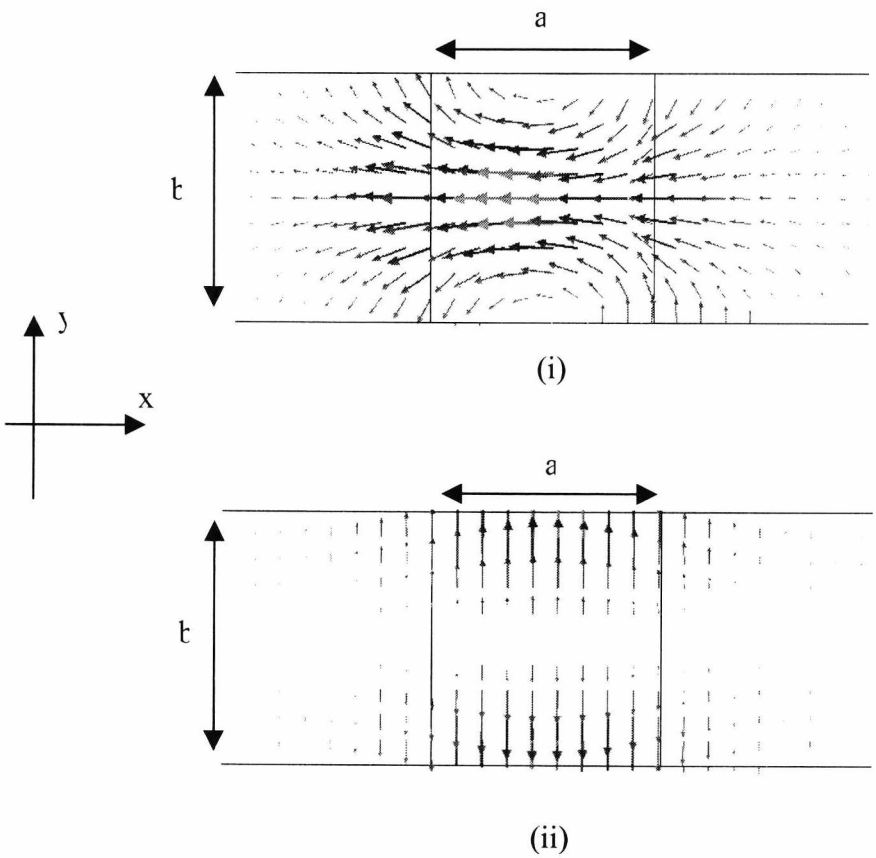

Figure 5.5 Simulated electric field lines in a cross-sectional plane of the nonradiative dielectric waveguide. Modes shown: (i) LSM_{11} (ii) LSE_{11}

5.2.1 Modes inside the NRD

As mentioned in the previous page, modes in an NRD are of the form LSM_{mn} and LSE_{mn}. These modes are not all nonradiative. Only those with field that varies in the vertical axis are confined in the dielectric core and cannot radiate. The modes of an NRD can be divided in four categories:

1) $LSM_{11, 21, 12, 22...}$ modes whose magnetic field varies in both the x and y directions. These modes are all nonradiative. E field along the x axis.

2) $LSE_{11, 21, 12, 22...}$modes whose electric field varies in both the x and y directions. These modes are also nonradiative, with E field along the y axis. However, this field orientation limits their practical use. LSM_{mn} modes are usually preferred to operate the NRD.

3) $LSM_{10, 20, 30, 40...}$ modes whose magnetic field varies along the horizontal but not along the vertical direction. This effectively implies that the electric field does not vary along the vertical axis which, of course, is not possible due to the presence of the metal plates on top and bottom of the NRD. Modes of this form cannot exist inside the NRD because of the top and bottom metal plates. E field along the x axis.

4) $LSE_{10, 20, 30, 40...}$ modes whose magnetic field varies in the x direction but not in y. These modes are radiative and can propagate inside the NRD irrespective of the distance between the metal plates. The presence of these modes can be avoided in the laboratory by selecting the correct excitation method for our NRD. E field along the y axis.

5.2.2 NRD Theory

The analysis of the NRD is an extension to the slab waveguide analysis. In the case of the Slab waveguide, the height of the dielectric sheet is infinite and hence there is no field variation along the vertical axis. In the case of an NRD waveguide, the presence of the top and bottom planes limits both the electric and magnetic fields. By adjusting the propagation constant expression of the slab waveguide appropriately, we derive formulas for the NRD guide. More specifically, the propagation constant of any waveguide is given by the general expression

$$k^2 = k_x^2 + k_y^2 + k_z^2 \tag{5.46}$$

where

$k = k_0\sqrt{\varepsilon_r}$, with k_0 being the propagation constant of the mode in free space and ε_r the effective permittivity of the dielectric waveguide.

For the slab waveguide it is assumed that there is no wave dependence on the vertical axis and hence $k_y^2 = 0$. The above expression is therefore modified for a slab waveguide to the following

$$\beta_z = \sqrt{\varepsilon_2 k_0^2 - k_x^2} \tag{5.47}$$

where the direction of propagation is along z. Also, at low frequencies $k_x^2 << \varepsilon_2 k_0^2$ and therefore equation above becomes

$$\beta_z = k_0\sqrt{\varepsilon_2} \tag{5.48}$$

and the effective permittivity is

$$\frac{\beta_z^2}{k_0^2} = \sqrt{\varepsilon_2} \tag{5.49}$$

which is equal to unity if ε_2=1

Unlike in the case of the slab waveguide, due to the presence of the metal boundaries on top and bottom of the NRD, the k_y^2 parameter is present and its value is given by the expression:

$$k_y = n\frac{\pi}{a} \tag{5.50}$$

where n is the number of half cycle variations, or mode order, and a is the separation between the top and bottom plates [3,4]. The initial expression for the propagation constant of the NRD waveguide now becomes

$$k_z = \sqrt{\varepsilon_2 k_0^2 - kx^2 - \left(n\frac{\pi}{a}\right)^2} \tag{5.51}$$

This expression cannot be solved analytically, but only using a graphical solution as in the case of the dielectric slab. For the purposes of this thesis, specially developed programming code has been used to calculate the cutoff frequencies of the modes inside the NRD. Figures 5.6 to 5.9 plot the dispersion characteristics of all the modes in an NRD guide with slab dimensions b = 6 mm, a=12 mm (b is the half width) ε_1 = 1, ε_2 = 10, where ε_2 is the permittivity of the central slab and ε_1 is the permittivity of the surrounding regions, i.e. air. The plots show effective permittivity (β^2 / k_0^2) against frequency.

The modes of figure 5.8, as mentioned before, can be avoided in the laboratory by careful excitation of the NRD guide. The modes of figure 5.9 do not exist by definition. The presence of the top and bottom plates of the NRD do not allow for such modes to propagate.

We are therefore dealing with the modes of figure 5.6 and 5.7. The mode of operation is LSM_{11} and its cutoff frequency is calculated from figure 5.6 to be 7.6 GHz. The bandwidth of the NRD stops at the cutoff frequency of the next higher order mode which, from figure 5.7, is the LSE_{12} at 10 GHz.

We also notice that the modes of figures 5.6 and 5.7 start with effective permittivity = 0 while the modes of figures 5.8 and 5.9 start with effective permittivity = 1. The explanation for this phenomenon is that for $\varepsilon_{eff}<1$ the modes of figures 5.6 and 5.7 have phase velocity greater than the speed of light. For that reason these modes are also called fast modes.

At very high frequencies, as expected, all of the modes are asymptotic to the permittivity of the dielectric slab ε_2 = 10.

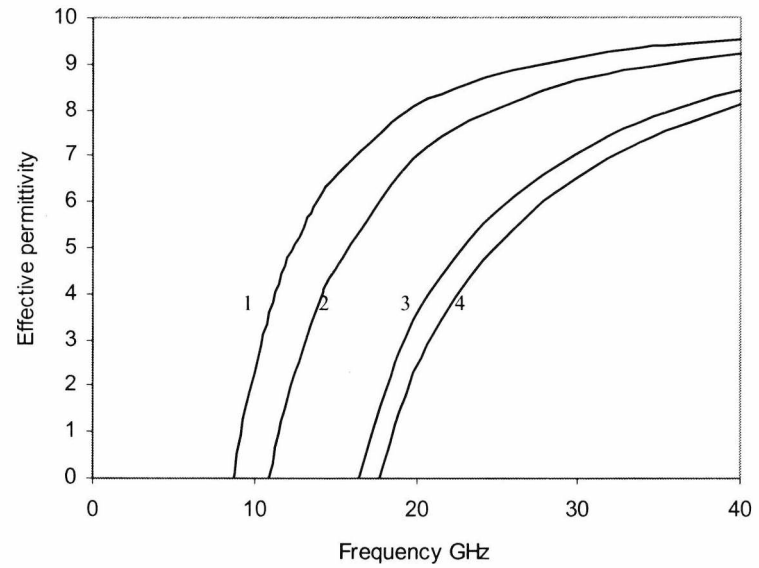

Figure 5.6. Modes of NRD guide. Line 1:LSM_{11}, 2: LSM_{12}, 3: LSM_{21}, 4: LSM_{22}

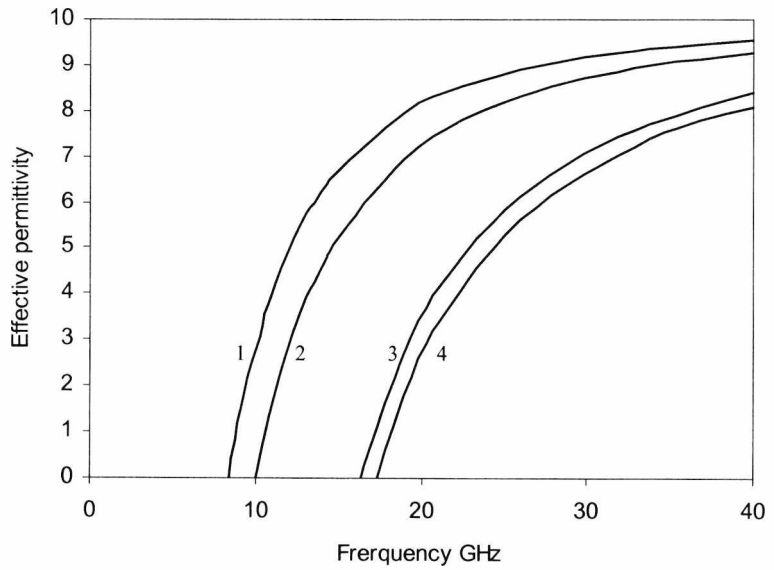

Figure 5.7. Modes of NRD guide. Line 1:LSE_{11}, 2:LSE_{12}, 3:LSE_{21}, 4:LSE_{22}

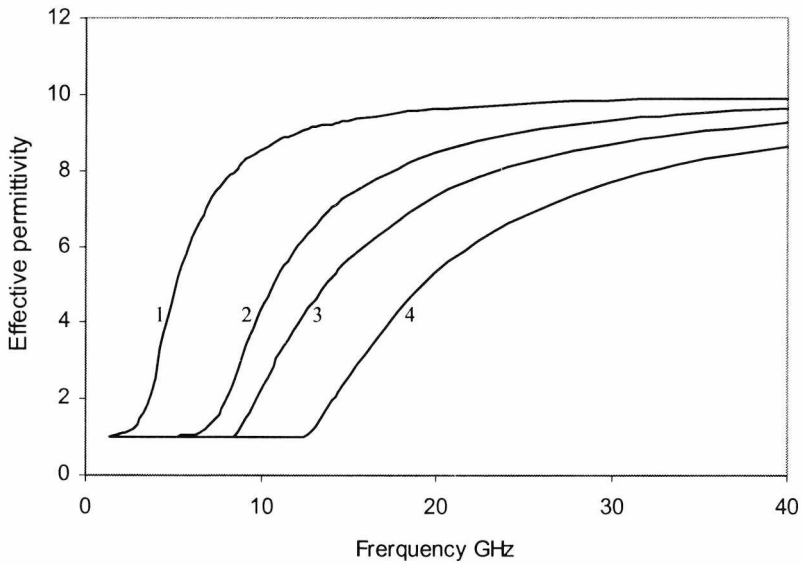

Figure 5.8. Modes of NRD guide. Line 1:LSM_{10}, 2:LSM_{20}, 3:LSM_{30}, 4:LSM_{40}

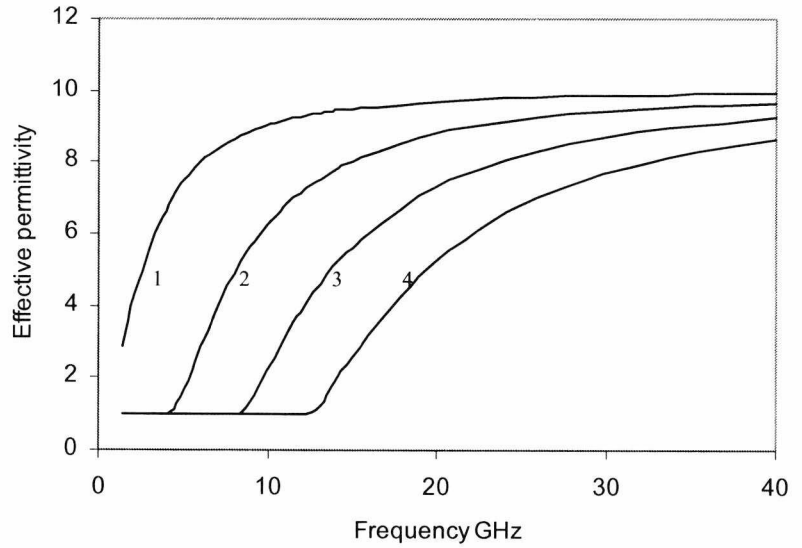

Figure 5.9. Modes of NRD guide. Line 1:LSE_{10}, 2:LSE_{20}, 3:LSE_{30}, 4:LSE_{40}

5.2.3 NRD design - optimisation

As in the case of Rectangular waveguides, NRDs can be designed to operate in different operating bandwidths by adjusting the dimensions of the dielectric slab and its electric permittivity. However, NRDs do not have a fixed relative bandwidth like rectangular waveguides. Consequently, apart from the standard design procedure, the NRD needs to be optimized for maximum relative bandwidth.

The analysis of NRDs begins by selecting the appropriate dielectric material that will form the dielectric strip of the NRPD. As mentioned before, the NRPD does not have any sidewall conduction losses, like in the case of a rectangular waveguide, and therefore the only propagation losses occur inside the dielectric. One of the most commonly used electromagnetic materials is FR-4, with a relative permittivity of ε_r=4.4. FR-4 is relatively cheap and quite robust, which makes it suitable for many practical applications, and comes at several thicknesses. Although FR-4 is sufficient for the purposes of our design, its loss tangent is not the lowest that you can get using a dielectric substrate. For that reason, some engineers prefer to use special types of duroid with a minimal loss tangent. Roggers^{TM} manufactures duroid substrates with tanδ=0.001 and various values of permittivity. In general, materials with high permittivities deliver greater NRD bandwidth but cost dramatically more. If a design is to be considered for mass production, a more economical value of permittivity should be considered. For example, NRDs work perfectly well on substrates with ε_r=4 or 3.

After the dielectric material has been selected the next step is to specify the centre frequency of operation. The bandwidth of an NRD comes close to that of a rectangular waveguide, but if a relative permittivity of 4 is used then the bandwidth is close to 80% of the bandwidth of the rectangular waveguide. The bandwidth of an NRD starts with the cutoff frequency of the LSM_{11} mode and ends at the cutoff frequency of the next higher order mode. The ratio of these two frequency points is referred to as *relative bandwidth*.

Using programming code specially developed for NRDs we can solve equation (5.51) at different frequencies and determine the value of b/a that gives the maximum available relative bandwidth, with b and a being the height and width of the NRD slab.

The design diagrams that we present here first appear in [5]. They describe the variation of relative Bandwidth as a function of $\sqrt{\varepsilon_r - 1}$ b/a, where ε_r is the relative electric permittivity of the dielectric slab.

Figure 5.10 shows how a higher permittivity dielectric material delivers higher relative bandwidth compared to a medium-low permittivity material such as FR-4.

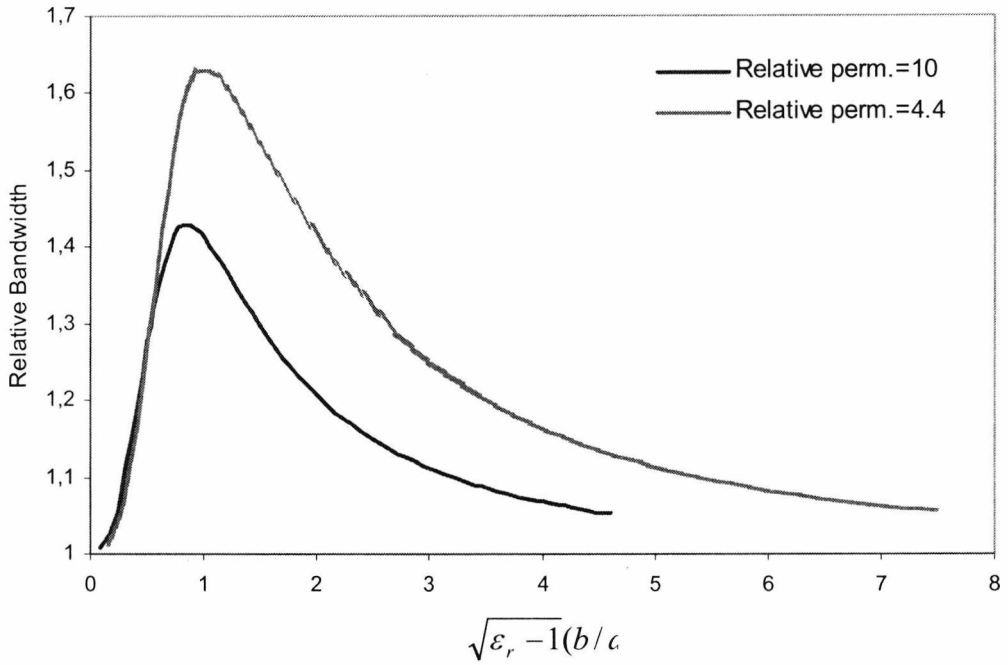

Figure 5.10 Relative bandwidth of NRD for two different permittivities of dielectric slab, $\varepsilon_r = 4.4$, $\varepsilon_r = 10$

5.2.4 NRD-based components and applications

Until today, the Nonradiative Dielectric waveguide has given rise to various applications owing to its low loss characteristics in the nonradiating propagation mode. NRDs are known as excellent stabilizing components for the design of variously shaped dielectric resonators [6]. The resonators are sandwiched between the metal plates and excited by the operating mode, usually the LSM11. Recently, microstrip-coupled NRD resonators [7] combine the advantageous features of the NRD and planar circuits while eliminating their critical advantages. The resonator is magnetically coupled to the input and output microstrip lines via two transversal slots etched in the common ground plane of the top NRD plate. This hybrid feature is also an efficient method of exciting Non-Radiative waveguides surpassing the impedance difference between NRDs and planar circuits.

Non Radiative Dielectric waveguides have been used to form high performance NRD guide circulators [8] by incorporating mode suppressors and half-Wavelength

dielectric strips. The fabricated circulators of this technology have proved to deliver less than 0.3 dB insertion loss and 20 dB isolation bandwidth of 20 GHz. Researchers in Japan [9] have successfully implemented NRD circulators for the design of high speed ASK modulators. Furthermore, these modulators are small in size because they do not require the use of bulky attenuators.

The list of NRD components also includes high quality filters. J.Malherbe and J. Coetzee [10] designed filters using rectangular resonators coupled to the center dielectric strip of an NRD. They presented a technique based on conventional synthesis for the formation of bandstop filters. Another type of NRD filters has been designed by researchers in Italy [11]. By introducing appropriate asymmetries, degenerate orthogonal modes were excited which proved to have filtering properties. The method could realize both bandpass and bandstop frequency selective devices while at the same time present low transmission losses and strong reduction of interference problems.

Although the NRD is popular for its radiation suppressing properties, changes introduced in the NRD topology cause the modes to leak and therefore create radiative elements that can be used as antennas or antenna feeders. The changes might include slots in the metal plane of the NRD [12, 13] or modifications to the geometry of the slab [14, 15].

All the above applications justify the use of NRD as one of the most suitable microwave device for wireless communication systems. Based on the high demand due to the rapid growth of Local area networks and vehicular radar systems NRD-guide technology is bound to plays key role in the market of communications. Figures 5.11 to 5.14 graphically illustrate some of the most important NRD-guide components.

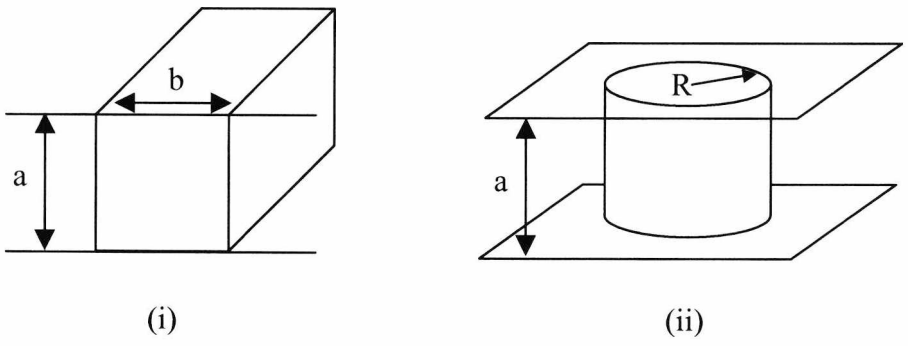

Figure 5.11. i) The non radiative dielectric waveguide ii) NRD-based dielectric resonator

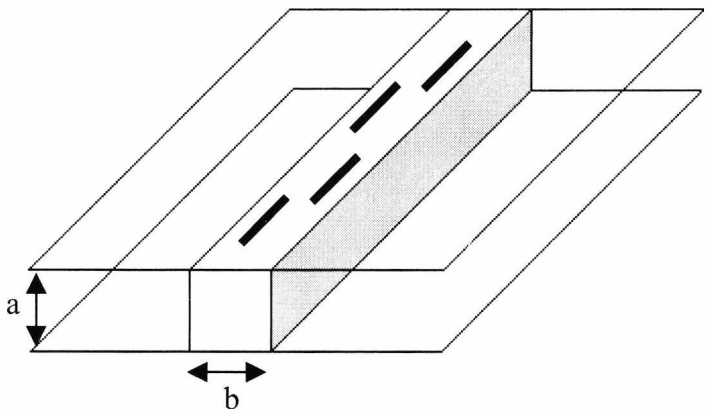

Figure 5.12. NRD guide operating as radiating element. The black lines represent slots on the top metal plate.

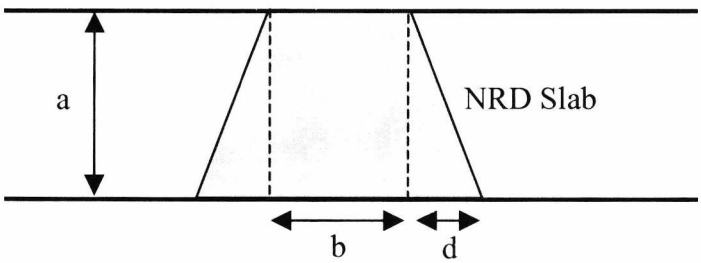

Figure 5.13. NRD with trapezoidal slab operating as Millimeter-Wave antenna. The structure is also referred to as *Leaky-Wave* NRD

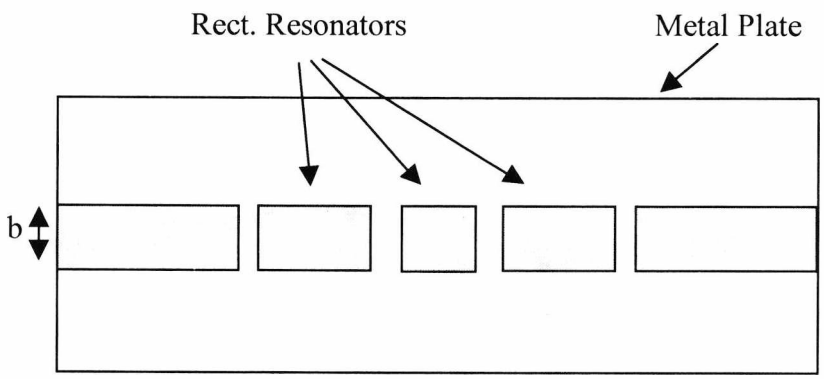

Figure 5.14. NRD Filter. By introducing air gaps in the dielectric slab we form successive rectangular resonators with filtering properties. Top view.

5.2.5 Disadvantages of the NRD

NRDs can suppress radiation and we saw how they can be optimized for maximum bandwidth. However, despite the attractiveness of the NRD guide, there are a number of cases where its use is not very practical. The most important problems are related to the mechanical support and assembly of the NRD central core and the alignment of the top and bottom metal plates. The disadvantages are even more when dealing with mass-consumer market applications where the production of a large number of devices is required at low cost.

For most applications, NRD Guides can be fabricated using conventional machinery but require accurate milling, which poses severe manufacture limitations. The problems become more evident at high frequencies, where extreme drilling precision is necessary. Manufacturing conventional NRDs at 100 GHz is a burdensome task due to the small dimensions of the design. Hence, the design of complex NRD applications like filters, resonators, endfire antennas and couplers would be impractical. Figure 5.15 shows an example of a filter using the NRD technology. For the correct operation of the filter, it is required that the individual blocks are in perfect alignment. At high frequencies, this task can be very expensive and cumbersome. Although some of these manufacturing difficulties could be overcome using micromachining, for mass production a simple and cheap means of fabrication needs to be found.

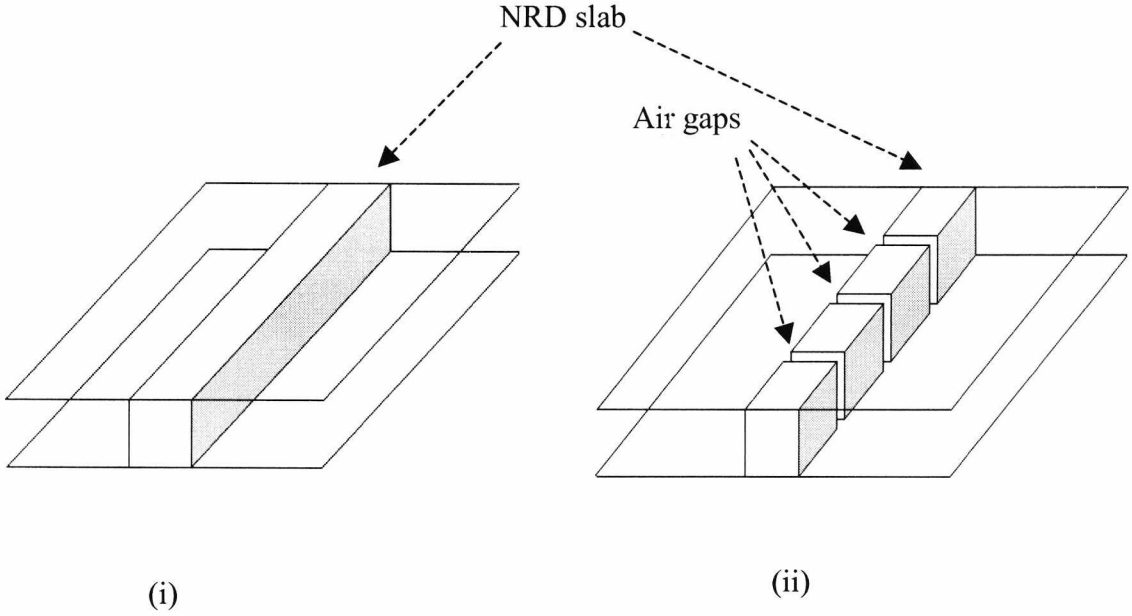

Figure 5.15 The design of NRD filter. (i) Pure NRD. (ii) NRD introduced with airgaps (filter)

5.3 Introduction to the Perforated NRD

In this section we introduce a structure which uses the geometry of conventional NRD with a modification concerning the air regions. This new design aims to surpass the problems related to mechanical support and assembly of conventional NRD central core as well as the alignment problems concerning the metal planes. Figure 5.16 shows the layout of our design. As with conventional NRD this new structure has two metal planes and a central waveguiding region but to the left and right, instead of air, we have perforated regions of the same material. We refer to this design as Non-Radiative Perforated Dielectric waveguide (NRPD). The principle of operation is analogous to that of an NRD. The perforated dielectric has lower electric permittivity than that of the central section and hence the guiding properties of the structure are based on the principle of total internal reflection. The permittivity of the perforated region can be controlled by the perforated lattice parameters.

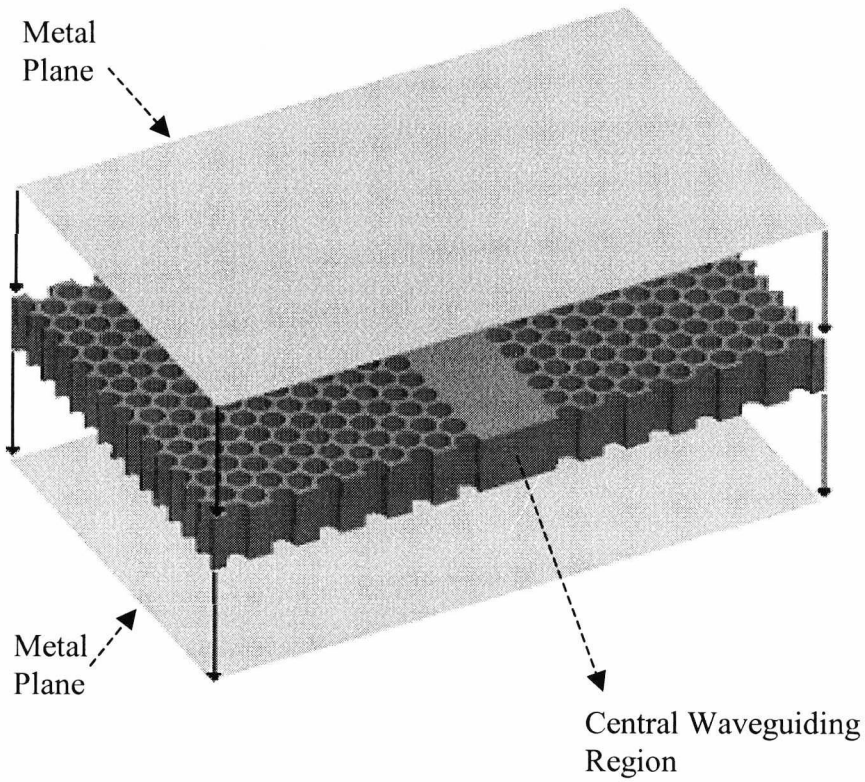

Figure 5.16. Layout of the Non Radiative Perforated Dielectric waveguide

The field inside the NRPD is maximum over the central core and decays exponentially over the perforated regions, in the same way as the field in the NRD. Since the entire dielectric lattice forms a self supporting structure, the alignment problems of the conventional NRD are eliminated, allowing complete systems to be fabricated out of a single layer of dielectric substrate. It is essential that the radius of each hole is significantly shorter than a guided wavelength so that the perforated regions appear homogeneous with respect to the guided wavelength. Holes of these dimensions can be fabricated using computer controlled CNC machines or laser cutting, allowing operation up to 50 GHz.

In the pages that follow, we present an in-depth analysis of the NRPD waveguide. We show the different types of perforated lattice and explain their features as well as the best conditions for their use. We also examine the wavelength sensitivity of the NRPD and show the excitation using rectangular waveguide. In addition we describe the NRPD optimization method and the manufacturing of the structure using conventional drilling methods in the workshop. At the end of this section we compare theoretical results with measurement.

5.3.1 Analysis of the perforated Regions – Permittivity expressions

The perforated lattice of an NRPD waveguide can have different patterns depending on the relevant positioning of the holes. For example if three of the closest neighbouring holes, inside the perforated dielectric, form an equilateral triangle then the lattice is called *triangular lattice*. If, on the other hand, four neighbouring holes form a rectangle then the lattice is referred to as *rectangular lattice*. The presence of the holes causes the permittivity of the perforated region to drop to a new value which we call *equivalent permittivity*. To derive formulae for the equivalent permittivity of each type of lattice we use the volume averaged permittivity expression, equation (5.52), where ε_r is the relative permittivity of the material and ε_o is the absolute permittivity of free space.

$$E_{eq} = \frac{\varepsilon_o \varepsilon_r A_m + \varepsilon_o A_h}{A_t} \tag{5.52}$$

where E_{eq} = equivalent permittivity of perforated lattice, A_m= area of material, A_h = area of holes, A_t = total area occupied by material and holes.

5.3.2 Triangular Lattice

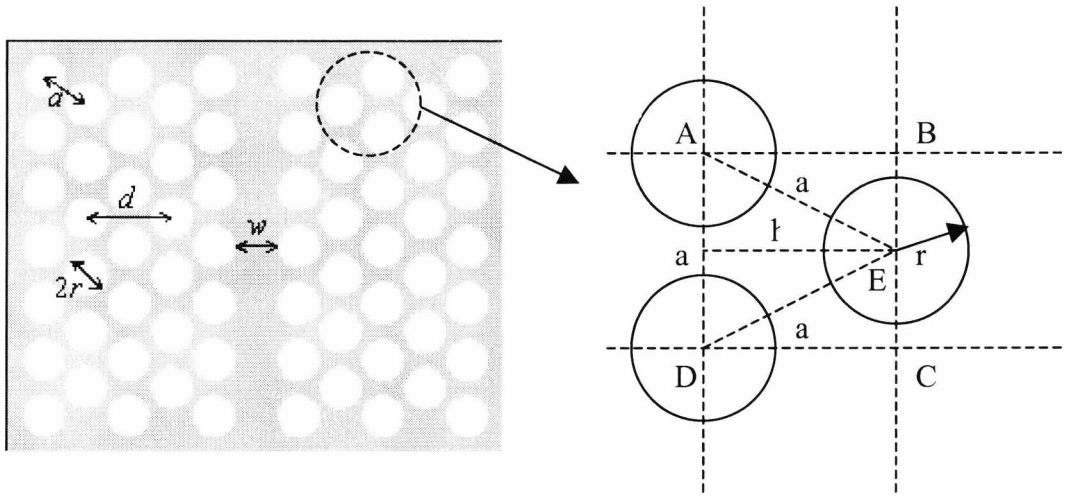

Figure 5.17. Triangular Perforated lattice i) Entire lattice ii) Elementary block

The perforated regions to the left and right of our waveguide appear homogeneous with respect to our operating frequency of 8 to 12GHz. In other words, over that operating bandwidth, the diameter of the holes is negligibly small compared to the guided wavelength. The volume averaged expression can be used, to calculate the value of equivalent electric permittivity of the perforated dielectric material. Since the structure is periodic, the equivalent permittivity of an elementary block will be the same as that of the entire area of material. Hence we shall focus our analysis on the elementary region ABCD, figure 5.17ii.

Height of equilateral triangle AED: $h = \frac{a\sqrt{3}}{2}$ (5.53)

Area of rectangle $ABCD = \frac{a^2\sqrt{3}}{2}$ (5.54)

Area occupied by holes: $\frac{\pi r^2}{4} + \frac{\pi r^2}{4} + \frac{\pi r^2}{2} = \pi r^2$ (5.55)

Therefore the area of material A_m is given by

A_m= Area of rectangle ABCD

$$- \text{Area of Holes in ABCD} = \frac{a^2\sqrt{3}}{2} - \pi r^2 \tag{5.56}$$

Substituting back to the equation (5.52):

$$E_{eq} = \frac{\varepsilon_o \varepsilon_r \left(\frac{a^2\sqrt{3}}{2} - \pi r^2 \right) + \varepsilon_o \pi r^2}{\frac{a^2\sqrt{3}}{2}} =$$

$$= \frac{\varepsilon_o \varepsilon_r \left(a^2\sqrt{3} - 2\pi r^2 \right) + 2\varepsilon_o \pi r^2}{a^2\sqrt{3}} = \varepsilon_o \varepsilon_r + \frac{2\pi r^2}{a^2\sqrt{3}} (\varepsilon_o - \varepsilon_o \varepsilon_r) \tag{5.57}$$

This final expression is the absolute equivalent permittivity. Dividing it with ε_r gives the relative permittivity expression. As such:

relative equivalent permittivity for the triangular lattice:

$$\varepsilon_{eq} = \varepsilon_r - \frac{2\pi}{\sqrt{3}} \left(\frac{r}{a} \right)^2 \left(\varepsilon_r - 1 \right) \tag{5.58}$$

Since the value of equivalent permittivity has been calculated, the NRPD guide is essentially equivalent to the structure of figure 5.18. As we are about to see in the next page, different types of lattices have different values of equivalent permittivity. Nevertheless, it is important that the equivalent permittivity is at least 50% less compared to that of the main guiding region so as to achieve good field confinement in the centre of the NRPD.

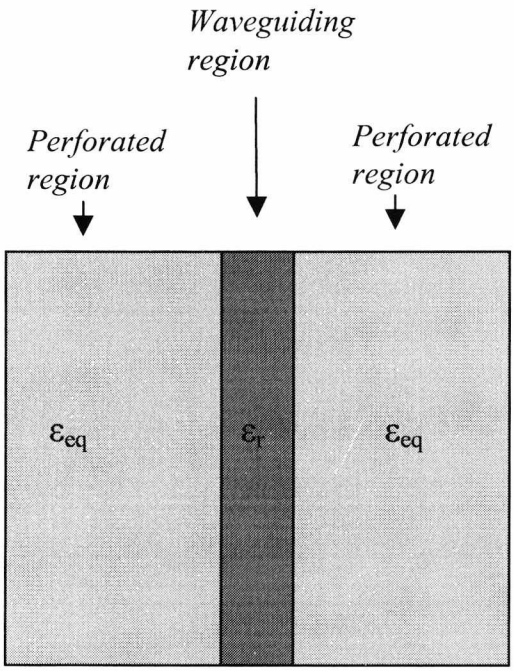

Figure 5.18. Top view of electromagnetic equivalent topology of the NRPD. For good field confinement in the center of the guide it should be $E_{eq}<1/2\ E_{eq}$

5.3.3 Analysis of the rectangular lattice

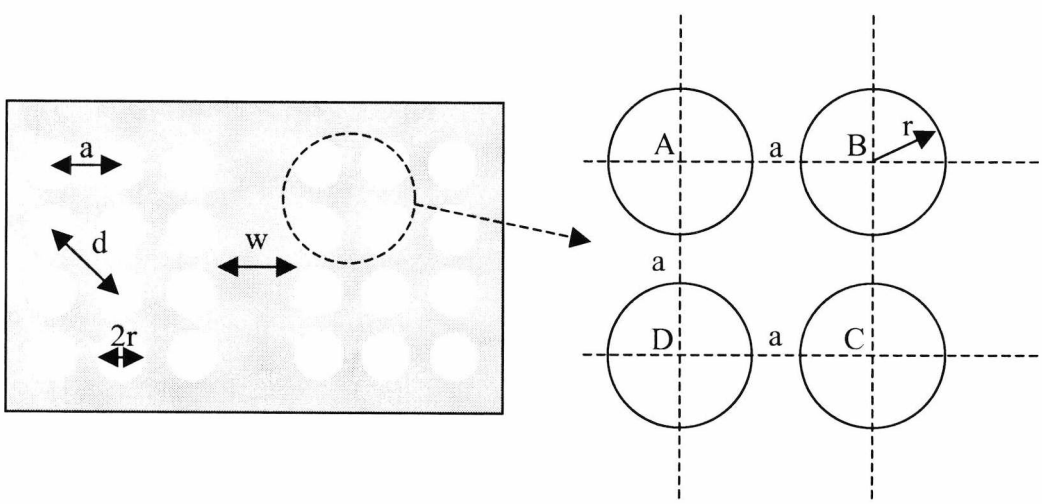

Figure 5.19. The rectangular perforated lattice i) Entire area ii) Elementary block of lattice

From figure 5.19 we have:

Area of rectangular ABCD = a^2 (5.59)

Area occupied by holes: $\frac{\pi r^2}{4}+\frac{\pi r^2}{4}+\frac{\pi r^2}{4}+\frac{\pi r^2}{4}=\pi r^2$ (5.60)

Therefore,

A_m = Area of rectangle ABCD
– Area of Holes in ABCD = $a^2-\pi r^2$ (5.61)

Substituting back to the volume averaged expression we get:

$$E_{eq}=\frac{\varepsilon_0\varepsilon_r(a^2-\pi r^2)+\varepsilon_0\pi r^2}{a^2}=$$

$$=\varepsilon_0\left(\varepsilon_r+\frac{\pi r^2(1-\varepsilon_r)}{a^2}\right)=\varepsilon_0\left(\varepsilon_r+\left(\frac{r}{a}\right)^2\pi(1-\varepsilon_r)\right) \quad (5.62)$$

and dividing by ε_o gives the relative permittivity expression for the rectangular lattice:

$$\varepsilon_{eq}=\varepsilon_r+\frac{\pi r^2(1-\varepsilon_r)}{a^2} \quad (5.63)$$

or

$$\varepsilon_{eq}=\varepsilon_r-\left(\frac{r}{a}\right)^2\pi(\varepsilon_r-1) \quad (5.64)$$

5.3.4 Comparison between triangular and rectangular lattice

The most common types of lattice are the triangular and the rectangular, but there are also other types which are usually more complex. For example the hexagonal lattice which is shown in figure 5.20.

The purpose of a perforated lattice is to reduce the electric permittivity of the region to which it is applied. The lattice of our project is required to lower the permittivity of the perforated material to the lowest possible value. For that reason we prefer the triangular lattice, which is the densest, and allows more of the material to be removed.

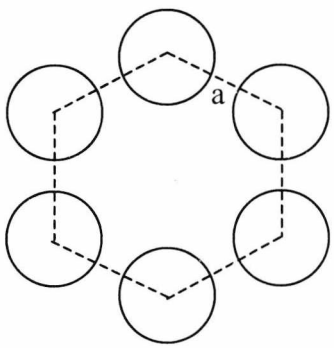

Figure 5.20. Perforated holes in hexagonal orientation of side a

Figure 5.21 compares the equivalent permittivities of the triangular and rectangular lattice. In theory, 0.5 is the maximum value that a lattice can have, i.e when $a=2r$. In practice we should choose a value of approximately 0.45 to avoid board breakdown, due to high concentration of holes. Soft materials such as Duroid can withstand very high concentration of holes, while FR-4 is more fragile due to its robust nature and requires careful handling. The drilling process of a dielectric sheet should be carried out before etching, as the metal planes provide some protection against board breakdown and keep the material together. In any case accurate drilling is required to achieve the value that was calculated through the volume averaged expression. Although the manufacturing process is automated, good knowledge of using the CNC drilling machine is required. While manufacturing the NRPD in the University of Kent we managed to produce an FR-4 triangular lattice whose distance between two neighbouring holes was 100 μm.

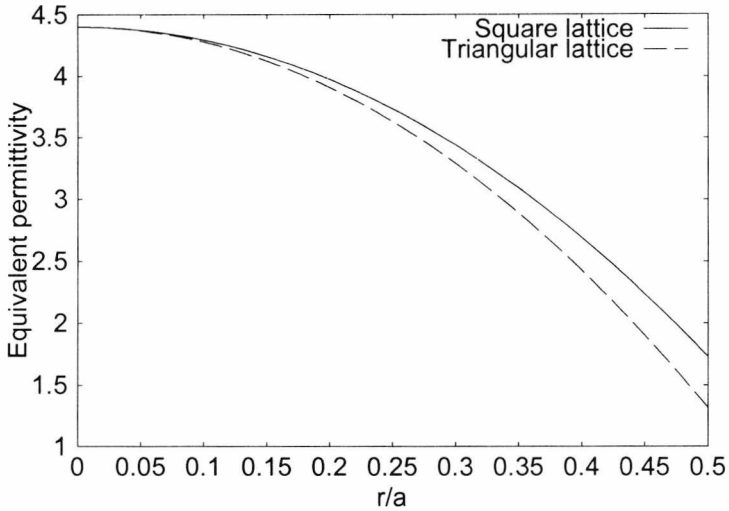

Figure 5.21. Comparison of relative permittivity versus r/a between triangular and rectangular lattice. ε_r=4.4, a=0.0033 m

Despite being denser the triangular lattice poses some practical limitations, especially in the design of rectangular cavities - resonators [16]. The relevant positioning of the holes interferes with the space occupied by the resonator. This problem can be solved with either using rectangular lattice figure 5.22 or simply reducing the *a* parameter of the lattice figure 5.23. There can also be designs in which a combination of both rectangular and triangular lattice are used. In that case the lattice will no longer be homogeneous and extra work might be required to account for the variations in equivalent permittivity. For practical reasons and to simplify the manufacturing process, the lattice used throughout chapter is triangular.

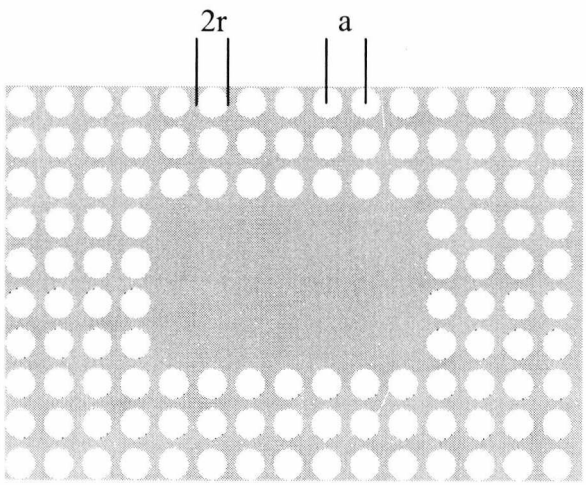

Figure 5.22. The resonator made using rectangular cavity. The rectangular lattice is better for the design of orthogonal structures.

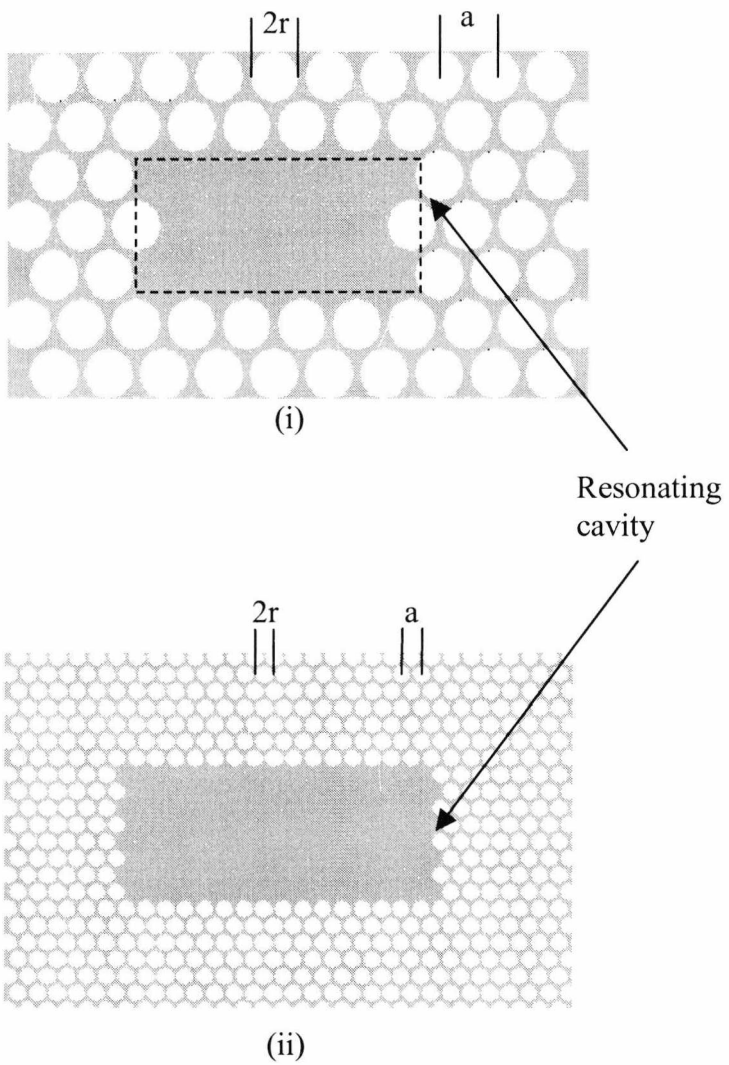

Figure 5.23. (i) Triangular lattice with a=1.65 mm, r=1.5 mm (ii) Triangular lattice with a=0.635 mm, r=0.5 μm. Increasing the lattice density results in better approximation of the rectangular cavity

5.3.5 NRPD Design and optimisation methods

Optimizing the NRPD is achieved in the same way as for NRDs. The same programming code is used to solve the modes inside the NRPD with the only difference being that the surrounding permittivity is no longer one. Figures one and two show the dispersion curves for the NRPD with a=9.3 mm, b=10.23 mm and ε_{eq} = 1.85. The bandwidth of this design is from 9.08 GHz to 10.95 GHz, i.e the cutoff frequencies of modes LSM_{11} and LSE_{12} respectively.

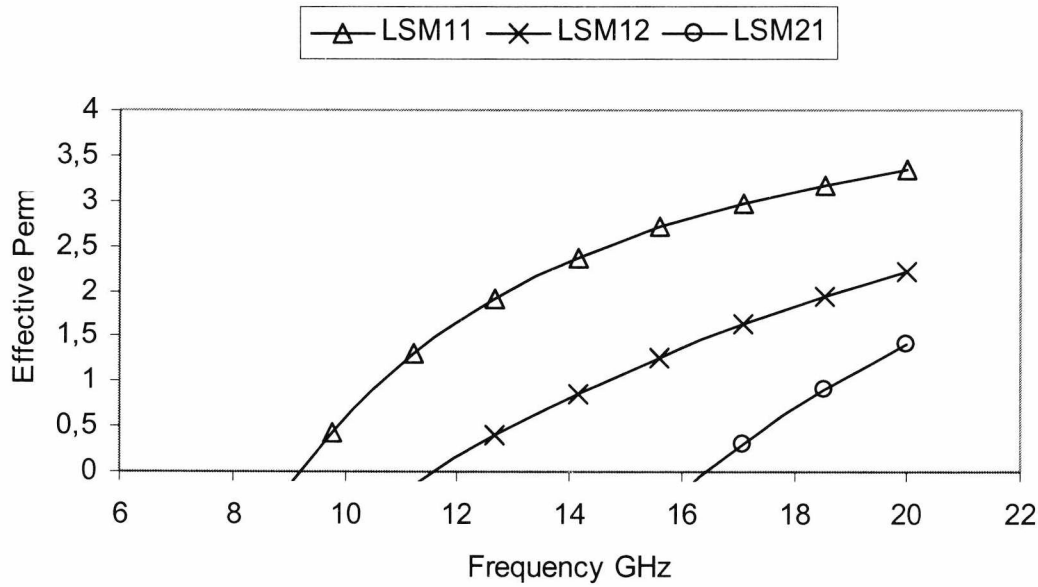

Figure 5.24 LSM modes of the NRPD

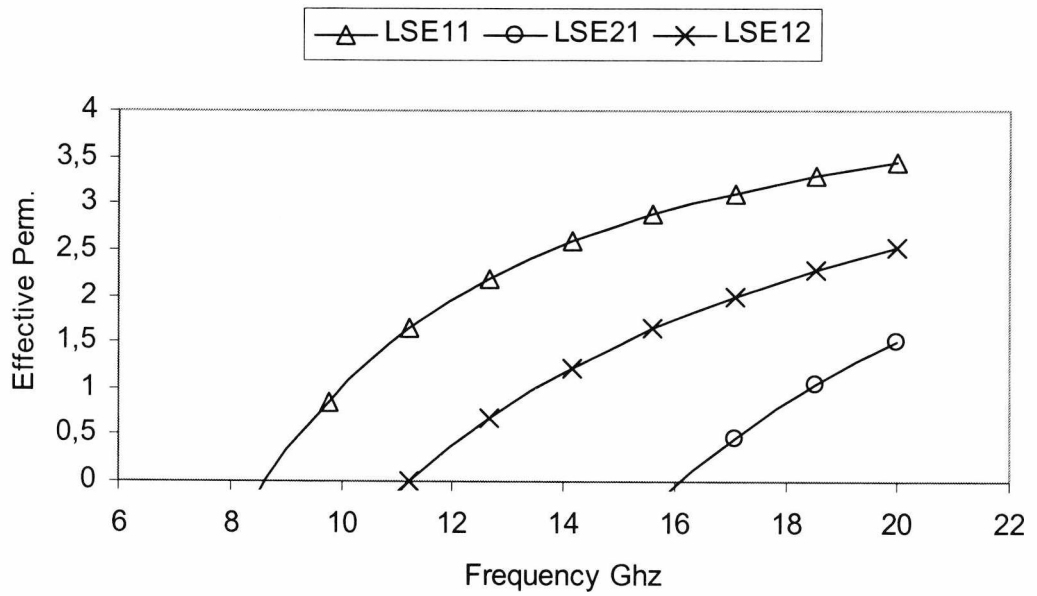

Figure 5.25 LSE modes of the NRPD

5.3.6 Excitation of the NRPD waveguide

The NRPD waveguide has been designed. At this point, before we proceed to fabrication of the design we need an effective excitation method. We can excite the

NRPD guide using the same methods as those used for conventional NRD waveguides. The most common excitation method is achieved through rectangular waveguide, figure 5.26. The central core of the NRD is extended beyond the metal plates and is inserted inside a hollow rectangular waveguide. The orientation of the rectangular waveguide is such that the E field of the TE_{10} mode is parallel to the metal planes of the NRD. The TE_{10} mode of the rectangular waveguide thus becomes the LSM_{11} as soon as it enters the NRD. There is no reason to assume that any other mode is being excited, since there is no physical obstruction to cause rotation of the E field.

The second method involves exciting the NRD through integration with a planar type of transmission line such as the microstrip line, figure 5.27. The excitation is achieved though magnetic aperture coupling due to the rectangular slot on the ground plane of the microstrip line, which is also the top metal plate of the NRD. The open ended microstrip line is placed in right angles to the NRD slab. The length of the microstrip line with respect to the coupling slot is of critical importance for the overall quality of the transition. Although this method offers the advantage of NRD-hybrid integration with planar circuitry, the manufacturing process is not as easy as that of the first method. It also takes more time to design.

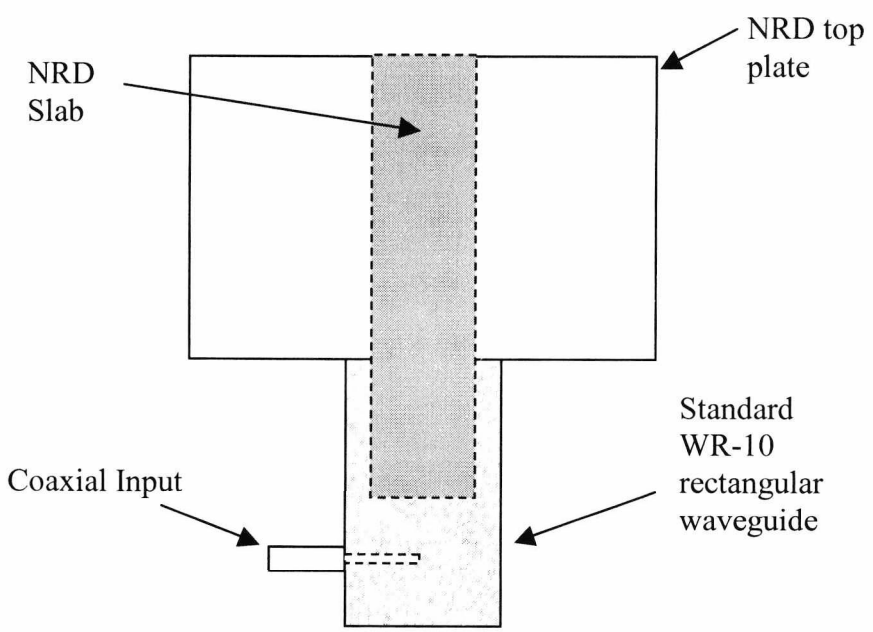

Figure 5.26 NRD Waveguide, excited by coaxially fed rectangular waveguide.

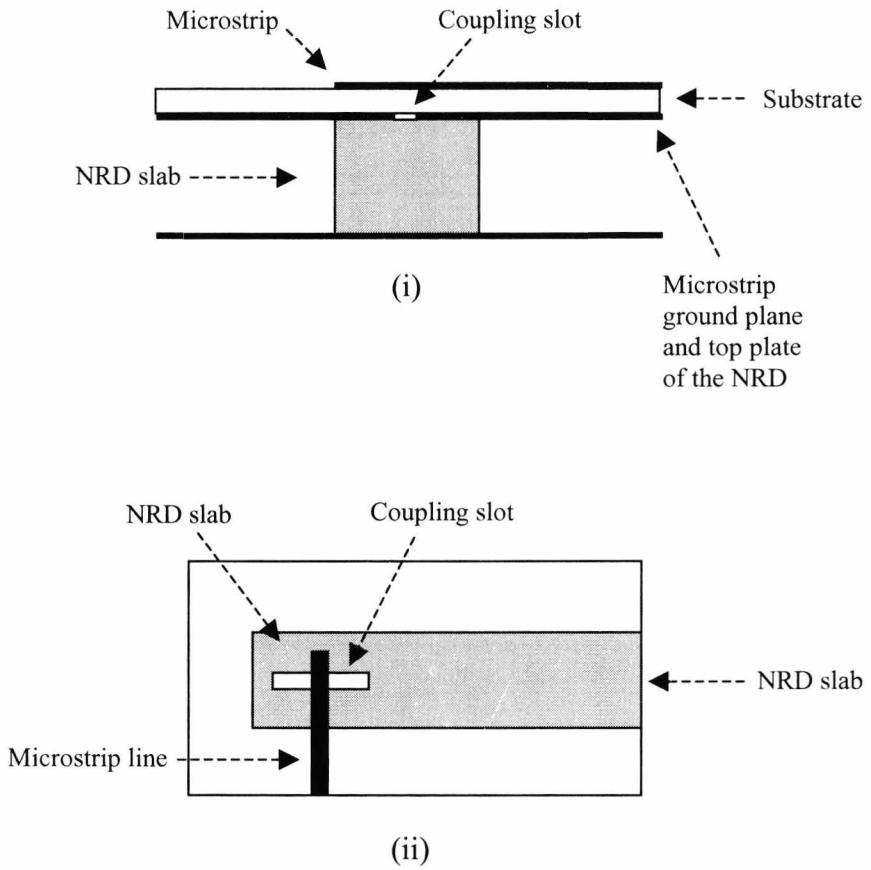

Figure 5.27. NRD guide excited through magnetic aperture coupling to a microstrip line (i) Side view (ii) Top view

For practical reasons, the excitation of our NRPD is realized using the first excitation method. The final form of the transition is shown in figure 5.28. The only difference to the conventional method is the tapered shape of the dielectric inside the rectangular waveguide. By tapering the dielectric we allow for smother propagation of the TE_{10} mode in the NRPD. Also, since the NRPD slab does not fill the entire space of the rectangular waveguide, some method must be found to securely fix the guide into the NRPD. This can be done by filling the rectangular waveguide with thin foam sheet and leaving a narrow space only for the NRPD slab. Alternatively, the NRPD slab can be designed, in advance, to match the height of the rectangular waveguide that will excite it. Then the two structures simply bond one inside the other applying a small amount of pressure. This method does not require any foam sheet but it might require compromise in the bandwidth of the NRD as it is not possible to independently choose *b/a*, centre frequency and maximum bandwidth all at the same time.

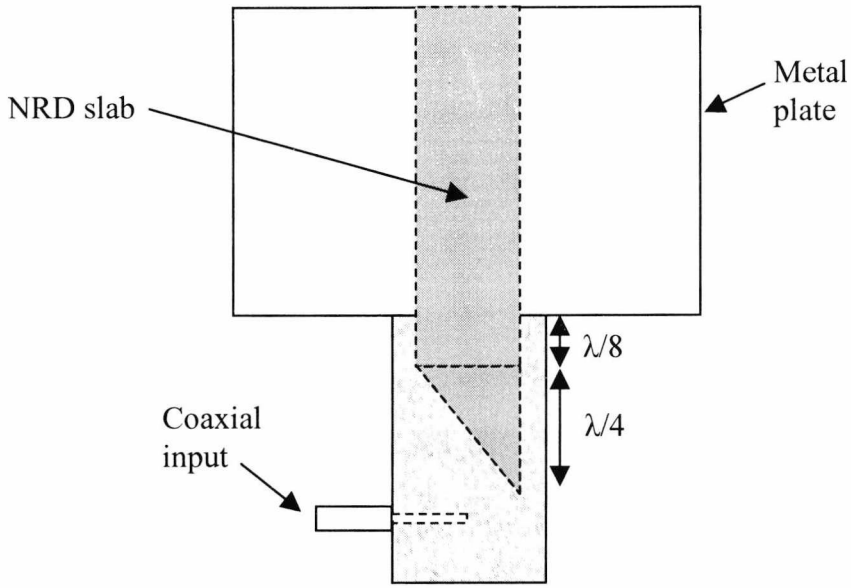

Figure 5.28 Excitation for the NRD. The slab inside the NRD is tapered to ensure better coupling.

5.3.7 Manufacturing the NRPD – Measurements

In this section a multilayer stack of three substrates are used to form an X band NRPD waveguide. The material and lattice parameters are $\varepsilon_r = 4.4$, $a = 3.3$ mm and $r = 1.5$ mm. This gives an equivalent relative permittivity of $\varepsilon_{eq} = 1.85$ i.e. reduction by more than half the original value. For non-radiative propagation the height of the waveguide must be less than $\lambda_{eq}/2$, where λ_{eq} is the wavelength in the equivalent dielectric. This allows the height to be set and the width can then be chosen to give optimal bandwidth. In our implementation the height is 10.5 mm and the channel width is 10.1 mm.

The lattice structure was fabricated using a computer controlled CNC machine. The substrates were then sandwiched between two conducting planes, figure 4.29. The complete structure was connected to X band rectangular waveguide using tapered transitions and a direct measurement of the guided wavelength was obtained using a field probe above a small slot cut in the top metal of the NRPD waveguide. Figure 4.30 shows measured and theoretical results for the NRPD waveguide. As can be seen the results are in good agreement with theoretical results for NRD surrounded with an equivalent permittivity calculated using volume averaged permittivity. The large discrepancy below 10 GHz is expected since the waveguide approaches cut-off at this

point and becomes very sensitive to parameter variation. Figure 4.31 shows the electric field variation of the LSM_{11} mode at the centre of the guide calculated using Ansoft's HFSS. It is seen that only about 5 holes are required to confine the mode.

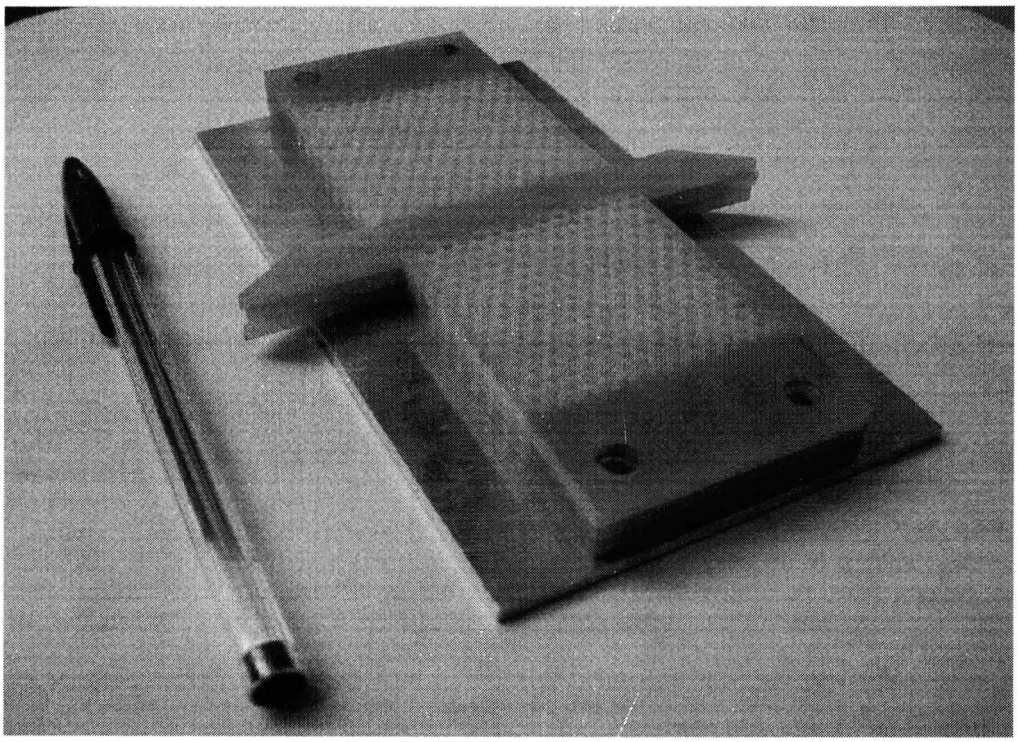

Figure 4.29. The perforated NRD. The top metal plate is not included such that the reader can see the topology of the dielectric substrate.

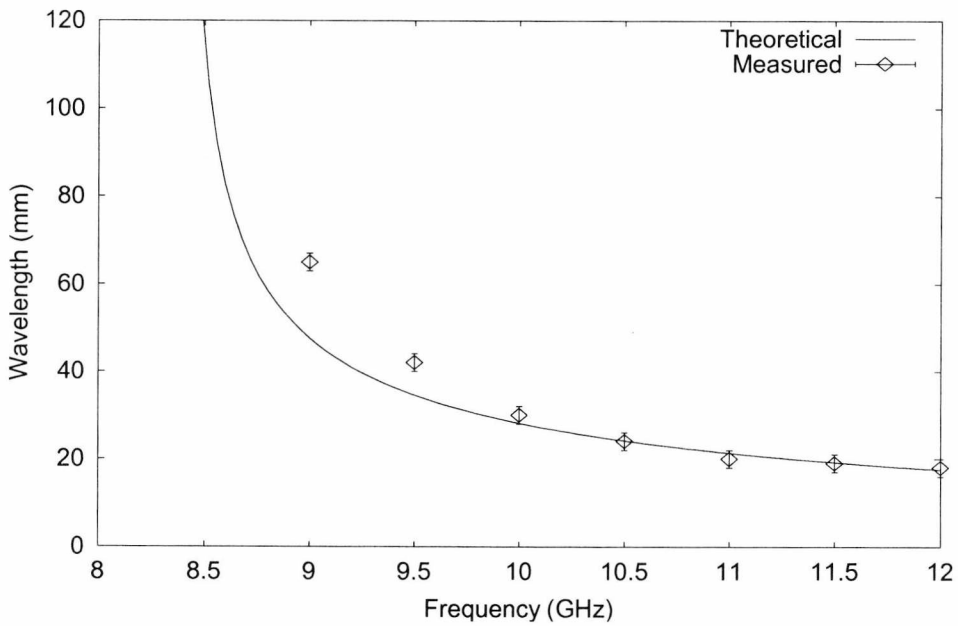

Figure 4.30. Measured and theoretical values of guided wavelength.

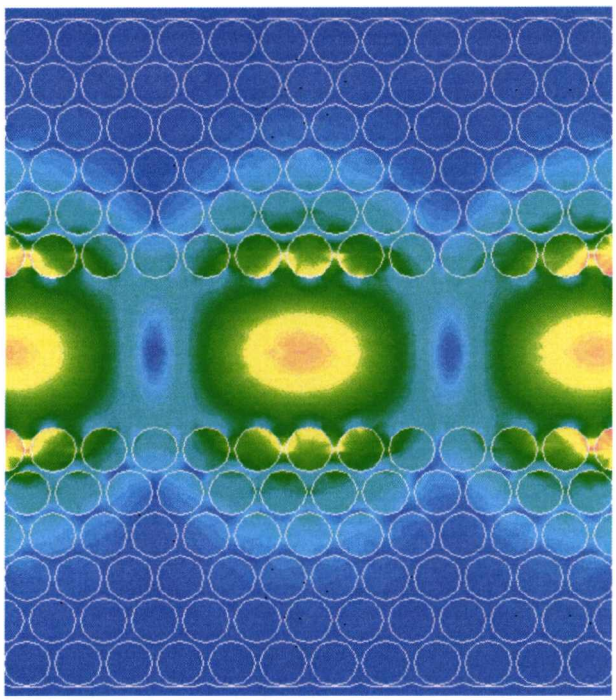

Figure 4.31. Electric field for LSM_{11} mode.

5.3.8 Wavelength Sensitivity

Expressions (5.28) and (5.64) in paragraph 5.3.1 show that the equivalent permittivity of a perforated dielectric depends on the ratio *r/a* rather that on the individual values of *r* and *a*. This effectively means that triangular lattice structures of different *r* will have the same ε_{eq} as long as the *a* parameter is changed accordingly. The same principle applies for any other type of perforated dielectric lattice.

In this paragraph we determine if there are any the limits in hole size inside the perforated region. By keeping the *r/a* ratio constant, we determine the effect of altering the value of lattice parameter *a* with respect to the wavelength inside the dielectric $\lambda=\lambda_0/\varepsilon_r^{-1/2}$. At 10 GHz the guided wavelength of the NRD is 14mm. Figure 5.32 compares the effective dielectric constant for a NRD guide surrounded by a homogenous dielectric and finite element results for lattice structures with $s=\lambda/a$ equal to 2, 3 and 4. Although a large hole would emulate free space better than a smaller one, it fails to optimally guide the mode of interest (LSM_{11}). On the contrary, a higher hole-density lattice works better, since the perforated dielectric appears homogeneous with respect to the wavelength. It is clear from Figure 5.32 that a value of s=2, or less, results in a significant variation in the value of equivalent permittivity

compared to the homogeneous value. In contrast, values greater than s=3 result in effective permittivity very close to the homogeneous value. The experimental results of Figure 3 are for s= 4.2 and correspond to a hole of just more than 3 mm of diameter. These results have been verified using both HFSS and CST.

Figure 5.32 clearly proves that altering the ratio λ/a effects the equivalent permittivity of the perforated dielectric region, despite the ratio r/a being constant. That phenomenon is better explained in Figure 5.33, which shows how the equivalent permittivity varies with λ/a. As λ/a increases the value of ε_{eq} decreases and,in the limit, as λ/a approaches a very large number, the equivalent permittivity of the surrounding dielectric converges to the homogeneous value of 1.85. Note that from Figure 5.32 the value of ε_{eq} is slightly smaller than 1.85 when λ/a is equal to 4. This is probably due to numerical error since many more holes are simulated and therefore the computational burden becomes very large.

We note that as s approaches unity the structure may, depending on the permittivity, exhibit an electromagnetic bandgap [17]. If this is case, by definition, energy cannot exist in the lattice region of the dielectric, and is therefore confined to the main core of dielectric material. This phenomenon forms a promising waveguide but due to its complexities it is beyond the scope of this thesis.

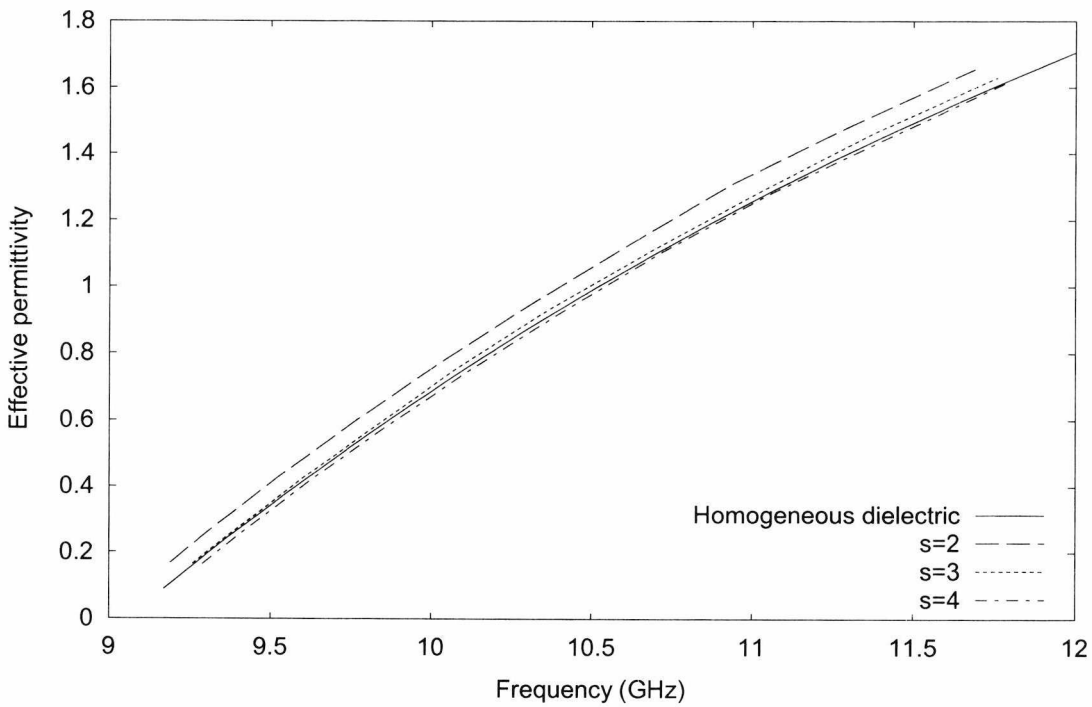

Figure 5.32. Effective permittivity for homogeneous dielectric and triangular lattice with $s = \lambda/a$ = 2, 3 and 4 at f=10 GHz.

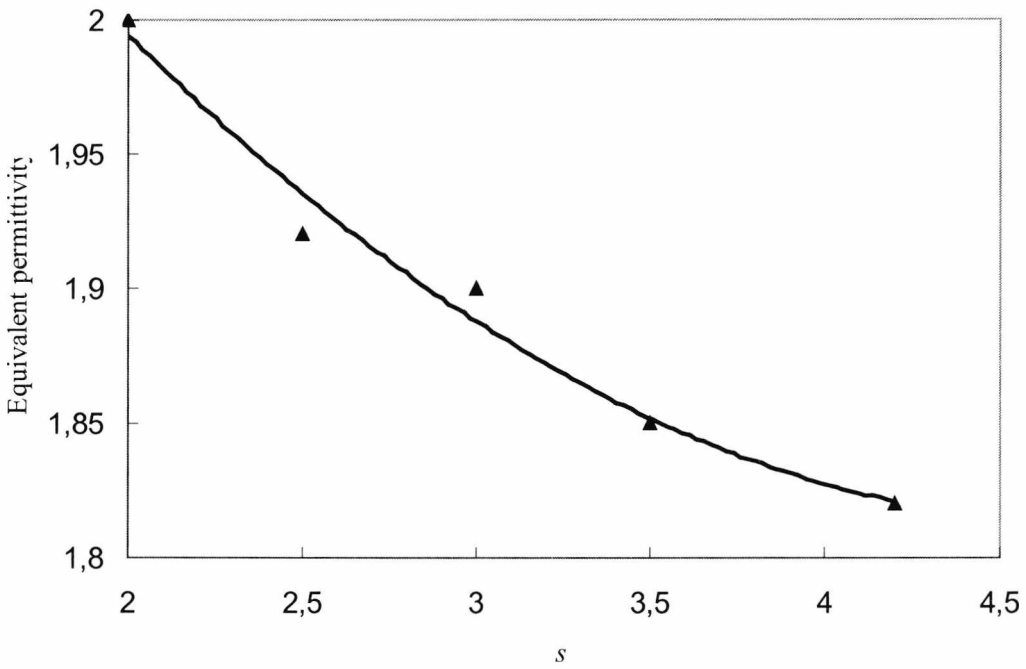

Figure 5.33. Equivalent permittivity as a function of $s=\lambda/a$. Triangles show HFSS results. The continuous line shows the fitted curve.

5.4 Summary

The NRD guide is attracting more and more interest from the scientific community, mainly due to its low loss properties and its ability to guide electromagnetic waves around bends with potentially no radiation loss. For that reason, a great number of microwave components such as filters, slot antennas, couplers and circulators is already based on the principles and benefits of NRD technology. However, at large scale production NRDs have manufacturing limitations related to the alignment of the metal plates.

In this chapter we have presented a simple technique to fabricate NRPD waveguide systems from single substrates. The structure is based on the NRD but, instead of air, the slab is surrounded by perforated dielectric. The NRPD has all the advantages of conventional NRD guides and no manufacturing limitations as it forms a self supporting structure.

Analysing the perforated lattice of the NRPD showed that three series of holes are enough to confine the mode in the center of the guide. Furthermore the s parameter of

the lattice was proven to be efficient as long as it $s<3$. For higher values the equivalent permittivity of the lattice becomes unreliable.

A 10 GHz prototype based on standard PCB has been presented and shown to be in good agreement with equivalent permittivity results. It is envisaged that high frequency examples could be easily fabricated using the newly immerging LTCC technologies. In this case the holes could either be punched or chemically etched using photoimageable LTCC. This would allow easy integration with planar circuitry and allow low cost mass production. Furthermore, multilayer structures could be formed where many NRPD's are stack on top of each other. By coupling between layers highly integrated systems based on high performance NRPD guides could be designed.

References

[1] P.R.Young "A study of coupled dielectric waveguides and their application to millimetre wave components" A thesis submitted for the degree of Doctor of Philosophy, Electronic Engineering Laboratories, University of Kent at Canterbury

[2] J. Dalaire and K.Wu, "Complete characterization of transmission losses in generalized non radiative dielectric waveguide" *IEEE Trans Microwave theory and Techs.*, vol48, no. 1, pp. 121-125, January 2000.

[3] *IEEE transactions on Mic. Theory and Techs.* Vol. 48, No. 1, January 2000 "Complete characterization of Transmission losses in Generalised Nonradiative Dielectric (NRD) Waveguide

[4] C.A. Balanis, Advanced Engineering Electromagnetics, New York: Wiley, 1989

[5] T. Yoneyama and S. Nishida. "Nonradiative dielectric waveguide for millimetre wave integrated circuits," *IEEE Trans. Microwave Theory and Tech.* Vol MTT-29, pp. 1188-1192, Nov. 1981

[6] Fabrizio Frezza and Alessandro Galli "Characterization of the resonant and coupling parameters of dielectric resonators for NRD-Guide filtering devices". *MTTS 1993 Symposium Digest*

[7] Ali A. Sayyah and Ke Wu, "Efficient Analysis of Microstrip-Coupled Nonradiative Dielectric Resonators for hybrid Integrated circuits", *IEEE Trans on Microwave Theory and Tech.* Vol. 47, No 2, February 1999.

[8] Hiroyuki Yoshinaga and Tsukasa Yoneyama, "Design and Fabrication of a Non_radiative Waveguide circulator", *Trans Microwave Theory and Techs.* Vol. 36 No 11, November 1988

[9] "Futoshi Kuroki and T. Yoneyama. High speed ASK Tranceiver Based on the NRD-Guide tecjnology at 60 GHz" *Microwave Theory and Techniques, IEEE Transactions on* Volume 46, Issue 6, June 1998 Page(s):806 - 810

[10] Johannes A. G. Malherbe and Jacob Coetzee, "Bandstop Filter in Nonradiative Dielectric Waveguide Using Rectanular resonators. *Trans on Microwave theory and Tech.* MTT-35 No. 12 december 1987.

[11] Carlo Di Nallo and Paolo Lampariello, "Experimental investigation on NRD-guide Dualt mode filters". *MTT-S Digest.* 1994

[12] K.Maamria, T. Yoneyama, "Leaky NRD Guide As a feeder for microwave planar antennas". *Microwave Trans, Microwave theory and Techs.* Vol 41 No 12 December 1993

[13] K. Sakakibara N. Gito, "High –gain and high Efficiency single layer slotted waveguide array for use in 22 GHz band. *Electronics letters* 15th February 1996 Vol 32 No 4

[14] Shanjia J. Xu and Ke Wu." Characteristics and design Consideration of Leaky wave NRD Guides for Use as millimeter Wave Antenna." *Microwave Microwave Trans, Microwave theory and Techs.* Vol 46 No 12 December 1998

[15] M.T. Lee K.M.Lulk. "Leaky wave antenna based on image NRD guide with staircase-shaped dielectric slab,". *Electronics Letters* 22nd June 2000 Vol 36 No 13

[16] A. Petosa, A Ittipiboon and S. Thirakoune. "Perforated dielectric resonator antennas", *Electronics Letters*, 21st November 2002 Vol. 38. No 24

[17] J. D. Joannopoulos, R. D. Meade and J. N. Winn, "Photonic Crystals – Molding the flow of light," Princeton University Press, 1995.

6. NRPD filters

The Non Radiative Dielectric waveguide has been the first dielectric waveguide that allowed low-cost and low-loss circuit design. NRDs suppress the inherent radiation loss of dielectric waveguide and allow for sharp bends and other geometrical discontinuities. For that reason, a large number of NRD-guide components have been developed as we saw in chapter 5. Unfortunately, conventional NRDs bare manufacturing limitations especially at high frequencies, due to mechanical assembly and support of the NRD central core as well as the extreme precision and alignment required by the metal plates. Hence the same problems arise for all NRD based components such as filters [1,2], resonators [3], couplers [4] and many more [5-9].

In this paragraph we demonstrate how the perforated dielectric technology that we used in the previous chapters can apply to NRD filters and therefore ease their fabrication at high frequencies at low cost. The filters that we analyze are based on discontinuities in the central core of the NRD. The equivalent circuit of the design is the same as the one used for the folded waveguides of chapter 4 and is based on the *Direct Coupled Cavity* principle.

6.1 Types of discontinuities

There can be many different types of discontinuities in an NRD waveguide. We name just a few, i.e. the ones that are most commonly used. Figure 6.1 shows three types of NRD-guide discontinuity. They are: i) air gap discontinuity ii) double step discontinuity and iii) notch discontinuity. All three types share the same characteristics, and the same guided-wave behavior. The usual mode of operation LSM_{11} can easily propagate along the discontinuity if the gap is too small or if, in the case of ii) and iii) discontinuities, the dielectric width is large. On the contrary, if the

air gap is too wide or if the dielectric width is narrow, the mode of operation becomes evanescent. The realization of an NRD filter is based on the placement of successive discontinuities in the central slab. Energy travels through the filter due to the coupling of the evanescent modes between the discontinuities.

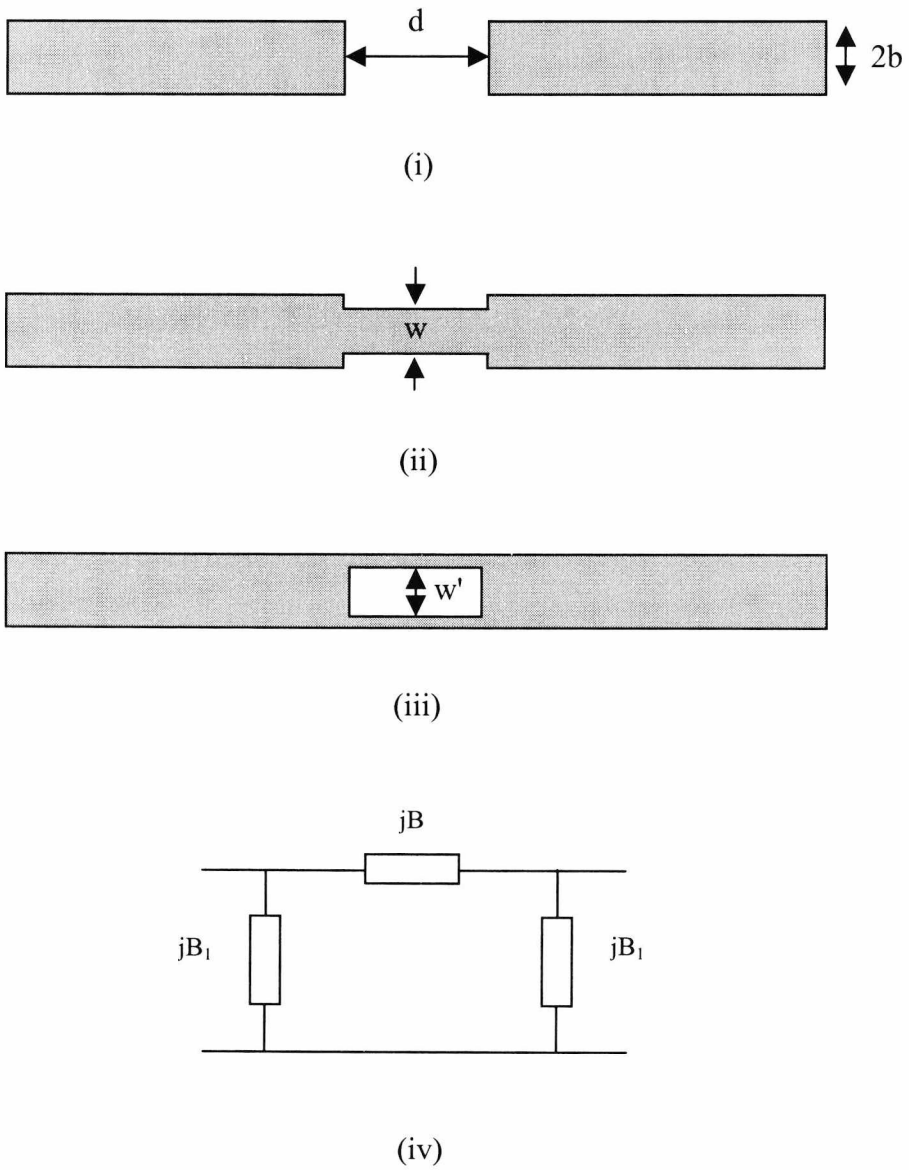

Figure 6.1. The common types of discontinuity used in NRD-guides for the design of filters. (i) Airgap discontinuity, (ii) Double step discontinuity, (iii) Notch discontinuity, (iv) Equivalent circuit for the discontinuities.

6.1.1 The airgap discontinuity

The design variable is the width of the air gap. The mode of operation is LSM_{11}. The filter can also work with other modes such as LSE_{10} or LSM_{10} although the NRD would no longer be non-radiative.

We begin the analysis by selecting the dimensions for the non-radiative dielectric slab. We have worked out that the a=9.3mm, b=10.23mm waveguide delivers good bandwidth, 9.24-11.31 GHz, with a surrounding lattice of ε_r = 1.85. The lattice parameters are r = 1.5mm and s = 3.3mm. We also calculate that a 5-pole filter with 0.1db passband ripple and centre frequency of 10.275 GHz requires the B and L values of table 6.1. From simulation we work out the *theta* values and the corrected lengths, table 6.2.

Figure 6.2 shows the simulation model of a single discontinuity. To reduce simulation time, instead of using perforated regions on either side of the central slab we use complete sections of the same ε_{eq} as the perforated lattice.

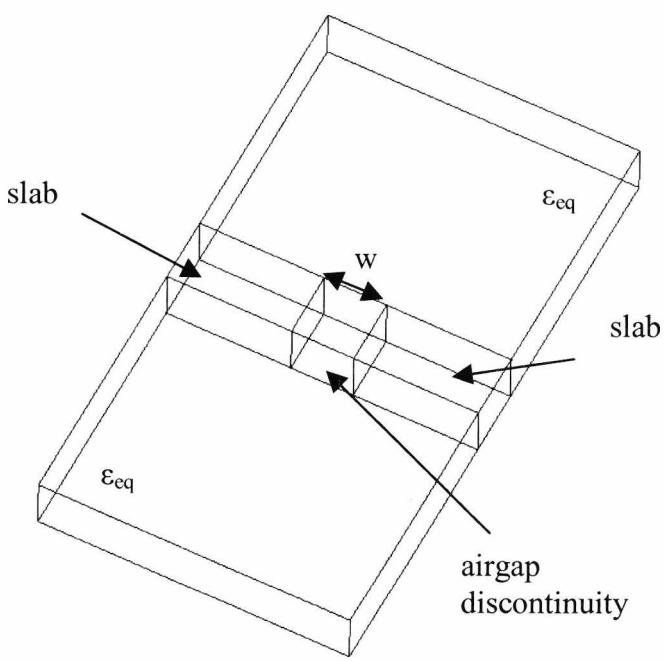

Figure 6.2. Model for simulation. A single airgap discontinuity in the centre slab of the NRD

B	L
1.4572	11.2
3.9892	12.6
5.3654	12.8
3.5654	12.6
3.9892	11.2
1.4572	

Table 6.1. B values and lengths for the NRPD filter

B	Correct L
1.4572	11.4792
3.9892	13.2932
5.3654	13.6788
3.5654	13.2923
3.9892	11.4792
1.4572	

Table 6.2. B values and corrected lengths for the NRPD filter

The complete filter with air gaps is shown in figure 6.3. The metal planes on top and bottom of the structure have been omitted such that the dielectric pattern is visible to the reader. The perforated regions to the left and right will be manufactured using the same drill size, while, different drill size should be used for each of the airgaps in the slab region. The theoretical bandwidth of this filter is 10.018 to 10.531 GHz with centre frequency 10.275 GHz.

The filter has been simulated and the results are shown in figure 6.4. Immediately we notice that the passband of the filter has been shifted. Instead of having a centre frequency of 10.275 GHz, the centre frequency is shifted to 10.5 GHz. I.e. there is an error of about 0.3 GHz due to the equivalent circuit which applies better to closed structures such as the folded guide.

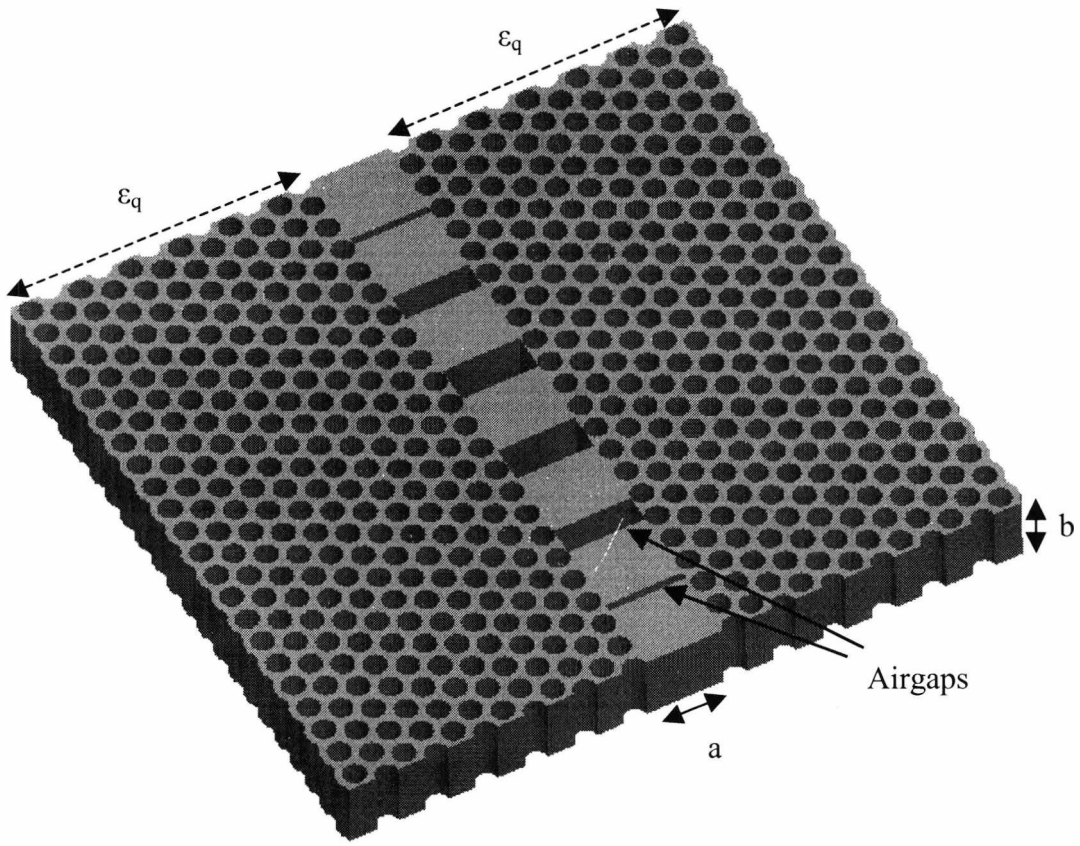

Figure 6.3. Perforated filter with airgap discontinuity

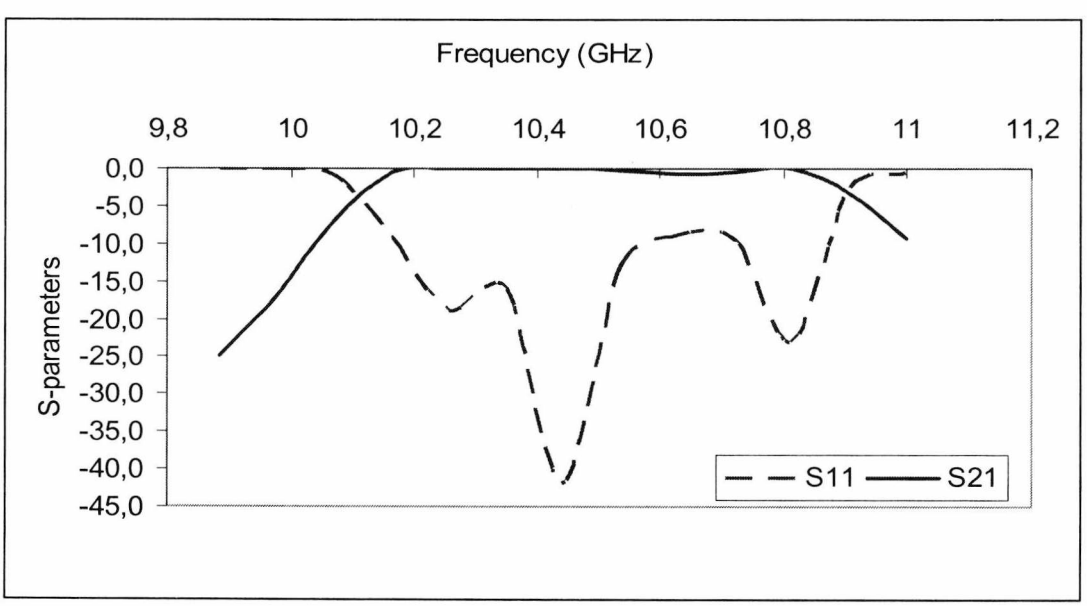

Figure 6.4. Simulated S parameters for the filter with airgap discontinuity

6.1.2 Air cylinder discontinuity

Another type of discontinuity that can used to form NRPD filters is the air-cylider discontinuity. Repeated simulations have shown that cylindrical air columns introduced in the centre slab of the NRD can form resonating cavities similar to those caused by the airgaps. The equivalent circuit is still the same used for the previous filters. Figure 6.5 shows the simulation model and Figure 6.6 shows the dielectric pattern used for such a filter. The metal planes are again omitted. The design variable for this filter is the radius of the cylinders. The same NRD guide is used with dimensions 9.3mm*10.23mm. The theoretical bandwidth of the filter is 10.018 to 10.531GHz. The filter has been simulated and the results are shown in figure 6.7. We notice that the pass band has shifted to a centre frequency of 10.7 for the same reason that it did in the airgap discontinuity.

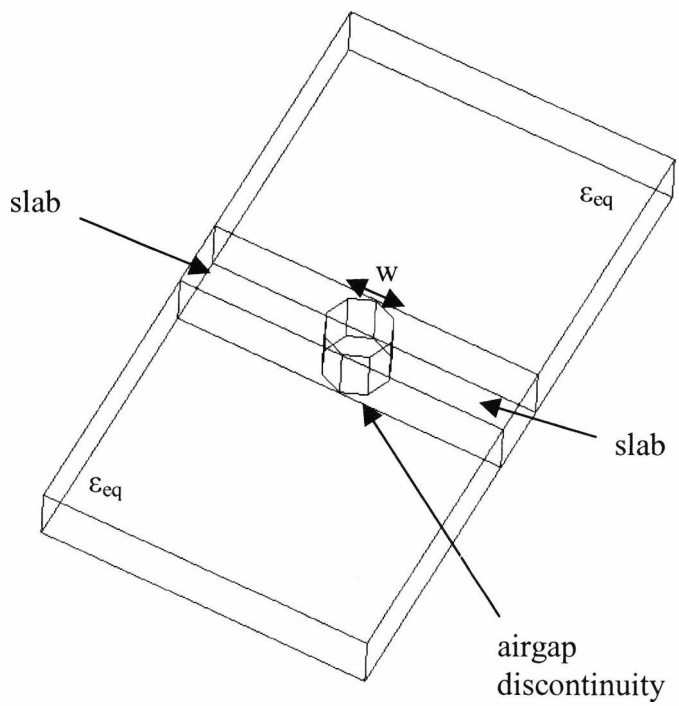

Figure 6.5 The single discontinuity of cylindrical air column in the slab of the NRD

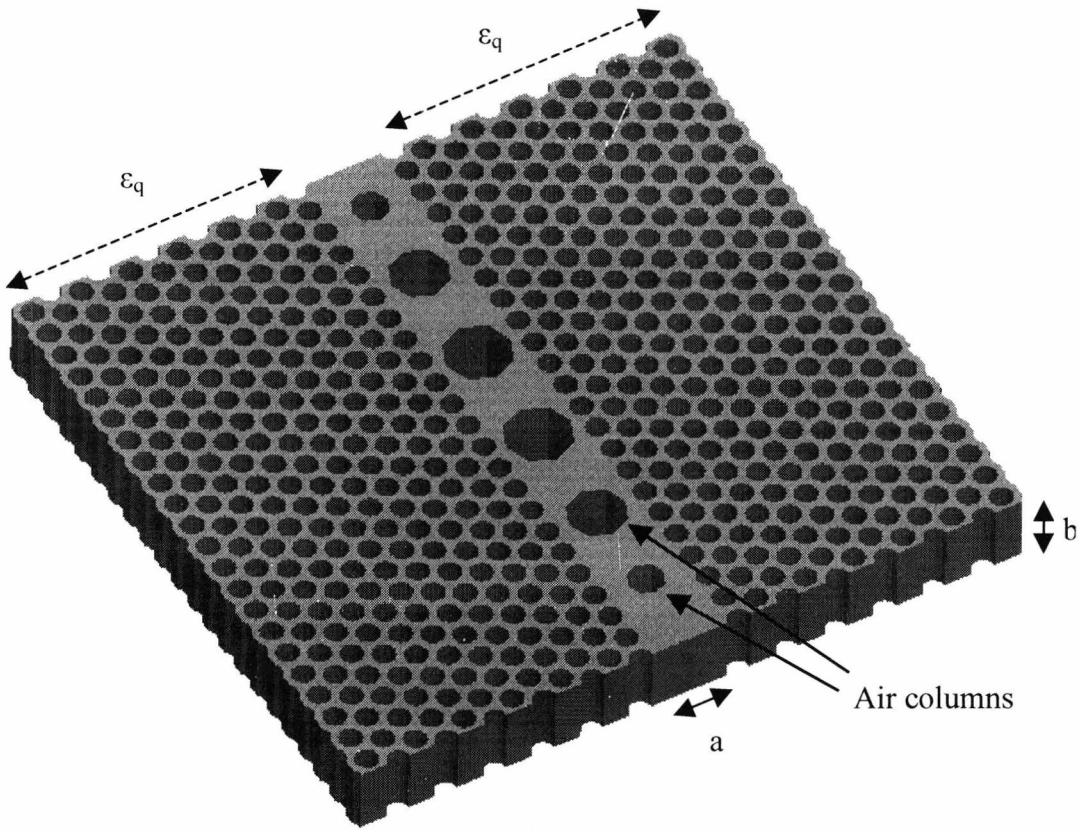

Figure 6.6 Perforated NRD filter made out of air columns in the slab

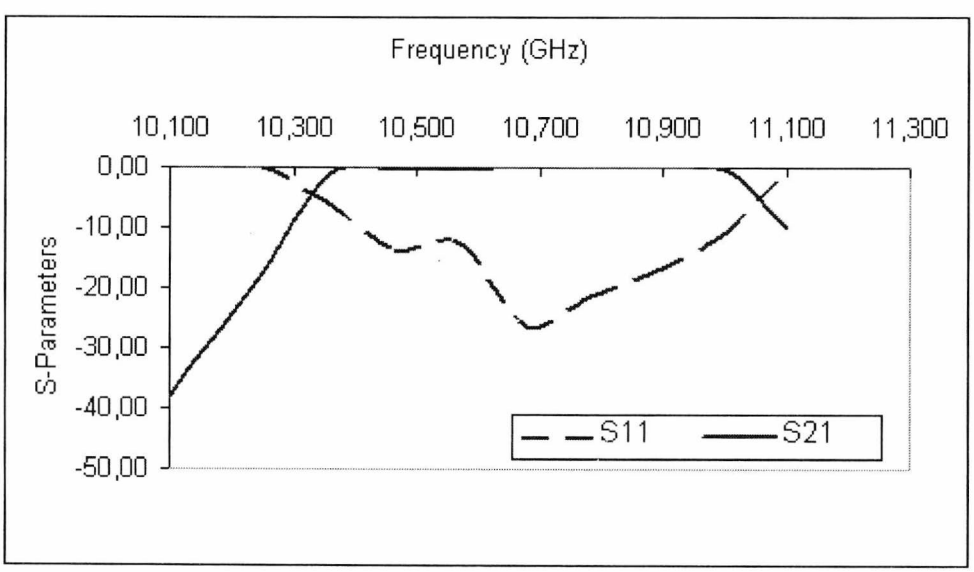

Figure 6.7. Simulated S-parameters for the cylindrical air columns filter

6.2 Summary

The NRD guide is known for its ability to guide energy around bends with potentially no radiation loss. Many components are therefore constantly designed on NRD principles. However all of these components suffer manufacturing limitations related to the alignment of the metal plated and the positioning of the central conductor.

In this chapter we have used the perforated dielectric technology to demonstrate the operation of NRPD filters. The operation is based on the resonating cavities formed by discontinuities in the central core of the NRD slab. We examined the airgap discontinuity and the air cylinder discontinuity and found them to have filtering properties but with a small amount of frequency shift. The reason for this phenomenon is probably the type of operating circuit which applies better to closed structures such as the folded guide or the rectangular waveguide.

Nevertheless, the NRPD filter surpasses the manufacturing limitations of conventional NRD filters and its manufacturing process is similar to that of an NRPD described in chapter 5.

References

[1] Jifu Huang and Ke Wu " A two-path Multimode Band pass Filter Using Non-Radiative Dielectric waveguide Technology" *IEEE MTT-S Digest*, 1995.

[2] Franqois Boone and Ke Wu, "Mode Conversion and Design Consideration of Integrated Nonradiative Dielectric waveguide (NRD) Components and Discontinuities", *IEEE Transactions on Microwave theory and Techniques*, Vol. 48, No 4, April 2000.

[3] Tomoyuki Goi, Shiego Kawasaki and Tsukasa Yoneyama," NRD Guide Couplers Combined with Microwave Integrated Circuits In Side-By Side alignment" *IEEE MTT-S Digest* 1998

[4] Fabrizio Frezza, Alessandro Galli and Paolo Lampariello, " Characterisation of the resonant and Coupling Parameters of Dielectric Resonators for NRD-Guide Filtering Devices," *IEEE MTT-S* Digest 1993

[5] "NRD-circuit compatible high permittivity dielectric radiator for multiple access LAN applications at 60 GHz," Kuroki, F.; Miyamae, A.; Yamaguchi, M.; *Antennas and Propagation Society International Symposium*, 2002. IEEE Volume 4, 16-21 June 2002 Page(s):402 - 405 vol.4

[6] "Filter-like design and optimization of NRD-guide mode suppressors," Jifu Huang; Ke Wu; Kuroki, F.; Yoneyama, T.;Microwave Symposium Digest, 1995., *IEEE MTT-S International* 16-20 May 1995 Page(s):995 - 998 vol.2

[7] "Slot array in non-radiating dielectric waveguide," Ghosh, B.; Shafai, L.; Ittipiboon, A.; Roscoe, D.J.;Antennas and Propagation Society International Symposium, 1997. IEEE., 1997 DigestVolume 4, 13-18 July 1997 Page(s):2508 - 2511 vol.4

[8] "Low-loss millimeter-wave propagation characteristics of NRD-guide surface-mounted on planar substrate for hybrid integrated circuit," Jinbang Tang; Xiangyin Zeng; Shanjia Xu; Ke Wu;Microwave Symposium Digest., 2000 *IEEE MTT-S International* Volume 3, 11-16 June 2000 Page(s):1679 - 1682 vol.3

[9] "Hybrid planar NRD-guide magic-tee junctionCassivi," Y.; Ke Wu;*Microwave Theory and Techniques, IEEE Transactions on* Volume 50, Issue 10, Oct. 2002 Page(s):2405 - 2408

7. Suggestions for further work

7.1. NRPD integrated with transition to slotline

In chapter 5, we described some of the most common applications of an NRD guide. We saw how it can be used to form filters and resonators or antennas and circulators. Nevertheless, what has not been achieved so far is the direct integration of NRD guide to Monolithic Microwave Integrated Circuits. MMICs, as they are called, play today a vital role in Microwave communications. They are circuits which combine active and passive devices on a single semiconductor substrate, hence the term monolithic. GaAs is probably the most common substrate for MMICs but other types of substrates such as Silicon, Silicon-on-Sapphire and indium Phosphide (InP) are also used. MMICs have the benefit of concentrating complete circuits in areas smaller than $1cm^2$. The weight of the structure is also extremely small. Due to these advantages MMICs are essential in the development of active microwave devices and are already used in a vast number of applications. Recently, state-of-the-art designs were been manufactured which use MMIC amplifiers to form power combiners for both spatial [1] and surface [2] power combining.

Conventional methods of coupling between MMICs and waveguides can use unilateral finlines inside rectangular waveguides [3] [4]. Previous work however has shown that this procedure is very time consuming and particularly expensive even for the simple designs. Furthermore, rectangular waveguides are heavy, robust structures and are not suitable for light, space-limited applications. NRD guide was integrated to MMICs in [5] but in that case the NRD is used in a leakage mode and the coupling is achieved through microstrip line outside the NRD. This paragraph demonstrates how a slotline-integrated NRPD can be a low cost alternative for energy coupling to MMICs chips without the manufacturing limitations of finlines.

7.1.1 Proposed NRPD guide with integrated tapered transition to slotline

An efficient type of impedance transformation must be employed in the NRPD core for wave transmission to MMICs. Although a quarter wave transformer can be used, its operation can be very narrow and unpredictable, especially when operating above 60 GHz. Hence, the best solution for this application is to use a tapered slotline, which delivers much wider bandwidth and has a relatively low return loss. Tapered slotlines are known for their design flexibility [6] and combine very well with the types of modes that propagate in side the NRD.

Due to its electric field orientation and low loss profile at increasing frequencies, mode LSM11 is the most suitable for our design, figure 7.1. The Electric field is predominately perpendicular to the direction of propagation and retains its maximum at the centre of the guide. Because of the confinement of LSM11 in the centre of the guide, exponentially tapered slotline can be used to couple the energy into a slot line mode, figure 7.2, which in turn can launch the energy into an MMIC. The transition must be placed in the middle of the guide core, where the field is at maximum. There are several types of tapered slotlines that can be used for the same purpose. Some of the most commonly used are the linear tapered slotline, half cosine and exponential taper and finally the *part of sine* taper, figure 7.3. The last, is a sine-curve plot from 0 to 120 degrees. In this project we have used only one type of tapered slotline, the exponential.

The taper can be modelled to match the physical characteristics of a waveguide, using design equations. Since the taper, by nature, forces the incoming wave to alter its geometry it generates reflected waves and radiation. However, if the tapered section is approximately λ/2 long all these reflections from inside the taper will cover a 360 degrees range in phase and add vectorially to a very small value, hence delivering low return loss characteristics [7]. Design equations for the tapers of figure 7.3 are:

$$y = mx \qquad \text{Linear taper} \qquad (7.1)$$

$$y = w * \exp(\frac{x}{l}) \qquad \text{Exponential taper} \qquad (7.2)$$

$$y = \frac{w}{2} * \cos\left(\frac{x}{l}\right) \qquad \text{Half cosine} \qquad (7.3)$$

$$y = A * \sin\left(\frac{x}{w}\right) \qquad \text{Part of sine} \qquad (7.4)$$

where m is the slope of the linear taper, w represents the total width of any taper, l is the total length of any taper, y represents dimension in length, x is dimension in width and A is a constant.

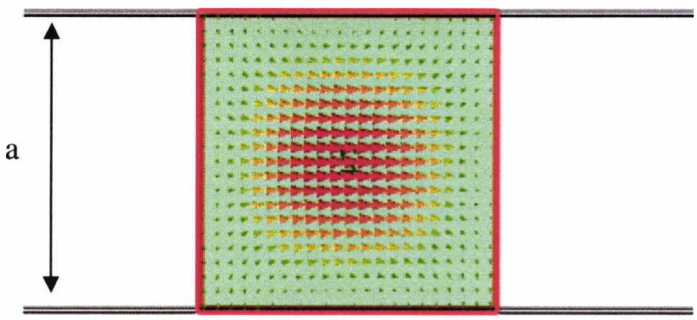

Figure 7.1. Illustration of the LSM11 inside a standard NRD guide mode considered in the design. The figure was produced with CST Microwave studio

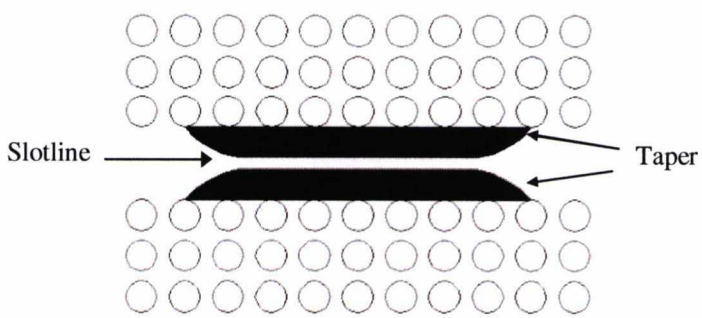

Figure 7.2. Top View. NRPD-guide with integrated back-to-back tapered transition to slotline. Black area is metal.

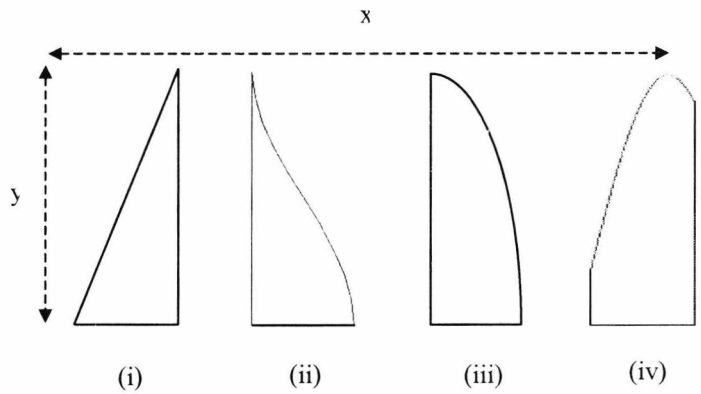

Figure 7.3. The different types of tapered slotlines: (i) linear, (ii) half cosine, (iii) exponential taper, (vi) part of sine

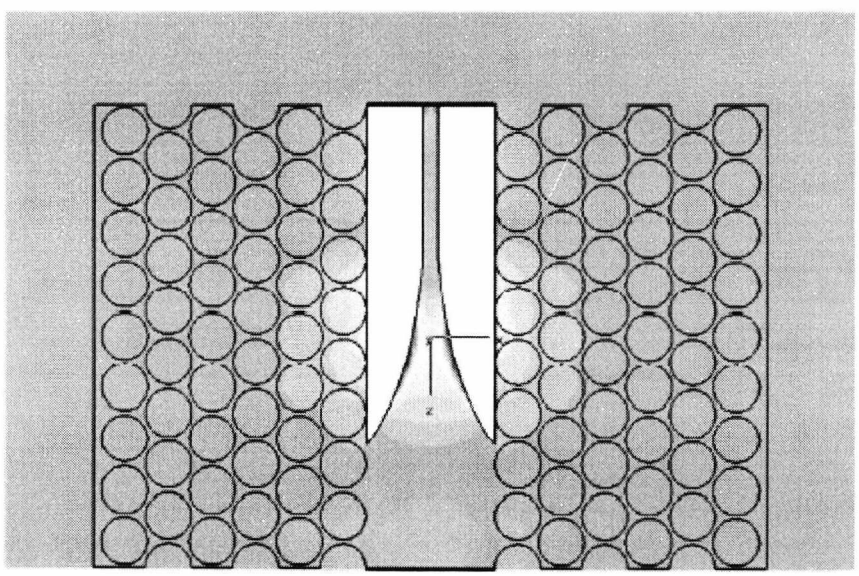

Figure 7.4. Simulated field plot of exponential slotline integrated with NRPD.

The NRPD waveguide has been simulated with an integrated exponential taper and the field plot is shown in figure 7.4. The field appears to enter the tapered transition just like it would to in the case of a finline. However, in this scenario there are no conducting walls surrounding the taper and hence there will be some leakage of energy. This problem can be handled by widening the taper so that it extends in the perforated region and by optimising the shape of the taper further. We have recently presented this idea, together with a publication, in [8]. Undoubtedly though, there is

a substantial amount of research still to be carried out before this structure is efficient, because we do not have a good set of S-parameters to accompany it.

Future work related to this application would be, at first, the improvement of a tapered transition that gives a better set of parameters and, secondly, a method to integrate the MMIC chip in the structure. The results that we have so far indicate that the structure works up to a certain degree but there is a lot of radiation and only a small part of the energy passes though the slotline.

Another issue that would require attention is the shape of the taper. We have shown in figure 7.3 that different shapes can be used, and each taper probably corresponds to a different response. The researcher that will continue this project is asked to investigate the usage of each taper and derive the best response. Nevertheless there can be another type of taper that might be very useful, the arbitrary taper. This type has no canonical shape. Instead its shape is produced through parametric simulations using a high frequency electromagnetic simulator. The taper is comprised of smaller segments of line which the simulator can position accordingly to achieve the lowest return loss, figure 7.5. The arbitrary taper can have any number of segments. A higher number gives greater detail and therefore approaches the ideal response at the expense of longer simulating time. Usually a compromise is chosen for practical reasons. This shape of taper is highly recommended for future work on this project.

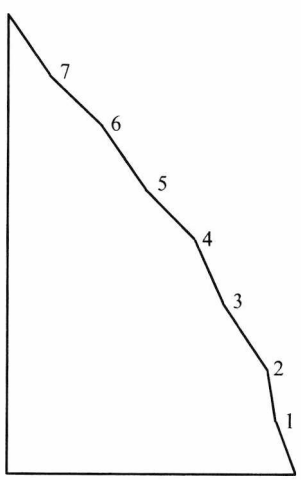

Figure 7.5. The ends of line segments are labelled with numbers. The simulator calculates the position of these segments for minimum return loss.

7.2 Antennas on folded waveguides

Folded waveguides broaden the horizons for a new class of substrate integrated structures that use the folded technology. We have already seen in chapter 4 the design of folded filters that offer reduced dimensions and good performance. Another novel type of structure that belongs to this class is the folded waveguide antenna. So far, several researchers have investigated slot antennas [9] and arrays [10] in substrate-integrated guide. We have used the folded technology to produce a microwave antenna with half the width of the other types of substrate-integrated waveguide [11]. Furthermore this new structure allows arrays of slot antennas to be more highly integrated.

Figure 7.6 shows the topology of the folded waveguide slot antenna. The antenna was fabricated using a substrate of dielectric constant $\varepsilon_r = 2.33$. The multilayer structure consisted of two layers of thickness 3.15 mm with the central metal etched on the bottom substrate. The side walls were formed using series of metallised vias, similar to the fabrication method of a folded waveguide. Excitation into the structure is achieved through tapered stripline. The length of the taper has been optimised for the lowest return loss. The antenna has been tested [12] and the results look very promising.

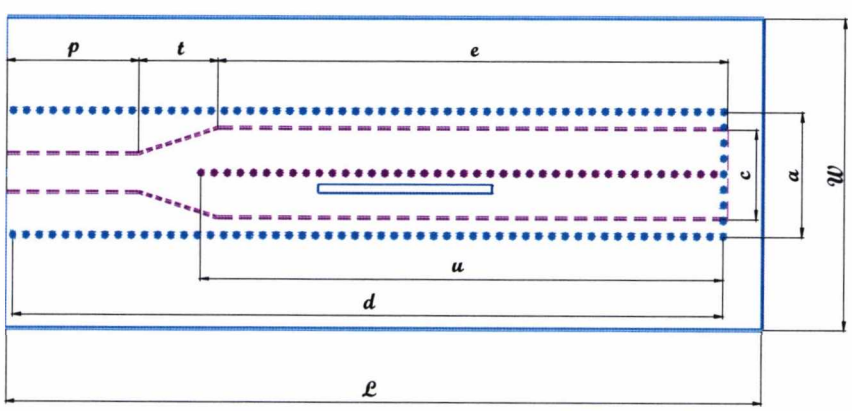

Figure 7.6. Folded antenna

This folded structure forms the basis for a new family of antennas. Future work would include folded antennas with arrays of slots rather than just one slot in the middle of the top plate. Arrays are very common in radiating structures and improve the directivity and radiation pattern of the antenna.

Also another type of future work would involve the design of folded antennas on Type 2 folded guide. Type 2 folded guides are known for their ease of fabrication. The only difference in the design would be the position of the slot, which, would have to go above the gapwidth of the guide since that is where the field is at maximum.

7.3. Summary

In chapter 5 we introduced the NRPD structure, an advanced alternative to the conventional NRD, with perforated regions of dielectric material surrounding the central slab. Due to the reduced permittivity of the surrounding regions the mode is confined in the middle in the form of a nonradiative mode, usually LSM11. Hence by introducing an exponentially tapered slotline in the slab we can couple the energy into a slot line mode which in turn can launch the energy into an MMIC. The transition must be placed in the middle of the slab core, where the field is at maximum. This design is analogous to a microwave finline but easier to fabricate. Future work on this project would include improvement of the transition.

In chapter 2 we introduced another novel type of structure, the folded waveguide. We described the two types of folded guides and demonstrated their superior bandwidth and reduced dimensions compared to the standard rectangular waveguide. Folded guides form the basis for a new class of folded based components such as the folded filters introduced in chapter 3. Following the same philosophy, we used folded waveguide type 1 to create a microwave slot antenna. The structure is double layered and therefore has reduced width compared to conventional slot antennas and is easily integrated to a tapered stripline. Future work on the folded antenna would be the design of slot-array antennas and the design of antennas on folded guide type 2.

References

[1] Pengcheng Jia and Robert A.York "Design of waveguide Filine arrays for Spatial Power Combining. *IEEE transactions on Microwave Theory and Techs*. Vol 49, No. 4, April 2001

[2] Alfred Richard And Tatsuo Itoh, "TM Surface-Wave Power Combining by a planar Active lens Amplifier" *IEEE transactions on Microwave Theory and Techs* Vol 46 No 6 , June 1998

[3] A.K.M. Saad "Design of Fin-line Tapers, Transitions and couplers" *11th European Microwave conference proceedings* pp. 308-350, 1981

[4] Jimmy Yip, Adam K. Jastrebski, Richard Collier and Diking Li." Properties of finlines" *International Microwave conference*. London 2001

[5] T.Goi, S.Kawasaki, T.Itoh and T.Yoneyama "NRD Guide Couplers Combined with Microwave Integrated Circuits in Side-by-Side Alignment" 1998 *IEEE MTT-S International Microwave Symposium*, June.1998, pp.1301-1304

[6] K.Singfrid Yngvenson, Daniel H. Scahubert and Thomas L. Korzeniows " Endfire Tapered slot antennas on dielectric sustrates" *IEEE Transactions on Antennas and Propogation*, vol. 33, pp. 1392–1400

[7] John D. Craus "Electromagnetics" McGraw-Hill International Editions, Fouth Edition, Electrical engineering series.

[8] *Non-Radiative Photonic Crystal Guide (NRPC) with Integrated Transition to Slotline for Millimetre-Wave Components*, N. Grigoropoulos, S. Tse and P.R.Young High Frequency Postgraduate Colloquium, Manchester 2004

[9] A. J. Farrall and P. R. Young, "Integrated waveguide slot antennas," Electron. Lett., vol. 40, No. 16, 5th August 2004, pp. 974-975.

[10] L. Yan, W. Hong, G. Hua, J. Chen, K. Wu and T. J. Cui, "Simulation and experiment on SIW slot array antennas," *IEEE Microwave Wireless Compon. Lett.*, vol. 14, No.9 September 2004, pp. 446-448.

[11] N. Grigoropoulos and P. R. Young, "Compact folded waveguides," *34th European Microwave conference*, Amsterdam 2004.

[12] Substrate-Integrated Folded Waveguide Slot Antenna, B. Sanz-Izquierdo, P. R. Young, N. Grigoropoulos, J. C. Batchelor, R. J. Langley, *IEEE International Workshop on Antenna Technology*, Singapore, March 2005.

8. Conclusion

Today we are living the Microwave era. More and more microwaves are being preferred, over other types of electromagnetic waves. Wavelengths of the order of centimeters fit humans and human-sized objects, which makes them attractive for radar and navigation. Microwaves have the largest absolute bandwidths of any RF waves before serious atmospheric attenuation sets in. They are therefore useful for wireless communications. Absorption in certain materials, especially water, is the basis for microwave industrial heating, cooking food and medical treatment. However we need to mention that uncontrolled exposure of live organs to Microwave radiation maybe be harmful, as in the case of mobile phones which operate on the lowest end of the Microwave spectrum. Hence caution is required for the safe usage of Microwaves, as is required for all other types of electromagnetic radiation.

The Microwave industry is one of the fastest growing industries. Originally (and still partially) driven by the military, especially in radar and electronic warfare, microwaves have now burst on the civilian scene and created the huge new industry of wireless communications. The Navy's needs for accurate navigation at sea resulted in the global positioning system (GPS), now available to anyone travelling by air, land or water. Microwaves have also started being used in the transportation industry. Specially developed integrated systems are used on modern vehicles to provide the driver with information concerning the condition of the road or the traffic ahead but also assist the driver by keeping safety distance from preceding vehicles or warn the driver of obstacles while reversing the vehicle.

It is clear that new types of microwave devices are often required, with efficient bandwidth and compact dimensions at low cost. They also need to meet the requirements of mass consumer market applications. Throughout this thesis we introduced two such new technologies in the field of Microwave engineering: i) The substrate integrated folded waveguide and ii) the Nonradiative Perforated Dielectric waveguide (NRPD). Chapters 2 and 5 analyzed extensively these new types of waveguide and described fabrication methods and measurements. Chapters 4 and 6 then proved that folded guides and NRPDs guides can form the basis for new types of components such as filters with efficient responses. NRPDs and folded guides are

therefore bound to play a vital role in the communication industry, both now and in the future.

For completeness, this chapter continues with a summary of what has been researched in this thesis and discusses the most important results.

8.1 Summary

Chapter 2 introduced a new type of microwave guide, the folded waveguide, a substrate integrated structure made from microwave laminates that can have two different geometrical formations i.e type 1 and type 2. Due to the closed nature of the folded guide, we based its analysis on the rectangular waveguide. Cutoff frequencies were derived and it was proved that a substrate integrated folded waveguide offers 50% more bandwidth and up to $\varepsilon_r^{-1/2}/3$ width reduction compared to standard air-filled rectangular waveguide. The same chapter explains how the folded guide can form multilayer stacks, resulting in further width reduction while at the same time offering wider bandwidth. Simulated results for Type 1 folded guide show that the relative bandwidth can reach values higher than 4. On the other hand, the bandwidth of folded guide type 2 does not change by increasing the number of layers. Furthermore, in the same chapter we presented design equations for both types of guide.

In chapter 3, the folded guide of type 1 and type 2 was fabricated in the workshop using conventional PCB fabrication techniques. Via hole technology was used to replace the perfect conducting sidewalls at low cost. The most suitable excitation method was proved to be the stripline, due to the orientation of electric field which is very close to that of folded guides. The transition was tapered and the length of the taper was optimised for minimum return loss. Two waveguides were measured and the results were in good agreement with simulation.

Chapter 3 also describes how folded guides can be designed at very high frequencies using thick film fabrication process. We designed both types of guide for operation up to 110 GHz. In order to form the side walls, thick film fabrication produced mettalised trenches 100microns wide. The substrate used had $\varepsilon_r=8$ and the structures were excited using microstrip line. Simulations showed very good performance throughout the entire bandwidth. The waveguides were sent for thick film fabrication to the University of Surrey. Unfortunately, at the time that this thesis was written the waveguides were not yet ready for measurement.

In chapter 4, we used the folded waveguide technology to form 5% bandwidth microwave filters. The filters were formed by periodically introducing discontinuities

in the folded waveguide and offer compact dimensions and good performance at low cost. Although both types of folded guide could be used we preferred to use the Type2 because of its manufacturing simplicity. A filter was designed, using via-hole technology and printed patch in the middle to deliver more accurate length of discontinuity. The filter operation was based on the principle of direct coupled cavity filters. The microwave filter was then measured in the lab with network analyzer with coaxial calibration and showed good performance. The return loss was a bit worse than expected but that was due to the SMA connectors and the stripline feeds that were not de-embedded. Nevertheless, the fabrication process was low cost and effective.

In chapter 5 we analyzed the Nonradiative Dielectric waveguide based on the theory of the slab waveguide and we derived equations for the calculation of propagation constants and cutoff frequencies. It was explained that the benefit of the NRD over simple dielectric waveguide is that it can guide electromagnetic waves around curved sections or discontinuities with potentially no radiation loss. Furthermore, NRD guides do not have the metal side walls of the rectangular waveguide which are the main cause of conduction losses. However, NRDs pose severe manufacturing limitations, especially at high frequencies. The most important problems are related to the mechanical support and assembly of the NRD central core and the alignment of the top and bottom metal plates. For that reason we introduced the Perforated Nonradiative waveguide which holds the advantages of the conventional NRD but eliminates its fabrication disadvantages. The NRPD was successfully manufactured in the workshop using computer controlled drilling machines which minimised the human involvement and the fabrication time. The NRPD was then tested for its wavelength sensitivity and we concluded that the diameter of the perforated lattice should be at least five times shorter than the guided wavelength. The wavelength of the NRPD was also measured and it was found to be in very good agreement with simulated results.

In the same chapter we analyzed different types of perforated lattice and concluded that the triangular lattice was the most suitable for the purposes of our NRPD. A triangular lattice with a =3.3mm and r =1.5mm can reduce the permittivity of a dielectric laminate by approximately 120%. Furthermore we demonstrated how three series of perforated holes were enough to confine the mode in the centre of the NRPD.

Excitation to the NRPD was achieved through rectangular waveguide and tapered transitions for the central slab. Microstrip line is also suitable of the same usage but the fabrication method would be a bit more complex.

Chapter 6 demonstrated how the perforated lattice can be used to form NRPD-based components such as filters, without the manufacturing limitations of conventional

NRD. The filter was formed by introducing airgaps in the central slab of the NRPD. Two types of discontinuities were simulated i) rectangular airgaps ii) cylindrical airgaps. The responses were good for both cases.

Chapter 7 discusses possible future projects arising from this thesis. Since the NRPD offers field confinement in its centre, a tapered slotline can be used to couple the NRPD mode into a slotline mode. Slotlines are commonly used in the fabrication of MMIC circuits inside rectanguilar waveguides. In our case we can house a MMIC in the central slab of the NRPD and use the slotline to get energy coupling. In other words we have a simpler alternative to the well known finline. Although we have already simulated this design, an efficient performance is yet to be achieved. Therefore extra work is required to achieve smoother excitation into the slotline.

Another application which requires some future work is the folded waveguide antenna which based on the folded guide technology. We designed a slot antenna on folded guide type 1 using conventional PCB techniques and via side walls. Excitation into the structure was achieved through tapered stripline. The length of the taper was optimised for the lowest return loss. The folded antenna was measured in the anechoic chamber and the directivity of the antenna was very good. The folded antenna has half the width of the other types of substrate-integrated waveguide antennas and forms the basis for a new family of antennas. Future work would include folded antennas with arrays of slots rather than just one slot in the middle of the top plate. Arrays are very common in radiating structures and improve the directivity and radiation pattern of the antenna. Also, since the antenna was designed for type 1 guide, it would be usefull to design an antenna using type2 especially since we know that type 2 guides are easier to fabricate.

Appendix - TRL method

The TRL technique is well known in mm-wave measurements and it is covered in the literature [1]. However for the sake of completeness we present a characteristic description of the technique in the following pages.

Every microwave integrated circuit (MIC) will need to have some form of transition on each side before it can be measured at high frequencies. Using the standard calibration procedures included in the network analyzer allows the user to obtain S-parameters of the circuit, i.e. transmission properties and return loss. Unfortunately, the two-port parameters will include the effects of the line and transition as well as reflections and losses. A de-embedding procedure is hence required that concentrates on the circuit contained within the line, microstrip, coplanar or other type. Such a procedure usually requires ideal or measured shorts, opens and/or resistive loads. At normal microwave frequencies a short circuit may appear as such but at mm-wavelengths a short appears inductive. At high frequencies a de-embedding technique is called through-reflect-load (TRL) and allows non ideal elements to be used for the procedure. These elements are the through (T) that connects the two transitions, the reflect (R) element, that can be anything, and the length of transmission line (L) connecting the two transitions. TRL is easy to implement on wafers that can use co-planar probes.

Figure A.1 shows the four measurements necessary for De-embedding. The TRL transitions A and B both include line lengths that meet somewhere in-between the reference point. In other cases the actual transitions could be quite different. Figure A.1.a shows the basic through structure and figure A.1.b shows the reflect measurement used. Since any two identical reflections can be used, it is simple to remove equal large sections from both sides of the reference position. Figure A.1.c shows the length measurement. The transitions A and B remain as in figure A.1.a apart from the extended length in the region surrounding the reference position. Figure A.1.d is the same as A.1.a except that the device to be measured is shown centered at the reference position. There might be cases where instead of the measurement with device, the user chooses another value of length. The four sets of measured data should be stored in data files for manipulation by the de-embedding program. The mathematics behind the procedure are discussed analytically in [2].

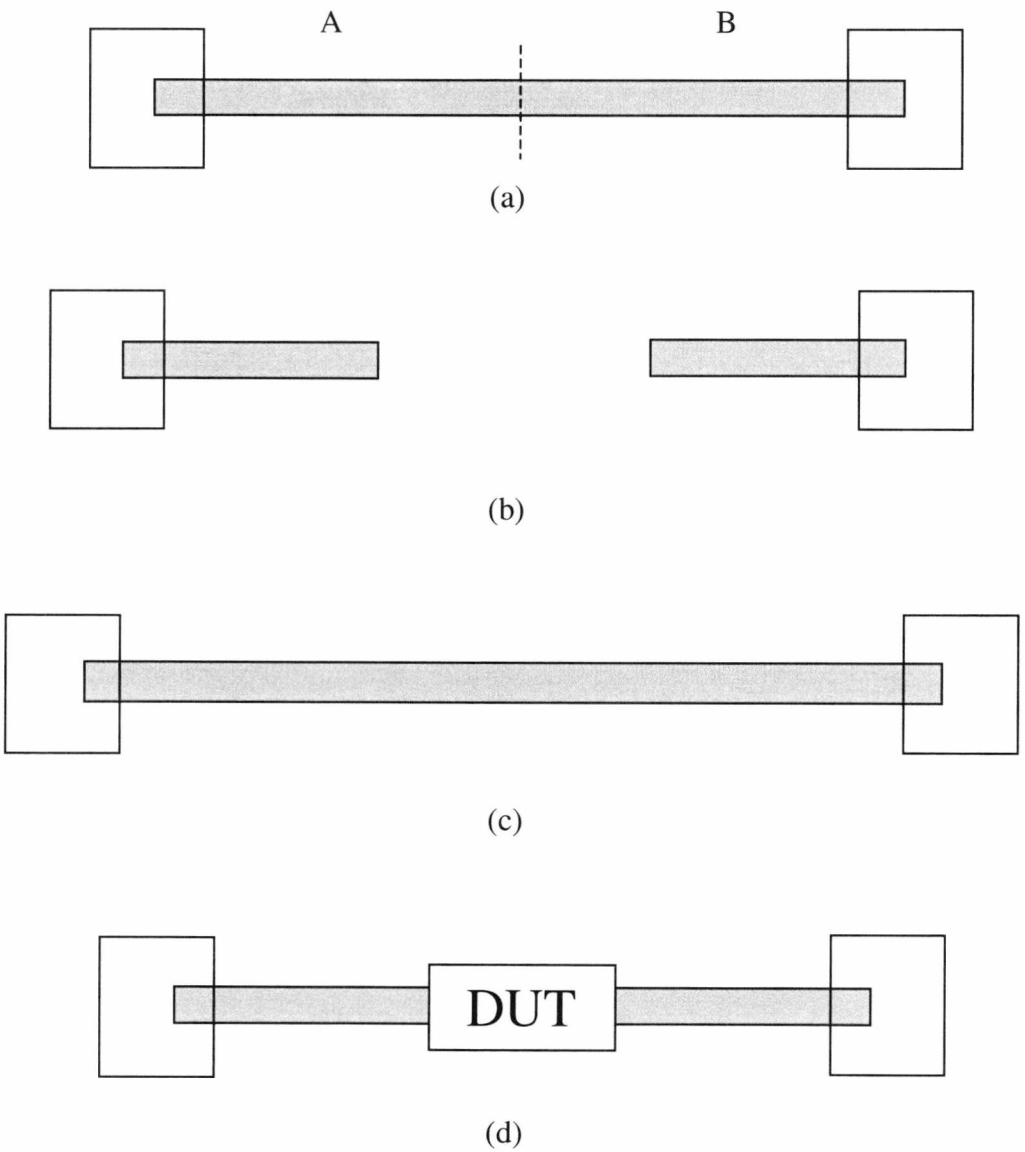

Figure A.1. The four measurements required for TRL de-embedding (a) through, (b) reflect, (c) length, (d) device

Following the TRL standard we prepared folded waveguide samples for fabrication in collaboration with the University of Surrey. For each waveguide we have four different variations. However, thick film fabrication is a multilayer process. Hence each individual guide is made of four layers. Figures A.2 and A.3 show each of the layers prepared for thick film and figures A.4 and A.5 show all the layers together.

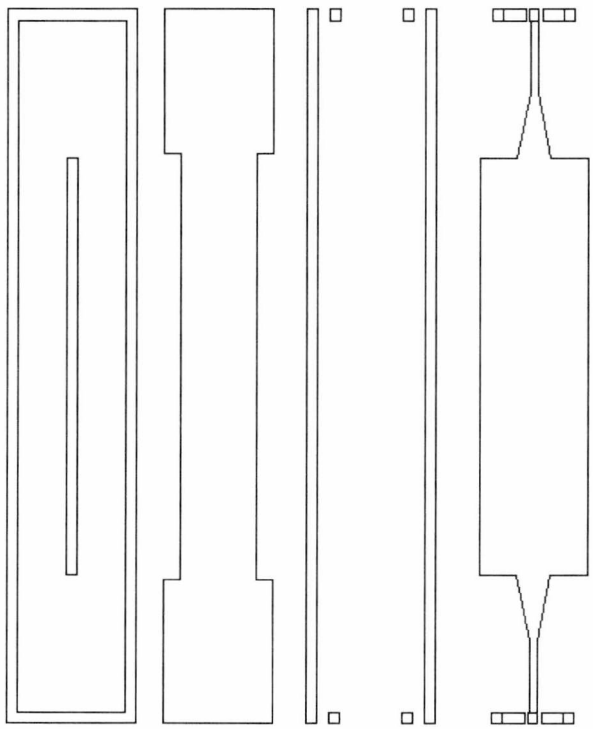

Figure A.2. From left to right - bottom to top layer for type 1 folded guide

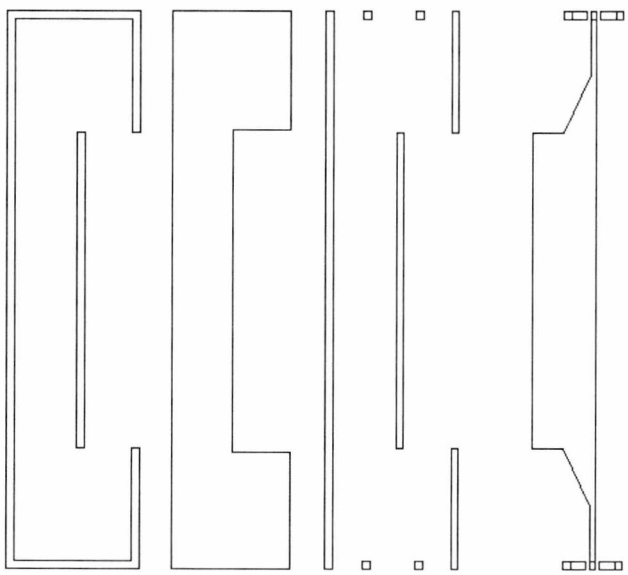

Figure A.3. From left to right – bottom to top layer for type 2 folded guide

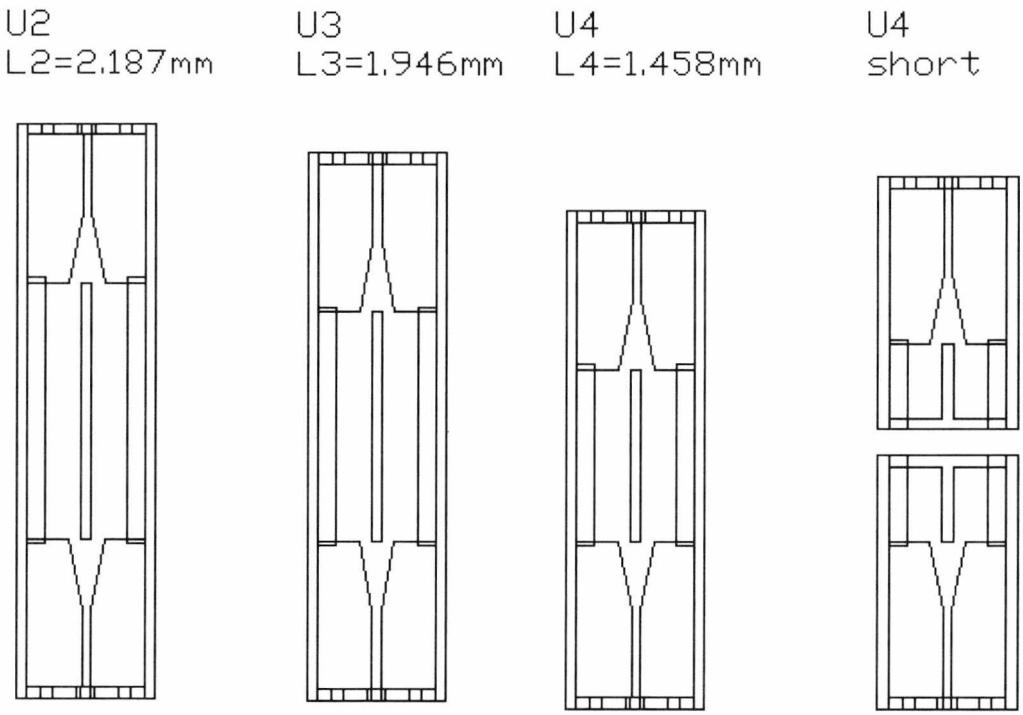

Figure A.4 Type 1 folded guide, four lengths for the TRL technique (a) Length1 (b) Length2, (c) Through, (d) Short

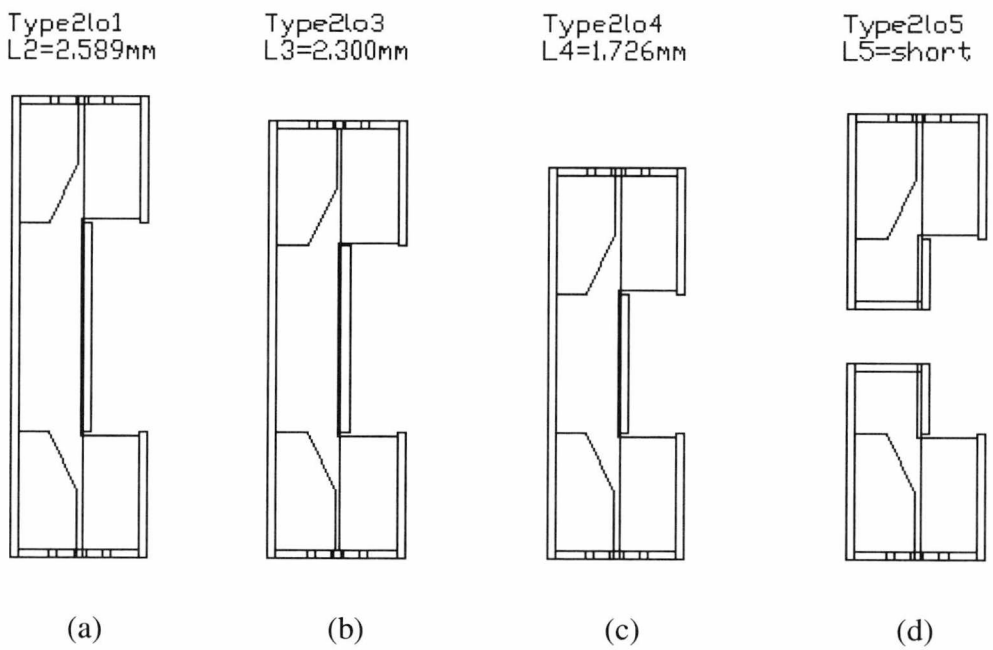

Figure A.5 Type 2 folded guide, four lengths for the TRL(a) Length1 (b) Length2, (c) Through, (d) Short

References

[1] G.F. Engen and C.A.Hoer-Reflect-Line: An improved technique for Calibrating the Dual Six-Port Automatic Network Analyzer. "*IEEE Trans. Microwave Theory Tech.*, VOl. MTT-27, No 12, Dec 1989

[2] David Rubin "De-embedding mm-Wave MICs with TRL". *Microwave journal* June 1990, pp141-148